# Eidesstattliche Erklärung

Vor- und Zuname: Martin Stockhausen
Geburtsdatum: 15.09.1979
Geburtsort: Solingen

Hiermit erkläre ich an Eides statt,

dass ich die vorgelegte Dissertation selbständig und ohne unzulässige fremde Hilfe angefertigt und verfasst habe, dass alle Hilfsmittel und sonstigen Hilfen angegeben und dass alle Stellen, die ich wörtlich oder dem Sinne nach aus anderen Veröffentlichungen entnommen habe, kenntlich gemacht worden sind;

dass die Dissertation ganz oder teilweise noch nicht zu einem früheren Zeitpunkt an der Christia*n*-Albrechts-Universität zu Kiel oder einer anderen i*n*- oder ausländischen Hochschule als Dissertation eingereicht worden ist.

Die Dissertation entstand unter Einhaltung der Regeln guter wissenschaftlicher Praxis der Deutschen Forschungsgemeinschaft.

Kiel, 24.09.2015 gez. Martin Stockhausen

# EXPERIMENTAL SIMULATION OF HYDROCARBON EXPULSION

*Dissertation*
*zur Erlangung des Doktorgrades*
*der Mathematisch-Naturwissenschaftlichen Fakultät*
*der Christian-Albrechts-Universität zu Kiel*

*vorgelegt von*

***Martin Stockhausen***

*Kiel, 2015*

| | |
|---|---|
| Erster Gutachter: | Prof. Dr. Lorenz Schwark |
| Zweiter Gutachter: | Prof. Dr. Brain Horsfield |

| | |
|---|---|
| Tag der mündlichen Prüfung: | 30.11.2015 |
| Zum Druck genehmigt: | 30.11.2015 |

gez. Prof. Dr. Wolfgang J. Duschl, Dekan

# Abstract

Investigating generation, expulsion and primary migration usually suffers from inadequate methodologies, failing in the provision of natural conditions, prevailing during the genesis of oil and gas. Destructive sample preparation, inappropriate pressure regimes and pyrolysis in closed mode and/or in the absence of water caused results not representative for natural processes. To overcome these limitations, a newly designed apparatus was developed and built, capable to perform pyrolysis experiments with intact rock samples under pressure regimes, prevailing during catagenesis. In detail, lithostatic (or overburden-) pressures and hydrostatic (or pore-) pressures, corresponding to 3000 m depth and beyond, can be simulated by this apparatus, the "Expulsinator" device. Additionally, the experiments are conducted as hydrous, semi-open pyrolysis, allowing the time-based sampling of the expelled products. Thus, generation/expulsion profiles are generated for each investigated source-rock.

Comparison of generation and expulsion efficiency of the Expulsinator with established pyrolysis methodologies (MSSV, HyPy, Rock Eval and closed small vessel pyrolysis (CSVP)) reveals striking differences: Expulsinator experiments yielded more bitumen and released lower gas amounts than classic pyrolysis. This is caused by secondary alteration of products in case of classic pyrolysis, e.g. oil to gas cracking at higher temperatures and polymerization to pyrobitumen. The open setup of the Expulsinator experiments prevents successfully secondary alteration, increasing the liquid product yields and lowering the gas formation. This is mirrored in TOC conversion rates as well: Expulsinator conversion exceeds 81 %, whereas those of hydrous CSVP remains at 65 %. Further, interactions between kerogen, bitumen, pyrobitumen and pyrite are reduced in case of Expulsinator experiments. In contrast, CSVP experiments residues show enrichment of nitrogen and oxygen and depletion of sulphur, indicating intense interaction between the mentioned components.

Investigating the impact of catagenesis onto the yields and composition of expelled products was carried out by a stepwise experimental setup, simulating burial depths of ~2000 m, ~2500 m and 3000 m, implementing overburden pressures from 600 bar to 900 bar and hydrostatic pressures from 200 bar to 300 bar. Each experiment step shows a distinct expulsion maximum of liquid hydrocarbons, reaching the total maximum at 3000 m. Confrontation of Expulsinator results with comparative CSVP and MSSV experiments reveal expulsion and primary migration effects onto the *n*-alkane distribution in dependence of maturation and subsidence. An *n*-alkane increase towards larger molecular size with ongoing expulsion is associated with molecular size controlled retention effects. The expulsion progress is mirrored in trends of isoprenoid-ratios (pristane vs. phytane) and isoprenoid – *n*-alkane-ratios (pristane vs. *n*-$C_{17}$), caused mainly by generation controlled effects. However, both ratios qualify as expulsion indicator, taking into account generation and expulsion are concurrent processes.

Generation/expulsion classification is done with eight different source-rocks (two type-I, type-II (-I/II), type-IIS and type-III kerogens, each) with different lithologies, using the catagenesis experiment setup described above. Again, formation of pyrobitumen shows to affect the maturity assessment of the source-rock, increasing the measured $T_{max}$ in case of kerogen type-I samples, but decreasing the measured value for type-II and –IIS kerogens. Type-III kerogen shows earliest onset of generation, followed by type-IIS and –II kerogen and type-I kerogen with the latest generation onset. The early generation and the concomitant high expulsion rate, observed for type-III kerogen, is contrasted by results of natural systems where this kerogen type usually shows very low expulsion rates. The Expulsinator setup provides excellent expulsion conditions, leading to early release of generated hydrocarbons. In contrast, accumulation within the kerogen pore space and subsequent condensation to solid bitumen leads to low generation and expulsion in natural systems. Differences between the generation/expulsion profiles of the different source-rocks are not only caused by the nature of the organic matter, but the lithology of the rock sample as well. Sturdy lithologies with very high pressure resistance and low permeability lithologies show lowered expulsion efficiency. An increase of the $CO_2$-yields with increasing temperatures and pressures was observed for lithologies with high inorganic carbon content.

# Abstrakt

Die Untersuchung von Öl- und Gas Expulsion und Migration wurde bisher durch unzureichende Methodiken erschwert, da Bedingungen, die während der Bildung freier Kohlenwasserstoffe vorherrschen, zumeist nicht oder nur teilweise durch diese Methodiken simuliert werden. Destruktive Probenvorbereitung, unzureichende Druckregime und Pyrolyse in geschlossenen Systemen und/oder in Abwesenheit von Wasser entsprechen nicht den Bedingungen natürlicher Prozesse. Um eine naturnahe Simulation der Generierung und Freisetzung von Öl und Gas zu ermöglichen, wurde im Rahmen dieser Arbeit eine Apparatur entwickelt, der „Expulsinator", der eine wässrige Pyrolyse mit einem intakten Erdöl-Muttergestein unter Druckbedingungen durchführen kann, die während der Katagenese vorherrschen. Im Einzelnen ist es möglich, lithostatische und hydrostatische Drücke (oder Porendruck) bis zu einer Tiefe von 3000 m und darüber hinaus zu simulieren. Die wässrige Pyrolyse wird in einem semi-offenen Modus durchgeführt, was eine zeitbasierte Beprobung der freigesetzten Produkte ermöglicht. Dadurch können individuelle Generierungs-/Expulsions-Profile für jedes untersuchte Muttergestein erstellt werden.

Ein Vergleich der Generierungs- und Expulsionseffizienz der Expulsinator-Versuche mit den Ergebnissen etablierter Pyrolyse-Methodiken (MSSV, HyPy, Rock Eval und closed small vessel pyrolysis (CSVP)) offenbart große Unterschiede. So wurden, verglichen zu klassischer Pyrolyse, durch Expulsinator-Versuche wesentlich größere Mengen an Bitumen generiert, bei gleichzeitig niedrigeren Gasmengen. Als Ursache werden sekundäre Abbaureaktionen gesehen, die im Falle der klassischen Pyrolysemethoden verstärkt zur Öl-zu-Gas Aufspaltung bei höheren Pyrolysetemperaturen und Polymerisation zu Pyrobitumen führen. Das offene Verfahren, das beim Expulsinator zur Anwendung kommt, verhindert dagegen sekundäre Reaktionen, was die Ausbeute flüssiger Produkte erhöht und gleichzeitig die Gasgenerierung reduziert, welches ebenfalls durch TOC Umwandlungsraten bestätigt wird: Während die Umwandlungsrate des Expulsinator-Versuchs 81 % übersteigt, erreicht die wässrige CSVP gerade einmal 65 %. Des Weiteren werden Reaktionen zwischen dem generierten Bitumen und dem verbleibenden Kerogen, dem Pyrobitumen und Pyrit im Falle des Expulsinators stark reduziert. Dagegen zeigt das Residuum von CSVP-Experimenten erhöhte Werte für Stickstoff und Sauerstoff sowie eine Abnahme an Schwefel, was ein Zeichen verstärkter Interaktion zwischen den oben genannten Komponenten ist.

Um den Einfluss der Katagenese auf die Menge und Komposition der freigesetzten Pyrolyseprodukte zu untersuchen, wurde ein Experiment mit schrittweiser Erhöhung der Drücke (lithostatisch: 600 bis 900 bar, hydrostatisch: 200 bis 300 bar) und Temperatur gewählt, wodurch Versenkungstiefen von ~2000 m, ~2500 m und 3000 m simuliert wurden. Jede einzelne Stufe des Experiments zeigte für flüssige Kohlenwasserstoffe ein deutliches Expulsionsmaximum, wobei das Gesamtmaximum bei 3000 m erreicht wurde. Die Gegenüberstellung der Expulsinator-Experimente mit CSVP- und MSSV-Experimenten zeigt deutlich eine Auswirkung von Expulsion und primärer Migration auf die *n*-Alka*n*-Verteilung und zwar in Abhängigkeit der Reife und der Versenkung. Mit fortlaufender Expulsion konnte dabei eine Zunahme von *n*-Alkanen mit zunehmender Molekülgröße festgestellt werden, was klar im Zusammenhang mit durch Molekülgröße beeinflussten Zurückhaltungseffekten steht. Isoprenoid-Verhältnisse (Pristan vs. Phytan) und Isoprenoid- *n*-Alka*n*-Verhältnisse (Pristan vs. *n*-$C_{17}$) zeigen Trends, die die Expulsionsentwicklung wiedergeben, was hauptsächlich durch Generierungseffekte beeinflusst wird. Allerdings eignen sich beide Verhältnisse dennoch als Expulsionsindikator, da Generierung und Expulsion zeitlich verbundene Prozesse sind.

Um eine Klassifizierung von Generierung und Expulsion durchzuführen, wurden insgesamt acht lithologisch unterschiedliche Muttergesteine (jeweils zwei Typ-I, Typ-II (-I/II), Typ-IIS und Typ-III Kerogene) mit dem oben beschriebenen Versuchsaufbau verglichen. Auch hier zeigt sich, das Pyrobitumen entscheidend die Reifebewertung eines Muttergesteins beeinflussen kann. Dabei wurde durch Pyrobitumen der gemessene $T_{max}$ im Fall vom Kerogen Typ-I erhöht, bei Typ-II und –IIS allerdings erniedrigt. Typ-III Kerogen zeigte einen sehr frühen Generierungsbeginn, gefolgt von Typ-IIS und –II und zuletzt Typ-I Kerogen mit dem spätesten Beginn der Generierung. Damit stehen die beobachtete frühe Generierung und die begleitende hohe Expulsionrate beim Typ-III Kerogen im Wiederspruch zu Beobachtungen in natürlichen Systemen, wo dieser Kerogentyp eher niedrige Expulsionsraten zeigt. Die Ursache liegt in den idealen Expulsions-Bedingungen, die durch den Expulsinator bereitgestellt werden und zu früher Freisetzung der generierten Produkte führt. Dagegen verursacht im natürlichen System Akkumulation von Bitumen im Porenraum des Kerogens und nachfolgende Kondensation zu festem Bitumen zu geringer Generierung und Expulsion. Weitere Unterschiede zwischen den Generierungs/Expulsions-Profilen der unterschiedlichen Muttergesteine werden nicht nur durch die unterschiedliche Beschaffenheit des organischen Materials verursacht, sondern auch maßgeblich durch die unterschiedlichen Lithologien. So zeigen widerstandsfähige Litho-Typen mit hoher Druckresistenz und mit niedriger Permeabilität verringerte Expulsionsraten. Des Weiteren zeigen Lithologien mit hohem Karbonatanteil mit Temperatur und Druck zunehmende $CO_2$-Mengen, was für einen hohen anorganischen Beitrag zum $CO_2$ spricht.

# Table of Contents

# Abbreviations

| | |
|---|---|
| CR | Conversion Rate |
| CSVP | Closed Small Vessel Pyrolysis |
| FID | Flame Ionisation Detector |
| GC | Gas Chromatography |
| HI | Hydrogen Index |
| HyPy | (Fixed-bed) Hydropyrolysis |
| MA | Monoaromatic Steroid |
| MDR | Methyldibenzothiophene Ratio |
| MS | Mass Spectrometer |
| MSSV | Microscale Sealed Vessel pyrolysis |
| MPI-1 | Methylphenanthrene Index |
| OC | Organic Carbone |
| OI | Oxygen Index |
| OM | Organic Matter |
| Ph | Phytane |
| Pr | Pristane |
| Py-GC | Pyrolysis coupled with Gas Chromatography |
| $R_0$ | Vitrinite Reflectance |
| TA | Triaromatic Steroid |
| TAI | Thermal Alteration Index |
| TCD | Thermal Conductivity Detector |
| TOC | Total Organic Carbone |

# List of Figures

# List of Tables

# 1 Introduction

Detailed knowledge of the processes involved in the formation of oil and gas are essential for efficient production and use of this resource. In recent years, considerable progress has been made in the lab-scaled simulation of the formation of petroleum. Thus, essential knowledge was gained about the generation of oil and gas. However, many questions remain unresolved, despite all the progress that has been made. Established methodologies focused on generation of hydrocarbons, but not on expulsion and primary migration of the oil. Thus, the accurate processes during the expulsion of oil are still unknown, although the latter is decisive for the assessment and modelling of basin systems. This study should provide a contribution to answer these questions.

## 1.1 Genesis of oil and gas

Organic matter (OM), primary produced by photosynthesis, accumulates under anoxic conditions and is incorporated into sediments. This process is facilitated by low-energy, fine-grained sedimentation. Most components which are easily utilizable by organisms, like proteins and polysaccharides, are recycled by biological activity during early digenesis. In result, the OM content drops sharply. Further reactions lead to an increase of the pH and formation of reducing conditions. Mainly responsible for this is the degradation of organic nitrogen to ammonia (pH) and the reduction of nitrates, sulfates and ferric hydroxide. Progressing diagenetic processes lead to the formation of complex geopolymers by condensation of humic acids (Bordenave, 1993), mainly by bacterial activity and delivery of methane and $CO_2$. Because of their high molar mass and degree of crosslinking, these macromolecules are insoluble in organic solvents and form kerogen, the precursor of oil and gas. It consists of aliphatic, aromatic and oxygen-containing functional groups (carboxylic acid, alcohol, carbonyl, ester, ether and amide) (Killops and Killops, 2009).

Further subsidence of the sediment and related increasing temperature and pressure conditions leads to beginning thermal degradation of the Kerogen. In this stage, the catagenesis, oil formation, is setting in. At temperatures of 100-150°C labile kerogen is thermally cracked to saturate-enriched oils. During this process kerogen is enriched on aromatic components and the H/O-ratio of the kerogen decreases (Behar and Vandenbroucke, 1987).

With increasing depth and temperature only gas (particularly methane) is released from the residual

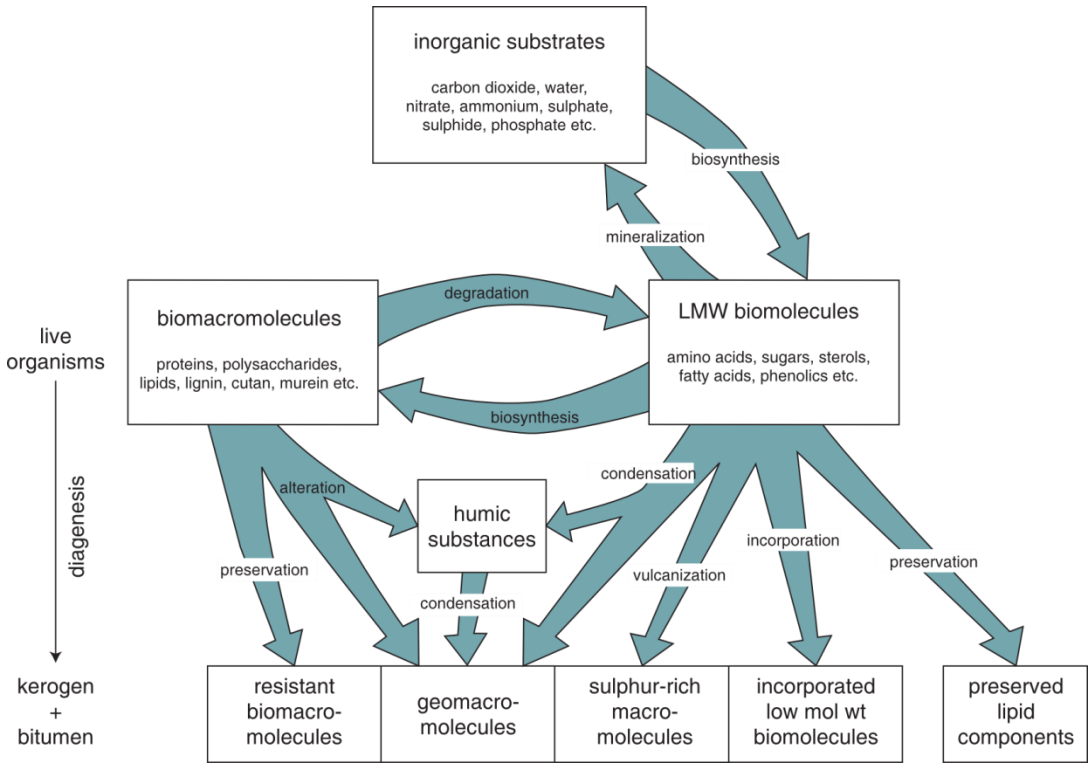


***Figure 1. Simplified process of kerogen formation (Killops and Killops, 2009).***

kerogen. This stage is called metagenesis and finally leads to the formation of pyrobitumen, a carbon-enriched highly polymer residuum.

### 1.1.1 Kerogen

Kerogen consists of polymerized networks, or geopolymers, derived from biological molecules (Bordenave, 1993). The biological precursors are lipids, carbohydrates, proteins and lignin in case of terrestrial-plant input. Easily utilizable components, like lipids and carbohydrates, were recycled mostly by microorganisms, increasing the content of lipid- and lignin-derived elements in kerogen. On elementary level kerogen consists mainly of carbon, hydrogen and oxygen and secondary amounts of sulphur and nitrogen. The relative amounts of C, H, and O forming the kerogen depend on the origin of the OM and of the thermal history of the kerogen. This allows a classification of kerogen with the H/C ratio and O/C ratio into subtypes of different origin (Killops and Killops, 2009) (see Figure 2). Main Kerogen types will be described in the following.

#### *Type-I Kerogen*

This Kerogen type results from lacustrine environments with anoxic, low energy sedimentary conditions. It contains significant amounts of lipid material with dominance of long-chain aliphatics. The origin of this material is alginate, algaenan, and smaller amounts of amorphous bacterial matter. Type-I kerogen has a very high H/C ratio and a low O/C ratio (see Table 1), resulting in a very high oil potential, but is relatively rare (Bordenave, 1993; Killops and Killops, 2009).

***Table 1. Kerogen types and corresponding H/C and O/C values (Killops and Killops, 2009).***

| Kerogen type | H/C | O/C |
|---|---|---|
| **Type I** | high (≥1.5) | low (<0.1) |
| **Type II** | high | low |
| **Type III** | low (<1.0) | high (up to 0.3) |

#### *Type-II Kerogen*

The composition of this kerogen is dominated by polyaromatic nuclei and ketone and also carboxylic acid groups in comparison to type I. However, aliphatic compounds are still present in larger amounts. Significant amounts of sulphur can occur in this kerogen type. High sulphur varieties are classified as type IIS (up to 8-14% organic S). Type-II kerogen is formed mainly in marine environments with allochthonous and autochthonous OM input. In consequence main sources of OM are phytoplankton and higher plant material. This Kerogen is characterized by high H/C values and low O/H values (Bordenave, 1993; Killops and Killops, 2009).

#### *Type-III Kerogen*

The main content of this kerogen type is formed by polyaromatic nuclei and ketone and also carboxylic acid groups. Aliphatic constituents are insignificant in comparison to the other content. Origins of kerogen type-III are vascular plants, resulting in a high content of vitrinite macerals. The oil potential is low and generated liquid hydrocarbons are dominated by phenols and aromatic hydrocarbons derived from lignin. However, at high thermal stress levels type-III kerogen is able to produce higher amounts of gaseous hydrocarbons (Killops and Killops, 2009).

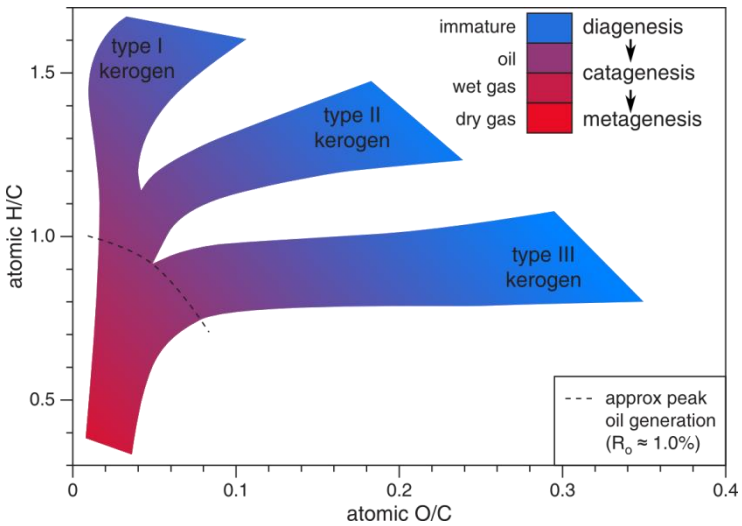


***Figure 2. Van Krevelen plot of different kerogen types (after Behar and Vandenbroucke, 1987).***

### 1.1.2 Bitumen and petroleum

Bitumen represents the OM in sediments, which is soluble by organic solvents. The term “bitumen” is used for both liquid and solid hydrocarbon deposits. Petroleum comprises liquid and gaseous hydrocarbons, i.e. oil and gas (Killops and Killops, 2009). Bitumen can be divided into three main fractions: aliphatic hydrocarbons, aromatic hydrocarbons and asphaltenes and resins (see Figure 3). The latter fraction is also called NSO-fraction (or NSO’s) as it is composed of heavy molecules with incorporated nitrogen, sulphur and oxygen content. Aromatics have a higher polarity in comparison to aliphatics (or saturates) (Killops and Killops, 2009).

### 1.1.3 Expulsion and primary migration

A very rough summary for expulsion and primary migration will be given in the following. More details are given in section 2.2.

Main driving force of expulsion and primary migration is lithostatic pressure, as it causes compaction and increasing internal pressure within the source-rock. First transport of generated hydrocarbons happens by diffusion within the kerogen network. By desorption, hydrocarbons are released from kerogen into the pore space of the source-rock (Mann et al., 1996). This process is cited as expulsion (Pepper and Corvi, 1995a). These expelled hydrocarbons accumulate and aggregation from the pore wall into the pore space takes place. Within the pore space pressure-driven fluid flow is possible, leading to primary migration within the source-rock (Pepper and Corvi, 1995a). By leaving the source-rock, secondary migration within the reservoir rock begins. The processes described above are influenced by a variety of effects and parameters, like fracturing, geochromatographically effects, adsorption and desorption by kerogen and bitumen and diffusion through kerogen networks (see section 2.2). The interactions of this effects and the impact to expulsion and primary migration is still unknown.

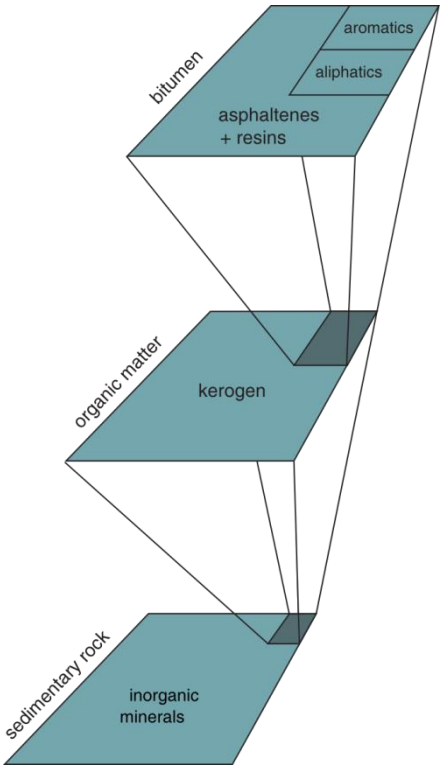


***Figure 3. Typical distribution of organic matter in a sedimentary rock (after Tissot and Welte, 1984)***

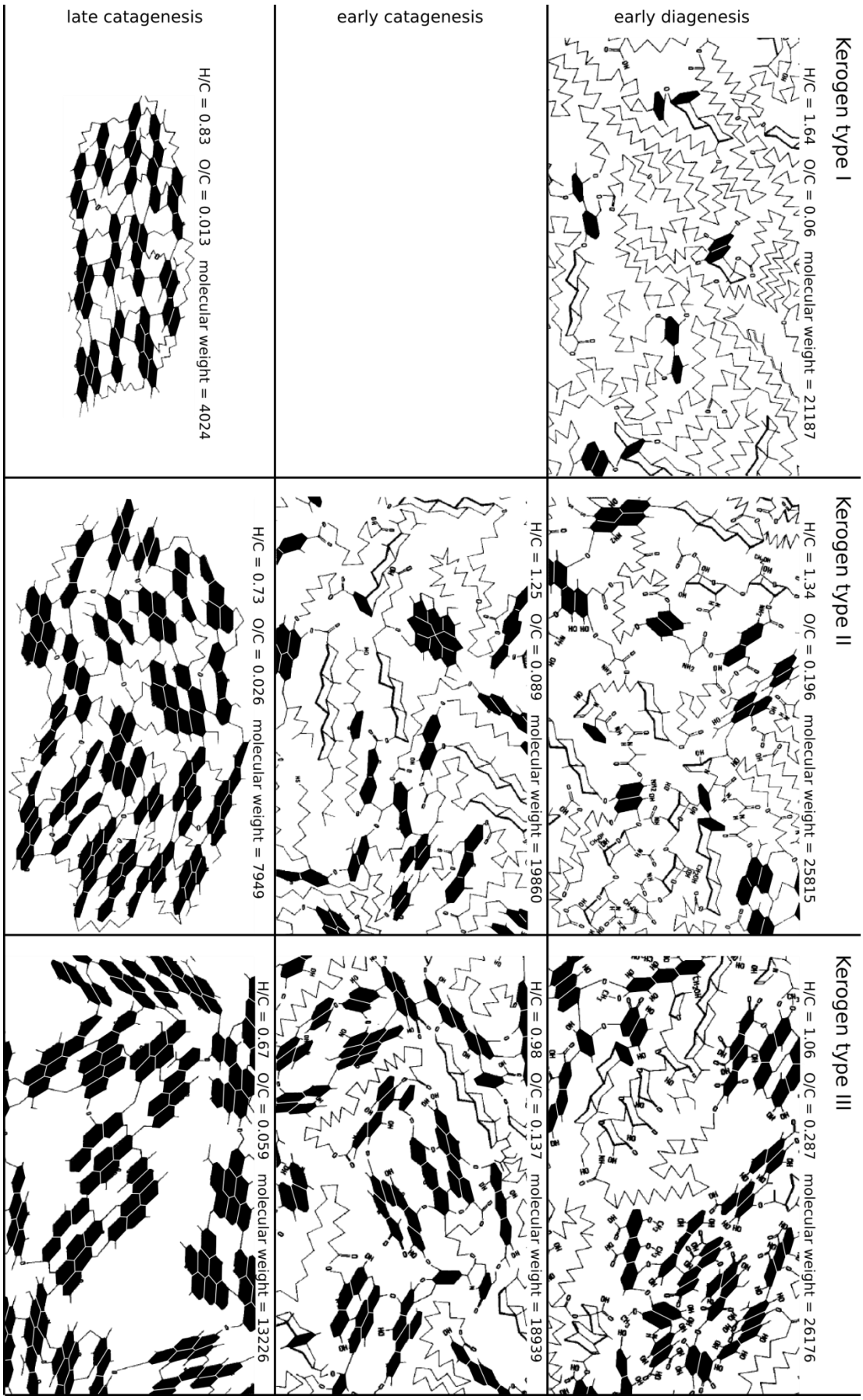


***Figure 4. Maturity related changes in different kerogen types (after Behar and Vandenbroucke, 1987).***

# 2 Motivation and overview of previous research

## 2.1 Objective of investigation

The precise understanding of processes, controlling the generation of hydrocarbons and expulsion (discharge of bitumen from kerogen) and primary migration (transport within the source-rock) into a reservoir rock is fundamental for the assessment of petroleum and gas plays. The composition of expelled petroleum is highly affected by processes in connection to primary migration and expulsion (Eseme et al., 2006b; Kelemen et al., 2006; Leythaeuser et al., 1988a, 1988b; Liao and Geng, 2009; Ritter, 2003). Influences towards maturity assessment and parameters used for oil to source correlation are especially important for exploration and evaluation of new oil/gas plays.

Objective of this study is a detailed investigation and quantification of generation and especially of expulsion and primary migration of hydrocarbons. Therefore, a method was developed to simulate the thermal maturation of an intact source-rock under different pressure regimes. A particular focus of this project was the natural simulation of pressure conditions as expected in natural subsidence systems. This means the production of a lithostatic load pressure in natural magnitudes and corresponding pore pressures. This study examines effects that are triggered by pressure induced expulsion effects to the composition of petroleum and corresponding products.

In addition to a generally improved understanding of the processes which take place during expulsion and primary migration, the results of this study are employable in a wide range of applications. Particularly model calculations will benefit from the empirical results contributed by this study. First early models integrated simple mass balancing calculations for prediction of generation and expulsion efficiency. Heuristic approaches (e.g. Cooles et al., 1986; Larter and Mills, 1991; Mackenzie and Quigley, 1988; Pepper, 1991; Quigley and Mackenzie, 1988; Rullkötter et al., 1988), based on simple empirical observations made in natural systems. Basically these models used mass balances from data which is obtained by comparison of mature source-rocks versus immature counterparts. However, these models show some uncertainties outside of their calibration area (Pepper and Corvi, 1995a), therefore the results only limitedly apply to nature systems. More advanced models use a deterministic approach for calculating the generation, expulsion and primary migration of oil and gas (Behar et al., 1992, 1991; Horsfield et al., 1992; Pepper and Corvi, 1995b; Pepper and Dodd, 1995; Schaefer et al., 1990; Tissot and Espitalié, 1975; Tissot et al., 1987; Waples, 1980). Basis of this models are kinetic calculations relating to the Arrhenius equation, which represents the chemical reaction rate $k$ in relation to the activation energy $E_a$ and absolute temperature $T$:

$$k = Ae^{-\frac{E_a}{RT}} \quad (1)$$

$A$ is the frequency factor (in case of 1st order reactions) and $R$ the gas constant. This equation enables the extrapolation of experimental data (gained from pyrolysis at elevated temperatures) to natural time frames. Generally it is assumed that the chemical reactions, taking place during generation of oil and gas, are 1st order reactions (Behar et al., 1992; Burnham and Braun, 1985; Pepper and Corvi, 1995b; Schaefer et al., 1990; Ungerer et al., 1988). This means that the amount of degraded kerogen $dc_k$ is proportional to the amount of generated oil and gas $c_o$ (Wei et al., 2012):

$$\frac{dc_k}{dt} = -kc_o \quad (2)$$

Other models exist as well, assuming nth-order reactions, as presented by (Delvaux et al., 1990). Various models used a set of n activation energies $nE_a$ and a single frequency factor $A$ (Delvaux et al., 1990; Reynolds et al., 1995; Schenk and Horsfield, 1998; Tissot et al., 1978; Vandenbroucke et al., 1999). Other models use a single $E_a$ and multiple $A$ (Welte and Yalçin, 1988), or a variation of $nE_a$ and $nA$ (Dieckmann, 2005; Dieckmann et al., 2002). Only few models also include expulsion and primary migration in their kinetic construct, as shown by Braun and Burnham (1992), Burnham and Braun (1990), Pepper and Corvi (1995a), Stainforth (2009) Ungerer (1990) and Welte and Yalçin (1988).

The benefit of these deterministic approaches is the possibility to make relative precise predictions about specific petroleum systems in case that the model is calibrated well by experimental data. However, in most cases the methodology of these experiments does not meet the naturally given geophysical conditions in no instance (see section 2.3). (Pepper and Corvi, 1995a) mention the difficulty of simulating realistic laboratory simulation. However, the quality of the date produced by the wide variety of models and different approaches summarized above depends on the calibrating process. In this study a methodology is developed to overcome the weaknesses of the classic pyrolysis experiments and generation simulations, especially in the focus of expulsion and primary migration.

## 2.2 Problem definition

Various causes are described in the literature as a possible driving force for expulsion. Many effects are discussed which might influence the expulsion of oil and gas. A natural simulation of generation and expulsion/primary migration is only possible in consideration of the given geophysical, petrological and mineralogical framework. Therefore, effects will be discussed in the following, which influence expulsion and primary migration in particular. An overview of the different mechanisms is shown in Figure 10.

### 2.2.1 Pressure and temperature

The prevalent pressure regimes in dependence of the depth are particularly important for simulation of expulsion and primary migration. All geophysical or geochemical processes discussed in the next subsections are directly or indirectly related to pressures, especially to the lithostatic pressure. Therefore, the aspect of lithostatic pressure will be discussed in more detail in the following:

The simulation should include at least the maximum of oil generation, or the peak of the oil window. Assuming a normal geothermal gradient of 33°C/km, oil generation reached a maximum in areas about 3 km depth (Bordenave, 1993; Tissot et al., 1987; Tissot and Welte, 1984) (see Figure 5). The lithostatic pressure can be calculated with the following formula (Sahay, 1999; Terzaghi and Peck, 1967):

$$p_l(z) = \vec{g} \int_0^z \rho_r(z)\, dz \qquad (3)$$

$p_l$ is the lithostatic pressure at given depth $z$. The density of the overlying rock is given by $\rho_r$. $\vec{g}$ is the acceleration due to gravity. Calculation (3) can be written simplified as:

$$p_l(z) = z \cdot \rho_r \cdot \vec{g} \qquad (4)$$

In a sedimentary basin an increase in lithostatic pressure of $0.23\ ^{bar}/_{m}$ to $0.31\ ^{bar}/_{m}$ will be accepted (Sahay, 1999), which corresponds to an average density of $2.31\ ^{g}/_{cm^3}$ to $3.06\ ^{g}/_{cm^3}$. It concludes that a lithostatic pressure of ca. 680 bar to 916 bar has to be simulated to comply with natural systems.

Concerning the hydrostatic pressure (or pore pressure), normal conditions are assumed. The reasons therefore are mainly technical aspects, as discussed in section 3.3. The calculation of the idealized hydrostatic pressure is similar to equation (4):

$$p_h(z) = z \cdot \rho_w \cdot \vec{g} \qquad (5)$$

$p_h$ is the hydrostatic pressure at given depth $z$, $\rho_w$ the density of the pore fluids. The fluid density is affected by the temperature, as more solids can be

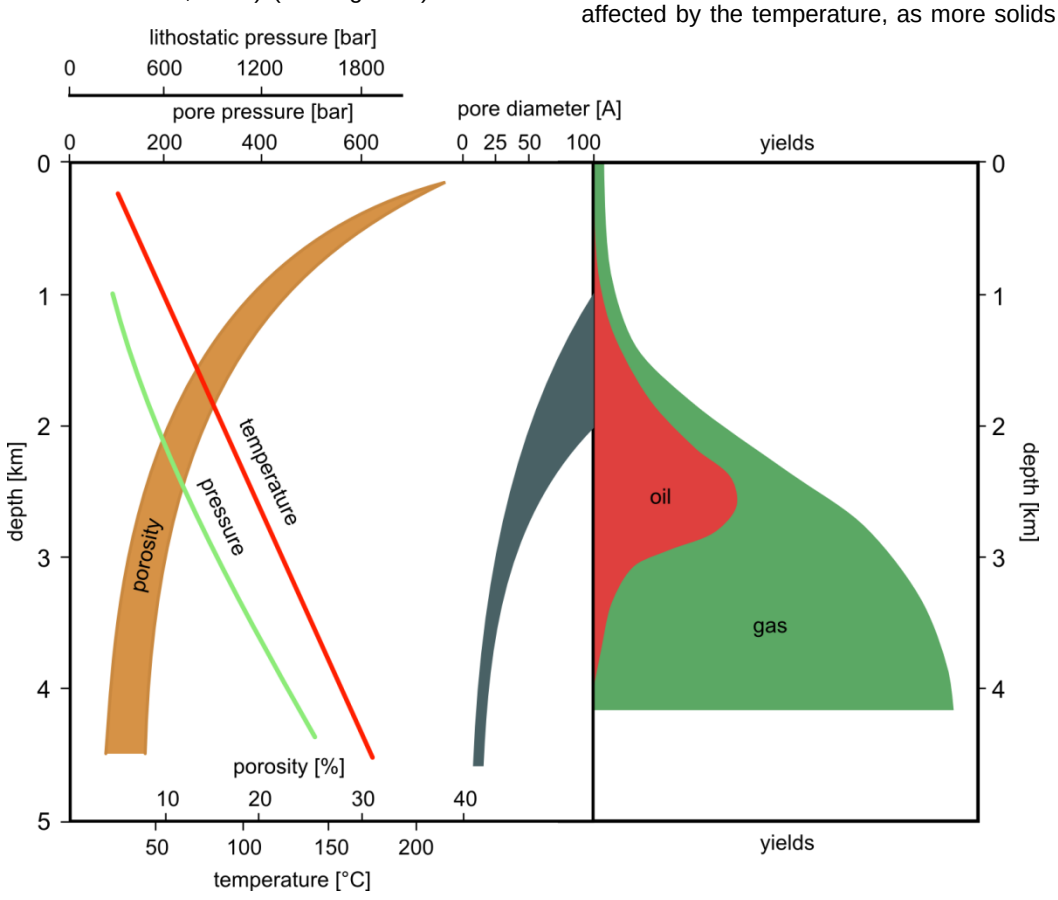


***Figure 5. Physical values of source-rocks and oil and gas yields vs. depth (after Tissot and Welte, 1984).***

dissolved at higher temperatures (increase of density) and gases are in solution with the liquid (decrease of density). In general, hydrostatic pressure gradients of 0.10 $^{bar}/_{m}$ (fresh and brackish water, $\rho_w = 1.00\,^{g}/_{cm^3}$) to 0.11 $^{bar}/_{m}$ (salt water, $\rho_w = 1.07\,^{g}/_{cm^3}$) are assumed (Sahay, 1999). The resulting hydrostatic pressures are in a range of ca. 295 bar to 316 bar. Simplified it can be said that the lithostatic pressure is three times higher as the hydrostatic pressure (Hanebeck, 1993).

A special case in simulating the generation and expulsion from hydrocarbons is the temperature. Under geological conditions, the temperature range of petroleum formation and oil expulsion is between 100°C and 150°C prevailing for periods of millions of years (Quigley and Mackenzie, 1988; Tissot and Welte, 1984). To accelerate the formation processes and the expulsion mechanisms in the laboratory, the temperatures have to be increased. In several different pyrolysis experiments (see section 2.3), temperatures of 350°C to 360°C have proofed to be adequate for experimental petroleum generation. Apart from this, higher temperatures result in a variety of technical problems due to the supercritical status of water at temperatures above 360°C (see section 3.3).

### 2.2.2 Micro-fractures as migration-pathways

The importance of mimicking natural pressure regimes is evident for simulation with focus on expulsion and primary migration. Lithostatic pressure leads to micro and macro-fractures within the source-rock, which represent important pathways for a hydrocarbon phase flow (Dickey, 1975; Leythaeuser et al., 1988a; Littke et al., 1988; Pepper and Corvi, 1995a; Ungerer, 1990). The generation of a pressure gradient, which only allows the flow of hydrocarbons, is mainly coursed by the lithostatic pressure (Rouchet, 1981) and by increasing pore pressure. Pore pressure increase is connected to the generation of fluid and gaseous hydrocarbons (Berg and Gangi, 1999; Mandl and Harkness, 1987; Ozkaya, 1988). The accompanying volume increase of fluid and gaseous components is contrary to the reduction of the pore diameter and loss of porosity caused by increasing compaction by lithostatic pressure. In this constellation, it is possible that overpressure arises (in comparison to the surrounding hydrostatic pressure) within the source-rock. This leads to an expulsion fracturing (Berg and Gangi, 1999; Littke et al., 1988; Ozkaya, 1988) and formation of migration pathways within the source-rock. Further reactions influence the available pore space: Secondary porosity arises by dissolution of minerals (e.g. calcite and clays) (Curtis, 1983) and pressure solution seams can act as pathways for primary migration (Leythaeuser et al., 1995).

### 2.2.3 Smectite-to-illite transformation

The lithostatic pressure has large impact to the clay mineralogy. Particularly the smectite-to-illite transformation is important for the processes observed by expulsion. A correlation between the relative abundance of illite compared to smectite and maturity of organic matter was observed by a variety of studies (Guthrie et al., 1986; e.g. Smart and Clayton, 1985; Velde and Espitalié, 1989; Velde and Lanson, 1993). The smectite-to-illite transformation seems to be driven mainly by temperature and time (Velde and Espitalié, 1989), but the lithostatic pressure has influence to the ratio of smectite and illite, too (Colten-Bradley, 1987). As shown by Colten-Bradley (1987), the dehydration process of smectite is supported by vertical effective stress (Figure 6 and Figure 7). The loss of water layers was observed as a stepwise process, wherein water layers are lost between 186-634 bar (third layer) and 310-1034 bar (second and first layer) at 25°C (see Figure 8). At elevated temperature ranges no load pressure is necessary to lose the second (67°-81°C) and first water layer (172°-192°). Colten-Bradley (1987) sees a connection between the formation of smectite with one water layer as less chemically stable complex under elevated pressures and the occurrence of smectite-to-illite transformation. Nevertheless, the loss of water layers would support the generation of internal overpressure, at least by the increase of fluid volume. In focus of expulsion and primary migration, smectite-to-illite transformation could rouse a sealing effect as discussed in Freed and Peacor (1989). The authors postulated that the ability of ion transportation is diminished by the conversion of smectite to illite, as the number of abundant dislocations for ion transport is reduced. On the other hand, the released water could support the transportation of hydrocarbons. Still, neither the kinetic of the transformation of smectite to illite, nor the illitization reaction is known in detail. Especially in shale the transformation to illite seems to follow several mechanisms (Altaner and Ylagan, 1997). Equation (6) (Hower et al., 1976) and (7) (Boles and Franks, 1979) show two different possible reaction ways:

$$4.5\,K^{+} + 8\,Al^{+3} + smectite \cdot 10\,H_2O \rightarrow illite + Na^{+} + 2\,Ca^{+2} + 2.5\,Fe^{+3} + 2\,Mg^{+2} + 3\,Si^{+4} + H_2O \quad (6)$$

$$3.93\,K^{+} + 1.57\,smectite \cdot 10\,H_2O \rightarrow illite + 1.57\,Na^{+} + 3.14\,Ca^{+2} + 4.78\,Fe^{+3} + 4.28\,Mg^{+2} + 24.66\,Si^{+4} + 57\,O^{-2} + 11.40\,OH^{-} + 15.7\,H_2O \quad (7)$$

$$\underbrace{KNaCa_2Mg_4Fe_4Al_{14}Si_{38}O_{100}(OH)_{20}}_{smectite}$$

$$\underbrace{K_{5.5}Mg_2Fe_{1.5}Al_{22}Si_{35}O_{100}(OH)_{20}}_{illite}$$

Remarkable is the significant loss of weight, descripted by equation (7). Freed and Peacor (1989) calculated a weight loss of 24%, assuming a reduction of 80% smectite layers to 20%. In opposite to equation (6) no additional $Al^{+3}$ is necessary in equation (7), where $Al^{+3}$ is delivered by cannibalization of smectite layers, why this reaction was seen as more likely (Boles and Franks, 1979; Freed and Peacor, 1989). Such a high weight and volume loss, descripted by equation (7), accompanied by water loss and dehydration processes of smectite, as explained above, could lead to a kind of squeezing effect, affecting the pore fluids within the source-rock. This could have big influence to the timing and efficiency of the expulsion of hydrocarbons.

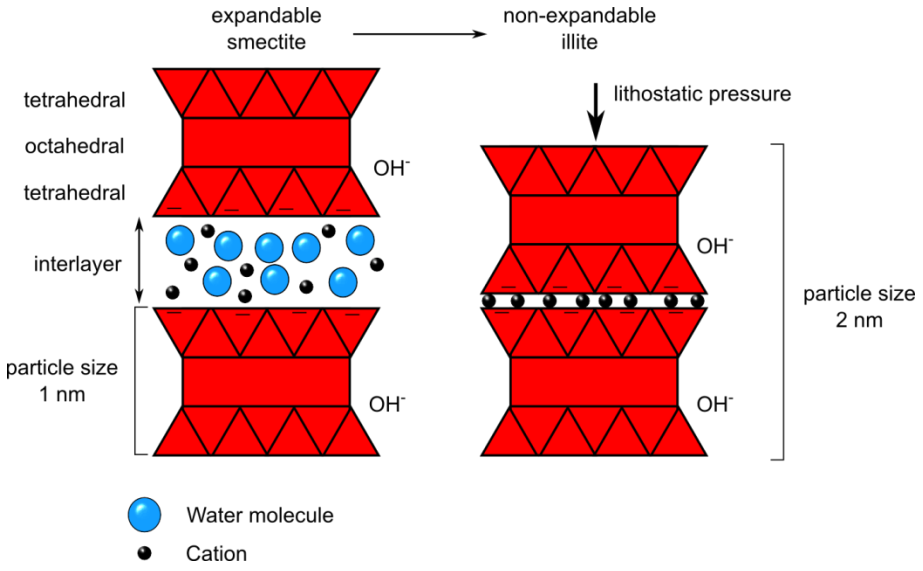


***Figure 6. Smectite to illite conversion supported by lithostatic pressure.***

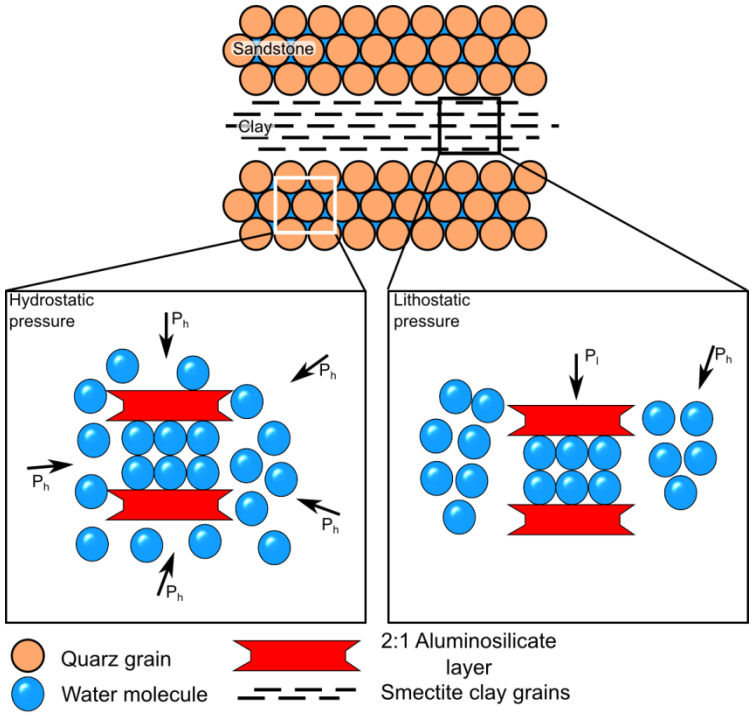


***Figure 7. Lithologically related differences of pressure conditions (after Colten-Bradley, 1987).***

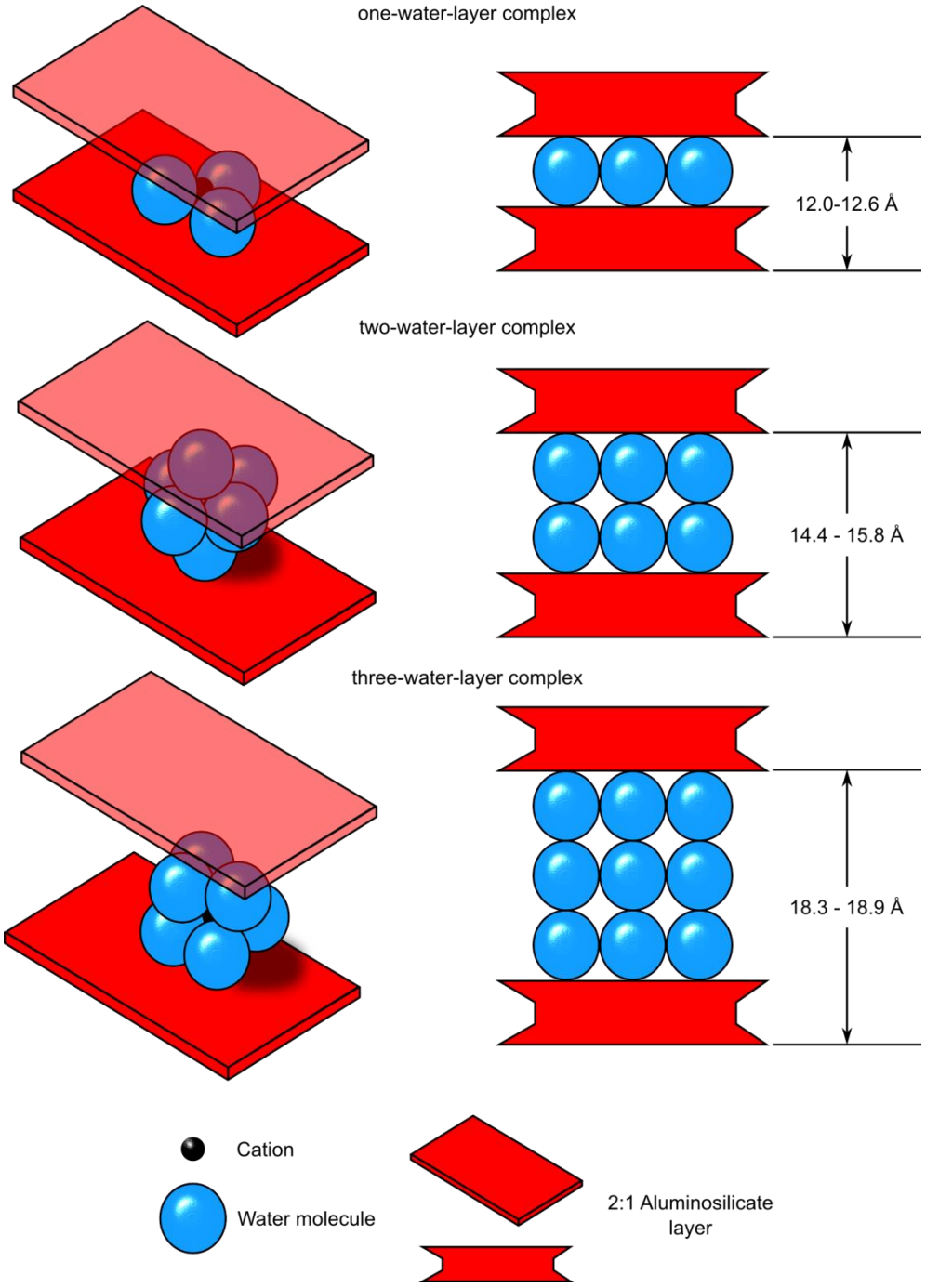


***Figure 8. Hydration states of smectite (after Colten-Bradley, 1987).***

### 2.2.4 Geochromatography

Of relevance for natural simulation of expulsion and primary migrations are absorption effects and catalytically active structures of minerals within the source-rock. Retention of component-groups with coherent properties is mostly called geo-chromatography and is investigated by several studies, as referred in Krooss et al. (1991). Crude oil composition compared to the extracted hydrocarbons of the source-rock shows preferred release of saturates, followed by aromatic components and NSO's, and a higher expulsion efficiency for *n*-alkanes in comparison to isoprenoids (e.g. Barker, 1980; Bonilla and Engel, 1986; Espitalié et al., 1984; Lafargue et al., 1990; Leythaeuser et al., 1984a, 1984b; Leythaeuser and Schaefer, 1984). The compound specific differences in expulsion efficiency are explained by adsorption-desorption processes and polarity differences of the expelled components (Lafargue et al., 1990; Leythaeuser et al., 1984a, 1984b) and is related to mineral particle size and temperature (Bonilla and Engel, 1986; Brother et al., 1991). An investigation of the impact of chromatographic effects to alkylated naphthalenes, phenanthrenes, benzo- and dibenzothiophenes were

performed by Leythaeuser et al. (1988b). Generally, a progressively higher depletion was observed with increasing expulsion distance to the source-rock, showing a higher impact for naphthalenes than for phenanthrenes and dibenzothiophenes. More important is that no fractionation was observed, concerning the relative ratios of $C_1$- and $C_3$-alkylnaphthalenes or $C_1$- and $C_2$-alkylphenanthrenes. So common maturity parameter, like the methylphenanthrene Index (MPI-1) and methyldibenzothiophene ratio (MDR) seem not to be influenced by chromatographic expulsion effects. Investigation of absorption effects of argillaceous minerals to the generation and migration of hydrocarbons was described in several studies (e.g. Eltantawy and Arnold, 1972; Espitalie et al., 1980; Krooss et al., 1991; Tannenbaum et al., 1986). It was observed that the impact of the retention power is related to the specific surface area of the different minerals (see Figure 9). Catalytic activity by minerals like montmorillonite ($Ca^{++}$ more than $Na^{+}$) leads to the formation of components of lower molecular weight, like olefins and aromatic hydrocarbons. However, it has to be considered that the experimental setup based on anhydrous pyrolysis. As pointed out by several authors (Espitalie et al., 1980; Espitalié et al., 1984; Krooss et al., 1991; Pepper and Corvi, 1995a), it is not very likely to find anhydrous conditions in natural systems. Thus, it is questionable to what extent these data can be applied to natural conditions.

Investigation of chromatographic effects in absence of water seems little expedient. In contrast to dry experiments, investigations performed with water-wet clays and silts (Fernandez and Quigley, 1985; Krooss et al., 1991; Larter et al., 2000) show a decreasing effect of water to fractionation of hydrocarbons. As mentioned by Brother et al. (1991), England et al. (1991), Fernandez and Quigley (1985) and Pepper and Corvi (1995a), hydrocarbons own much lower dielectric constants than water. Therefore, it is very likely that sorptive sites of clay minerals are blocked by water molecules, diminishing fractionation effects for hydrocarbons. A greater chromatographic impact is shown for non-hydrocarbons in the form of carbazoles (Larter et al., 1996, 2000; Li et al., 1997). These compounds seem to be useful as tracer for secondary migration over grate distances (Larter et al., 1996), though Clegg et al. (1998) notes that facies and maturity are probably more relevant, rather than partition.

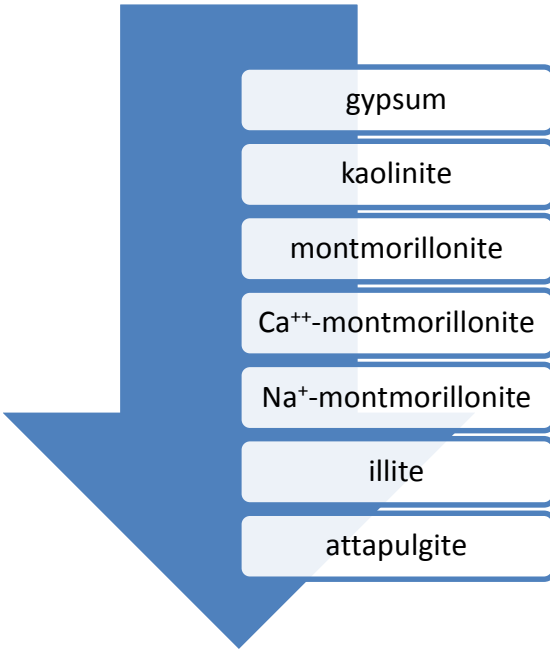


***Figure 9. Increase of retention power with increase of the specific surface area (from top to bottom) (after Espitalié et al., 1984).***

### 2.2.5 Adsorption-desorption effects of kerogen

The role of a chromatic effect for the fractionation of a petroleum fluid phase is called into question by several authors (e.g. Pepper and Corvi, 1995a; Sandvik et al., 1992; Thomas and Clouse, 1990a, 1990b, 1990c). They argue that it is more likely that the described effects are rather due to interactions with the kerogen than to geochromatography. Retaining of components through the kerogen network by adsorption, as discussed in (Sandvik et al., 1992; Thomas and Clouse, 1990a, 1990b, 1990c), is a possible alternative model to explain fractionation, observed by the aforementioned studies.

Swelling experiments are a possibility to investigate the capability of adsorption of different components (solvents) by kerogen. Thereby, the absorbing capacity of a kerogen for a specific solvent or a solvent mixture is measured volumetric (Green et al., 1984) or gravimetric (Sanada and Honda, 1966). In Table 2 solvent properties and the volumetric swelling ratio ($Q_v$, volume of initial kerogen vs. volume of swelled kerogen) for different solvents are listed. The swelling ratio is lowest for saturates and increased for aromatics and NSO's. Conversely, this means that saturates will be released first by kerogen, then by aromatics and NSO's (Sandvik et al., 1992; Thomas and Clouse, 1990c). The problem here is the methodology applied for investigation of swelling behaviour of kerogen. The swelling is investigated in a depressurized system and mainly with isolated kerogen. Under natural conditions you will find overburden pressure and a compact rock matrix, which counteract the swelling of the solid organic matter. It is unclear how far these factors will influence the adsorption of hydrocarbons, but it is very likely that swelling will diminish by confining pressure.

***Table 2. Solvents, solvent properties and mean volumetric swelling ratio for kerogen Type-II (Draupne formation) (Ertas et al., 2006).***

| *solvent* | *solubility parameter* $(J/cm^3)^{1/2}$ | *molar volume* $(cm^3)$ | *mean swelling ratio* $(Q_v)$ |
|---|---|---|---|
| *n*-decane | 15.8 | 195.9 | 1.228 |
| *n*-hexa-decane | 16.3 | 294.1 | 1.212 |
| Cyclo-hexane | 16.8 | 108.7 | 1.287 |
| decalin | 17.7 | 154.2 | 1.245 |
| toluene | 18.2 | 106.9 | 1.338 |
| tetralin | 19.4 | 136.3 | 1.328 |
| 1-methyl-naphtha-lene | 20.2 | 139.4 | 1.400 |
| 2-5 dimethyl-pyrrole | 20.3 | 101.7 | 1.320 |
| pyridine | 21.9 | 80.6 | 1.415 |
| benzo-furan | 21.1 | 108.3 | 1.360 |
| benzo-thiophene | 21.8 | 124.7 | 1.362 |

### 2.2.6 Diffusion through kerogen network

Sorption and desorption lead to another transport mechanism, which is discussed in literature (e.g. Durand, 1988; Hanebeck, 1993; Krooß, 1985; Stainforth and Reinders, 1990; Thomas and Clouse, 1990a, 1990b, 1990c): diffusion of hydrocarbons through a kerogen network. Important for diffusion is the chemical potential of the bitumen, respectively of the hydrocarbons. This potential is created by a concentration gradient, or by a pressure gradient, e.g. a micro-fracture, which represents a pressure depression (Hanebeck, 1993; Thomas and Clouse, 1990c). Diffusion experiments show a certain efficiency concerning the transport of bitumen through a kerogen network, though not in the order of magnitude necessary to correspond with natural mass flows alone (Hanebeck, 1993; Thomas and Clouse, 1990c). As mentioned by Hanebeck (1993), a swelling of polymers (like kerogen) can lead to the formation of a case II diffusion. This results in a swelling front which moves quickly along the chemical potential, accelerating the diffusion (Thomas and Windle, 1982). For reasons mention before, this is very unlikely under confining pressure conditions. In addition, other arguments are against a major role of diffusion: Thomas and Clouse (1995b) show that lighter hydrocarbons diffuse much easier through a kerogen network than heavier hydrocarbons, corresponding to observations in nature. However, it is also shown that aromatics diffuse faster than naphthenes and naphthenes faster than paraffins, which is the reverse order as it was observed in nature. This order correlates to the swelling ratio (Table 2) and corresponds therefore to the adsorption power. Interesting in this context is the observation of Stainforth and Reinders (1990). The authors postulate that the preferred pathways would be the aliphatic parts of the kerogen. Therefore, with increasing maturity and aromaticity of kerogen, diffusion would become difficult or even impossible. That would also mean that the ability to adsorb aliphatic compounds would decrease in favour of aromatics, which fits to the fractionation effects, mentioned before. Another aspect that should be mentioned is that you need a continuous kerogen network for high diffusion efficiencies. Lithostatic pressure might be supportive by compaction of the rock. Thereby adjacent kerogen structures could be pressed together, forming a continuous network over greater distances.

## 2.3 Established pyrolysis methodologies and their suitability for investigation of expulsion and primary migration

Laboratory investigations applied in simulating thermal maturation of source-rocks to generate and expel oil and gas has a long history in geoscience. A variety of methodologies have been developed over the years with different emphases concerning the sample size, the pre-treatment of the sample material, medium (hydrous/anhydrous), temperature range and pressure conditions. Experiments were performed in open or closed systems, in gold or glass tubes or in stainless steel reactors. Results produced by the different methodologies are often not comparable and suffer from a variety of inconsistencies with natural conditions. Most methods focused purely on generation of hydrocarbons and are therefore unsuitable for investigation of expulsion and primary migration. In the following, specific methods will be examined and their advantages and disadvantages with focus on expulsion will be discussed. Primary focus here is on aspects that can be derived from section 2.2, and are considered important for a natural simulation of generation, expulsion and primary migration. Specifically that would be the maintenance of a coherent mineral matrix, simulating natural pressure conditions and product transport through a water saturated pore space.

### 2.3.1 Anhydrous open pyrolysis

One of the most used tools in investigation of the potential of source-rocks, maturity assessment and source-rock characterisation is anhydrous open pyrolysis. Various methods were developed, which

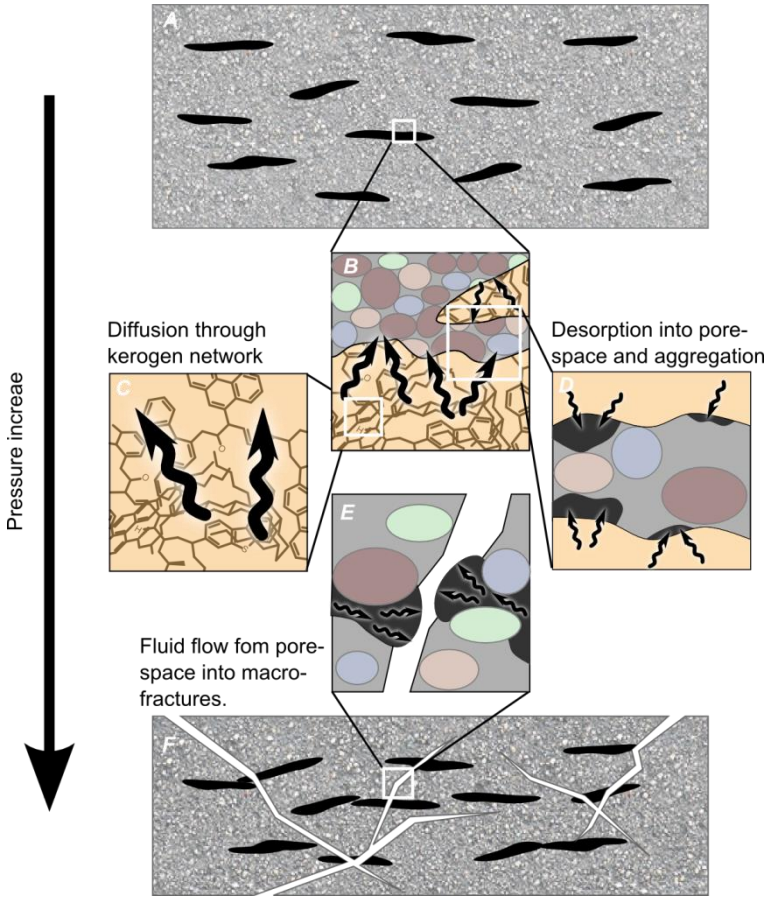


***Figure 10. Various expulsion and migration pathways: Unfractured rock with incorporated kerogen (A); Kerogen and mineral matrix (B); Diffusion (C); Expulsion (D); Primary migration (E); Fractured rock (F).***

based on high temperature pyrolysis of a source-rock, using inert gases (e.g. Nitrogen or Helium) to flush out the produced and vaporized hydrocarbons. The principals of this pyrolysis techniques are described in Bordenave et al. (1970) Giraud (1970) and Gransch and Eisma (1970), whereas in this early studies isothermal pyrolysis were performed. The development of these pyrolysis techniques led to the establishment of methods which worked with programed temperature gradients (Claypool and Reed, 1976; Tissot and Espitalié, 1975).

### *Rock-Eval pyrolysis*

Especially mentionable is the Rock-Eval pyrolysis method (Espitalie et al., 1986, 1985a, 1985b; Espitalié et al., 1977), as it is used widely by the petroleum industry. The methodology is described in detail in various literature (e.g. Bordenave, 1993; Horsfield et al., 1996). However, in the following Rock-Eval pyrolysis and related pyrolysis methods will be described shortly and discussed with special emphasis on the objectives of this investigation.

Small amounts of crushed and powdered rock (10 mg – 100 mg) are used for standardised Rock-Eval analysis. The pyrolysis is performed under a Helium atmosphere (Rock-Eval VI: optional Nitrogen). The sample runs through a temperature program, starting with an isothermal heating at 300°C for three minutes. Subsequently the temperature is raised to 550°C (Rock-Eval VI: 600°C) at 25°C/min. Generated Products are flushed out by a Helium flow to a flame ionisation detector (FID). During the first heating phase (300°C, isothermal), free hydrocarbons already present in the source-rock (oil/gas) were mobilized by vaporization and quantitatively measured by the FID. The value thus obtained is called $S_1$-peak (mg HC/g rock) and contains mainly free hydrocarbons from $C_1$ to $C_{33}$ (Espitalie et al., 1985b). Heavier components, which are counted to “free hydrocarbons” (NSO compounds like resins and asphaltenes; usually soluble in solvents), were vaporized only partially and therefore be detected in the next temperature stage. The $S_1$ represents bitumen, oil and gas which are already generated by the source-rock. The increase of temperature (300°C to 550°C or 600°C) leads to cracking reactions of the kerogen whereby free hydrocarbons are generated and vaporized together with the heavier compounds still remaining in the sample. These were measured quantitatively by the FID, too, creating the $S_2$-peak (mg HC/g rock). The $S_2$-peak is useful to estimate the current potential of a particular source-rock and can be placed directly in relation to the amount of oil and gas which still can

be generated from the source-rock by increasing thermal maturity. The temperature at which the $S_2$-peak reached its maximum is called $T_{max}$ (°C) and is related to the maturity of the analysed rock sample: With progressing maturity of the source-rock higher thermal energy is necessary to crack the residual kerogen. For this reason the $T_{max}$ raise with increasing maturity of the analysed source-rock. During the heating, between 300°C and 390°C oxygen compounds decomposed to $CO_2$ and were measured by an thermal conductivity detector (TCD), resulting in the $S_3$-peak (mg $CO_2$/g rock). In standard application, Rock-Eval delivers several useful parameters. Beside the assessment of the quantity of already produced hydrocarbons, the still remaining potential for hydrocarbon generation and the maturity of the source-rock, it can be used for determination of the kerogen Type. Therefore the hydrogen index (HI) and the oxygen index (OI) has to be calculated:

$$HI = {}^{S_2}/_{TOC} \cdot 100 \quad (8)$$

$$OI = {}^{S_3}/_{TOC} \cdot 100 \quad (9)$$

The resulting values can be plotted in a HI vs. OI diagram (pseudo Van Krevelen diagram) and enable the deviation of kerogen Types.

Rock-Eval delivers reliable data for evaluation of the potential of source-rocks, maturity and kerogen Type. However, the benefit of Rock-Eval pyrolysis for investigation of expulsion is very limited and it cannot be used for examination of primary migration. By destroying the rock matrix, new reaction sides were created, resulting in an accelerated expulsion. Effects like diffusion trough kerogen networks or adsorption-desorption effects were almost completely eliminated by grounding the rock. Because it is a anhydrous pyrolysis, geochromatographic effects can be seen only from a theoretical point of view (Espitalie et al., 1980; Espitalié et al., 1984) and it is not possible to transfer observations in this regard into natural systems. In addition, the methodology only delivers bulk parameters and no evaluation of the influence of expulsion to molecular markers is possible. However, it is possible to determine gross kinetic parameters with Rock-Eval pyrolysis (Burnham et al., 1987; Delvaux et al., 1990; Ungerer, 1990) without the influence of effects mentioned above.

***Pyrolysis coupled with gas chromatography (py-GC)***

Quite similar to Rock-Eval pyrolysis proceeds thermal pyrolysis coupled with gas chromatography (GC), as described early by Bordenave et al. (1970), Giraud (1970) and Leplat (1967). Thereby the furnace unit is not directly connected to an FID, but the produced hydrocarbons are collected in a cooling trap and released to a GC-FID or GC-MS (mass spectrometer) after the pyrolysis is completed. Also combined systems are possible (Bjorøy et al., 1986; Solli et al., 1984), enabling the simultaneous measurement of bulk parameter $S_1$ and $S_2$ and measurement of molecular compounds by GC. The main differences between the developed systems are found in the heating units (Bordenave, 1993). For example Maters et al. (1977) introduced Curie point pyrolysis, where a Curie point filament is heated inductively. Other techniques used micro-furnace (Behar and Pelet, 1985), capacitive boosted filaments (Allan and Larter, 1983) or even laser beams (Larter et al., 1977).

The results of these techniques show certain differences to natural observations. First of all the high yields of alkenes has to be mentioned (Behar and Pelet, 1985) and a higher grate of aromatization. Since the consistency of the sample and the pyrolysis method itself is similar to those in the Rock-Eval pyrolysis, the same limitations exist in this respect. Expulsion will be accelerated due to new reaction sides and effects, caused by a kerogen network, are eliminated. Through the use of GC it is possible to obtain molecular data; however, the pyrolysates were collected cumulative and cannot be assigned to specific pyrolysis phases. However, there are exceptions, were multiple cold traps are used to sequentially collect the generated hydrocarbons (Behar et al., 1997b). The focus of this method is clearly the generation and not the expulsion.

***Fixed-bed hydropyrolysis***

A more recent development in pyrolysis techniques is the fixed-bed hydropyrolysis (HyPy). This method works with a constant pressurized hydrogen flow (>100 bar) and dispersed sulphided molybdenum catalyst as reaction accelerator (Bolton et al., 1988, 1987; Carter et al., 1994; Robinson et al., 1991; Snape et al., 1991). For HyPy, kerogen concentrates were usually produced by acid treatment of the sample and washout of the solved mineral matrix. This should increase the yields of the pyrolysis due to the fact that only small amounts of sample can be used (~250 mg). Generated hydrocarbons are flushed out by the hydrogen flow and collected in a cold trap filled with silica. Although the pyrolysis is performed in hydrogen atmosphere, the method is referred in this study as anhydrous pyrolysis due to the leak of fluid water. The methodology aims to allow kerogen covalent bond cleavage at relative low temperatures due to the use of a catalyst. For this purpose, usually moderate heating rates are used (e.g. 8°C/min) at end temperatures of 500°C. Hydrogen as flushing agent should act as protection of the generated hydrocarbons, minimizing post-generative isomerization (Love et al., 1995; Roberts et al., 1995). Out of this reason, HyPy were mainly used to

study kerogen-bound bio- and geomarkers, due to the intention to obtain unaltered compounds after pyrolysis (Bishop et al., 1998; Love et al., 1995; Putschew et al., 1998; Russell et al., 2004).

The definite focus of HyPy is the generation of hydrocarbons and the release of covalent bonded compounds. Due to the strong pre-treatment of the sample material (grounding, acid treatment), natural effects regarding expulsion were eliminated. The pyrolysis in hydrogen atmosphere and admixed with a catalyst is not related to natural conditions in no instance. This will lead to unnatural reaction behaviour of the kerogen and will complicate the extrapolation to natural systems. Therefore, HyPy is useful for analysing the composition of kerogen, but not for evaluating expulsion or primary migration.

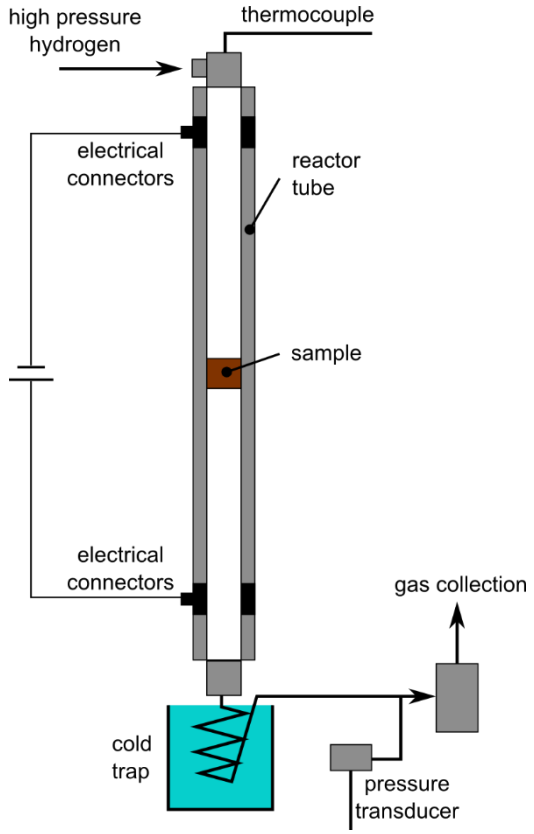


***Figure 11. Schematic representation of a HyPy apparatus.***

### *Pyrolysis in a self-purging reactor*

Based on a standard Fischer assay apparatus, a self-purging reactor was introduced by several authors (Burnham and Singleton, 1983; Campbell et al., 1978). In this device, a powdered sample material was pressed to a pellet with about 10 % remaining porosity. Reason therefore was the aim to reduce oil vapour residence time (Burnham et al., 1988). The self-purging reactor released gas, steam and oil vapours through a frit in the bottom of the reactor into an oil collection assembly. By adding a backpressure valve, the pyrolysis could be carried out at elevated pressures and even gas collection was possible.

Overall, the results did not fit to geological composition of bitumen, oil and gas. Experiments performed at different heating rates (2°C/min and 2°C/h) showed extremely different amounts of produced bitumen, oil and gas, whereas the yields were significantly lower for the slow heating rate (Burnham, 1991). The experiments also showed, especially considering the slow heating rate, abnormal high yields of alkenes in comparison to alkanes, which contrasted the results delivered by closed hydrous pyrolysis (see section 2.3.4). Burnham (1991) observed a high degree of aromatization and formation of large amounts of carbon residue, too. It is possible to make kinetic calculations with data produced by the self-purging reactor (Burnham, 1991; Burnham and Braun, 1990), but especially compared to kinetic parameters received from closed hydrous pyrolysis, large differences concerning activation energy and frequency factor were observed. Regarding to expulsion and primary migration, the self-purging reactor is not employable. Neither the sample material, nor the geophysical parameters meet the conditions, specified by natural systems.

### *Uniaxial pressure pyrolysis*

A device, used mainly for artificial maturation and examination of primary migration within terrestrial source-rocks, was used by several authors (Geng et al., 1998; Liao et al., 2004; Liao and Geng, 2009). Experiments were performed at elevated temperatures up to 510°C and lithostatic pressures up to 800 atm (~810 bar) (Liao et al., 2004). Based on different coals, significant isotopic fractionation effects could be observed in primary migration (Liao and Geng, 2009). No isotopic fractionation effects could be observed for Type-II kerogen, as reported by Liao et al. (2004).

For investigation of expulsion and primary migration under natural conditions, the used device does not appear to be particularly useful. The pyrolysis is performed as anhydrous pyrolysis and hydrous pressure is completely absent. The absence of water could influence observed fractionation effects dramatically.

### *Triaxial pressure pyrolysis*

A very interesting device was introduced by Hanebeck (1993). In this apparatus, it is possible to insert an intact rock disc and apply lithostatic pressure by a piston and confining pressure over a sealing membrane. The high-pressure cell employed supported temperatures up to 350°C, lithostatic pressures up to 1000 bar and confining pressures of 300 bar. Capillary vents enabled the implementation of diffusion experiments, but were also suitable for releasing of oil and gas during the experiment. The apparatus was used by Hanebeck (1993) to perform

diffusion experiments as well as artificial maturation of oil shales. The same apparatus was used by Eseme (2006) and Eseme et al. (2012, 2007, 2006b), to investigate expulsion and primary migration effects. Diffusion experiments showed a higher efficiency for the transportation of hydrocarbons by diffusion within the kerogen network than through volume flow of the oil phase through pores (Hanebeck, 1993). The transportation through diffusion is influenced by adsorption and kerogen swelling-effects (see section 2.2.5 and 2.2.6) and affected mainly non-polar components. The author notes that transportation through open pore space is much more important for soluble components. High-temperature compaction tests (Eseme et al., 2012) led to believe that fracture permeability as a primary pathway for migration occurs in dependency of saturation levels of the pore space. Employing petrophysical, geochemical and petrological methods, Eseme (2006) studied Permian to Miocene oil shales. Besides elucidating a variety of material specific values for the different oil shales, this study considered the formation and distribution of aliphatic, aromatic and polar compounds. The author did not observe fractionation based on molecular weight. Little preferential expulsion of *n*-alkanes relative to acyclic isoprenoids was observed, comparing generated and expelled petroleum with extracted material of the untreated sample (Eseme, 2006; Eseme et al., 2007). Thus, the conclusions of these studies are in stark contrast to previous observations, including in natural systems. Pressure experiments showed a final volume reduction of the source-rock during artificial maturation, which is related to the genesis and release of hydrocarbons (Hanebeck, 1993). The volume reduction was 2-3 times smaller than expected for natural conditions. The author notes that volume reduction rates for hydrous pyrolysis matched the natural conditions much better.

In summary, the triaxial pressure pyrolysis presented by Hanebeck (1993) is an interesting approach for laboratory simulation of maturation and expulsion. However, the system performed only anhydrous pyrolysis. As described above, this caused several differences to observations of natural systems and to hydrous pyrolysis.

### 2.3.2 Anhydrous closed pyrolysis

#### *Microscale sealed vessel pyrolysis*

Horsfield et al. (1989) introduced a small scaled method of artificial maturation in a microscale sealed vessel (MSSV). Here 5-10 mg aliquots of source-rocks were matured at 300° to 400°C under anhydrous conditions in a sealed glass tube for certain periods. After generation the glass tube is placed in a crushing tool, connected to a GC. In this way hydrocarbons can be transferred lossless to the GC, which enables accurate measurements even of

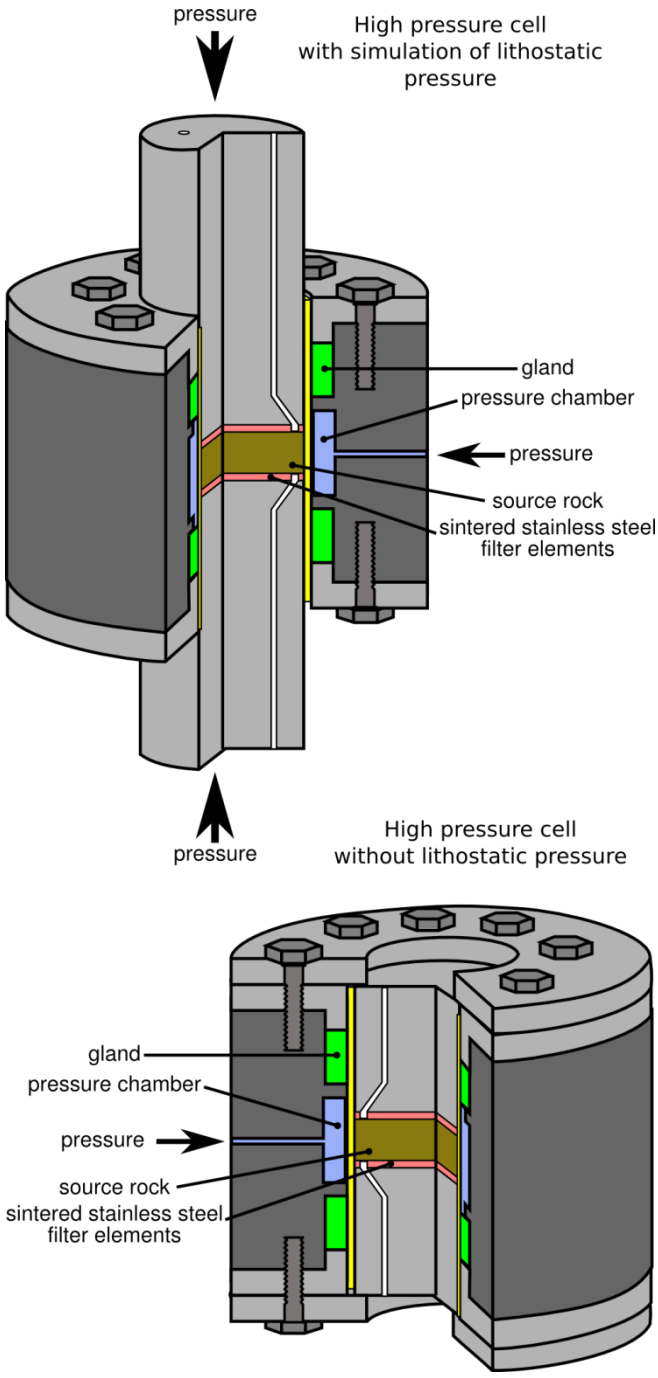


***Figure 12. Triaxial pressure cell (above) and confied pressure cell (below) used by (Hanebeck, 1993).***

lighter compounds, which normally are subject to evaporation. As a cheap method, different application fields were established for MSSV. It is used for kerogen typing (Horsfield, 1990) or kinetic modelling (Dieckmann et al., 2000; Horsfield et al., 1992; Schenk et al., 1997; Schenk and Horsfield, 1993). In this context Dieckmann et al. (2000) observed a dependency of the composition of petroleum and heating-rate, which are considered in 1$^{st}$ order parallel reaction models. In that study, an enrichment of *n*-alkanes was observed with decreasing heating rate. This observation is coherent to results of Burnham (1991), showing increasing aromatization with slower heating-rate. This could be an artefact of

the anhydrous pyrolysis or, in the case of MSSV, to secondary cracking reactions.

### *Anhydrous closed small vessel pyrolysis*

Under this designation (closed small vessel pyrolysis; CSVP) all methods are combined, which are using small stainless steel or alloy reactors without additional water and a gas filled (e.g. Nitrogen or Helium) reaction space. An explanation of this method is given by Lewan (1997). In that study, reactors are used with a volume of 543 $cm^3$, filled with a crushed and grounded, organic rich rock. After sealing the vessels, the tightness of the reactor was tested by filling the reactor with at least 69 bar of Helium. After successfully passing the pressure test, the reactor was filled with the required headspace medium (vacuum or Helium for anhydrous conditions). In comparison to other methods, like MSSV, CSVP benefits from the possibility to use different media and to monitor pressures during pyrolysis. The relative large volume of the reactors enables the use of larger sample amounts, increasing the petroleum yields of pyrolysis. Because the reactors are the same, also used for closed hydrous pyrolysis, this method is often utilised for comparative studies of the influence of water to petroleum generation (Behar et al., 2003; Koopmans et al., 1998; Lewan and Roy, 2011; Uguna et al., 2012). Generally, the generation is in focus of this technique and not the examination of expulsion.

### *Gold tube pyrolysis*

Various studies used gold tube pyrolysis for artificial maturation experiments of kerogen and source-rocks. A small amount of sample (~50 – 500 mg) is filled into a gold tube under a protective gas atmosphere (e.g. Argon). The gold tube is then placed into a heating unit, which is commonly able to generate hydrostatic pressure onto the gold tube. Such a device is described by Monthioux et al. (1985), for example. The advantages of gold tube pyrolysis are the inert properties of gold and that it is resistant to high temperatures (up to 550°C) and relatively high pressures. The ability to exert confining pressure onto the sample makes this method ideal for investigation of relationships between pressure and petroleum formation (Blanc and Connan, 1992; Hill et al., 1996). In the first of the two studies, it is shown that higher confining pressures cause a decrease of the yield of $C_{13+}$ oil fraction and favours the formation of aromatics. In contrast to this results, the authors of the second study notice only small influences to generation by pressure, secondary to the effects caused by temperature. The possibility to add water to the sample and to perform hydrous pyrolysis led to comparative studies, which examine the influence of water to the products of pyrolysis (Jin et al., 2009; Monthioux et al., 1985; Pan et al., 2010). Regarding to expulsion, the same limits exist which were discussed for MSSV and CSVP.

### *Confined pressure pyrolysis*

Closed pyrolysis under confined pressure conditions was performed by Lafargue et al. (1990, 1994) in order to investigate primary migration behaviour of source-rocks. The experiments were realised with intact source-rocks and attempted to differentiate the role of temperature and pressure. The experiments employed a high-pressure cell, in which a column of oil shale with an underlying artificial reservoir was exposed to high confining pressures under dry conditions. Two different procedures were applied: In the first one, an immature oil shale was first matured artificially at temperatures of 300°C and 1 kbar for 48 hours. The

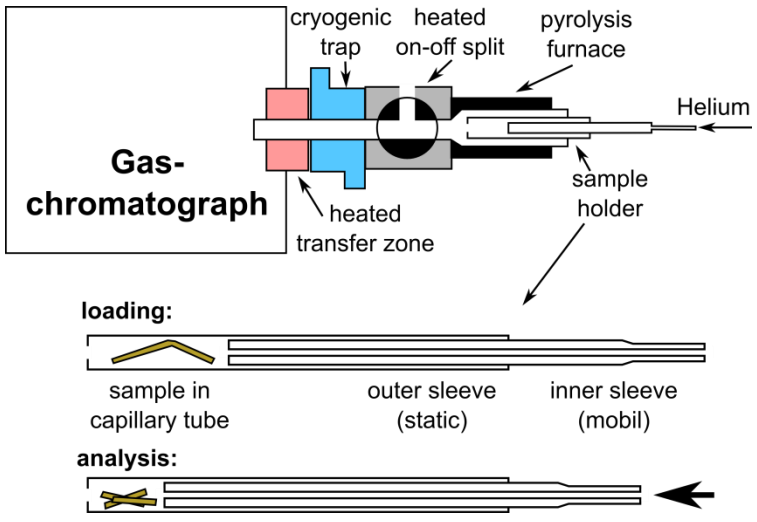


***Figure 13. Schematic representation of a MSSV apparatus (Horsfield et al., 1989).***

final expulsion experiment was conducted at a pressure of 3 kbar and a temperature of 150°C. These conditions were held up to one month. The second procedure used already matured natural samples. Beside a general exponential increase of expelled hydrocarbons with increasing temperature and pressure, Lafargue et al. (1990) noticed an preferential expulsion of saturated hydrocarbons and aromatics. Also the *n*-alkane to isoprenoid ratio decreased in the reservoir, confirming observations descripted in section 4.7. Lafargue et al. (1994) emphasizes the influence of permeability and pressure as important parameter for primary expulsion.

This approach tries to separate generation and expulsion of petroleum. It is questionable, if this process is expedient, since these processes in natural systems could proceed simultaneously. Here, too, the methods of the generation do not correspond to natural conditions, as it is performed with anhydrous pyrolysis.

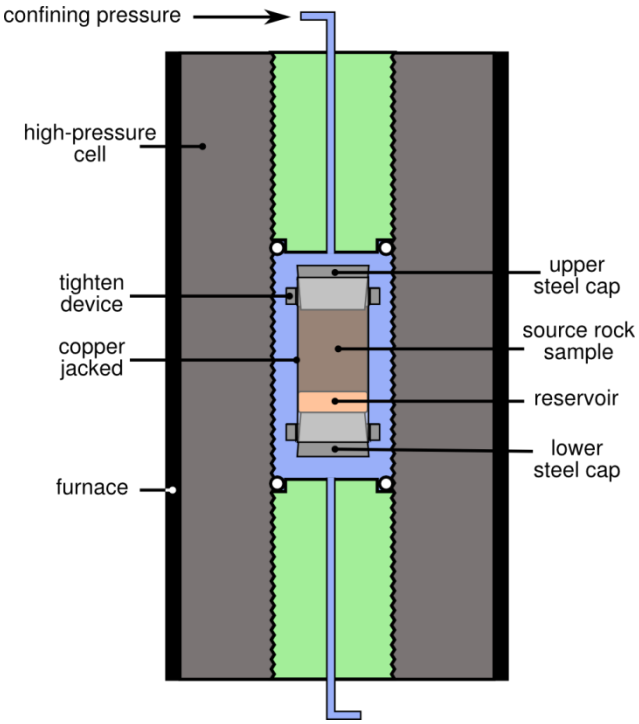


***Figure 14. Confined pressure cell, used by (Lafargue et al., 1990, 1994).***

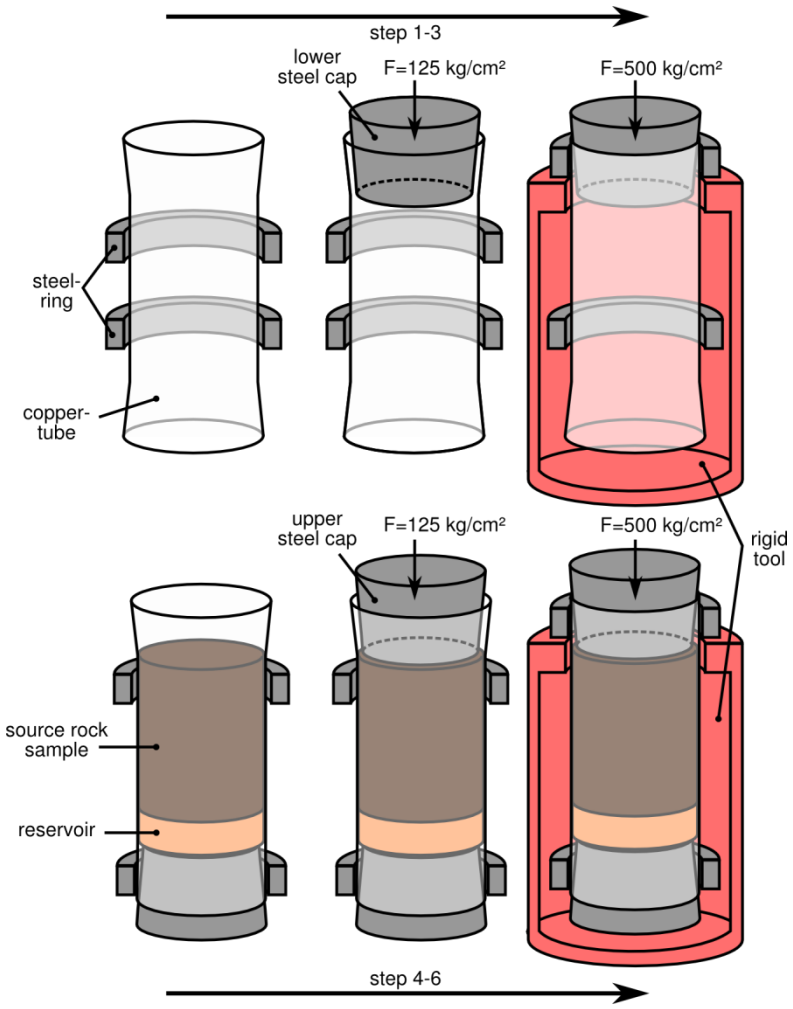


***Figure 15. Arrangement of sample source-rock and reservoir, as well as method of sealing, used by Lafargue et al. (1990, 1994).***

### 2.3.3 Hydrous open pyrolysis

The implementation of hydrous pyrolysis with open conditions is very difficult from the technical point of view. Therefore, only very few examples exist. One approach was presented by Seewald et al. (1998), using a standard stainless steel vessel. In that study, it was only possible to collect fluids discontinuously by a gas-tight syringe mounted on the top of the reactor. A pump was used to maintain the pressure during the withdrawal of the sample. The experiment was performed at 360°C and 350 bar in maximum. The study examined the gaseous hydrocarbons dissolved in the water phase and showed the dependence of gas production to temperature and time.

### 2.3.4 Hydrous closed pyrolysis

***Gold tube pyrolysis***

As already stated in section 2.3.2, it is possible to perform hydrous gold tube pyrolysis. Therefore, the same apparatus is used as it has been described previously for anhydrous pyrolysis. It is necessary to carry out the hydrous gold tube pyrolysis under confining pressure conditions to counteract the high pressures generated within the gold tube by hydrous pyrolysis. The method of gold tube pyrolysis is preferably used for anhydrous pyrolysis. The hydrous pendant was used by some studies for investigation of the influence of water on pyrolysis (Jin et al., 2009; Monthioux et al., 1985; Pan et al., 2010). For bulk parameters (elementary analysis, Rock-Eval) no difference between hydrous and anhydrous pyrolysis was noticed by Monthioux et al. (1985). A large impact on gas generation and carbon and hydrogen isotopic fractionation was observed by Jin et al. (2009). In this study, oils were matured artificially with and without addition of water. It was observed that hydrous pyrolysis results in smaller $C_{1\text{-}5}$ alkane yields and in lighter carbon and hydrogen isotopic ratios in comparison to anhydrous pyrolysis. In the study of Pan et al. (2010) observed decreasing maturation rates of hopanoids and steranes with addition of water.

Although the addition of water may provide more natural results, the limitations with respect to the expulsion still exist. These include the destruction of the coherent mineral and kerogen matrix and unnatural pressure regimes.

***Hydrous closed small vessel pyrolysis***

As already described previously, this designation (closed small vessel pyrolysis; CSVP) combines all methods, using a small stainless steel or alloy reactor with additional water, or water and gas filled (e.g. Nitrogen or Helium) reaction space. An early description of a procedure to produce oil-like pyrolyzates is given by Lewan et al. (1979) and later in more detail by Lewan (1997). A reactor is filled with a crushed and grounded organic rich rock. The rock is hold in place during pyrolysis by a sinter-filter on the top of the powdered sample. The following procedure is similar to the method described for anhydrous CSVP: After sealing of the vessels, the tightness of the reactor was tested by filling the reactor with at least 69 bar of Helium. After the pressure test has been passed, the reactor was filled with distilled water. The amount of water is calculated using steam tables and measured bulk rock densities to ensure that the rock is in contact with liquid water at every moment of the experiment (Lewan et al., 2008). The headspace volume was filled by pressurised gas, normally Helium.

With this procedure or similar to this, a large number of experiments were performed and many studies exist, describing different aspects of hydrous pyrolysis supported by the assumption that hydrous pyrolysis would mimic natural conditions best (Lewan, 1997; Lewan et al., 1979) (see section 2.4.1). An example for an application of hydrous pyrolysis is the investigation of stabile isotopes. Relationship between maturity and $\delta^{13}C$ values of expelled bitumen and its components was investigated by Lewan (1983). He observed an initial enrichment of $^{12}C$ in the bitumen, caused by bitumen generation, followed by depletion of $^{12}C$ with increasing maturity, caused by decomposition of the bitumen. With the aim to determine hydrogen exchange reactions between kerogen or water and hydrocarbons generated upon maturation, Schimmelmann et al. (1999) employed hydrous pyrolysis using deuterated water. The D/H isotope ratio of kerogen, bitumen, oil and water, was then examined for source-rocks of different kerogen Types (I, II, IIS and III). The study shows that (depending on temperature and time of artificial maturation) between 45% and 79% of the total amount of carbon-bound hydrogen in kerogen is derived from water and that the influence of water contributing hydrogen to different Types of kerogen is: IIS>II≈III>I. Schimmelmann et al. (2001) performed further hydrous pyrolysis experiments to investigate the effects of thermal maturation on D/H and $^{13}C/^{12}C$ ratios of kerogen, bitumen and oil. The experiments showed large isotopic transfers between water-derived hydrogen and organic hydrogen during maturation, but only small effects to the organic $^{13}C/^{12}C$ ratio. The $\Delta\delta D$ values for water and organic hydrogen were primary affected by the rock/water ratio. The experiments implemented that the H-isotopic transfer between hydrogen of water and hydrogen of organic matter increased with larger rock permeability and smaller rock grain. The authors were uncertain about the effects of an increase of the hydrostatic pressure. The generation of oxygen-rich species as precursor of $CO_2$ was investigated by Stalker et al. (1994), using $^{18}O$ labelled water and

model compounds (3,4-dimethylphenol, dodecanoic acid and xanthene), or a Type-II kerogen. The results showed an almost complete oxygen exchange in dodecanoic acid, only ~14% oxygen exchange in dimethylphenol and no exchange in xanthene. The oxygen of mono-, di-, and trimethylphenols, released from Type-II kerogen, consisted of 40% incorporated $^{18}O$. The authors concluded that the neoformation of phenols influenced the mass balance concerning the generation of $CO_2$.

The shown examples elucidate the possible rule of water for the formation of oil and gas. However, the use of mainly crushed sample material is not corresponding to natural conditions. In comparison to an oil shale with very low permeability under load pressure, the kerogen in the pyrolysis experiments has a much larger contact surface to the water. Thus, it is questionable, whether water plays such a big role during generation within the source-rock. Since water is present in large quantities in the reservoir, it is likely that many of the effects shown above take place after primary migration. Therefore, the standard hydrous pyrolysis is not suitable to simulate expulsion and primary migration. One exception is the experiment performed by Bonilla and Engel (1986). In this study, an oil shale was placed in the bottom of a reactor and wet sand was filled on the top, leaving 0.5 cm headspace. The reactor was closed, purged and pressurized with helium. The pyrolysis and expulsion was performed at 300°C. The results of this experiment did not show any change in *n*-alkane vs. isoprenoid ratio with migration distance as described previously. Reason for this could be the sand, which has lower adsorption effectiveness than clay. However, the experimental pressures did not correspond to pressures of geological systems.

## 2.4 Impact of different pyrolysis parameters

As shown in section 2.3, various methodologies were developed with different focus areas. This makes it necessary to take a closer look to aspects, which may influence the results of pyrolysis.

### 2.4.1 Hydrous vs. anhydrous pyrolysis

Various opinions exist about a possible influence of water on the pyrolysis and the strength of this influence.

***Yields of hydrocarbons (oil and gas)***

An early study performed with gold tube pyrolysis of kerogen Type-III did not show an impact of water on bulk parameters like Rock-Eval or elementary analysis (Monthioux et al., 1985). Data presented by Ritter et al. (1995) support this observation. In contrast, Behar et al. (2003) reported that the vitrinite reflectance values for anhydrous experiments were on average 0.2 % $R_0$ lower in comparison to hydrous experiments. In addition, the remaining carbon generation potential after anhydrous pyrolysis was 16 $\frac{mg}{g\ lignite}$ higher, compared to hydrous pyrolysis. The authors concluded that there is a better release of the pyrolysis products in the hydrous systems from the kerogen network once generation occurs. Investigations made with kerogen Type-II (Andresen et al., 1993) show an increase of the bitumen generation for hydrous pyrolysis, although it must be said that the methods described for hydrous and anhydrous closed pyrolysis in that study are only poorly comparable. Lewan (1997) studied the role of water in petroleum formation and noticed that the thermal conversion of kerogen to bitumen was not significantly affected by the presence or absence of liquid water at temperatures less than 330°C. Above this temperature and in absence of water, formation of insoluble pyrobitumen was the dominant reaction. In the presence of liquid water the generation of saturate-enriched oil is dominant, which is similar to natural crude oil. Comparative pyrolysis experiments of coals (Kuangzong et al., 1994) revealed higher yields for hydrous pyrolysis with higher amounts of aliphatics and aromatics, a significantly lower content of resins and a higher amount of asphaltenes. A short comparison of low-pressure anhydrous pyrolysis, high-pressure anhydrous pyrolysis and hydrous pyrolysis is given by Burnham (1993). He postulated that the main differences between the various methodologies are driven by temperature and not by the presence of water or by pressure. In conclusion, he assessed that hydrous and high-pressure pyrolysis follow the natural “van Krevelan” trend more closely. Therefore, hydrous pyrolysis is preferable to anhydrous pyrolysis, if conditions close to those prevailing in nature are to be met. Higher yields of bitumen for hydrous pyrolysis are stated by Uguna et al. (2012). Michels et al. (1995) reported that hydrous pyrolysis inhibited aromatization of the residual kerogen. Due to the different behaviour of the residual kerogen of hydrous and anhydrous pyrolysis and due to the different products generated upon artificial maturation, the authors implied different hydrogen sources (water or the residual kerogen) and hydrogen exchange mechanisms, which are involved during the maturation process. Much higher yields for $C_{14+}$ components produced by hydrous pyrolysis are reported by Behar et al. (2003). The difference to anhydrous pyrolysis is explained by cracking reactions leading to liquid products in case of hydrous pyrolysis and to formation of char in case of anhydrous pyrolysis. Cross-linking reactions and trapping of generated products within the coal network are further explanations. The comparison of the gas yields in this study of closed anhydrous pyrolysis and the gas yields of hydrous pyrolysis showed that closed anhydrous pyrolysis generated on the average 14 % more gas than hydrous

experiments. The proportionality of the produced gases was essentially the same for both pyrolysis systems.

***Yields of $CO_2$ and incorporation of hydrocarbons***

The yields of $CO_2$ are frequently higher in hydrous pyrolysis as in corresponding anhydrous pyrolysis (Andresen et al., 1993; Behar et al., 2003; Lewan, 1997). The high amounts of $CO_2$ in hydrous pyrolysis were interpreted as indication that water acts as exogenous source of hydrogen (Lewan, 1997). The author presented two possible reaction ways to explain the excess of $CO_2$:

1. Oxidation of carbonyl groups by water, forming hydrogen and carboxyl groups. Finally, $CO_2$ is formed by decarboxylation.
2. Formation of hydrogen-terminated free-radical sites by interaction of hydrogen or oxygen of water with unpaired electrons. Oxidation of the latter would generate $CO_2$ and hydrogen.

Comparative pyrolysis experiments with lignite of Behar et al. (2003) show similar results. The $CO_2$ production reached maximum in hydrous pyrolysis, which was 37% higher than closed pyrolysis. The authors traced it to selectively oxidization of specific functional groups within the lignite by water, as described earlier by Lewan (1997). In contrast, hydrous oil cracking experiments showed a higher production of hydrogen, but a lower formation of $CO_2$ in comparison to anhydrous pyrolysis (Jin et al., 2009). This indicates that main reactions forming $CO_2$ are linked to kerogen-to-bitumen decomposition and not to further oil cracking. This observation fits the assumptions of Lewan (1997), who linked the formation of $CO_2$ with kerogen-to-bitumen reactions as well. The formation of large amounts of $CO_2$ is connected to a higher availability of hydrogen, which is supposed to reduce the rate of cross linking and promotes thermal cracking, as stated in different studies (e.g. Behar et al., 2003; Lewan, 1997; Lewan and Roy, 2011).

Experiments performed with deuterated water show that high amounts of hydrogen are incorporated into the expelled hydrocarbons (Hoering, 1984; Lewan, 1997; Schimmelmann et al., 2001, 1999; Stalker et al., 1998, 1994). Several experiments suggest that the deuteration takes place during the decomposition of kerogen (Lewan, 1997; Stalker et al., 1998, 1994), which underlines the importance of water during thermal maturation of kerogen.

***Free radical vs. catalytic reaction pathways***

Radical reaction pathways are preferred by most studies to explain the results of hydrous pyrolysis. However, Larsen (1999) argues that various chemical parameters speak against reactions involving free radicals. He noted that radicalization of hydrocarbons happened much faster than the abstraction of hydrogen from water. The formation of alkyl radicals by β-scission at 330°C is 300 times faster than the provision of hydrogen by water (Larsen, 1999). The result would be the formation of a large amount of alkenes, which was not observed for hydrous pyrolysis. This argument is supported by results of Lewan (1997), received by pyrolysis experiments with added $H_2$. No significant change in the product distribution was observed, although hydrogen can be removed much easier from $H_2$ as from water (119.1 kcal/mole for water vs. 104.2 kcal/mole for $H_2$ (Larsen, 1999)). In addition, hydrogen-balance calculations of hydrous and anhydrous pyrolysis show that water does not contribute to the net amount of initially bonded hydrogen in the products of hydrous pyrolysis (Lewan et al., 1979). Moreover, experiments which were carried out with pure compounds (Weres et al., 1988) or with oils (Jin et al., 2009) show high yields of alkenes, which should be prevent by hydrogen donors like water. Larsen (1999) see in this the proof that the role of radical reactions is secondary in formation of oil and gas from kerogen. In contrast Weres et al. (1988) emphasizes the role of highly aromatic kerogen and bitumen as hydrogen donor and explained the higher yields of alkenes with the lack of these components in their experiments. Furthermore, the authors see water in hydrous pyrolysis primary as inhibition of catalysis by clays and in limiting the loss of generated products by volatilization and for pressurizing the system (see section 2.4.3). Several authors disagree (Larsen, 1999 and cited studies there) and presented catalytic reaction pathways like the following:

$$\underbrace{3Fe_3O_4}_{Magnitite} + 4.5SiO_2 + -CH_2 \rightarrow \underbrace{4.5Fe_2}_{Fayalite} + CO_2 + H_2O \quad (10)$$

$$1.5Fe_2SiO_4 + -CH_2\_CH_2\_ + H_2O \rightarrow 2 - CH_3 + 1.5SiO_2 + Fe_3O_4 \quad (11)$$

Results which support these reaction pathways even in presents of water were presented by Eglinton, (1987). The yield of carboxylic acids formed by hydrous pyrolysis of Kimmeridge clay increased significantly after adding limonite to the pyrolysis. This reaction model would not need additional water. However, it has to be considered that mineral conversions (e.g. smectite to illite) will supply water. This and the role of kerogen and bitumen as hydrogen donor are arguments, explaining why the yields of alkenes of anhydrous closed pyrolysis not exceed the yields of hydrous pyrolysis, as shown by several studies (e.g. Hoering, 1984; Horsfield et al., 1989).

***Formation of a separate oil phase***

Another important effect of liquid water in hydrous pyrolysis is described by Lewan (1997). The formation of a saturate-enriched oil phase separated from polar-enriched residual bitumen impregnating the rock was only observed in pyrolysis performed with liquid water phase. Both phases (oil and bitumen) are mutually soluble with one other, making it difficult to explain separation in natural and artificial system. The author explained this effect with the increasingly saturate-enriched oil, which is miscible with the bitumen due to the dissolved water in the bitumen. This water is able to dissolve in bitumen and kerogen at temperature conditions present in hydrous pyrolysis as descripted by Larsen (1999). The solubility parameter $\delta$ can be calculated with following formula:

$$\delta = \left(\frac{\Delta E_{vap}}{V_{mole}}\right)^{1/2} = \left(\frac{\Delta H_{vap} - RT}{V_{mole}}\right)^{1/2} \quad (12)$$

In this equation $\Delta E_{vap}$ is the energy of vaporization, $\Delta H_{vap}$ the enthalpy of vaporization and $V_{mole}$ the molar volume. $R$ is the gas constant and $T$ the temperature. Using this calculation, water reached values for $\delta$ of $9.1\ cal^{1/2}cm^{-3/2}$ and $7.4\ cal^{1/2}cm^{-3/2}$ at 350°C and 360°C respectively. Kerogen Type-I is supposed to have approximately $9.75\ cal^{1/2}cm^{-3/2}$ (Larsen, 1999). With these values it is likely that water is able to solve in kerogen and will have access to almost all areas of the kerogen network at conditions which are present at hydrous pyrolysis. However, in nature temperatures did not reach necessary levels to provide solubility of water in kerogen. In addition, the factor of lithostatic pressure is not considered in this theory.

Maybe the separation-effect could be explained with simple chemo-physical processes. The solubility of hydrocarbons in water increased with decreasing molecular weight (Weres et al., 1988) and increasing temperature and pressure (Economou et al., 1997; Heidman et al., 1985; Tsonopoulos and Wilson, 1983). Since saturates are released preferentially by kerogen (Sandvik et al., 1992; Thomas and Clouse, 1990c), and aromatics are retained by adsorbing-effects of the kerogen, it can be assumed that an early enrichment of saturated oil-like hydrocarbons occur within the pore space. If water acts as simple transporting and separation agent, the saturated hydrocarbons will be separated from the residual OM (kerogen and absorbed bitumen) maybe by simple convection or buoyancy. After completion of the pyrolysis, the separate oil phase is accumulated as a film on the water surface. There will not be any distribution of bitumen within the water due to its higher density. In anhydrous pyrolysis, oil-phases and bitumen will vaporize and condense later on both the reactor wall and cap.

***The role of water in pyrolysis summarized***

The processes of a hydrous pyrolysis are complex and far from being completely understood. The following tries to summarize the essence of recent results: During the thermal breakdown of kerogen to bitumen radical reactions occur, maybe supported by catalytic reactions including mostly reactive clay minerals. In addition, water seems to course selective oxidation of specific functional groups within the Kerogen, too. Crosslinking and therefore the formation of pyrobitumen are diminished by provision of sufficient amounts of hydrogen. Hydrogen donors are kerogen, bitumen and water, supplied by clay mineral conversion or by artificially added water. In any case, these reactions are directly connected with the thermal breakdown within the kerogen or bitumen, as experiments with isolated products (without kerogen or bitumen) lead to abnormal yields of alkenes.

After generation of bitumen, a separation between bitumen and a single oil phase took place. Water dissolved in bitumen could drive out the oil phase from the bitumen. Also conceivable would be a chemo-physically driven separation of a primary released oil-phase by water as transporting and separation agent.

Water seems to play an important role for artificial maturation of kerogen with the aim to match natural products. However, there are still some uncertainties about the exact role of water. It would be necessary to determine whether water is important for the kerogen to bitumen thermal breakdown or if water only diminishes crosslinking and support cracking reactions after generation of bitumen.

### 2.4.2 Open vs. closed pyrolysis

In open pyrolysis, as descripted in section 2.3.1, generated products are just removed out of the system at the moment of formation. Therefore reactions with residual kerogen, bitumen or with released water are prevented. This leads to differences to closed pyrolysis, most evident in the yields of alkenes and aromatics. In open anhydrous pyrolysis higher yields of alkenes were observed than in closed pyrolysis techniques (Behar and Pelet, 1985; Solli et al., 1984). If the products are not removed immediately after generation, like in closed pyrolysis, they can be alkylated or hydrogenated by present hydrogen donors (kerogen, bitumen, water). Other differences were noted in several studies, some are partially contradictory:

Significant lower yields production rates for open pyrolysis were reported by Andresen et al. (1993). However, no significant differences were observed by Arneth and Matzigkeit (1986), concerning yields and carbon isotope composition. Behar et al. (2003)

recognised a great difference between the liquid product quantities of closed anhydrous pyrolysis and open anhydrous and hydrous pyrolysis. The highest production rate for high molecular weight liquid products ($C_{14+}$) exists for open anhydrous and hydrous pyrolysis with similar values. These yields were more than 70 wt% higher than the yields for closed anhydrous pyrolysis. The authors observed the highest amount of hydrocarbon gas production for open anhydrous pyrolysis, reaching 20 % and 29 % higher yields as closed anhydrous pyrolysis and hydrous pyrolysis, respectively.

This contradictions show that comparisons of open and closed pyrolysis methods are difficult, due to the large differences in the methodology. This is especially evident in the conflicting data presented in literature. It should be noted that only open systems were compared as descript in section 2.3.1. These methods are all anhydrous procedures, missing effects caused by water, as descripted before.

### 2.4.3 Influence of confining pressure

Different effects have been described in literature, which are caused by confining pressure. An retarding effect of pressure is reported by several authors for the generation of hydrocarbons by hydrous pyrolysis (Jackśon et al., 1995; Michels et al., 1995; Uguna et al., 2012). Experiments with confining pressure for hydrous and anhydrous pyrolysis show that the retarding effect was less pronounced in anhydrous pyrolysis (Michels et al., 1995). The same study showed that the yield maximum shifted to higher temperatures with increasing pressures. The reason for the retardation is most likely an increase of the activation volume by increasing pressure (Jackśon et al., 1995; Uguna et al., 2012). However, temperature is the primary factor for the reaction rate and superior to pressure effects (Hill et al., 1996; Jackśon et al., 1995).

Confining pressure seems to have positive influence on the alkene/alkane formation ratio. The ratio decrease with increasing pressure (Weres et al., 1988), as low-pressure experiments decrease the rate of reactions among the cracking products. As stated by Weres et al. (1988), in low pressure pyrolysis alkenes and alkanes boil off into gas phase before they are able to react and are preserved during pyrolysis.

Increased pressure is required to ensure that liquid water is present during pyrolysis and not water vapour. Expansion fractures were observed within rock flakes after hydrous pyrolysis (Lewan and Roy, 2011). In absence of liquid water, the rock chips did not show any expansion fracturing. The authors assumed that water promotes reactions like thermal cracking, causing a net-volume increase. Net-volume

***Table 3. Comparison of the results of different pyrolysis techniques, using Type-III kerogen (Behar et al., 2003).***

| ***Product parameter*** | ***hydrous vs. anhydrous CSVP*** | | ***hydrous CSVP vs. open pyrolysis*** | | ***anhydrous CSVP vs. open pyrolysis*** | |
|---|---|---|---|---|---|---|
| | *match* | *mismatch* | *match* | *mismatch* | *match* | *mismatch* |
| **hydrocarbon gases** | | | | | | |
| quantity | a, b | - | - | a, c | - | a, d, c |
| composition | a, b | - | - | c | - | d, e |
| **non-hydrous gases** | | | | | | |
| quantity | - | a, b | - | a, c | - | a, d, c |
| composition | - | a, b | - | c | - | d, e |
| **liquid pyrolyzates** | | | | | | |
| quantity | f | a, b | - | a, c | - | a, d, e |
| fractions (saturates, aromatics, NSO's) | a, f | - | a | c | a | - |
| Gas-chromatogram | a, f | - | a | - | a | - |
| **residual lignite** | | | | | | |
| elemental analysis | a, f | b | - | c | - | d, g |
| vitrinite reflectance | f | a, h | - | - | - | d |

a (Behar et al., 2003, p. 200); b (Artok et al., 1998); c (Kuangzong et al., 1994); d (Behar et al., 1995); e (Arneth and Matzigkeit, 1986); f (Michels et al., 1995); g (Monthioux et al., 1985); h (Huang, 1996)

decrease reactions were in favour of anhydrous reactions.

Summarizing the results, it is clear that increasing confining pressure reduced the yields of oil and gas in low extend. In contrast, confining pressure supports formation of natural oil and gas by providing liquid water, preventing the vaporization of product and permitting further reactions.

## 2.5 Thermal maturity parameters and their application in pyrolysis

The chemical components forming kerogen, oil and gas are thermally unstable over time (Hunt, 1996; Peters et al., 2005a; Tissot and Welte, 1984). Differences of the decomposition rate of components or the relative abundance of precursor compounds to their thermally rearranged or degenerated products enables to estimate the thermal history of an oil, gas or kerogen.

Source-rock maturity can be assessed by classic methods like Rock-Eval, vitrinite reflectance ($R_0$) or thermal alteration index (TAI). However, these parameters are not applicable to oils. For this, molecular maturity-related parameters have to be used. In the following, maturity parameters are shown in more detail with a particular focus on expulsion and primary migration. An overview of various maturity parameters is given in Figure 16.

### 2.5.1 Rock-Eval

Rock-Eval pyrolysis as described in section 2.3.1 is an easy way to estimate the thermal maturity of a source-rock. From the four parameters, measured by Rock-Eval ($S_1$, $S_2$, $S_3$ and $T_{max}$) $S_2$ and $T_{max}$ are especially suitable for maturity assessment.

The $S_2$ value is corresponding to the amount of components generated from kerogen by thermal heating with temperatures up to 550°C. Related to the $S_2$-parameter is the HI-value (see equation 8), which is essentially a measure of hydrogen richness. Therefore, HI values vary with kerogen type (Table 4)

However, due to thermal decomposition of kerogen during time, the HI-value is supposed to decrease with increasing thermal maturity. This is a very rough method for maturity assessment and will therefore only give an idea of the thermal history of a source-rock.

The $T_{max}$-value is related to the $S_2$-value, as it is the temperature at which the generation of hydrocarbons during Rock-Eval pyrolysis reaches the maximum. The $T_{max}$-value increases with increasing thermal maturity, as more thermal energy is necessary to release remaining molecules from the thermally altered kerogen. $T_{max}$-values show good correlation with vitrinite reflectance, confirming the maturity dependence. However, $T_{max}$-values depend from kerogen type, too (Bordenave, 1993). For Type-I kerogen oil genesis starts at $T_{max}$-values of 440 °C and $R_0$-values of about 0.7 %. During oil genesis $T_{max}$ will remain relative constant and $R_0$ will reach 1.00 %. For Type-II kerogen oil generation will start at around 0.60-0.65 % and at $T_{max}$ of around 435 °C. At $R_0$ of 1.0 %, the $T_{max}$ value reaches around 455 °C. The $T_{max}$-values for the gas and condensate zones will be in a range of 455-470 °C. Type-III kerogen starts with $R_0$-values around 0.6-0.7 % and a $T_{max}$ higher than 435 °C. The condensate zone will start around a $R_0$ of 1.3 % and $T_{max}$ of 470 °C. For Type-III kerogen the production of hydrocarbons exceed $R_0$-values of 1.6 % and corresponding $T_{max}$-values of 600 °C.

***Table 4. Kerogen type and corresponding HI-value (Miles, 1994).***

| Kerogen type | HI [mg/g TOC] |
|---|---|
| **Type I** | 600-900 |
| **Type II** | 400-600 |
| **Type III** | 0-300 |

### 2.5.2 Vitrinite reflectance

Vitrinite reflectance is a common application to estimate the thermal maturity of a source-rock. With decreasing O/C and H/C ratios the reflectance of any OM increases (Bordenave, 1993). The vitrinite reflectance is related to the maturity-related changes in reflectance of polished vitrinite particles (Miles, 1994). They are examined microscopically and the reflectance is measured at monochromatic light (546 nm), about one hundred times per sample. The result represents the mean value expressed as a reflectance histogram. As already shown in section 2.5.1, the correlation between vitrinite reflectance and thermal maturity is influenced by the type of kerogen to a certain degree, but are normally in a range as shown in Table 5.

***Table 5. Typical vitrinite reflectance values and corresponding thermal maturity stages (Miles, 1994).***

| | Vitrinite reflectance [%$R_0$] | |
|---|---|---|
| | Oil generation | Gas generation |
| **Immature** | < 0.5 | <0.7 |
| **Mature** | 0.5-1.3 | 0.7-3.0 |
| **Overmature** | >1.3 | >3.0 |

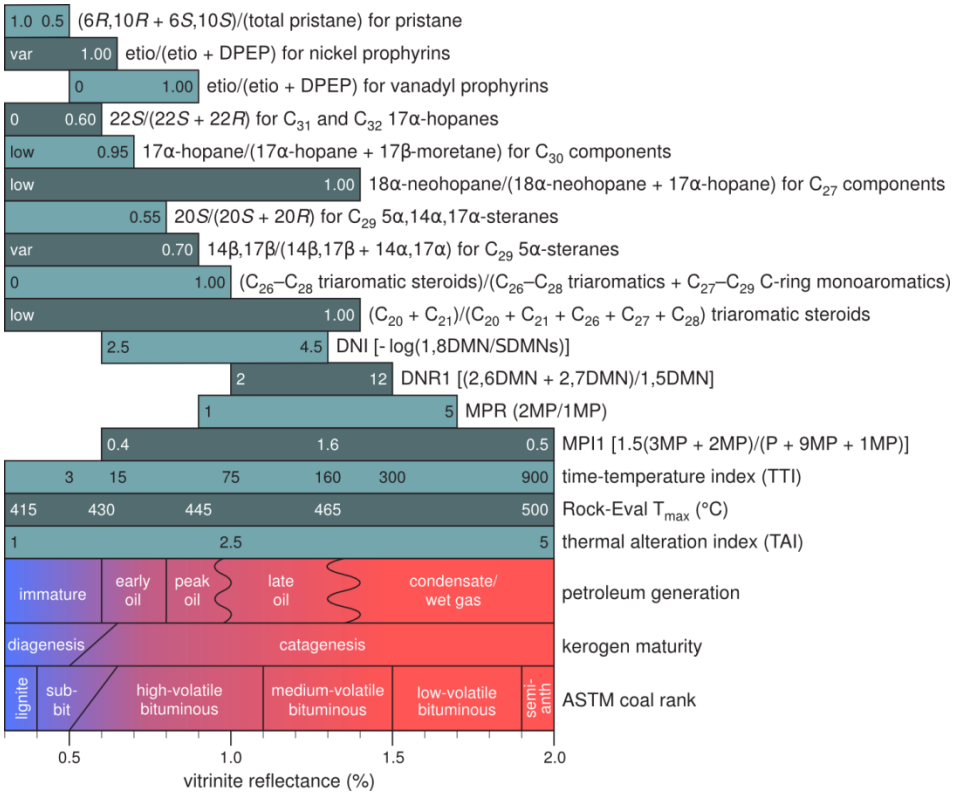


***Figure 16. Maturity parameter and corresponding maturity range (after Killops and Killops, 2009).***

### 2.5.3 Molecular non-biomarker maturity parameters

#### *Isoprenoid and isoprenoid/n-alkane ratios*

Commonly used for the calculation of ratios are pristane (Pr), phytane (Ph), *n*-$C_{17}$ and *n*-$C_{18}$ due to their usually high abundance in crude oils (Peters et al., 2005a). Pr/Ph ratio is usually not taken for maturity assessment, but will be discussed shortly since it is examined in this study in context of expulsion and primary migration. Pristane and phytane have biological precursors and are mostly derived from phytol (the side chain of chlorophyll). Beside this source, many other possible sources are discussed which could influence the Pr/Ph ratio, like unsaturated isoprenoids in zooplankton and higher animals, tocopherols and archaeal ether lipids (Peters et al., 2005a and cited studies there). Pr/Ph can be influenced by maturation as shown in several studies. Low values for Pr/Ph were frequently observed for immature oils and source-rocks in contrast to higher values in corresponding samples with higher maturity (Volkman and Maxwell, 1986). Experiments simulating natural sulphurization show that the release of sulphur-bound phytols during early maturation could possibly an explanation (De Graaf et al., 1992). Pr/Ph at higher maturity shows a more variable behaviour, as shown by a variety of studies (Peters et al., 2005a and cited studies there). A generally increasing Pr/Ph ratio with increasing maturity was observed for petroleum, which was explained by a higher abundance of pristane precursors in kerogen (Koopmans et al., 1999). However, some studies observed that the ratio first increased until the main oil formation zone followed by an decreasing ratio at higher maturities (e.g. Albrecht et al., 1976; Brooks et al., 1969; Radke et al., 1980). This effect could be explained by preferential release of pristane compared with phytane at early maturity stages.

Generation of pristane from kerogen was observed in generation and expulsion experiments (Eseme et al., 2006b). This affected the Pr/Ph ratio with beginning petroleum generation. Tang and Stauffer (1995) investigated pristane and phytane by open and closed pyrolysis. They observed same formation rates for pristane and phytane, but faster decomposition of phytane. Since they suggested that the formation rate is constant with increasing maturation, a faster decomposition would lead to increasing Pr/Ph ratios. No significant influence of maturation was observed in comparative anhydrous and hydrous pyrolysis (Lewan, 1997).

The ratio of isoprenoids vs. *n*-alkane decreased with increasing thermal stress (Tissot et al., 1971). The decrease of the ratio is reasoned by an increase of the relative abundance of *n*-alkanes compared to isoprenoids, as *n*-alkanes are generated by thermal cracking from kerogen.

Several studies observed a relation between ongoing expulsion/primary migration and decreasing values for Pr/*n*-$C_{17}$ and Ph/*n*-$C_{18}$ (Bonilla and Engel, 1986; Lafargue et al., 1990; Leythaeuser et al., 1984a, 1984b; Leythaeuser and Schaefer, 1984; Mackenzie et al., 1983), explaining this with geochromatographic effects.

***Methylphenanthrene ratios***

Ratios, using the relative abundance of phenanthrene (P) and methyl-homologues (MP) (Figure 18) were investigated by various studies (Peters et al., 2005a and cited studies there). Most commonly used is the MPI-1 ratio, introduced by Radke et al. (1982) and Radke and Welte (1983). The ratio based on the relative abundance of the thermally more stable β-isomers (2-MP and 3-MP) to the thermally less stable α-isomers (1-MP and 9-MP) and phenanthrene (see equation 13).

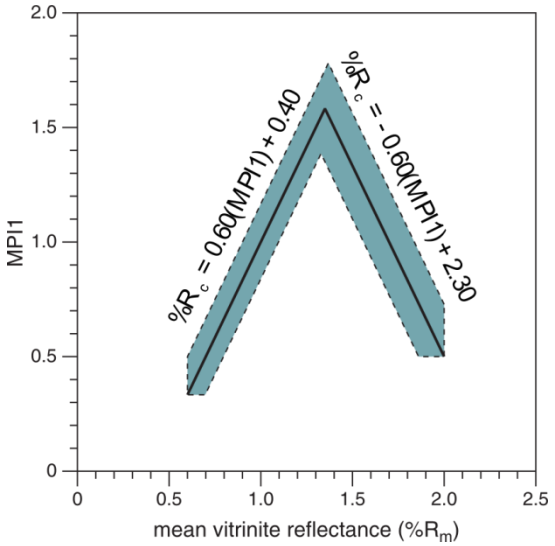


***Figure 17. MPI vs. vitrinite reflectance for type-III kerogens (from Peters et al., 2005a; after Radke and Welte, 1983).***

Phenanthrene is derived from biological sources like steroids and triterpenoids. 1-MP and 2-MP could have biological precursors, too, but more likely is methylation of phenanthrene to explain the abundance of the four isomers (Radke et al., 1982; Radke and Welte, 1983).

$$MPI\text{-}1 = \frac{1.5 \cdot (2\text{-}MP + 3\text{-}MP)}{P + 1\text{-}MP + 9\text{-}MP} \qquad (13)$$

$$MPI\text{-}1 = \frac{1.89 \cdot (2\text{-}MP + 3\text{-}MP)}{P + 1.26(1\text{-}MP + 9\text{-}MP)} \qquad (14)$$

Equation 14 represents a modified version of the MPI-1, including different response factors by using m/z 178 and 192 mass chromatograms (Cassani et al., 1988). Phenanthrene is acting as reference point in this ratio. Other modifications of the methylphenanthrene ratio waive the reference point, as shown by the PP-1:

$$PP\text{-}1_A = \frac{1\text{-}MP}{2\text{-}MP + 3\text{-}MP} \qquad (15)$$

$$PP\text{-}1_B = \frac{1\text{-}MP + 9\text{-}MP}{2\text{-}MP + 3\text{-}MP} \qquad (16)$$

Equation 15 was introduced by (Alexander et al., 1986) and equation 16 by (Cassani et al., 1988).

Comparison of the MPI-1 with vitrinite reflectance showed a positive linear correlation between 0.65-1.35% $R_0$ (oil window) and negative correlation for 1.35-2.00% $R_0$ (Figure 17) (Radke and Welte, 1983). Reason could be different rates of generation and destruction of phenanthrene and α- and β-isomers (Peters et al., 2005a).

The MPI-1 seems not to be affected by primary migration (Leythaeuser et al., 1988b).

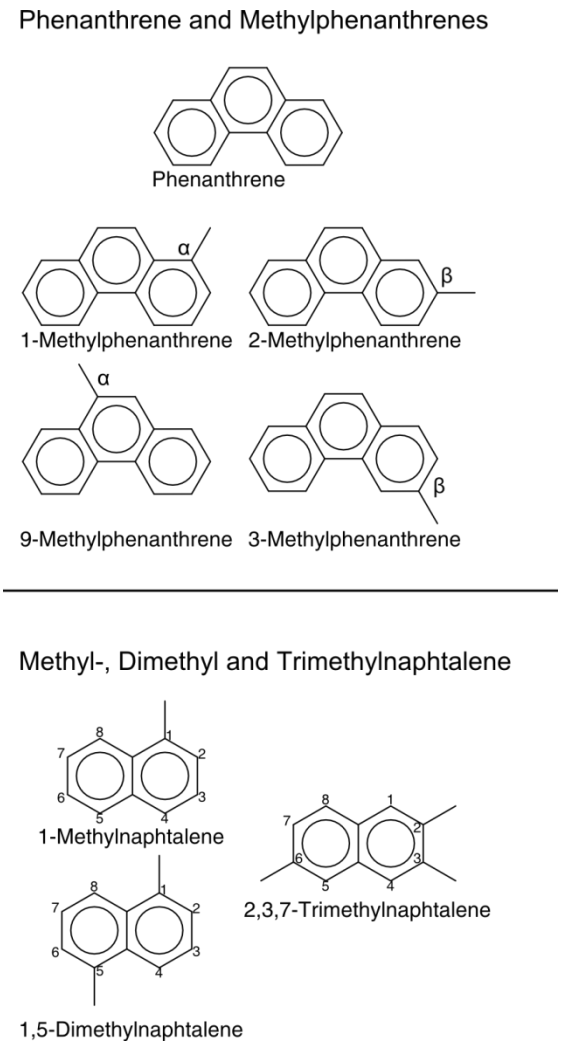


***Figure 18. Phenanthrene, methylphenanthrene and methyl-, dimethyl- and trimethylnaphthalene.***

***Naphthalene indices***

Indices based on isomers related to naphthalene (methyl-, ethyl-, dimethyl- and trimethylnaphthalene, Figure 18) are typically specific for high thermal maturity, starting at ~0.9% $R_0$ (Peters et al., 2005a). The ratios based on the rearrangement of thermally less stable isomers and the resulting relative increase of the more stable isomer.

$$MNR = \frac{2\text{-}MN}{1\text{-}MN} \quad (17)$$

$$ENR = \frac{2\text{-}EN}{1\text{-}EN} \quad (18)$$

$$DNR\text{-}1 = \frac{2{,}6\text{-}DMN + 2{,}7\text{-}DMN}{1{,}5\text{-}DMN} \quad (19)$$

$$TNR\text{-}1 = \frac{2{,}3{,}6\text{-}TMN}{1{,}4{,}6\text{-}TMN + 1{,}3{,}5\text{-}TMN} \quad (20)$$

$MNR$: $Methylnaphthalene\ Ratio$
$MN$: $Methylnaphthalene$

$ENR$: $Ethylnaphthalene\ Ratio$
$EN$: $Ethylnaphthalene$

$DNR$: $Dimethylnaphthalene\ Ratio$
$DMN$: $Dimethylnaphthalene$

$TNR$: $Trimethylnaphthalene\ Ratio$
$TMN$: $Trimethylnaphthalene$

No impact of expulsion or primary migration was reported for naphthalene rations (Leythaeuser et al., 1988b).

### 2.5.4 Maturity-related biomarker parameter

#### *2.5.4.1 Thermal stress induced aromatization*

In immature rocks biomolecules are present in their biological favoured isomerization. During dia- and catagenesis and with increasing thermal stress these molecules are converted gradually by isomerization, resulting in a mix of biological and geological epimers (Figure 19 F, G). The rank of isomerization can be correlated to the thermal stress the OM has underwent. In contrast, the investigation of biomarker maturity parameters by Farrimond et al. (1998) led to the assumption that the ratios are mainly affected by increasing concentrations of individual isomers due to release of biomarkers from kerogen. The authors saw isomerisation secondary to generation effects.

***Homohopane isomerization 22S/(22S+SSR)***

Homohopane isomerization is applicable for maturity ranges from immature to early oil generation (Peters et al., 2005a). Isomerization occurs at C-22 in the $C_{31}$-$C_{35}$ 17α-hopanes and starts at vitrinite reflectance of ~0.5% (Schoell et al., 1983) (Figure 19 B). The ratio 22S/(22S+22R) can be calculated for any or all of the $C_{31}$-$C_{35}$ compounds, whereas R is the biological isomerization, and S the geological one. The ratio can start at zero for immature samples and increase to an equilibrium value at around 0.6. The equilibrium value depends on the used homologe and increased usually with higher homologe (Zumberge, 1987).

Values of around 0.50-0.54 are typical for beginning oil generation, whereas samples with values around 0.57-0.62 reached or surpassed the main stage of oil formation (Peters et al., 2005a).

***Table 6. Equilibrium values of different homologes for 22S/(22S+22R) (Zumberge, 1987).***

| Homologe | equilibrium |
|---|---|
| **$C_{31}$** | 0.55 |
| **$C_{32}$** | 0.58 |
| **$C_{33}$** | 0.60 |
| **$C_{34}$** | 0.62 |
| **$C_{35}$** | 0.59 |

***$C_{29}$ ααα-sterane isomerization 20S/(20S+20R)***

$C_{29}$ 5α,14α17α(H)-steranes were isomerized at C-20 forming 20S/(20S+20R) ratio (Figure 19 C). The biological epimere has R isomerization, forming a mixture of R and S $C_{29}$ ααα-sterane configurations. The ratio ranges from 0 to 0.52-0.55 as equilibrium value (Peters et al., 2005a) and is applicable for immature to mature samples.

***Steranes - $C_{29}$ ββ/(ββ+αα) isomerization***

Isomerization occurs at C-14 and C-17 in the $C_{29}$ 20S and 20R regular steranes, forming the ββ/(ββ+αα) ratio (Figure 19 D). This maturity parameter reached to somewhat higher maturity levels in comparison to 20S/(20S+20R) as the equilibrium is reached slower (Peters et al., 2005a). The values reached from zero to the equilibrium value around 0.67-0.71.

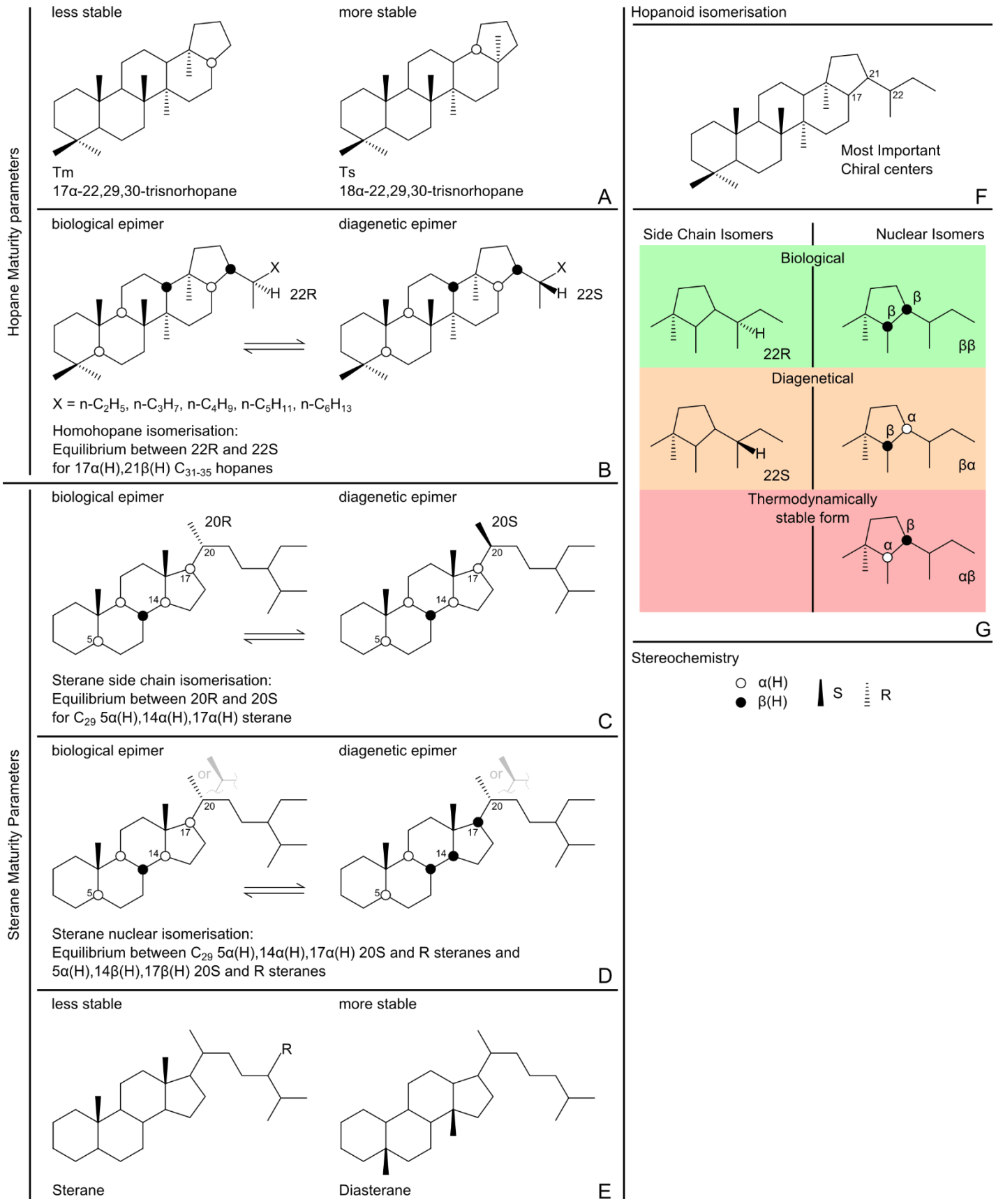


***Figure 19. Hopane and sterane maturity parameters (A-E) and hopanoid isomerisation (F, G; after Farrimond et al., 1998; Mackenzie, 1984)***

### 2.5.4.2 *Maturity assessment based on different thermal resistance of components*

Molecules of biological parentage were decomposed to related compounds by thermal stress. The degree of decomposition and so the ratio between the parental and the newly formatted component is related to the level of thermal stress the source-rock or oil has undergone. This allows using these ratios to assess the maturity of an oil or source-rock.

***Moretanes/hopanes***

The moretanes/hopanes ratio is based on the correlation between thermally less stable $C_{29}$ or $C_{30}$ 17β,21α(H)-moretanes to $C_{29}$ or $C_{30}$ 17α,21β(H)-hopanes. The ratio is controlled by different energy barriers and follows a reaction scheme discussed by Seifert and Moldowan (1980) (Figure 21).

The biologically imprinted initial molecule is the 17β,21β(H)-moretane. It therefore has the ββ configuration, which is thermally unstable, and usually absent in crude oils. The ββ-moretane converts to βα-moretane and αβ-hopane (Figure 20), overcoming the energy barriers $\Delta G_2$ and $\Delta G_1$. At higher temperatures and therefore at higher energy levels the conversion of βα-moretanes to αβ-hopanes and vice versa is possible with ββ-moretanes as intermediate step. This requires that the energy barriers $\Delta G_3$ and $\Delta G_4$ are overcome. As $\Delta G_4$ is higher than $\Delta G_3$, the resulting mixture will favour αβ-hopanes with increasing maturity with equilibrium by ~20:1 (Peters et al., 2005a). The moretanes/hopanes ratio will decrease from ~0.8 for immature samples to 0.15 for mature samples and will reach a minimum at 0.05 (Peters et al., 2005a; Seifert and Moldowan, 1980). This maturity parameter is useful for immature samples and covers the early oil generation.

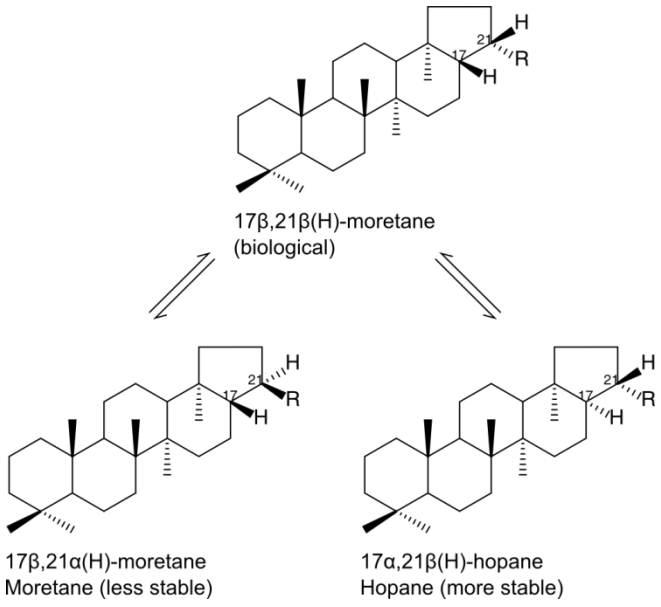


***Figure 20. Relationship between 17β,21β(H)-hopane,17β,21α(H)-moretane and 17α,21β(H)-hopane.***

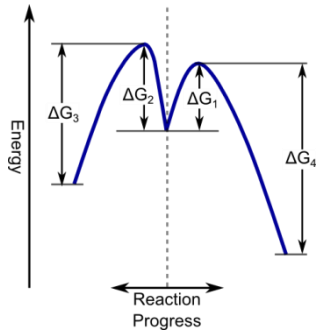


***Figure 21. Energy schematic for the moretane/hopane relationship (Seifert and Moldowan, 1980).***

***Ts/(Ts+Tm)***

Thermal stress caused a faster decomposition of the less stable $C_{27}$ 17α-22,29,30-trisnorhopane (Tm) in comparison to $C_{27}$ 18α-22,29,30-trisnorhopane (Ts) (Seifert and Moldowan, 1978) (Figure 19 A). The importance of catalytically effects by clay minerals is discussed in several studies and shown by the unusual values of Ts/(Ts+Tm) obtained from calcareous source-rocks (e.g. Price et al., 1987; Rullkötter et al., 1985).

***Table 7. Mono- and triaromatic steroids used for TA/(MA+TA) ratio.***

| Aromatic steroid | Compound |
|---|---|
| MA | $C_{29}$ 5α10β($CH_3$),20R,24R |
| | $C_{29}$ 5α10β($CH_3$),20R,24S |
| | $C_{29}$ 5α10β($CH_3$),20S,24R |
| | $C_{29}$ 5α10β($CH_3$),20S,24S |
| | $C_{29}$ 5β10β($CH_3$),20R,24R |
| | $C_{29}$ 5β10β($CH_3$),20R,24S |
| | $C_{29}$ 5β10β($CH_3$),20S,24R |
| | $C_{29}$ 5β10β($CH_3$),20S,24S |
| | $C_{29}$ dia-5β($CH_3$)10β,20R,24R |
| | $C_{29}$ dia-5β($CH_3$)10β,20R,24S |
| | $C_{29}$ dia-5β($CH_3$)10β,20S,24R |
| | $C_{29}$ dia-5β($CH_3$)10β,20S,24S |
| TA | $C_{28}$ 20R24R |
| | $C_{28}$ 20R24S |
| | $C_{28}$ 20S24R |
| | $C_{28}$ 20S24S |

***Diasteranes/steranes***

In the presence of acidic catalysts (e.g. acidic clays) sterenes are converted to diasterenes, the precursors of diasteranes (Peters et al., 2005a) (Figure 19 E). These are thermally more resistant as steranes, resulting in increasing values for this ratio with thermal maturation. Calcareous source-rocks have usually low content of diasteranes due to their lack of acidic clay minerals. However, several studies reported higher diasterane abundance in carbonate rocks leading to the assumption that also other acid mechanisms are possible for the conversion to diasteranes (e.g. Moldowan et al., 1991). Artificial maturation of source-rocks in the postmature range lead to a strong increase of the diasteranes/steranes ratio (Peters et al., 1990). This was explained either by direct rearrangement of steranes by hydrogen-exchange reactions without acidic catalysis (Rullkötter et al., 1984), or preferred destruction of steranes at high levels of maturity (Peters et al., 2005a). This maturity parameter is applicable in a range from early mature to early postmature.

### *2.5.4.3 Aromatic steroids*

***Monoaromatic steroid aromatization TA/(MA+TA)***

Monoaromatic steroids (MA) with C-ring aromatization convert to triaromatic steroids (TA) with ABC-ring aromatization during thermal maturation involving a loss of a methyl group at position C-10 and of the asymmetric centre at position C-5 (A/B-ring junction). The ration includes the major known C29 monoaromatic steroids (8 regular and 4 diasteroids) and four C28 triaromatic steroids (see Table 7).

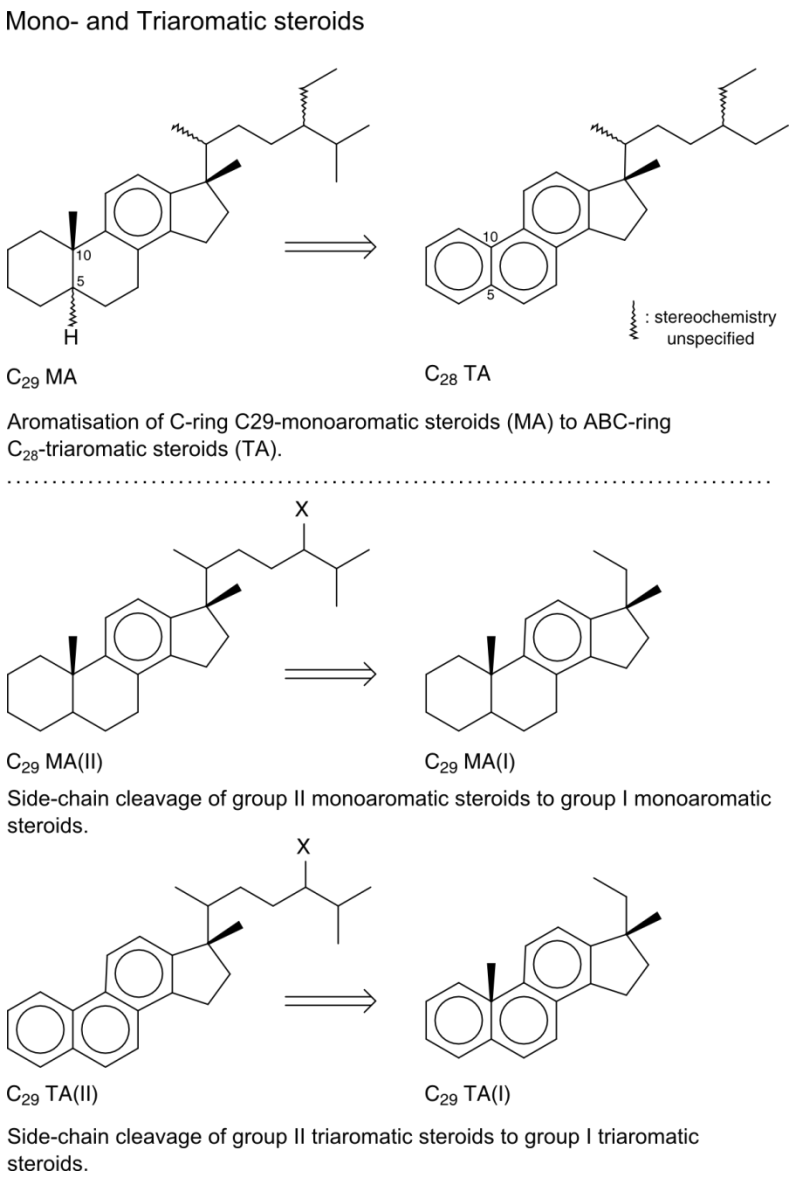


***Figure 22. Maturity parameter based on mono- and triaromatic steroids.***

In Hydrous pyrolysis a retaining effect was observed affecting mainly the triaromatic steroids. This was explained by charged sites on minerals, retaining preferred the more polar triaromatic steroids (Peters et al., 1990). Also discussed were effects of migration affecting the ratio (Hoffmann et al., 1984), mainly reasoned by the higher aromatization of triaromatic steroids. TA/(TA+MA) covered the immature to mature range.

***Conversion of group II MA and TA to group I MA and TA***

Side-chain scission affected both, monoaromatic steroids and triaromatic steroids with increasing thermal stress, leading to an increase of the short chain steroids in comparison to the long chain precursors (Mackenzie et al., 1981; Seifert and Moldowan, 1978). This increase could be caused by cracking-controlled conversion of long-chained steroids to short-chain steroids, greater thermal weakness of long-chain steroids, or both (Peters et al., 2005a).

For monoaromatic steroids the ratio is calculated as MA(I)/MA(I+II) and include for MA(I) $C_{21}$ and $C_{22}$ and for MA(II) the sum of the major $C_{27}$-$C_{29}$ monoaromatic steroids. In correspondence, the ratio for the triaromatic steroids is calculated as TA(I)/TA(I+II). TA(I) is formed by $C_{20}$ and $C_{21}$ and TA(II) included the sum of $C_{26}$-$C_{28}$ (20S+20R) triaromatic steroids (Peters et al., 2005a). MA(I)/MA(I+II) is applicable from an early mature to late mature range. Since triaromatic steroids are derived from monoaromatic steroids. TA(I)/TA(I+II) is applicable for a higher maturity.

# 3 Laboratory simulation of oil/gas generation and expulsion under near-natural conditions – the "Expulsinator" device

## 3.1 Abstract

Investigating generation and expulsion of hydrocarbon with pyrolysis is limited by methodologies incapable of simulating conditions close to those prevailing in natural systems. Destructive sample preparation, inappropriate pressure regimes and pyrolysis in closed mode and/or in the absence of water caused results not representative for natural processes. We here present a new approach for a laboratory scaled simulation of generation, primary migration and expulsion under natural conditions, using the "Expulsinator" device. Near-natural conditions have been realized by application of lithostatic pressure onto a source-rock disc with intact pore network and by hydrous pyrolysis, conducted in open flow through mode. The efficiency in generation and expulsion of this new methodology has been compared with established pyrolysis methodologies, like MSSV, HyPy, Rock Eval and closed small vessel pyrolysis (CSVP). Expulsinator experiments released higher amounts of bitumen than CSVP or HyPy. This has been attributed to increased cross-linking reactions of bitumen in case of the classic pyrolysis, favouring formation of pyrobitumen. Differences in yields and composition of *n*-alkanes were controlled not by generation (kinetics) exclusively but also by expulsion effects, in particular delayed expulsion via geochromatography. Expulsinator conversion rates of TOC exceeded 81 %, whereas those of hydrous CSVP remained at 65 %. Higher Expulsinator TOC conversion was accompanied by lower gas generation compared to CSVP. This has been attributed to the open setup of the expulsion experiment preventing secondary alteration of products, particularly polymerization to pyrobitumen and oil to gas cracking at higher temperatures. MSSV pyrolysis and HyPy of Expulsionator pyrolysis residues verified a low generation potential remaining after the expulsion experiment. In case of CSVP nitrogen and oxygen content of the pyrolyzate were enriched and sulfur content was lowered by interaction- between kerogen, bitumen, pyrobitumen and pyrite. The immediate removal of Expulsionator products by the mobile hydrous phase reduced such effects. The Expulsinator-device generates oil and gas generation data, which can be applied in numerical modelling exercises.

## 3.2 Introduction

Migration of expelled oil through the kerogen network will impact on its composition by desorption and adsorption effects. Hereby, for a given component, its absorption-capability in kerogen will increase with polarity. As a consequence, NSO's will adsorb more intensively than aromatics and the latter more than saturates (Sandvik et al., 1992; Thomas and Clouse, 1990c). After hydrocarbons have been released from kerogen, they first migrate through the source-rock and here interact with the mineral surfaces of the sediment. Active sides in clay minerals may cause fractionation of migrating oils by geochromatography (Krooss et al., 1991), though pore water or mineral-bound water could diminish this effect. Upon burial, a source-rock will be exposed to increasing lithostatic pressures causing micro- and macro-fractures within the rock. These fractures are pressure lows, where hydrocarbons will accumulate and form a single oil-phase. Therefore, micro- and macro-fractures represent important pathways for hydrocarbon phase flow (Dickey, 1975; Leythaeuser et al., 1988a; Littke et al., 1988; Pepper and Corvi, 1995a; Ungerer, 1990).

Water plays an important role in the genesis and migration of oil and gas, as it is supposed to reduce the rate of cross linking and to promote thermal cracking (Behar et al., 2003; Lewan, 1997; Lewan and Roy, 2011). Most commonly free radical reactions are used to explain decomposition of kerogen to hydrocarbons (e.g. Hoering, 1984; Lewan, 1997; Lewan and Roy, 2011; Michels et al., 1995; Weres et al., 1988). In this case water would act as exogenous source of hydrogen, support cracking reactions and reduce the generation of pyrobitumen (Lewan, 1997).

Pressure systems in source-rocks consist of a lithostatic and hydrostatic component. In oil and gas formation, a retardation effect of hydrostatic pressure has been observed, diminishing hydrocarbon yields via an increase of the activation volume by progressing pressure (Jackśon et al., 1995; Michels et al., 1995; Uguna et al., 2012). However, elevated hydrostatic pressure may exert a positive effect onto the alkane/alkene ratio of artificially generated petroleum (Weres et al., 1988). In laboratory simulation of oil and gas formation, an elevated hydrostatic pressure ensured the presence of liquid water instead of water vapour during pyrolysis. Supressed hydrocarbon vaporization led to intensified reactions among cracking products (Weres et al., 1988).

The conditions and experimental parameters described above define the boundary conditions for lab-scaled simulation of hydrocarbon expulsion and primary migration. In detail, these conditions are lithostatic pressure, hydrostatic pressure and the

presence of a coherent mineral matrix with an undestroyed kerogen network. A sample used for artificial expulsion must have sufficient lateral expansion, i.e. parallel to bedding plane. This allows investigation of geochromatography effects, those induced by micro- and macro-fracturing, and mineral-conversion reactions. Temperatures should be between 350 °C and 360 °C to accelerate the reactions to a time frame suitable for the laboratory (Lewan, 1997; Lewan et al., 1979).

In addition it has to be considered that natural systems are open for expelled hydrocarbons to migrate off, thus diminishing secondary cracking reactions. Only open pyrolysis will ensure to generate and release hydrocarbons compositionally unaltered by secondary reactions.

## 3.3 Technical description and methodology of the experiments

A laboratory simulation of the natural processes of generation, expulsion and primary migration has to cover the maximum of oil generation, which is equivalent to a burial depth of ~3000 m at a normal geothermal gradient of 33 °C/km (Bordenave, 1993; Tissot et al., 1987; Tissot and Welte, 1984). In a sedimentary basin, this usually equals lithostatic pressures between 680 to 920 bar and hydrostatic pressures between 290 to 320 bar (Sahay, 1999). In natural systems, the hydrocarbons generated and expelled will migrate and thus be removed from the kitchen area. This implies an open system solution to simulate a near-natural generation and expulsion of hydrocarbons.

### 3.3.1 Technical description of the expulsion simulation device

The specific demands of near-natural simulation of oil and gas expulsion required development of a suitable experimental device, in the following termed “Expulsinator”. A high-pressure reactor, capable of holding hydrostatic pressures up to 300 bar at a maximum temperature of 360 °C, facilitated oil and gas generation in the Expulsinator. The reactor was heated by a thermal jacket, adjustable at an accuracy of ±1 °C. The hydrostatic pressure was produced by an HPLC-pump with an accuracy of ±2 bar.

The Expulsinator received intact rock-samples with their authentic pore and kerogen network

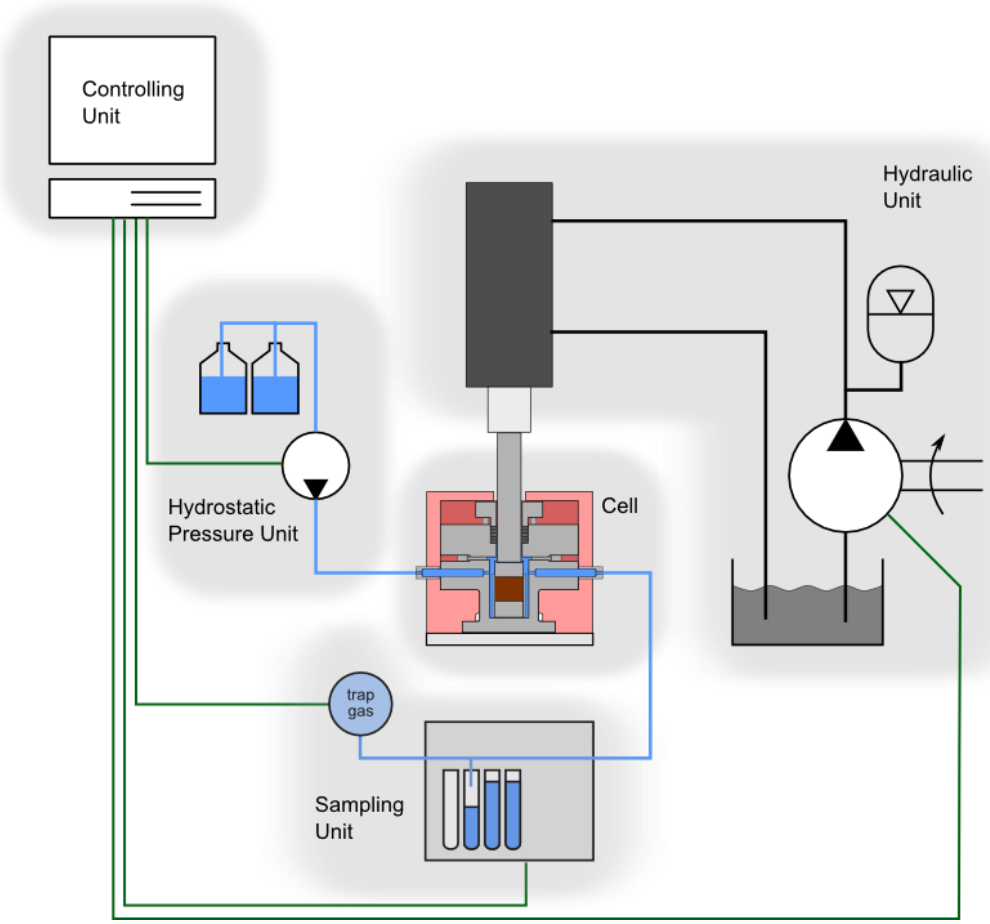


*Figure 23. Simplified schematic representation of the ”Expulsinator” device.*

preserved. Plugs with a diameter of 50 mm and a thickness of several cm can be employed. Overburden/lithostatic pressure was applied onto the sample by a hydraulic-driven piston, conducted through the specially designed reactor cap. The system worked at a maximal internal pressure of 250 bar, which was computer-controlled with an accuracy of ±2 bar. The effective lithostatic pressure acting upon the sample was measured indirectly and could be calculated according to the following equations:

$$P = \frac{F}{A} \tag{21}$$

$$P_{Lith} = \frac{P_{hydraulic} \cdot A_{cylinder}}{A_{sample}} \tag{22}$$

$P$ was the pressure, $F$ the force, and $A$ the area of the contact surface. Equation 22 was derived from equation 21 giving the relation between the lithostatic pressure ($P_{Lith}$), the hydraulic pressure ($P_{hydraulic}$) and the surfaces area of the hydraulic cylinder ($A_{cylinder}$) versus that of the sample ($A_{sample}$). A theoretical maximum lithostatic pressure of 2560 bar resulted for a cylinder diameter of 160 mm and a sample diameter of 50 mm. In our instrumental setup, the minimum internal hydraulic pressure was 25 bar, giving a minimum pressure of 256 bar acting on the sample.

The Expulsinator sampling unit facilitated continuous product collection in flow-through mode. For practical reasons, a semi-continuous collection of pyrolysis effluents over programmable time intervals was preferred. Fluids were collected at atmospheric pressure in gas tight vials. Gases were directed into a flask, filled with a sealing liquid. The gas volume produced was estimated by weighing of the displaced liquid. Reactor effluent recovery was optimized by activation of a release valve in case that the hydrostatic pressure exceeded the predefined value.

All units described above were computer controlled via a program developed with LabVIEW™. Pressures and temperatures could be preselected as constant values over time or as ramp function with freely selectable heating and pressure rates. The program not only operated the Expulsinator during autonomous experiments, but also recorded and stored all incoming data (pressures, temperatures, gas production).

***Implementation of an expulsion experiment***

Intact rock samples were used in Expulsinator experiments. Therefore, core plugs were drilled out of a rock plate by a low spinning drill bit. This prevented overheating while avoided cooling liquids, prone to cause pre-experimental swelling of clay minerals, like smectite and montmorillonite. Plugs were lathed parallel to final a sample dimension of 50 mm in diameter and between 18 and 30 mm in height. Sample weight varied between 70 and 100 g. The source-rock specimen was arranged in an assembly consisting of a metal sinter disk below and above the sample and a sinter metal sleeve surrounding the plug. These permeable units were supposed to act as artificial carrier beds. In order to avoid physical deformation and shearing of the rock plug by lithostatic pressure, the assembly was placed tightly into a stainless steel stabilization sleeve.

The cell interior and all parts installed within the cell (capillaries, sinter-filter tubes or discs and other parts) were cleaned carefully with DCM/MeOH (1:1) to remove organic contamination. Removable parts were annealed in a muffle furnace at 450 °C. Following placement of the cell assembly into the reactor, the latter was closed gas-tight and the piston adjusted. After filling the reactor with HPLC-grade water, a lithostatic pressure starting at 300 bar was applied onto the sample and the system was tested for tightness under a hydrostatic pressure of 100 bar. Subsequently, the programmed pressure (P) and temperature (T) program was executed. The P/T programme chosen depended on the scope of a particular experiment.

Products were collected continuously in a flow through mode for preselected intervals of 12 h. To flush out expelled hydrocarbons from the artificial carrier bed effectively, the flow rate of the HPLC-pump was increased for a short time period every 20 min. The volume of each flushing process was set to 4 ml, resulting in 144 ml of fluid sample recovered after 12 h.

Quantitative purging of fluid products from the artificial carrier bed into which they had been expelled required additional stimulation. Previous experiments had shown large deficits in the withdrawal efficiency of pure water. Only a small proportion of expelled oil was flushed out by pure water, whereas the major part (>80 %) remained within the cell due to its poor miscibility with the water phase, even at elevated temperatures of 360 °C. The oil expelled was retained within the pore space of the artificial reservoir by adhesion forces, because the amounts generated and expelled were insufficient to form a separate oil phase capable to overcome adhesion forces by buoyancy. To sequentially obtain oil when it had been expelled, a modifier (*n*-hexane/2-propanol 85:15) was pumped into the cell over defined short intervals to increase the system´s purge performance. The modifier was purged into the cell every 5 h for 45 min, corresponding to 4-6 ml. Residence time of the modifier within the cell was determined to < 2 h. The modifier stayed in direct contact with the source-rock surface for < 40 min. Based on the high lithostatic pressure and low permeable lithology, no invasion of the source-rock by the modifier was noted. Due to high temperature

prevailing inside the cell, 2-propanol partly dehydrated to propene and oxidized to acetone. The artefact formation of propene interferes with the analysis of gases generated upon source-rock maturation. In future experiments, alternative modifiers with 6 to 9 carbon atoms will be employed.

After experiment termination, the Expulsinator cooled down passively to ambient temperature. Remaining water was removed and collected from the cell and the residual plug was dismantled carefully by a removal tool for further examination. The interior of the cell, as well as the cell assembly, were dried and rinsed with DCM/MeOH (93:7) to recover residual oil. Gas samples were taken as an aliquot from the collecting flask and transferred into a headspace vial.

The collected fluids represented oil-water emulsions, which were separated into a water and an organic phase by liquid-liquid extraction with DCM. The resulting extract encompassed the $C_{10}$ to $C_{40}$ components. Compounds in the carbon range of $C_6$ to $C_9$ could not be recovered due to the liquid extraction step.

An aliquot of artificially matured source-rock was ground and solvent-extracted by Accelerated Solvent Extraction (ASE) (50 bar, 75 °C) with DCM/MeOH (93:7) to recover non-expelled hydrocarbons. The extract residue was analysed by Rock-Eval and elemental analysis for the composition of the bulk organic matter after completion of the experiment.

### 3.3.2 Comparative pyrolysis experiments

In order to validate the Expulsinator procedure, a suite of experiments employing other established pyrolysis methods were performed on the same source-rock. Details of pyrolysis procedures are given below. Briefly, closed hydrous and anhydrous pyrolysis was conducted as closed small vessel pyrolysis (CSVP) and microscale sealed vessel pyrolysis (MSSV). Open pyrolysis was performed as fixed-bed hydropyrolysis (HyPy) and Rock Eval. The experiments were conducted with pre-extracted rock samples (CSVP) and with decalcified material (MSSV, HyPy) in order to increase the kerogen content for pyrolysis. Additionally, experiments were performed using residue from the expulsion experiments in order to estimate the remaining potential after the simulation (Rock Eval, HyPy, MSSV; see Table 8).

To obtain sufficient quantities of pre-extracted material, ground and homogenized sediment was solvent extracted twice with a Büchi SpeedExtractor E-914 at 50 bar and 75 °C with DCM/MeOH(93:7) as solvent mixture. The extracted sediment was recovered, dried, homogenized and then employed in artificial maturation experiments. The amount of extracted bitumen was determined gravimetrically.

***Table 8. Method validation experiments.***

| | pre-extracted | pre-extracted & decalcified | untreated sample | residue of expulsion experiments |
|---|---|---|---|---|
| **CSVP** | x | | | |
| **MSSV** | | x | | x |
| **HyPy** | | x | | x |
| **Rock Eval** | | | x | x |

For decalcification, the sample was weighed into a glass-centrifuge tube and hydrochloric acid (HCl) (25 %) was added until reaction ceased. Then, the sample was centrifuged, the acid phase removed and the sample washed with water (HPLC-grade) several times until pH-neutral. Finally, the sample was dried in an oven at 80 °C for 48 h.

***Closed hydrous and anhydrous pyrolysis***

For CSVP, stainless steel tubes of 30 ml volume were used. Two different pyrolysis procedures were executed in CSVP to allow comparison with the expulsion treatment. Standard continuous pyrolysis (single-step) or stepwise pyrolysis (multi-step) were conducted. The latter was carried out with the intention to match better to Expulsinator conditions, concerning the removal of generated hydrocarbons. Both types were performed as hydrous and anhydrous pyrolysis. For both sets of experiments, the temperatures applied were identical and ranged from 210 °C to 360 °C in 30 °C steps and finally to 375 °C. For single-step pyrolysis, 3 g of immature pre-extracted sediment was used for each temperature level. In case of the multi-step procedure, sample material already pyrolyzed in the previous step was solvent-extracted, an aliquot (500 mg) was retained for further analysis and the residual material was re-applied in the next pyrolysis step. The initial quantity of the sample material in case of the multi-step pyrolysis was 8 g. Apart from the differences described above, the experimental procedure for both CSVP-variants was identical. The vessels were cleaned with DCM/MeOH (1:1) and annealed in a muffle furnace at 450 °C before pyrolysis. The vessels were loaded with powdered source-rock and, in case of hydrous pyrolysis, 20 ml water (HPLC-grade) was added. The headspace was evacuated with nitrogen and reactors were closed tightly. Then the vessels were heated at a rate of 25 °C/min to the aimed temperature, which was kept constant for 72 h.

The weights of the vessels were recorded before and after the pyrolysis. In case of divergence to the

starting weight, the sample was discarded due to leakage. After the termination of the experiment, liquid and solid samples were removed and processed for analysis. Gaseous samples were not collected.

In case of hydrous CSVP, the product was filtered to separate the liquid phase from the residual rock followed by liquid-liquid extraction to separate the organic from the water phase. The still-wet filter cake was first rinsed with MeOH and afterwards with DCM/MeOH (1:1) to obtain bitumen still bound to the mineral surface. Since solvents absorb? water during the rinsing process, they were dried afterwards over a molecular sieve (3 Å). The filter cake was dried at 80 °C for 48 h and subsequently extracted with ASE (50 bar, 75 °C; DCM/MeOH (93:7)). Extracts from liquid-liquid extraction, from rinsing and from ASE-extraction were merged, concentrated and prepared for further analysis.

For anhydrous CSVP, the solid rock residue was extracted by ASE (50 bar, 75 °C; DCM/MeOH (93:7)), to obtain the bitumen generated and expelled. The vessels were rinsed with DCM/MeOH (7:3), extract and rinsing fluids merged, concentrated and prepared for further analysis. The residual rock was analysed with Rock-Eval and elementary analysis after extraction.

The methodology for MSSV corresponds largely to the procedure described in Horsfield et al. (1989). An aliquot of 5-18 mg of sample material was weighed into glass tubes (ca. 40 µl volume) together with glass beads and flame-sealed under helium. Glass tubes and beads had been previously cleaned by annealing. The sealed glass tubes were placed into a furnace and heated for 72 h at 300 °C, 330 °C, 360 °C and 390 °C. Due to the low remaining HC-generation potential of the source-rock residue recovered after the expulsion experiments, high amounts of sample material were used. This led to high gas pressures especially at 390 °C, which caused bursting of tubes. Therefore, 390 °C-MSSV only succeeded for the immature sample, where less material had been employed. Analysis was performed with a GC-FID equipped with a purpose-build sample holder. This enabled crushing the glass tubes and releasing the pyrolyzates under a helium stream (30 ml/min) at elevated temperatures of 300 °C. The hydrocarbons were collected in a cooling trap, operated with liquid nitrogen. After collecting, the trap was heated from -196 °C to 300 °C in 30 sec and the hydrocarbons transferred onto the GC-column.

***Open anhydrous pyrolysis***

For HyPy ca. 250 mg of pre-extracted and decalcified sample was mixed with 25 mg sulfided molybdenum catalyst as reaction accelerator (Bolton et al., 1988, 1987; Carter et al., 1994; Robinson et al., 1991; Snape et al., 1991) and 250 mg quartz sand to break up the mixture. This was placed on a sample bed in the middle of a reactor tube. The pyrolysis was performed with a constant hydrogen flow of 5-6 L/min and a pressure of 145 bar. First the sample was heated to 250 °C at 50 °C/min and then to 500 °C at 8 °C/min. Hydropyrolyzates generated were flushed out by the gas stream and adsorbed directly onto a bed of silica.

The silica gel was extracted by ASE (50 bar, 75 °C; DCM/MeOH (93:7)) and the pyrolyzed rock residue analysed by Rock-Eval.

The methodology of the Rock-Eval analysis has been described in detail (Espitalie et al., 1986, 1985a, 1985b; Espitalié et al., 1977). For Rock-Eval pyrolysis 20 - 100 mg of untreated sample was used. The sample was heated isothermally at 300°C for 3 min to release free hydrocarbons measured by FID to give the $S_1$-peak (mg HC/g rock). Temperature was then raised to 550 °C at 25 °C/min. Hydrocarbons released by thermal decomposition of kerogen were measured by FID to give the $S_2$-peak (mg HC/g rock). The temperature of maximum pyrolysis yield was recorded as $T_{max}$ (°C). Organic oxygen compounds decomposed to $CO_2$ between 300 °C and 390 °C were measure by TCD, to give the $S_3$-peak (mg $CO_2$/g rock).

### 3.3.3 Analytical processing

***Elemental analysis***

For determination of total carbon (TC), total sulfur (TS) and total nitrogen (TN) samples were analysed by a VARIO EL III elemental analyser. To measure the total inorganic carbon (TIC), the analyser was equipped with a TIC-module in which the sample carbonate was dissolved by HCl (10%) at 50 °C. The released $CO_2$ was purged from the reactor by He, and measured by TDC to give the inorganic carbon content.

***Compound class separation***

For GC-analysis, the extracts were separated into an aliphatic, an aromatic and a NSO-fraction. Separation was carried using 8 ml SPE-columns with 4 ml of activated silica gel as stationary phase. 5 mg of extract dissolved in DCM were sorbed on silica gel and applied onto the column, which had been conditioned with 20 ml of *n*-hexane. Aliphatics were eluted with *n*-hexane (5 ml), aromatics with *n*-hexane/DCM (3:1; 6 ml) and the NSO-fraction with DCM/MeOH (1:1; 6 ml).

***GC-FID and GCMS measurement***

Extract fractions were analysed on an Agilent 7820A GC coupled to a 5975 MSD mass-spectrometer. The GC was equipped with a HP 5 fused silica capillary column (5 % phenyl, 95 %

methylsilicone) of 30 m length, 0.25 mm inner diameter and 0.25 µm film thickness. Helium flow was set to 1.5 ml/min. The GC-oven was programmed as followed: 60 °C isothermal for 5 min, heating to 325 °C at 4 °C/min and held constant at 325 °C for eight minutes.

For MSSV a SGE forte BP1 column was used (50 m length, 0.32 mm inner diameter and 1 µm film thickness). Helium flow was set to 2.5 ml/min. The GC-oven was programmed as followed: 40 °C for 13 min, heating to 320 °C at 5 °C/min and isothermal for 25 min.

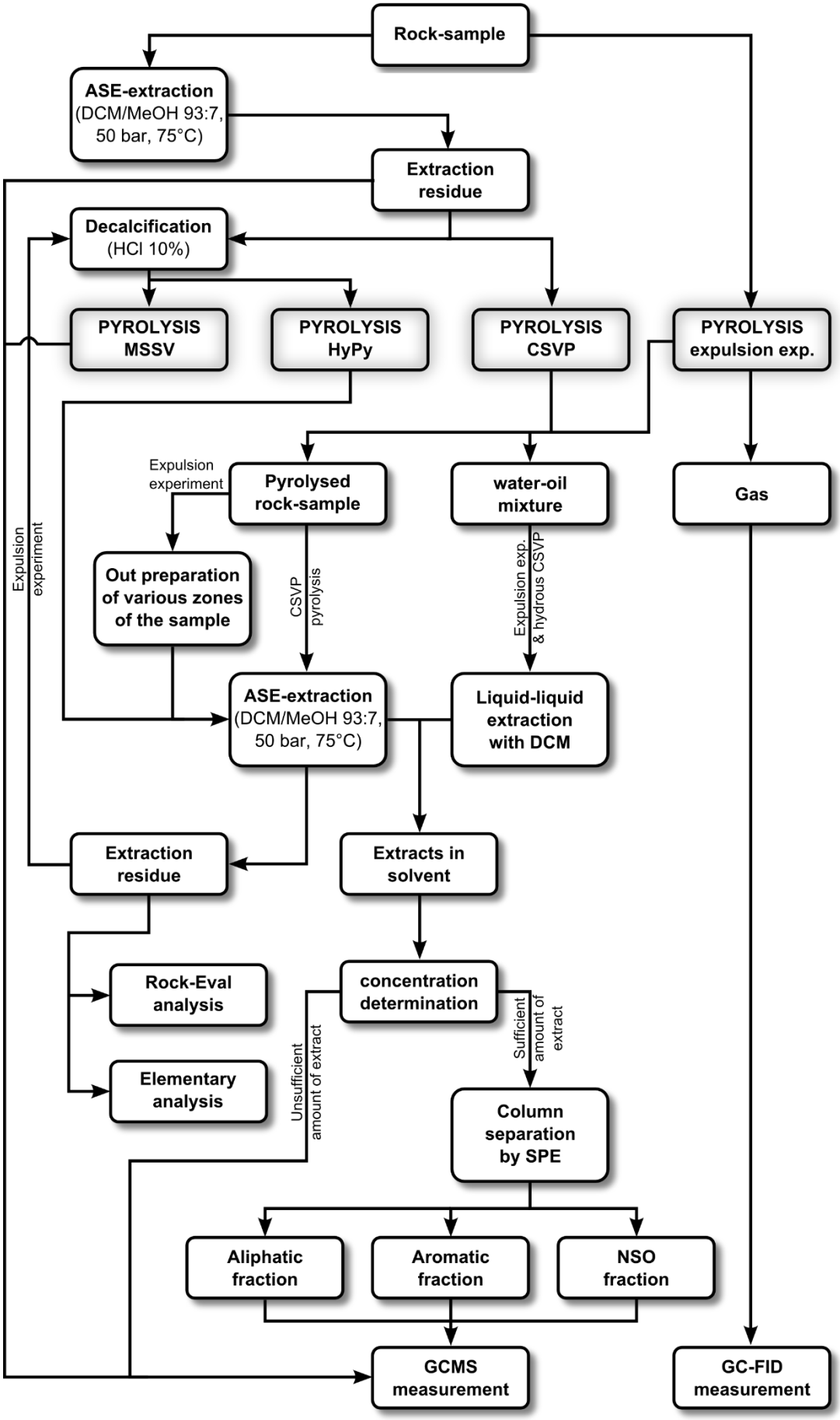


***Figure 24. Experimental flow chart with pyrolysis procedures, sample collection, processing and measurement.***

## 3.4 Sample description

For implementation of generation and expulsion simulation, sample material was selected to fulfil the following parameters. An immature source-rock with high contents of OM and well-known composition was required. To compare results from multiple experiments, large quantities of homogenous material were needed. Considering this requirements, Posidonia Shale from the HOLCIM quarry near Dotternhausen (SW-Germany) was selected. This source-rock was deposited during the Lower Toarcian, a period characterized by extensive transgression (Frimmel et al., 2004; Röhl et al., 2001) over a shallow shelf area. Under restricted water circulation, anoxic areas developed during extended episodes, leading to sedimentation of thick black shale deposits.

Posidonia shale from the HOLCIM quarry has high initial TOC-values of up to 15 % at low maturity ($T_{max}$ from 411 °C to 433 °C). According to Frimmel et al. (2004) the black shales provide high HI (>700 mg HC/g TOC) and low OI values (< 20 mg $CO_2$/g TOC). Three lithostratigraphic units show particularly high TOC values, caused by excellent preservation and high production. The units are located in the exaratum and elegans subzones of the falciferum ammonite zone (Riegraf, 1985). Samples used in this study originated from upper exaratum to lower elegans ammonite subzone. Plugs (K01206 and K001207) were drilled from rock plates with a thickness of 40-100 mm. Both rock-samples gave high TOC and HI but low OI values at relatively

***Table 9. Bulk parameter of the used Posidonia shale (cf=carbonate free).***

| | K001206 | K001207 |
|---|---|---|
| ***carbonate [%]*** | 34.6 | 19.5 |
| ***TOC [%]*** | 9.75 | 10.76 |
| ***$TOC_{cf}$ [%]*** | 14.91 | 13.36 |
| ***S [%]*** | 3.68 | 4.66 |
| ***$S_{cf}$ [%]*** | 5.62 | 5.79 |
| ***$S_1$ [mg HC/g rock]*** | 4.78 | 4.68 |
| ***$S_2$ [mg HC/g rock]*** | 67.39 | 78.63 |
| ***$T_{max}$ [°C]*** | 427 | 428 |
| ***HI [mg HC/g TOC]*** | 686 | 731 |
| ***OI [mg $CO_2$/g TOC]*** | 7 | 11 |
| ***extract [mg/g TOC]*** | 95.6 | 108.7 |

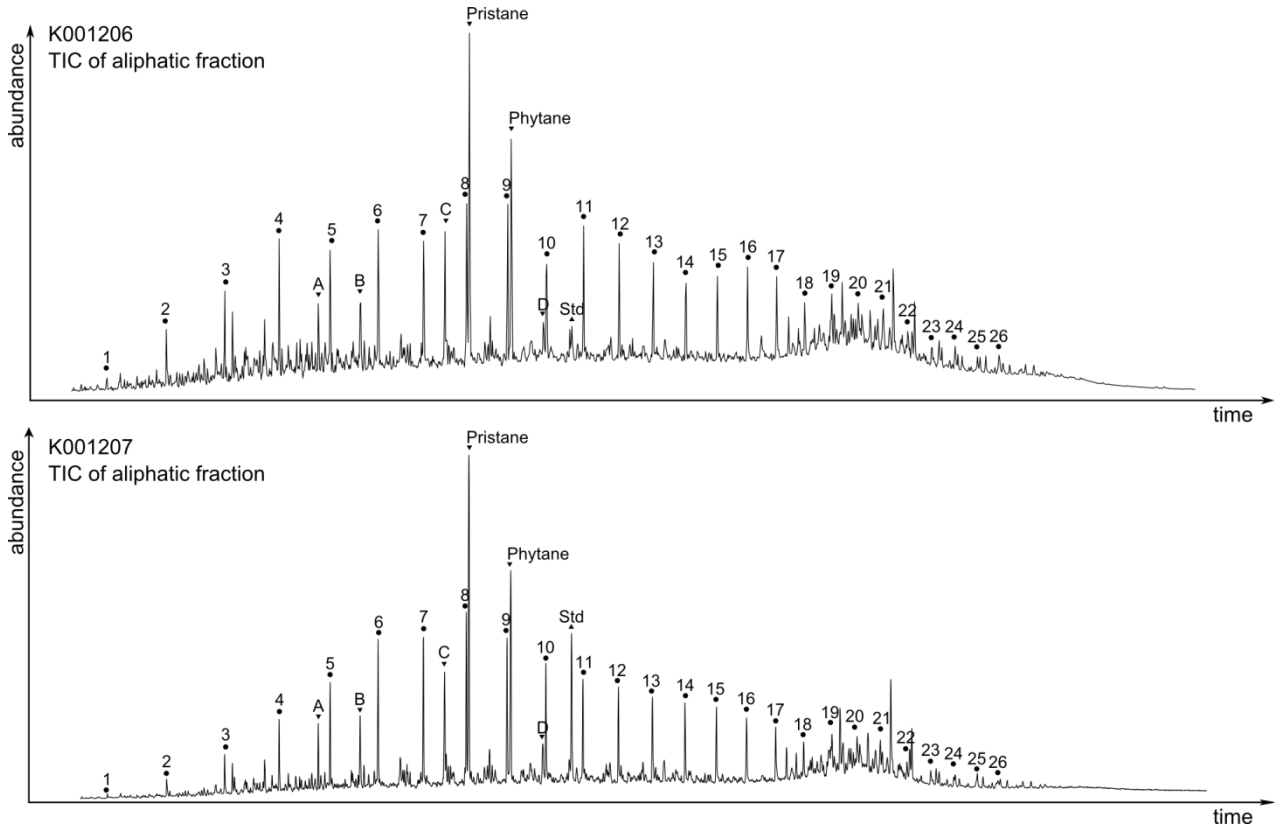


***Figure 25. Chromatograms depicting aliphatic hydrocarbons of untreated Posidonia Shale. Numbers denote n-alkanes (1-26: $nC_{10}$ – $nC_{35}$). A: farnesane, B: $C_{16}$-isoprenoid, C: norpristane, D: $C_{21}$-isoprenoid.***

*Table 10. Experimental conditions applied in expulsion experiments.*

| | | Stage 1 | Stage 2 | Stage 3 | Stage 4 |
|---|---|---|---|---|---|
| **Exp. A** | Duration | 72 h | 72 h | 120 h | - |
| | Temp. | 300 °C | 330 °C | 360 °C | - |
| | hyd. P. | 200 bar | 250 bar | 300 bar | - |
| | lith. P. | 600 bar | 750 bar | 900 bar | - |
| **Exp. B** | Duration | 48 h | 48 h | 48 h | 101 h |
| | Temp. | 210 °C | 260 °C | 310 °C | 360 °C |
| | hyd. P. | 150 bar | 200 bar | 250 bar | 300 bar |
| | lith. P. | 450 bar | 600 bar | 750 bar | 900 bar |

low $T_{max}$-values (Table 9) confirming a type I/II kerogen type. Both samples had similar bulk and molecular organic composition (Table 9, Figure 25), allowing for comparison of results.

## 3.5 Efficiency of formation and expulsion

Laboratory experiments, simulating generation and expulsion as described here, represent a new approach to converge towards natural conditions of oil and gas formation. Expulsinator efficiency of generation and expulsion is compared to established classic pyrolysis methodologies. Two Expulsinator experiments, characterized by a stepwise parallel increase of temperature, hydrostatic and lithostatic pressure are supposed to mimic dia/catagenesis in a near-natural fashion. Comparison with other pyrolysis methods is facilitated by an identical stepwise increase of maturation in those experiments.

Experiment A was carried out with a starting temperature of 300 °C and pressure conditions corresponding to a depth of ~2000 m ($P_{lith}$: 600 bar; $P_{hyd}$: 200 bar). These conditions were kept constant for 72 h. Subsequently the temperature was raised by 30 °C to 330 °C and the pressures were increased to $P_{lith}$ of 750 bar and $P_{hyd}$ of 250 bar (corresponding burial depth ~2500 m) and held constant for 72 hours. In the final step, the temperature was set to 360 °C and the pressures corresponded to a depth of ~3000 km ($P_{lith}$: 900 bar; $P_{hyd}$: 300 bar). This final stage was kept constant for 120 h, or until expelled hydrocarbon yields reached a minimum. To simplify the comparison between the Expulsinator experiments, a theoretical linear heating and pressure rate from the stepwise increase was calculated by forming a regression for the different parameters:

$$T = 0.42\ {}^{°C}/_{h} \cdot t + 285\ °C \quad (23)$$

$$P_{Lith} = 2.08\ {}^{bar}/_{h} \cdot t + 525\ bar \quad (24)$$

$$P_{hyd} = 0.69\ {}^{bar}/_{h} \cdot t + 175\ bar \quad (25)$$

$$\{t \in \mathbb{R} \mid t < 180\ h\}$$

Experiment B included lower temperature and pressure ranges and shorter time intervals (48 each, with the exception of the last stage), representing faster theoretical heating and pressure rates. Starting temperature was 210 °C at a simulated depth of ~1500 m ($P_{lith}$: 450 bar; $P_{hyd}$: 150 bar). Following this stage heating to 260 °C corresponded to a depth of ~2000 m ($P_{lith}$: 600 bar; $P_{hyd}$: 200 bar). Temperature was then increased to 310 °C to reach a simulated depth of ~2500 m ($P_{lith}$: 750 bar; $P_{hyd}$: 250 bar). Finally, the temperature was increased to 360 °C at a depth of ~3000 m ($P_{lith}$: 900 bar; $P_{hyd}$: 300 bar). This was held constant for 108 h. The theoretical linear heating and pressure rates are as followed:

$$T = 1.04\ {}^{°C}/_{h} \cdot t + 185\ °C \quad (26)$$

$$P_{Lith} = 3.13\ {}^{bar}/_{h} \cdot t + 375\ bar \quad (27)$$

$$P_{hyd} = 1.04\ {}^{bar}/_{h} \cdot t + 125\ bar \quad (28)$$

$$\{t \in \mathbb{R} \mid t < 168\ h\}$$

*Table 11. Deviation in extract yield between hydrous and anhydrous CSVP.*

| | Difference between hydrous & anhydrous CSVP | |
|---|---|---|
| | **single-step** | **multi-step** |
| **300°C** | 114 % | -3 % |
| **330°C** | 22% | 39 % |
| **360°C** | 52 % | 31 % |
| **375°C** | 103 % | 34 % |

### 3.5.1 Extract yields and thermal maturation levels

In comparison to classic pyrolysis methods, the expulsion experiments showed large differences concerning the generation and expulsion efficiency. This is evident from extract yields shown in Figure 26.

The diagram depicts the total amounts of extractable hydrocarbons of expulsion experiment A and B compared to the total extract yields of hydrous and anhydrous CSVP and to HyPy at 500 °C.

The different temperature and pressure steps of expulsion experiments were interpreted by defining

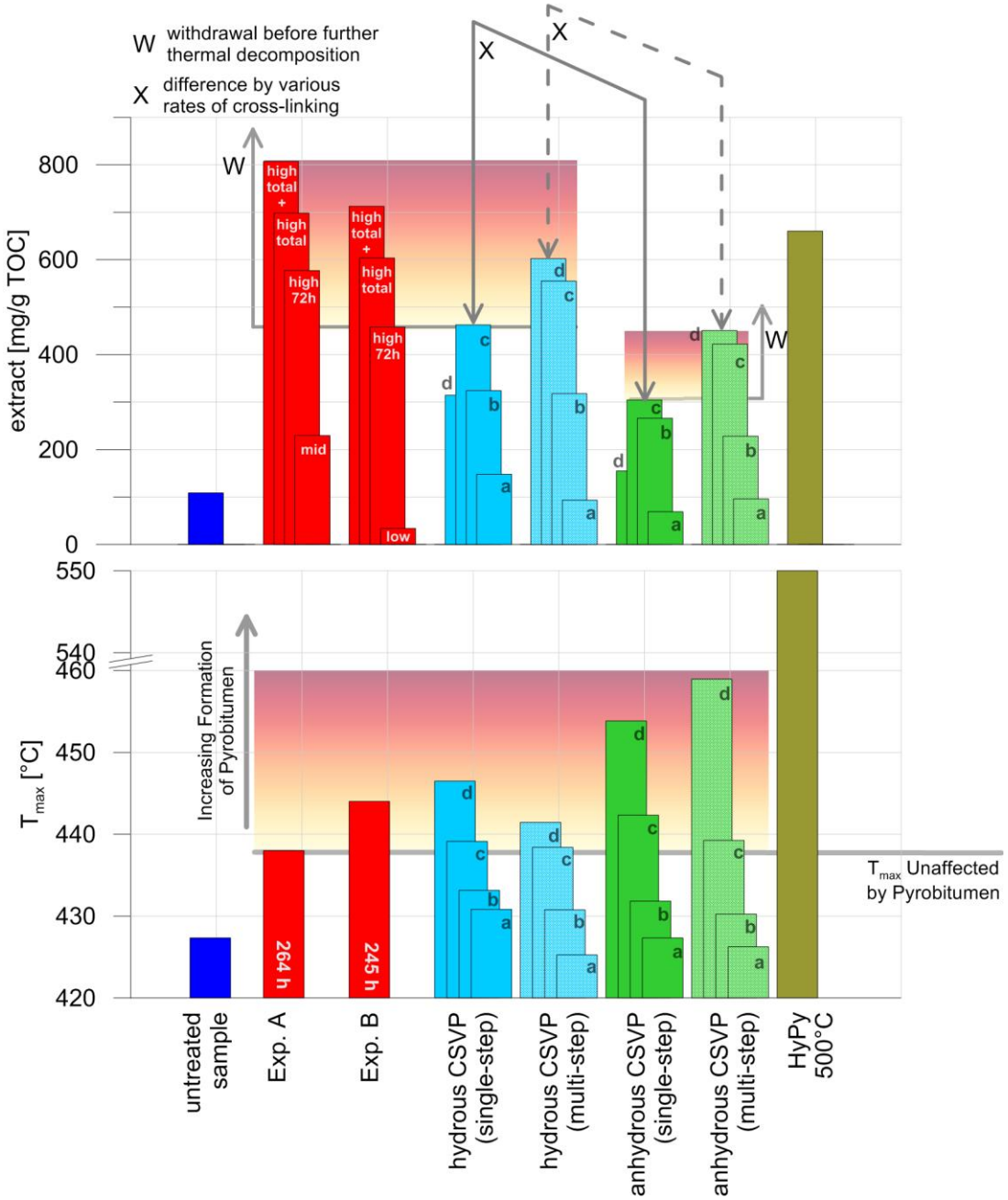


***Figure 26. Extract yields (above) and $T_{max}$ values (below) of pyrolyzates. Expulsion experiments are labelled A and B. Abbreviations as below:***

| | |
|---|---|
| ***Expulsinator experiments*** | ***low ≤ 310 °C; mid ≤ 330 °C; high ≤ 360 °C (calculated cumulatively after substraction of UT-extract, except for exp. A at 300 °C due to UT exceeding expelled extract yield)***<br><br>***For high stage indices denote: 72h = yield accumulated over low and mid stage plus the first 72 h at 360 °C, compatible with CSVP duration; total = yield accumulated over entire pyrolsis experiment; total+ = total plus extract yield of UT.*** |
| ***CSVP*** | ***a: 300 °C, b: 330 °C, c: 360°C, d: 375 °C (each for 72 h). Extract yields of single-step CSVP were calculated cumulatively.*** |

sets of equal temperature. To enable comparison of CSVP conducted over 72 h with Expulsinator experiments, Expulsinator yields up to 360 °C were cumulated. CSVP-experiments were performed with pre-extracted material, which was impossible in Expulsinator experiments employing intact source-rock plugs. Therefore, extract yield of the untreated sample was subtracted from the Expulsinator yields. All expulsion experiments performed at low start temperatures (≤ 310 °C) show poor extract yields for the lower temperature range. The extract yields of the low-temperature stages did not reach the extract quantities of the untreated sample ($E_{UT}$). This can be explained by time delays caused by mineral interaction or retardation effects and low expulsion efficiency at low-pressure conditions. Since subtraction of the extract yields of the untreated sample from the yields of low-temperature stages would result in negative values, these temperature stages were not shown in Figure 26.

The CSVP-experiments gave results as previously described. Hydrous CSVP generated larger amounts of extractable material in comparison to anhydrous CSVP. This was evident for all temperature steps, but especially pronounced at a low temperature of 300 °C and at higher temperatures of 360 °C and 375 °C (Table 11). The effect is less distinct in multi-step pyrolysis. This difference has been observed in several studies (e.g. Andresen et al., 1993; Koopmans et al., 1999; Kuangzong et al., 1994; Uguna et al., 2012). A comparative “hydrous versus anhydrous closed pyrolysis” study of lignite up to 350 °C resulted in differences in yields of up to 70 % (Behar et al., 2003). In CSVP-experiments of our study the addition of water increased the extract yields by 52 % at 360 °C and by 103 % at 375 °C pyrolysis temperature.

The reason for these large differences in pyrolyzate yields was seen in increased cross-linking reactions of bitumen in anhydrous pyrolysis, favouring formation of unsolvable pyrobitumen (Behar et al., 2003; Koopmans et al., 1998; Lewan and Roy, 2011). This was previously explained by free radical reactions (Jin et al., 2009; Lewan, 1997; Weres et al., 1988), where hydrogen is abstracted from bitumen. In case of hydrous pyrolysis, thermal cracking led to β-scission of the neoformed free radicals by incorporation of hydrogen delivered by water. In the absence of water as hydrogen donor, cross-linking occurred between radical sites and adjacent carbons, leading to aromatized, cyclic compounds (Lewan, 1997). Extract yields of multi-step CSVP exceeded that of single-step CSVP, because products generated were withdrawn, avoiding further thermal decomposition. Hydrous multi-step CSVP reached 20 % higher extract yields at 360 °C than hydrous single-step CSVP. For anhydrous CSVP, this difference was even higher with 39 %, due to intensified formation of pyrobitumen. The latter was seen as one reason for decreasing extract yields at 375 °C, both for anhydrous, as well as for hydrous single-step CSVP.

The other reason was propagated oil to gas cracking at 375 °C, a process requiring high pyrolysis temperatures (≥ 365 °C) for a minimum of 72 h (Lewan et al., 2008). This leads to rates of thermal cracking exceeding those of generation (Curry, 2003). Due to cumulative calculation of extract yields for multi-step CSVP, the calculated pyrolyzate yields increased even for 375 °C experiments.

$T_{max}$-values of the CSVP-experiments supported the observation of pyrobitumen formation favoured under anhydrous conditions. In general, the $T_{max}$-values of experiment A and B and of the CSVP-experiments were only slightly higher compared to the initial value of the sample ($T_{max\text{-}UT}$=428 °C). Low $T_{max}$-values remaining invariant at different pyrolysis maturity levels are typical for type-I kerogen (e.g. Huizinga et al., 1988; Lewan and Roy, 2011; Tissot et al., 1987). The Posidonia Shale comprised a mixture of type-I and type-II kerogen and seemed to respond like a type-I kerogen concerning $T_{max}$-values.

Due to its graphitic structure (Bordenave, 1993), pyrobitumen represents a fraction with high thermal resistance compared to residual kerogen (Huc et al., 2000). A high pyrobitumen content with a simultaneously lower amount of kerogen preserved will result in higher $T_{max}$-values. The $T_{max}$-values of CSVPs met these expectations at higher temperatures (>360 °C), when pyrobitumen exerted a higher impact on the $T_{max}$-value. For hydrous CSVP at 360 °C however, $T_{max}$ revealed no evidence for pyrobitumen formation, neither for single-step ($T_{max}$=439 °C), nor for multi-step CSVP ($T_{max}$=438 °C). At 375 °C the formation of pyrobitumen was recognized by elevated $T_{max}$-values in hydrous CSVP, especially for single-step ($T_{max}$=446 °C) when compared to multi-step ($T_{max}$=441 °C) pyrolysis. This was attributed to effective removal of early released bitumen by multi-step pyrolysis, preventing further thermal alteration of bitumen to pyrobitumen in case of multi-step CSVP. For anhydrous pyrolysis at 360 °C the $T_{max}$ increased via pyrobitumen to 442 °C (single-step) and 439 °C (multi-step). The strongest increase in $T_{max}$ by pyrobitumen formation was observed at 375 °C. For anhydrous single-step CSVP, $T_{max}$ reached 454 °C and for multi-step CSVP 459 °C. The fact that $T_{max}$ in anhydrous multi-step CSVP was higher than in single-step CSVP was caused by incomplete generation and removal of bitumen in preceding temperature steps.

The HyPy experiment represented a special case concerning both extract yield and $T_{max}$-value. The extract yield exceeded the yields in hydrous and

anhydrous CSVP, but not the yields of Expulsinator experiments. $T_{max}$-values were not comparable due to 500 °C reached in HyPy experiments, thus approaching the maximum of the measurable $T_{max}$-value by Rock Eval pyrolysis (550 °C). The use of a catalyst ensured high conversion rates and led to high extract yields and low amounts of residual hydrocarbons. Differences to the Expulsinator in liquid extract yields could have been caused by higher rates of gas generation in HyPy at pyrolysis temperatures of 500 °C.

Comparison of experimental expulsion methods revealed large differences. The highest expulsion yield was obtained in Expulsinator experiment A. This applied to both the yield after 72 h at 360 °C and the total yield. The yields of exp. B however remained behind, both in yield after 72 h at 360 °C and in total yield. The difference in the extract yields between experiments A and B could not be explained by the marginally longer duration of experiment A. The reason inferred was an imbalance between generation and expulsion rate in experiment B. Due to ineffective generation at low temperature stages at the onset of experiment B, the amount of hydrocarbons generated was exceptionally high when approaching 360 °C pyrolysis temperature. Therefore, the generation rate exceeded the expulsion rate (e.g. by exceeding the capacity of migration avenues) and led to accumulation of hydrocarbons generated within the rock´s pore space and absorbed within the kerogen polymer, where it was exposed to further thermal decomposition. Moderate heating rates in exp. A resulted in the highest extract yields. In this experiment, the production exceeded the expulsion rate at no time, resulting in almost 100 % of the hydrocarbons produced to be expelled. This was reflected in the $T_{max}$-values of experiments A and B (Figure 26). Experiment A reached a $T_{max}$ of 438 °C after pyrolysis, which corresponded to the value reached by hydrous multi-step CSVP. Experiment B showed elevated $T_{max}$-values of 444 °C: respectively, interpreted as an indication that bitumen had been trapped within the source-rock during pyrolysis. This caused thermal bitumen alteration, producing pyrobitumen of higher thermal stability.

Comparing the extract yields of Expulsinator experiments with CSVP, revealed larger quantities of extractable material obtained by the former method. After 72 h at 360 °C, experiment A produced 25 % more extract than hydrous single-step CSVP and 4 % more extract than hydrous multi-step CSVP. The total extract yield in experiment A was 51 % higher than in hydrous single-step CSVP at 360 °C and 16 % higher than in hydrous multi-step CSVP at 375 °C. Due to formation of pyrobitumen, the yields of experiment B were not as high as from experiment A. However, the total extract yields of experiment B exceeded the yields reached by hydrous single-step CSVP at 360 °C by 30 % and those of hydrous multi-step CSVP at 375 °C by 0.2 %. Only for the interval at 330 °C, the yields of experiment A are lower than in CSVP. This could be due to lower Expulsinator efficiency caused by lower lithostatic pressure, which reduced the generation of migration pathways in form of fractures. The differences of the yields between Expulsinator experiments and CSVP at 360 °C were mainly produced by higher rates of cross-linking and pyrobitumen formation in CSVP.

The distribution and yield of *n*-alkanes generated and released in Expulsinator experiment A and CSVP is shown in Figure 27. Recovery rates of short-chain *n*-alkanes were highly affected by different sample treatment after the pyrolysis. To ensure comparability between Expulsinator experiments and CSVP, the varying impact of processing needed compensation. Therefore, a recovery standard (deuterated $nC_{14}$ and $nC_{24}$) had been added to samples in CSVP and Expulsinator experiments.

This allowed calculation of the evaporative loss during work-up. Respective loss of CSVP and experiment A was corrected using anhydrous CSVP as reference, as this methodology showed the lowest evaporative loss of *n*-alkanes. To calculate correction factors for evaporative loss of each *n*-alkane from $nC_{10}$ to $nC_{23}$, a linear equation was formed. First, the average of the ratio of $nC_{24}$ to $nC_{14}$ is calculated (29) for every methodology used. The evaporative loss factor for $nC_{14}$ in relation to anhydrous CSVP was then calculated by division of the ratio of the respective method by the ratio of anhydrous CSVP (30). This allowed the slope (31) and the intercept (32) of the linear equation (33).

$$A_{C24/C14\ method.} = \frac{1}{n}\sum_{i=0}^{n}\left(\frac{C_{24}}{C_{14}}\right)_i \tag{29}$$

$$f_{C14\ method.} = \frac{A_{C24/C14\ method.}}{A_{C24/C14\ anh.CSVP.}} \tag{30}$$

$$m_{method.} = \frac{1 - f_{C14\ method.}}{24 - 14} \tag{31}$$

$$b_{method.} = \frac{24 \cdot f_{C14\ method.} - 14 \cdot 1}{24 - 14} \tag{32}$$

$$f_{Cx\ method.} = m_{method.} \cdot x + b_{method.} \tag{33}$$

The factors calculated indicate higher evaporation of short-chain *n*-alkanes in Expulsinator experiments compared to anhydrous CSVP (Table 12). The artefact in sample treatment after the Expulsinator experiment is caused by the oil-water emulsion obtained. Separating the bitumen from the

water phase resulted in higher evaporative loss of low boiling components.

When comparing the different pyrolysis methods it had to be considered that in CSVP pre-extracted material had been used. This was impossible in case of Expulsinator experiments, where intact sediment plugs were employed. To obtain a correct value for the *n*-alkane yields of experiment A, as shown in Figure 27, the total *n*-alkane yield of the untreated sample (in-situ bitumen) was subtracted from the yields of experiment A on a percentage basis.

For 300 °C pyrolysis temperature the yields of *n*-alkanes generated by exp. A exceeded the yields of the other pyrolysis methods and were three times higher than those of CSVP. For a pyrolysis temperature of 330 °C identical observations were made. For pyrolysis at 360 °C, the yields for short-chain *n*-alkanes ($n$C$_{10}$-$n$C$_{14}$) of exp. A greatly exceeded the CSVP yields. Hydrous single-step pyrolysis reached identical values for a range from $n$C$_{15}$ to $n$C$_{19}$, whereby the other experiments remained under the level of exp. A in this carbon number range. At a certain chain-length, the yield of CSVP exceeded that of exp. A, with the exception of anhydrous multi-step CSVP. For hydrous single-step this point was $n$C$_{19}$ and for hydrous multi-step and anhydrous single-step it was $n$C$_{21}$. The values of anhydrous multi-step pyrolysis matched those of exp. A from $n$C$_{23}$ onward. The higher total *n*-alkanes yields of the Expulsinator experiment mirrored the higher extract yields reached by this methodology (see Figure 26).

***Table 12. Fit line values (slope m and intercept b) and calculated n-alkane factors for exp. A and hydrous CSVP.***

| | Exp. A | hyd. single-step CSVP | hyd. multi-step CSVP |
|---|---|---|---|
| **m** | -0.38 | -0.13 | -0.15 |
| **b** | 10.12 | 4.09 | 4.64 |
| **f$_{C10}$** | 6.32 | 2.80 | 3.12 |
| **f$_{C11}$** | 5.94 | 2.67 | 2.97 |
| **f$_{C12}$** | 5.56 | 2.55 | 2.82 |
| **f$_{C13}$** | 5.18 | 2.42 | 2.67 |
| **f$_{C14}$** | 4.80 | 2.29 | 2.52 |
| **f$_{C15}$** | 4.42 | 2.16 | 2.37 |
| **f$_{C16}$** | 4.04 | 2.03 | 2.21 |
| **f$_{C17}$** | 3.66 | 1.90 | 2.06 |
| **f$_{C18}$** | 3.28 | 1.77 | 1.91 |
| **f$_{C19}$** | 2.90 | 1.64 | 1.76 |
| **f$_{C20}$** | 2.52 | 1.52 | 1.61 |
| **f$_{C21}$** | 2.14 | 1.39 | 1.46 |
| **f$_{C22}$** | 1.76 | 1.26 | 1.30 |
| **f$_{C23}$** | 1.38 | 1.13 | 1.15 |
| **f$_{C24}$** | 1.00 | 1.00 | 1.00 |

The large difference between CSVP and exp. A concerning the short-chain *n*-alkanes suggested influences of expulsion effects onto *n*-alkane composition. Geochromatography, as described by Krooss et al. (1991), could lead to selective retention of *n*-alkanes with longer chain-length, aromatics and other polars within the source-rock. This would have led to further cracking and to enrichment in short-chain *n*-alkanes. Geochromatograpy as described in literature causes selective retention, controlled by the different polarities of the components (e.g. Barker, 1980; Bonilla and Engel, 1986; Espitalié et al., 1984; Lafargue et al., 1990; Leythaeuser et al., 1984a, 1984b; Leythaeuser and Schaefer, 1984). However, selective retention caused by different molecular size is conceivable, too.

A further explanation could be catalytic effects. Several studies observed effects by argillaceous minerals in the generation and migration of hydrocarbons (e.g. Eltantawy and Arnold, 1972; Espitalie et al., 1980; Krooss et al., 1991; Tannenbaum et al., 1986). Especially catalytically active minerals like smectite supported the formation of lower molecular weight components, like olefins and aromatic hydrocarbons. The application of lithostatic pressure onto the natural rock matrix could play an important role in catalytic reactions, as it supports dehydration of smectite and leads to smectite-to-illite transformation (Colten-Bradley, 1987). Such a process could have provided more active mineral sites supporting the formation of aliphatic compounds. This assumption was supported by the fact that smectite-to-illite transformation can be correlated with maturation of organic matter in nature (Guthrie et al., 1986; Smart and Clayton, 1985; Velde and Espitalié, 1989; Velde and Lanson, 1993).

In case of CSVP, interactions between hydrocarbons generated and residual bitumen could also have caused a decrease in *n*-alkane yields. Expulsinator experiments diminished such interactions, since expelled hydrocarbons were removed from the system avoiding further thermal decomposition.

Unexpectedly, multi-step attained lower yields than single-step CSVP, although being methodologically closer to the Expulsinator experiment than single-step pyrolysis. This was even more surprising, as the multi-step variant produced higher amounts of extract than the single-step pyrolysis. An explanation could be the removal of products generated at each temperature of multi-step pyrolysis, preventing these from thermal decomposition in following temperature steps. In

Expulsinator experiments, retention effects of the mineral and kerogen matrix caused enrichment in *n*-alkanes in general, and in short-chain components in particular.

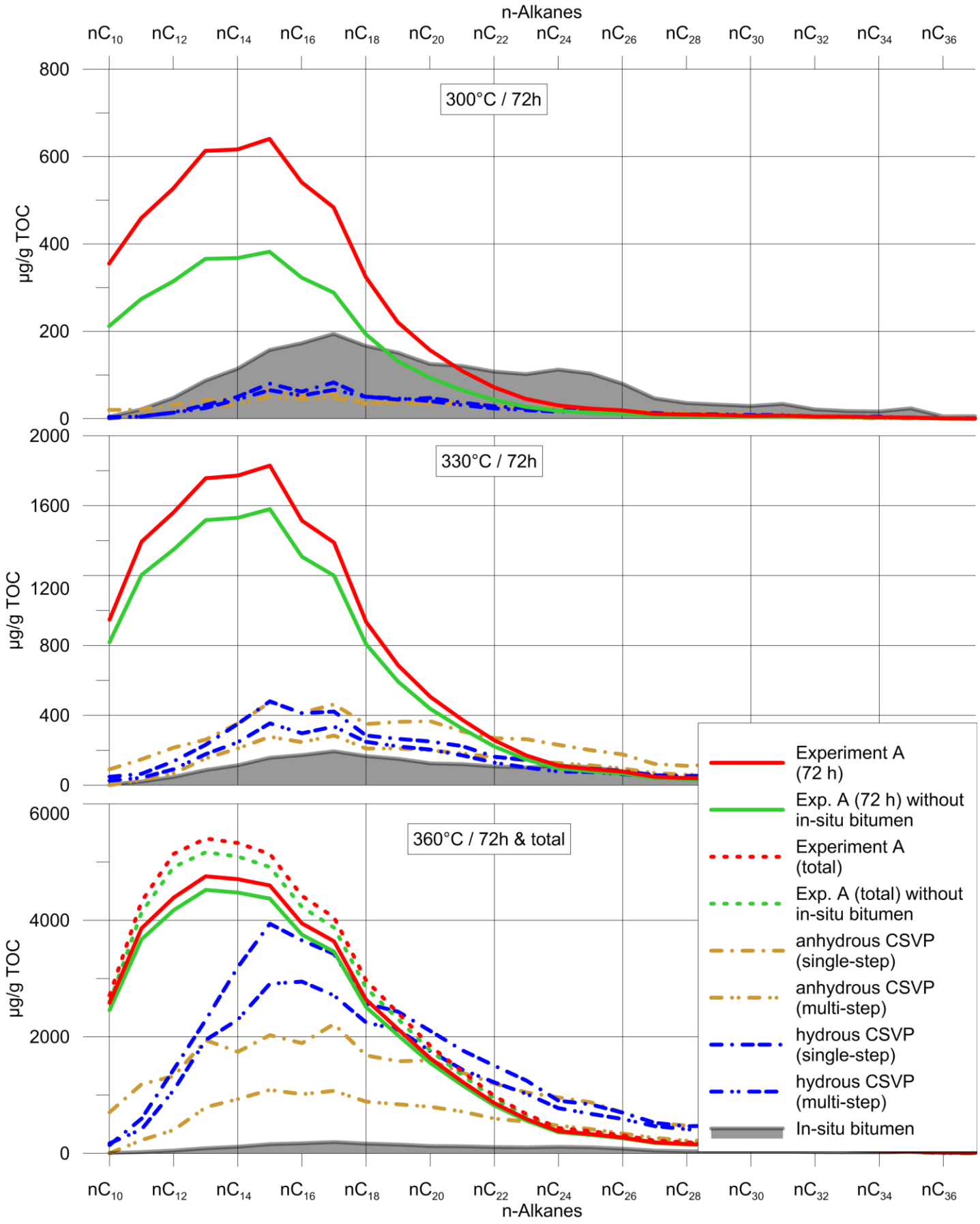


***Figure 27. n-Alkane yields of exp. A and CSVP. CSVP was performed using pre-extracted rock. Unextracted in-situ n-alkanes in exp. A are indicated as grey areas. Processing artefacts were corrected by applying factors given in Table 12.***

### 3.5.2 Conversion rates and gas generation

Higher extract yields in Expulsinator experiments were reflected by lower TOC- and $S_2$-values of the pyrolysed residual rock-samples (Figure 28). All expulsion experiments showed lower residual TOC- and $S_2$-values in comparison to CSVP at 375 °C. Formation of pyrobitumen, as well as lower transformation rates, explained the high TOC-values of anhydrous CSVP compared to other experiments. Generally the TOC- and $S_2$-values of multi-step CSVP were lower than in single-step CSVP. This complied with higher extract yields obtained by multi-step CSVP. Higher TOC- and $S_2$-values in anhydrous CSVP compared to hydrous CSVP and single-step CSVP compared to mutli-step CSVP were a strong indication for cross-linking. Pyrobitumen increased overall TOC and $S_2$, as long as it could be cracked at temperatures reached by Rock-Eval.

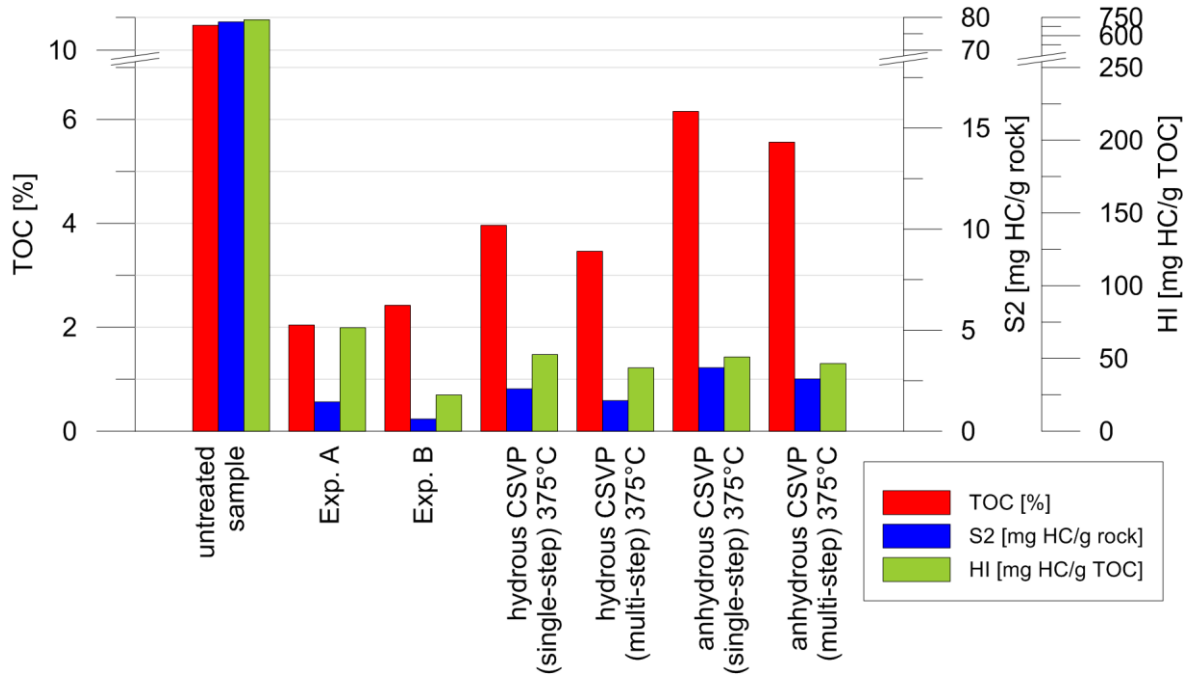


***Figure 28. TOC, $S_2$ and HI-values of untreated sample, expulsion experiments and CSVP at 375 °C.***

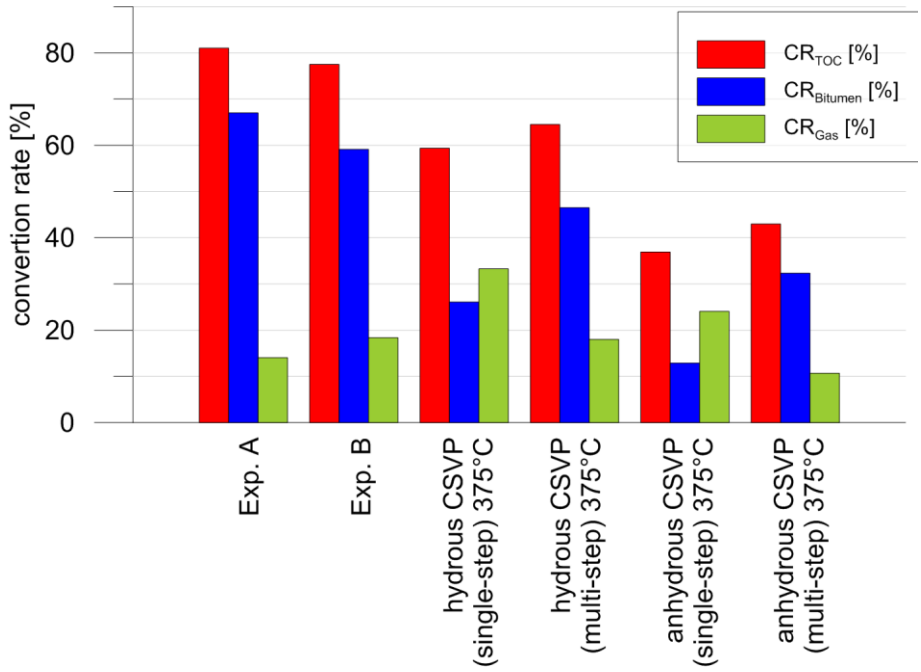


***Figure 29. Conversion rates (CR) of Expulsinator and CSVP (375 °C) experiments based on TOC-values. The OC fraction of bitumen was predefined to be 83 wt.% (Peters et al., 2005) for $CR_{Bitumen}$ and $CR_{Gas}$ calculations.***

Residual HI-values reached similar values in CSVP, but were higher after single-step (51.0 – 52.9 mg HC/g TOC) than multi-step CSVP (43.9 – 46.6 mg HC/g TOC). The highest variation in residual HI-values was observed for expulsion experiments. Exp. B had the lowest HI-value due to a low $S_2$-value combined with an increased TOC content (compared to exp. A) of the residual rock. The low $S_2$-peak indicated a high generation and expulsion ratio on the one hand, the increased TOC a minor formation of pyrobitumen on the other. The slightly elevated HI-value of exp. A was attributed to the low TOC content of the residual sample (2.04 %), being the lowest of all pyrolysis experiments. In context with the large extract yields of this experiment, it demonstrated the high generation and expulsion efficiency reached by selection of suitable pressure and temperature regimes.

Conversion rates ($CR_{TOC}$) for expulsion experiments and CSVP are presented in Figure 29, calculated on the basis of the TOC-value before ($TOC_{UT}$) and after pyrolysis ($TOC_{py}$). For CSVP experiments gas formation was not measured. However, estimation of gas production is possible by calculating the carbon content of the bitumen obtained and subtracting this value from the TOC converted. A hypothetical carbon content of the bitumen of 83 wt.% was used (Peters et al., 2005b). The conversion-rates were calculated with the following equations:

$$CR_{TOC} = \frac{TOC_{UT} - TOC_{py}}{TOC_{UT}} * 100 \qquad (34)$$

The resulting value indicated the degree of conversion in weight percent. A proportionate conversion rate of bitumen ($CR_{Bitumen}$) and gas ($CR_{Gas}$) could be calculated on basis of the assumed organic carbon content of the bitumen ($OC_{Bitumen}$) and the resulting $OC_{Gas}$:

$$OC_{Bitumen} = Extract\,[\%\ of\ rock] \cdot 0.83 \qquad (35)$$

$$OC_{Gas} = TOC_{UT} - OC_{Bitumen} \qquad (36)$$

$$CR_{Bitumen} = \frac{OC_{Bitumen}}{TOC_{UT}} \cdot 100 \qquad (37)$$

$$CR_{Gas} = CR_{TOC} - CR_{Bitumen} \qquad (38)$$

The conversion rates as presented in Figure 29 show higher conversion reached by the Expulsinator in comparison to CSVP at 375 °C. In exp. A, 81 % of the initial TOC is converted to $OC_{Bitumen}$ and $OC_{Gas}$. In exp. B 78 % of the TOC was converted. In contrast, the highest conversion rate of CSVP was reached by hydrous multi-step CSVP with 65 %. The conversion rates achieved by the Expulsinator were very high. However, the results are reproducible (exp. A and exp. B) and in a range confirmed by literature. For type-I kerogen a conversion rate of 70 to 80 % is accepted (Bordenave, 1993).

In Expulsinator experiments, bitumen yields outweighted gas yields. The highest gas amounts were produced by exp. B, followed by exp. A. The lower gas conversion in exp. A compared to B could be explained by the different temperature stages reached in the experiments. Longer pyrolysis duration at 300 °C and 330 °C of exp. A converted higher amounts of labile kerogen to bitumen and oil. Due to lower thermal energy at these pyrolysis stages, the hydrocarbons generated have not been thermaly cracked to gas. This happened partially in exp. B., which was performed with temperatures too low and pyrolysis duration too short for intensive labile kerogen cracking during the first two pyrolysis stages. This resulted in elevated proportions of labile kerogen remaining within the source-rock, until high pyrolysis temperatures (360 °C) were reached. Upon maximum pyrolysis temperature labile kerogen was cracked to bitumen and oil and also partly converted to gas directly, which did not occur in exp. A. In general the gas yields of the Expulsinator were lower compared to CSVP due to the open pyrolysis setup. Oil to gas cracking was diminished because the oil generated was released immediately after generation.

Comparing the different CSVP-experiments which each other revealed hydrous CSVP to release a higher total amount of gas. In parallel, a higher proportion of the TOC converted was released as gas instead of bitumen in anhydrous CSVP. This effect was caused by intensified cross-linking processes in anhydrous pyrolysis, leading to thermal alteration of the already produced bitumen. The total pyrolyzate yields obtained in anhydrous CSVP diminished, causing higher proportions of gas in total conversion. The difference between single-step and multi-step followed the same effect: The extractable hydrocarbon yield was significantly larger for multi-step pyrolysis, caused by lower pyrobitumen formation. An even greater suppressive effect in gas production was the removal of oil generated after each successive temperature step in multi-step CSVP.

A comparison of the results calculated here with those from literature proved to be difficult. In part this was ascribed due to a lack of differentiation between hydrocarbon gases and $CO_2$ in this study. However, different comparative studies showed higher yields for $C_1$ to $C_5$ hydrocarbons in anhydrous pyrolysis and a significantly higher yield of $CO_2$ for hydrous pyrolysis (Andresen et al., 1993; Behar et al., 2003; Lewan, 1997). The higher gas yields, achieved via hydrous pyrolysis in this study, were seen as an indication for higher $CO_2$-generation.

### 3.5.3 Expulsion efficiency and residual potential

Hydrocarbons generated upon artificial maturation were expelled with a very high efficiency, as shown in Figure 30. The amounts of extractable organic matter retained were very low in all expulsion experiments. The values of matrix-retained *n*-alkanes were similarly low, with 2.8 % and 2.8 % for exp. A and B, respectively.

The residual potential remaining after Expulsinator experiments was investigated by performing MSSV at 360 °C for 72 h and HyPy at 500 °C on pyrolyzed rock from exp. A. The m/z=85 mass fragmentograms from MSSV experiments (Figure 31) of untreated sample and pyrolyzate of exp. A demonstrate that small amounts of *n*-alkanes could still be released from the pyrolyzed material. However, it has to be considered that in the course of the sample preparation for MSSV the pyrolyzed rock of exp. A was grounded and decalcified. In this way, matrix-trapped hydrocarbons could become MSSV amenable. The *n*-alkane yields achieved for the pyrolyzed rock of exp. A reached only 0.23 % of the yields of MSSV of the untreated sample (Table 13). The total yields obtained from pyrolyzed rock in comparison to the untreated samples were calculated based on total ion chromatogram intensities. Exp. A reached 1.45 % of the yields of the untreated samples.

MSSV of the pyrolyzed rock of exp. A released mainly gaseous products, emphasizing the low remaining generation potential of the sample. Figure 32 (A-E) shows the development in the MSSV-release of low molecular weight aromatics, in particular benzene, toluene, ethylbenzene and xylenes (BTEX), in dependence of pyrolysis temperature. BTEX were detected from 300 °C to 360 °C (exp. A) and 300°C to 390 °C (untreated sample). The development of gas generation for exp. A is opposite to that of the untreated sample. While all BTEX-components for the untreated sample from 300 °C to 360 °C rose sharply, the values decreased in case of exp. A for benzene and toluene. The values for the methylated and ethylated components of exp. A remained almost constant but at very low concentrations.

In case of the untreated material, it can be assumed that with increasing pyrolysis temperature more BTEX-components were released from the kerogen by thermal cracking and from precursors by dehydration and dealkylation. The decreasing amounts of BTEX-components at 390 °C do not stand in opposition to this assumption, as at these high temperatures, the rate of decomposition and thermal cracking exceeded the rate of generation. This was already shown by the CSVP experiments at 375 °C (see above). As result, a much higher amount

***Table 13. Deviation in MSSV and HyPy yield between Expulsinator pyrolyzates and untreated sample.***

| | Yields of pyrolyzed rocks compared to untreated material [%] | |
|---|---|---|
| | **Sum ion m/z= 85** | **Sum TIC** |
| **MSSV (360°C)** | 0.23 | 1.45 |
| **HyPy (500°C)** | 3.90 | 2.26 |

of HC was decomposed to smaller molecules and to $CO_2$. This lowered the yields of all BTEX-components, but especially those of the methylated and ethylated components.

In case of exp. A, a different picture emerged: Here the main source of the BTEX-component was not kerogen, but already generated and trapped hydrocarbons, which were released during sample preparation for MSSV. At 300 °C, only low thermal

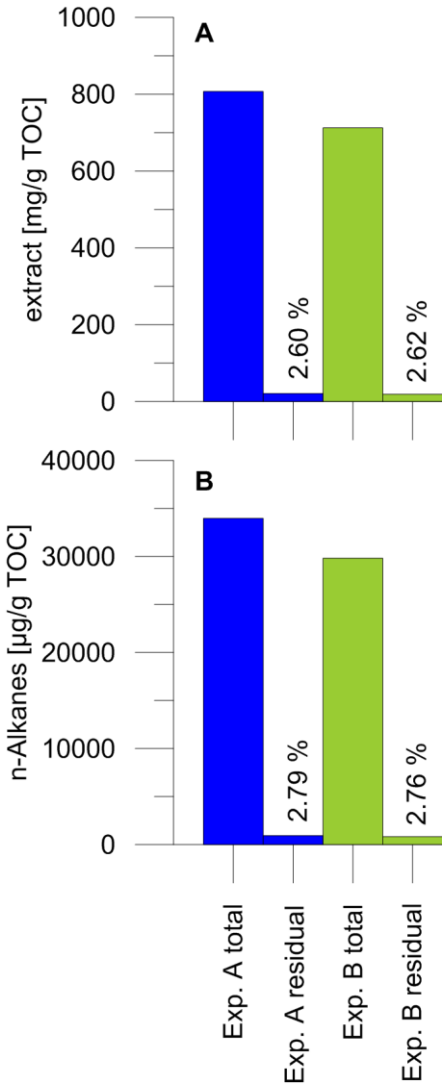


***Figure 30. Residual extractable material (A) and n-alkanes (B) in the rock after expulsion experiment.***

alteration of this OM led to the highest yields of BTEX-components. With higher temperature, the remaining OM was more affected by thermal decomposition. This, and the lack of additional generation of BTEX-components from the exploited kerogen, provided a similar constellation to that of the untreated sample at 390 °C: an imbalance between the generation rate and the degradation rate with advantage for the degradation rate.

The distribution of BTEX-components for MSSV at 360 °C (Figure 32 F) supported these observations. For the untreated sample the yield for (m+p)-xylene was highest, followed by toluene and o-xylene. For exp. A, a significant shift in the yields towards benzene and toluene was observed. The amounts of ethylated and methylated components were only very small in comparison to the untreated sample. Most of these components and of their precursors had already been released during the Expulsinator experiment. The very small amounts, which were left within the sample, were thermally decomposed and dealkylated to benzene or even smaller molecules. The trend in generation of BTEX-components led to the assumption that higher temperatures would not initiate a significant increase of the yields obtained by MSSV of the pyrolyzate residue of exp. A.

***Table 14. Bond-dissociation energies (Blanksby and Ellison, 2003).***

| Bond | Bond-dissociation energy | |
|---|---|---|
| | [kJ/mole] | [kcal/mole] |
| $CH_3$-$CH_3$ | 377 | 90 |
| $CH_2$-$CH_2$ | 416 | 99 |
| H-H | 436 | 104 |
| HO-O | 498 | 119 |

HyPy of the untreated sample produced relatively high amounts of *n*-alkenes beside *n*-alkanes - an effect not observed in HyPy of the pyrolyzed rock of exp. A. Obviously for untreated sediment, the quantities of hydrocarbons released

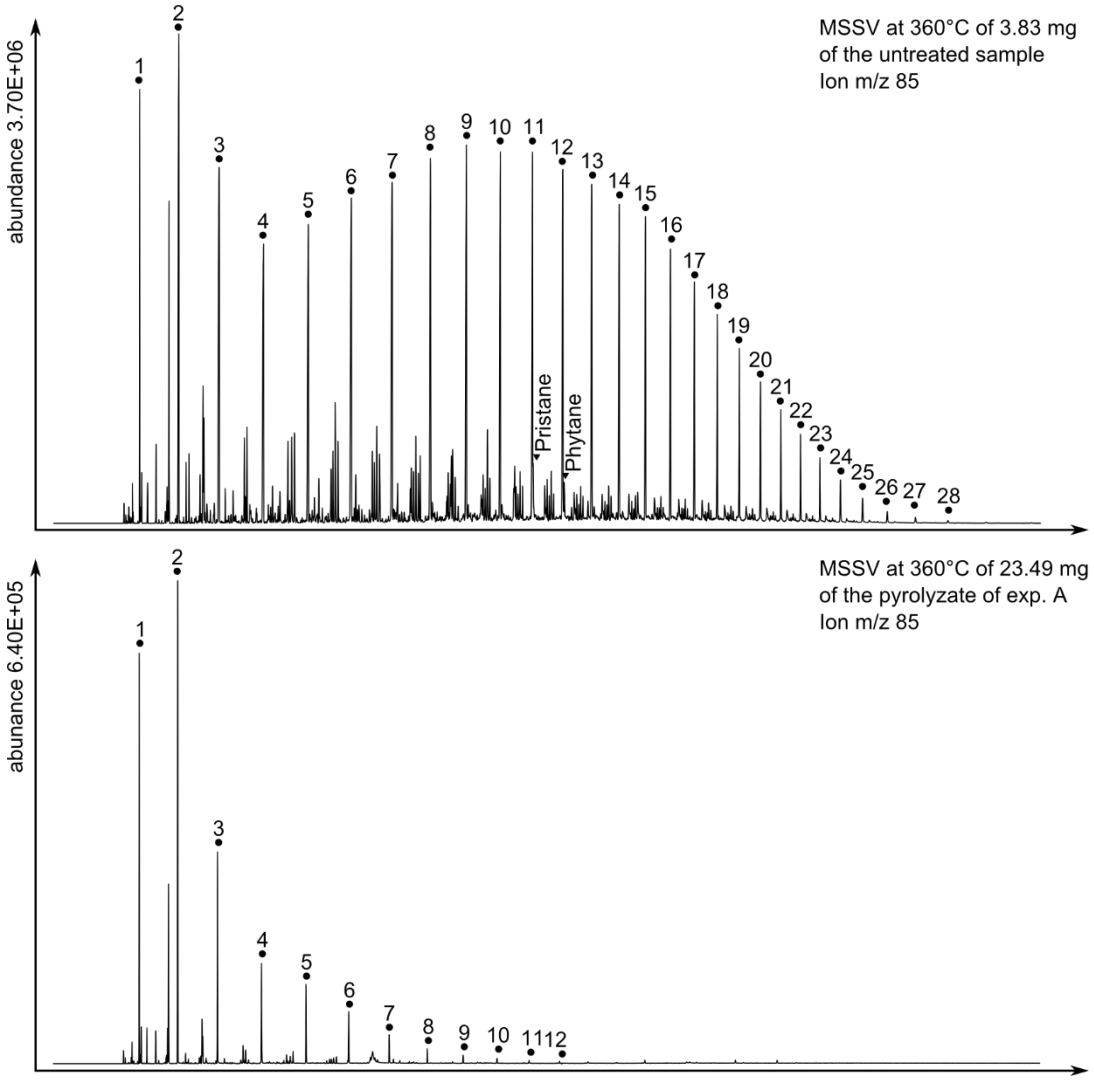


***Figure 31. MSSV-fragmentograms (m/z=85) for untreated sample (above) and exp. A pyrolyzate (below). Numbers denote n-alkanes (1-28: $nC_7$ – $nC_{34}$).***

exceeded those of free hydrogen available to generate unsaturated *n*-alkenes instead of *n*-alkanes. Hydrocarbons generated by cleavage of O-bearing bonds immediately after generation were transported out of the heated zone into the cold trap. β-scission of hydrocarbons by thermal cracking is a faster reaction than the abstraction of hydrogen from water or $H_2$ (see Table 14), which diminished the role of $H_2$ and water as hydrogen donor, especially in consideration of the short residence time of hydrocarbons and $H_2$ within the HyPy-reactor. Evidence for this effect was the low impact of additional hydrogen onto the composition of products generated in closed pyrolysis (Larsen, 1999; Lewan, 1997). To compare the amount of *n*-alkanes obtained from the pyrolyzate of exp. B with the results of the untreated sample required calculating the sum of *n*-alkenes and *n*-alkanes of the HyPy of the untreated sample.

The yields of *n*-alkanes of the pyrolyzate of exp. A reached only 3.9 % of the yields of *n*-alkanes of the untreated sample after HyPy (see Table 13). The distribution of summed *n*-alkanes and *n*-alkenes (Figure 33) showed a similar pattern for HyPy of the untreated sample and of the pyrolyzate, even though the distribtion curve of the pyrolyzate was shifted slightly to lower chain lengths. This suggested that a proportion of *n*-alkanes originated from already generated, but trapped hydrocarbons. Concerning the total extract after HyPy, the amount obtained from the pyrolyzed sample of exp. A reached 7.3 % of the extract yield generated by the untreated sample. These results had to be interpreted in the context of the methodology applied.

For HyPy the sample preparation was identical to the preparation for MSSV and made trapped hydrocarbons accessible by grinding and decalcification. The temperatures of HyPy experiments reached 500 °C and were higher than the maximum temperatures used in expulsion experiments. The higher temperatures and the support of a catalyst caused cracking of the more stable kerogen and led to the release of some remaining gas potential from the source-rock.

Of the remaining TOC-content of the exp. A pyrolyzate 12 % was converted by HyPy. The untreated sample lost 86 % of its TOC (see Table 15). Interestingly the untreated sample reached a lower TOC-value after HyPy than the pyrolyzate of exp. A. This was an indication for the generation of thermally highly stable components like pyrobitumen during the Expulsinator experiment, albeit on a small scale.

### 3.5.4 Interactions between kerogen, bitumen, pyrobitumen and pyrite

The large differences between the Expulsinator and classic CSVP experiments could not be explained by different rates of cross-linking and

***Table 15. TOC-content of exp. A pyrolyzate versus untreated sample before and after HyPy.***

| | pyrolyzed rock of exp. A | untreated sample |
|---|---|---|
| **TOC [wt.%]** | 2.04 | 10.76 |
| **$TOC_{cf}$ [wt.%]** | 2.43 | 13.36 |
| **$TOC_{cf\ HyPy}$ [wt.%]** | 2.14 | 1.92 |
| **$TOC_{conv.}$ [%]** | 12.12 | 85.64 |

formation of pyrobitumen exclusively, even though this may have played the most important role. To estimate the impact of pyrobitumen formation on the different pyrolysis methodologies, the TOC converted was plotted versus the converted $S_2$-value (Figure 34 A). In case of minor pyrobitumen formation we expected both, a high $TOC_{conv.}$ and a high $S_{2\ conv.}$. At high formation rates of pyrobitumen, the $TOC_{conv.}$ would be low due to an insoluble pyrobitumen carbon contribution. Only labile pyrobitumen components would be measured as $S_2$, leading to a lower impact of $S_{2\ conv.}$ versus $TOC_{conv.}$. For low pyrobitumen formation rates the value of $TOC_{conv.}/S_{2\ conv.}$ would approach unity. With increasing pyrobitumen formation the ratio would decline due to a stronger decrease in $TOC_{conv.}$. The values of $TOC_{conv.}$ vs. $S_{2\ conv.}$ fitted to this estimation (Figure 34 A), as anhydrous pyrolysis showed medium values for $S_{2\ conv.}$ and low values for $TOC_{conv.}$. Slightly higher conversion of TOC indicated lower formation of pyrobitumen for hydrous in comparison to anhydrous pyrolysis. Highest conversion rates, both for $TOC_{conv.}$ and for $S_{2\ conv.}$, were evident for low formation rates of pyrobitumen in exp. A and B.

In Figure 34 B, C and D, the conversion of total nitrogen, the alteration of the $CO_2$-content and the conversion of total sulphur were plotted versus pyrolysis temperature respectively. For nitrogen conversion, an increase was observed in CSVP, starting near zero at 300 °C and rising to a maximum at 360 °C, whereby the maximum conversion for hydrous pyrolysis was higher (42 - 45 %) than for anhydrous pyrolysis (19 - 24 %). At 375 °C the conversion rates decreased, indicating nitrogen incorporation into the residual rock. The conversion rates at 375 °C were lowest for anhydrous CSVP and single-step CSVP reached lower values than multi-step CSVP. The conversion rates corresponded to the degree of pyrobitumen formation (Figure 34 A). This, in case of CSVP, meant increasing formation of pyrobitumen led to incorporation of nitrogen into the pyrobitumen formed. The decrease of nitrogen conversion rates corresponded to the quantity of the pyrobitumen generated. Nitrogen incorporation is typical for pyrobitumen formation (Kelemen et al., 2010, 2008). Increasing aromatisation of the residual bitumen and the pyrobitumen formed was seen as a reason for this effect, due to the favoured retention of nitrogen within aromatic structures.

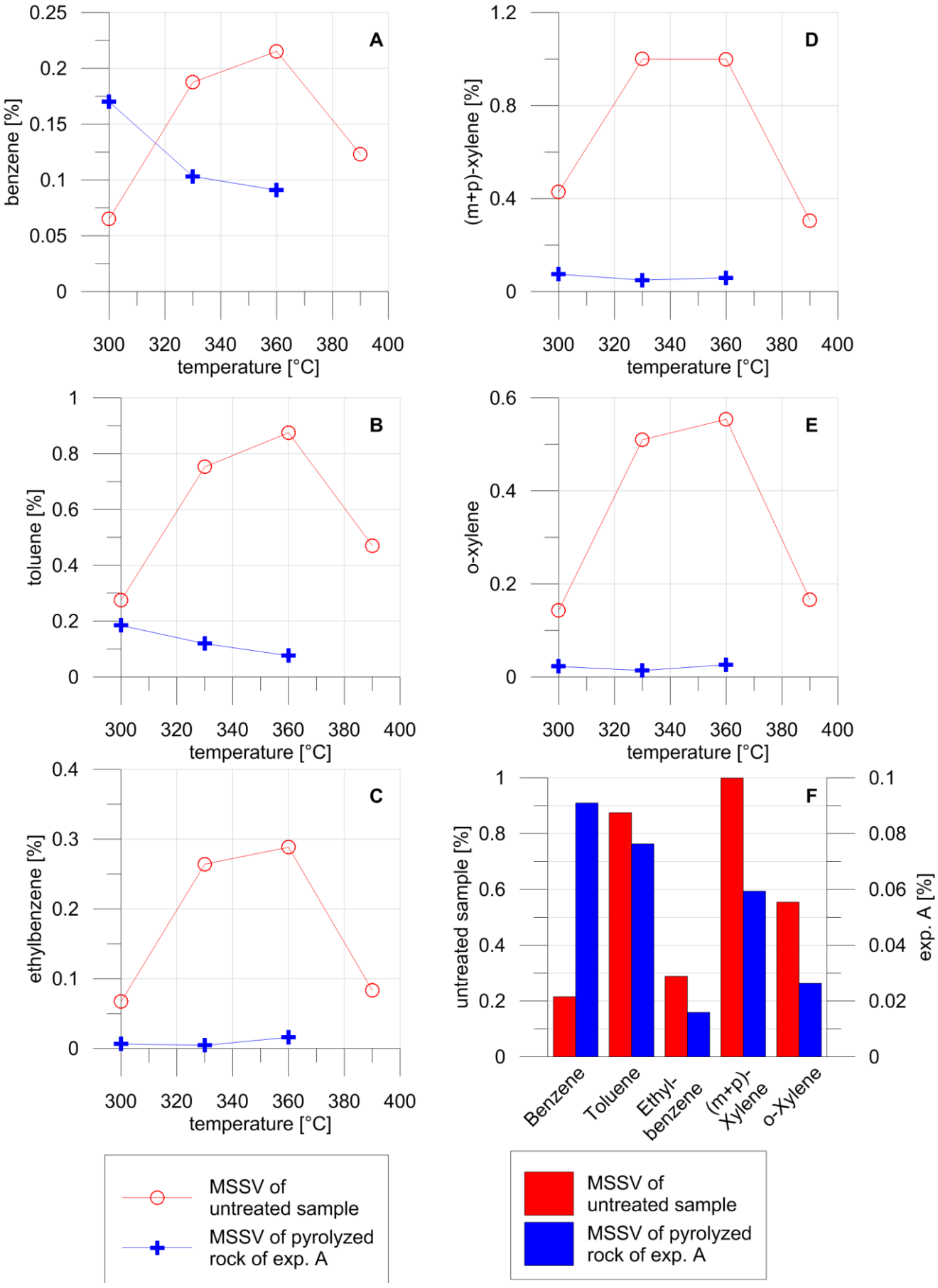


***Figure 32. Temperature dependent BTEX trends, obtained by MSSV of untreated sample and exp. A pyrolyzate. Diagram A to E: Benzene, toluene, ethylbenzene, (m+p)-xylene and o-xylene, respectively. Diagram F reveals relative BTEX proportions of MSSV of untreated sample at 360 °C versus exp. A pyrolyzate (normalized to (m+p)-xylene of the untreated sample).***

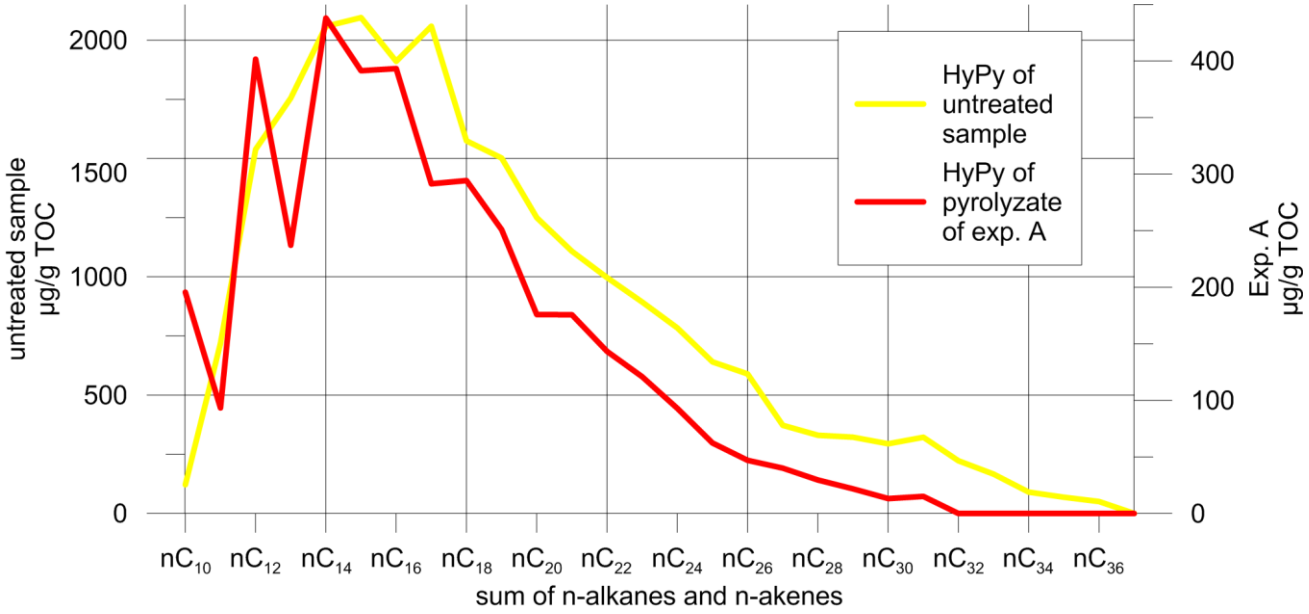


***Figure 33. Distribution of HyPy generated n-alkanes from exp. A pyrolyzate versus distribution of cumulated n-alkanes and n-alkenes in untreated sample.***

The conversion rates observed for the expulsion experiments were similar to maximum values of hydrous CSVP (exp. A) or slightly higher (exp. B). In case of exp. B this result was surprising given the small amounts of pyrobitumen generated. The open setup of the Expulsinator experiments may explain this behaviour. Released nitrogen was expelled into the artificial reservoir and flushed out of the reactor, being unavailable for incorporation into pyrobitumen.

The alteration of the $CO_2$ content was calculated by subtracting the residual from the initial $S_3$ value to yield, $S_{3\ alteration}$ representing the change in oxygen content of the kerogen. At low temperatures of 300 °C CSVP showed uniform $S_3$-reduction of about -100 %, indicating the amount of oxygen doubled. With increasing temperature, the main difference is between multi- and single-step CSVP and only secondary between hydrous and anhydrous CSVP. $S_{3\ alteration}$ of multi-step CSVP increased to values between -12 % (anhydrous) and -27 % (hydrous) at 330 °C and to values between -1 % (anhydrous) and -18 % (hydrous) at 360 °C. Finally the values increased to 28 % for anhydrous and to 40 % for hydrous multi-step CSVP at 375 °C. Conversion in single-step CSVP at 330 °C remained unaltered when compared to 300 °C and rose to values between -5 % (anhydrous) and 29 % (hydrous) at 360 °C.

The conversion rates were similar to those reached at 375 °C. Elevated amounts of oxygen at low pyrolysis temperatures compared to initial oxygen levels indicated neoformation of oxygen-bearing compounds, like free or kerogen-bound acids or phenols (Stalker et al., 1994). Further pyrolysis temperature increase initiated thermal decomposition of these species, which were ultimately oxidized to $CO_2$. The decomposition of these compounds seemed to occur faster in case of multi-step CSVP, as the $S_3$ values reached pre-pyrolysis levels earlier. This was attributed to a longer total pyrolysis time at which kerogen had been exposed to elevated temperatures. For the first step (210 °C) the duration was 72 h, but for completion of the next step the cumulative pyrolysis time was 144 h. The values of $S_{3\ alteration}$ for expulsion experiments were higher than the corresponding values of CSVP experiments and reached 89 % for both, exp. A and B. Responsible for the lower values for CSVP could have been a metastable equilibrium between oxidized carbon-bearing species (such as $CO_2$, $HCO_3^-$, $CH_3COOH$, $CH_3COO^-$, $CH_3CH_2COOH$, $CH_3CH2OO^-$) within the water-phase and the oil (Helgeson et al., 1993), or bitumen, pyrobitumen and remaining kerogen. As in the expulsion experiments, expelled components were removed from the reactor, leaving the system unbalanced between organic matter within the rock and the oxidized species. As a result, higher amounts of oxidized organic species were released from the kerogen. Alternatively, it was considered that in CSVP reactions between kerogen, pyrobitumen and aqueous oxidized carbon-bearing species continued to occur after termination of the heating phase. In such a scenario, oxygenated carbon species could have become re-incorporated into the organic matrix.

Covariation between thermal stress and conversion of sulfur occurred in CSVP, but not in Expulsinator experiments (Figure 34 D). For CSVP no impact of pyrolysis at 300 °C and 330 °C was observed but a strong increase in conversion rates of sulfur between 330 °C and 375 °C. At 375 °C the

conversation rate reached a maximum of 30 % and 25 % for hydrous pyrolysis and 25 % and 20 % for anhydrous pyrolysis (single-step and multi-step, respectively). No sulfur was converted in Expulsinator experiments. In pyrolysis experiments pyrite, the main component of sulfur-containing minerals in the sediments used could have been transformed into ferrous sulfide (FeS) and reactive sulfur. This has been shown to occur at temperatures above 570 °C at 1 bar, or at 400 °C at 30 or 50 bar hydrostatic pressure (Chen et al., 2000). Pyrolysis experiments conducted with coals and pure pyrite have shown that the addition of lignite lowers the temperature for the onset of pyrite decomposition by about 100 °C (Chen et al., 2000). Effective transformation has been observed at temperatures above 360 °C (Yani and Zhang, 2010). The catalytic effect has been attributed to the ability of coals to donate hydrogen resulting in $H_2S$ and FeS generation. Presence of water during pyrolysis had no influence on the temperature of pyrite transformation (Yani and Zhang, 2010). In such experiments water seems to have played only a secondary role as hydrogen donor.

In case of our CSVP experiments we expect the role of coal as reaction partner to have been taken

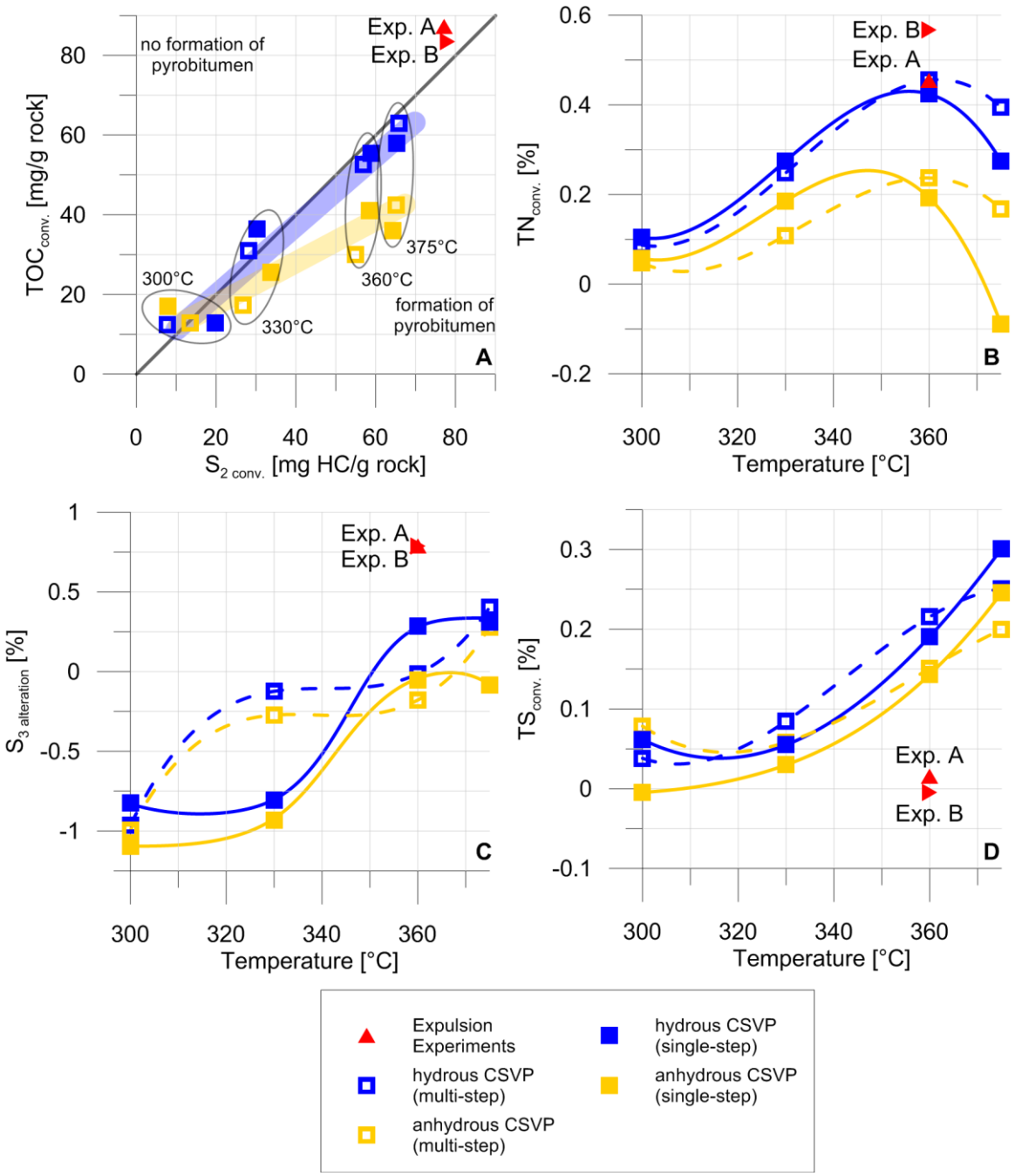


***Figure 34. Impact of pyrobitumen formation and interactions between products, kerogen and pyrobitumen onto specific conversion rates. Diagram A: Converted TOC versus converted $S_2$. Diagram B to D: Converted total nitrogen (TN), alterated $S_3$ and converted total sulfur (TS) vs. pyrolysis temperature. Curves are plotted as third-order polynomial.***

over by the neoformed labile pyrobitumen. Pyrobitumen formation would lower the temperature necessary to transform pyrite into FeS and S, or rather $H_2S$. In hydrous pyrolysis higher vapour pressures were generated, lowering the transformation temperature even further. This became evident from higher conversion rates of sulfur in hydrous versus anhydrous CSVP. The Expulsinator generated no (exp. A) or very low amounts of pyrobitumen (exp. B), exerting no effect on the transformation temperature of pyrite.

## 3.6 Conclusion

The Expulsinator experiments presented here showed high generation and expulsion efficiency. Trace amounts of extractable material remained within the source-rock and more than 97 % of the hydrocarbons generated were expelled into the artificial reservoir. The residual source-rock potential after the Expulsinator experiment was extremely low. Even after grinding and decalcification, minimal additional hydrocarbons were released by MSSV after 72 h at 360 °C.

The Expulsinator experiments showed differences compared to classic hydrous and anhydrous pyrolysis. This was evident in the extract yields obtained and in the quantities of the *n*-alkanes released. For both products, Expulsinator experiments exceeded the yields reached by classic closed vessel pyrolysis by a multiple. The maximum yields of the expulsion experiments presented in this study were at least 16 % higher as the yields of comparative hydrous pyrolysis (hydrous multi-step CSVP). The large differences in the extract yields could be explained by the intensified cross-linking reactions in case of classic pyrolysis, which led to the formation of pyrobitumen instead of free hydrocarbons. Cross-linking reactions favoured β-scission via thermal cracking, provided that neoformed radical sites were not terminated by free hydrogen (Lewan, 1997). Therefore, the availability of free hydrogen was seen as limiting factor in free hydrocarbon formation. If the generation rate exceeded the rate of hydrogen provision, this resulted in increasing cross-linking and formation of double carbon bonds or cyclization. This was most pronounced in single-step CSVP at 360 °C and 375 °C, where very high generation rates exceeded hydrogen availability. Multi-step CSVP revealed higher extract yields and lower rates of cross-linking. We attributed this to a removal of hydrocarbons already generated during previous temperature steps, thus reducing the amount of bitumen formed upon subsequent temperature rise. Consequently, the amount of hydrocarbons released did not exceed that of hydrogen provided in the corresponding temperature step. In addition, secondary cracking was diminished even further reducing hydrogen consumption. In multi-step pyrolysis the proportion of pyrobitumen formed could be reduced further by increasing the number of pyrolysis steps, thus reducing the exposure time of bitumen generated in each pyrolysis stage. The open pyrolysis in our expulsion setup and the stepwise temperature increase over a longer period (up to 150 h) ensured that at no time hydrocarbon generation surpassed hydrogen availability or that secondary cracking consumed larger amounts of hydrogen. Water seemed to have played an important role as hydrogen donor, due to anhydrous CSVP showing much higher rates of cross-linking than hydrous CSVP. For the expulsion experiments it remained open, whether the surrounding water or hydrogen itself was able to penetrate the source-rock itself, supporting thermal kerogen cracking. Although it has been shown in other expulsion experiments (Larsen, 1999) that water may penetrate kerogen at elevated temperatures, in concert with the lithostatic pressures applied in our experiments this was considered unlikely. Reactive hydrogen could have been provided by water released by pressure supported smectite to illite transformation (Colten-Bradley, 1987). Alternatively, hydrogen may have been derived from kerogen or bitumen aromatization (Weres et al., 1988).

Interactions between residual kerogen and other components played an important role in classic pyrolysis and showed large differences compared to expulsion experiments. Pyrobitumen formation in CSVP was related to interaction with nitrogen which became incorporated into aromatic pyrobitumen substructures. Pyrobitumen seemed to have lowered the temperature of pyrite transformation as recognized in CSVP experiments. In the context of hydrogen limitation, pyrite transformation could further diminished free hydrogen, as reactive sulfur could have bound free hydrogen to produce $H_2S$.

Large differences were observed in the oxygen content of pyrolyzed samples for both, the Expulsinator and classic pyrolysis experiments. The Expulsinator released higher amounts of oxygenated organic compounds compared to classic pyrolysis. This was attributed to open pyrolysis applied in the Expulsinator, where re-incorporation of oxygen compounds into kerogen has been diminished by removal of these components through the mobile water phase.

The natural simulation of generation, expulsion and primary migration of hydrocarbons via the Expulsinator showed differences to classic pyrolysis. The formation of polymerized pyrobitumen seemed to have been predominantly methodology-affected by the classical, but not by the Expulsinator experiments. Continuous effluent withdrawal in the Expulsinator, regarded similar to conditions prevailing in nature, affected the composition of the

products generated. However, further work is required to investigate the impact of lithostatic and hydrostatic pressure and of temperature gradients onto the formation of oil and gas.

# 4 Behaviour of *n*-alkanes and isoprenoids during artificially simulated catagenesis of an Toarcian black shale (Posidonia shale)

## 4.1 Abstract

In this study, the results are presented of a lab scaled, close to nature simulation of generation, primary migration and expulsion of hydrocarbons during catagenesis. This simulation was carried out with a newly designed apparatus, developed and built in the institute of geosciences in Kiel. By this new approach, it was possible to overcome limitations in previously used methodologies, concerning the investigation of processes prevailing during primary migration and expulsion of hydrocarbons in petroleum systems. The experiment, which is presented here, was performed in a stepwise setup, simulating burial depths of ~2000 m, ~2500 m and 3000 m by implementing overburden pressures from 600 bar to 900 bar, and hydrostatic pressures from 200 bar to 300 bar. The experiment was conducted as hydrous pyrolysis with a semi-open setup, which allowed collecting expelled hydrocarbons during the simulation. The obtained extract yields showed a clear maximum for each expulsion step, with the highest yields at 3000 m simulated depth. To compare the results of this new method, accompanying classic pyrolysis experiments were performed (closed small vessel pyrolysis and microscale sealed vessel pyrolysis). Expulsion and primary migrations showed to affect the distribution of *n*-alkanes with ongoing maturation and increasing subsidence. Retention affects in dependence of the molecular size were observed, leading to an *n*-alkane increase towards larger molecular size with ongoing expulsion. Isoprenoid-ratios (pristane vs. phytane) and isoprenoid – *n*-alkane-ratios (pristane vs. *n*-$C_{17}$) showed trends correlating with the expulsion progress. For both trends, generation related effects were primarily responsible for the observed behaviour. However, both ratios could be useful expulsion indicators, as generation, expulsion and primary migration are concurrent processes, which cannot be considered separately. Thus, both ratios deliver information about expulsion processes and the migration history in natural systems.

## 4.2 Introduction

It is fundamental for the assessment of petroleum and gas plays to understand the processes, which control the generation of hydrocarbons, the expulsion (discharge of bitumen from kerogen) and primary migration (transport within the source-rock) into the reservoir rock.

On the way from the kerogen into the reservoir, many factors influence the composition of the petroleum. This starts with the nature of the source material, reflected by the compositional differences of oil, originate from type I, type-II or type-III kerogen. Considering the compositional changes of the released petroleum over time, then kerogen has further influence onto the released hydrocarbons. During the migration of free hydrocarbons through the kerogen network, the composition of the expelled petroleum will be affected by desorption and adsorption effects. The impact of the adsorption depends on the polarity of the compounds, which cause fractionation of expelled hydrocarbons (Sandvik et al., 1992; Thomas and Clouse, 1990c). The migration through the rock matrix of the source-rock could cause further fractionation by interactions between the expelled petroleum and active sides of minerals (Krooss et al., 1991 and cited studies there).

Expulsion and primary migration efficiency is highly affected by the prevailing pressure regimes within the oil play. Increasing lithostatic pressure during the catagenesis leads to the formation of micro- and macro-fractures within the rock, which represent important pathways for hydrocarbons (Dickey, 1975; Leythaeuser et al., 1988a; Littke et al., 1988; Pepper and Corvi, 1995a; Ungerer, 1990). The pore pressure within the source-rock influences the expulsion and migration behaviour as well, for example by expulsion fracturing. Thereby, the pore pressure increases sharply due to the expulsion of fluids and gases into the pore space (Berg and Gangi, 1999).

Water is an important factor for the generation and the subsequent migration of oil and gas. It acts as pressure mediator for hydrostatic pressures and as hydrogen donor in case of free radical reactions, which are likely to happen during the decomposition of kerogen to hydrocarbons (Jackśon et al., 1995; Michels et al., 1995; Uguna et al., 2012). Furthermore, water will support migration, for example by differences in density between the released petroleum and pore water and supported migration along of pressure gradients. Secondary migration, supported by water as well, will cause the transport of the hydrocarbons away from the kitchen area, preventing secondary effects like cracking and condensation reactions.

In summary, it is necessary to use an untreated source-rock with intact mineral matrix and kerogen network, as well as natural pressure regimes for a nature near simulation of generation, expulsion and primary migration. In addition, it is required to perform the source-rock maturation under hydrous conditions to mimic natural conditions and the released hydrocarbons have to be removed from the heated zone to prevent secondary reactions.

Different approaches were made to represent the above-mentioned factors on a laboratory scale to investigate their impact onto the composition of oil and gas. Most of these methods focused on only one single aspect, either the formation or the migration of hydrocarbons. This leaded to misinterpretation of results and incorrect impact-assessment onto generation, expulsion and migration of petroleum. Most methodologies focused on the generation of hydrocarbons and left the aspect of expulsion and migration unnoticed (e.g. standardised hydrous or anhydrous pyrolysis). In many cases, the sample preparation (grounding, decalcification) destroyed the mineral matrix and the kerogen network, which diminished expulsion and migration effects. For the reasons mentioned above, anhydrous methodologies too are insufficient to mimic natural conditions. However, a separate contemplation of the formation of petroleum on the one hand and of expulsion and primary migration on the other hand will be unrewarding, as both processes will run contemporaneous in nature.

To overcome methodical limitations, a newly designed apparatus was developed and built in the institute of geosciences in Kiel, referred to as Expulsinator. This device allows performing artificial maturation of an intact rock sample by hydrous pyrolysis and the release of petroleum under pressure conditions, prevailing during the subsidence of a source-rock. In addition, it is possible to collect the generated oil and gas after the expulsion and migration process in a semi-open setup during the simulation. The more detailed technical specifications were given in chapter 3, so in the following only a brief description is given:

The core of the Expulsinator is a high-pressure cell, which is characterized by a special cap design (see Figure 35). This allows applying of lithostatic pressure onto the rock sample of up to 2560 bar by hydraulic pressure transmission. In addition, the high-pressure cell is able to handle hydrostatic pressures of up to 300 bar (± 2 bar; generated by a HPLC-pump) and temperatures of up to 360 °C (± 1 °C). All parameters are computer controlled, recorded by the controlling unit and are freely programmable for a fully automatic experimental run. Expulsion simulation is carried out with an intact rock disc of 50 mm in diameter and of variable high (depending on the nature of the sample material). During the simulation, the rock disc is surrounded by an artificial reservoir, consisting of a porous sinter filter (stainless steel; 50 % porosity) and a protection tube to prevent lateral plastic flowing of the rock disk due to increasing lithostatic pressure. During simulation, the high-pressure cell is flooded with HPLC-water. By a directed inlet and outlet system, it is possible to flush out migrated and released hydrocarbons without pressure decrease and to collect the fluids and the gaseous products separately by the sampling unit.

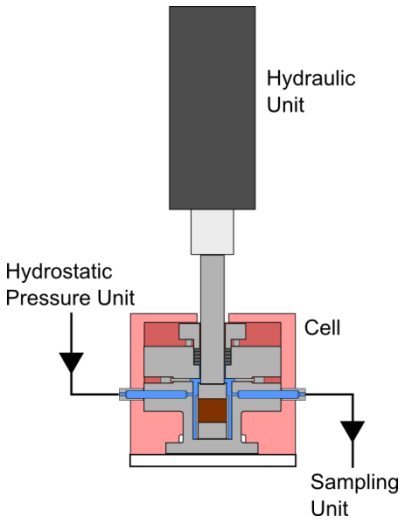


***Figure 35. Greatly simplified schematic representation of the expulsion apparatus.***

## 4.3 General experimental conditions

Simulation of the formation and expulsion of hydrocarbons in the curse of catagenesis required pressure conditions present during the generation of oil and gas. This includes hydrostatic and lithostatic pressures prevailing during the burial history of a source-rock. Considering a geothermal gradient of 33 °C/km, the maximum of oil generation is exceeded at 3 km depth (Bordenave, 1993; Tissot et al., 1987; Tissot and Welte, 1984). Assuming an average density of 2.31 $^{g}/_{cm^3}$ to 3.06 $^{g}/_{cm^3}$ of the rocks in a sedimentary basin the lithostatic pressure increases by 0.23 $^{bar}/_{m}$ to 0.31 $^{bar}/_{m}$ (Sahay, 1999), resulting in pressures between 680 bar and 916 bar at 3 km depth. For hydrostatic pressures (or pore pressures) pressure gradients of 0.10 $^{bar}/_{m}$ (fresh and brackish water, $\rho_w = 1.00$ $^{g}/_{cm^3}$) to 0.11 $^{bar}/_{m}$ (salt water, $\rho_w = 1.07$ $^{g}/_{cm^3}$) are assumed (Sahay, 1999), resulting in a pressure-range of ca. 295 bar to 316 bar at 3 km depth. This corresponds to hydrostatic pressures, which are three times higher as hydrostatic pressures (Hanebeck, 1993).

Under geological conditions, the temperature range at main petroleum formation and oil expulsion is between 90 °C and 150 °C, prevailing for periods of millions of years (Quigley and Mackenzie, 1988; Tissot and Welte, 1984). To accelerate the formation processes and the expulsion mechanisms in the laboratory the temperatures have to be increased to temperatures between 300 °C and 360 °C.

Corresponding to the assumption above, a catagenesis simulation was carried out with three

different pyrolysis steps (see Figure 36). The first step corresponded to a depth of ~2000 m (T: 300°C; $P_{lith}$: 600 bar; $P_{hyd}$: 200 bar) and was performed for 72 h. Afterwards, the pressures and temperature were increased to simulate conditions corresponding to a depth of ~2500 m (T: 330°C; $P_{lith}$: 750 bar; $P_{hyd}$: 250 bar). These conditions were kept constant for 72 h. In the following, the temperature and the pressures were increased to a corresponding depth of ~3000 m (T: 360°C; $P_{lith}$: 900 bar; $P_{hyd}$: 300 bar). This final stage was kept constant until the yields of expelled hydrocarbons reached a significant minimum. The Expulsinator experiment was terminated after 120 h.

The generated and expelled hydrocarbons were collected cumulatively for time intervals of 12 h. In every time-interval, products within the artificial reservoir were flushed out every 20 min with a Volume of 4 ml, resulting in 144 ml of fluid sample after 12 h. To increase the solubility of the expelled petroleum in the water and to prevent precipitation of asphaltenes, a small amount of a modifier (< 9 ml, *n*-hexane/2-propanol 85:15) was pumped through the artificial reservoir ever 5 h for 45 min. In total, 23 liquid samples were obtained, quantified and processed for further analysis. In addition, the untreated sample and the rock sample after the experiment were extracted and prepared for analysis.

### 4.3.1 Experimental conditions of comparative pyrolysis experiments

Established pyrolysis methods were used to compare the results of the newly developed approach. Additional pyrolysis experiments were conducted with closed small vessel pyrolysis (CSVP) and microscale sealed vessel pyrolysis (MSSV). The detailed technical proceedings were explained chapter 3. Therefore, only a short description of the methodologies is given.

For CSVP grounded, pre-extracted sample material was used. For MSSV the pre-extracted rock-sample was decalcified additionally to increase the kerogen content for pyrolysis. The pre-extraction was performed with a Büchi SpeedExtractor E-914 with a preselected pressure of 50 bar and at 75 °C and a mixture of DCM and methanol (93:7). The inorganic carbon content was removed via hydrochloric acid (HCl; 25 %).

CSVP were performed as a single-step and as a multi-step variant, with additional water (hydrous) and without addition of water (anhydrous). All CSVP-variants were conducted with the same temperature

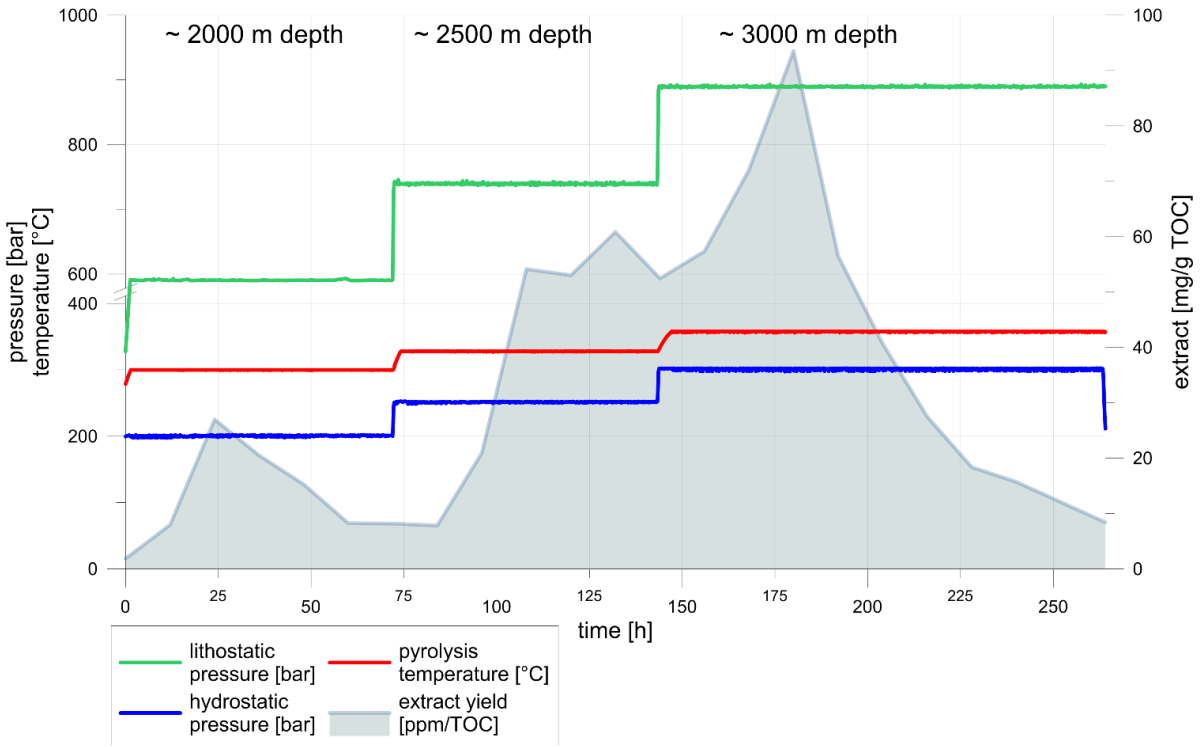


***Figure 36. Experimental pressure and temperature conditions and the expulsion profile of the catagenesis simulation.***

sets, ranging from 210 °C to 360 °C in 30 °C steps and 375 °C. For the multi-step variant 8 g and for the single-step variant 3 g of sample material were used. In case of the multi-step variant, the pyrolyzed rock sample was removed after each temperature step and generated products were obtained by raising of the reactor and extraction of the pyrolyzed rock. Afterwards, an aliquot (500 mg) was retained for further analysis and the pyrolyzed and by now extracted rock sample was inserted into the reactor again, to be pyrolyzed at a higher temperature. This procedure was repeated until the final temperature step was reached. In case of the single-step variant, fresh pre-extracted sample material was used for every temperature step.

The used MSSV-methodology is described by Horsfield et al. (1989) and in chapter 3. A small amount of sample material (5-18 mg, mixed with glass beads) was pyrolyzed in glass tubes (ca. 40 µl volume) for 72 h at 300 °C, 330 °C and 360 °C. After the pyrolysis, the glass tubes were inserted into a purpose-build sample holder connected to a GC-FID. The glass tubes were crushed within the sample holder and the pyrolyzates were released, vaporised at 300 °C and transported into the GC-FID by a helium stream.

### 4.3.2 Analytical processing

The content of total carbon (TC), total sulphur (S), total nitrogen (N) and total inorganic carbon before and after analysis were measured with the VARIO EL III elemental analyser.

For molecular-geochemical investigation of the liquid samples, the oil-water mixtures were extracted by liquid-liquid extraction with dichloromethane (DCM). The extracts were separated into an aliphatic, an aromatic and a NSO-fraction by column separation.

GCMS measurements were performed with an Agilent 7820A GC-system coupled with a 5975 MSD Agilent mass-spectrometer. The analysis were carried out with a HP 5 fused silica capillary column (30 m length, 0.25 mm inner diameter, 0,25 µm film thickness). The temperature program of the GC-oven started with 60 °C isothermal for 5 min, then heating to 325 °C at 4 °C/min., which was finally held isothermal for eight minutes.

MSSV was measured with a SGE forte BP1 column (50 m length, 0.32 mm inner diameter and 1 µm film thickness). The temperature program was as followed: 40 °C for 13 min, then heating to 320 °C at 5 °C/min. This temperature is held for 25 min. Finally, the temperature is raised to 330 °C at 5 °C/min and hold for 10 min.

### 4.3.3 Sample description

The sample material was Posidonia shale from the HOLCIM quarry near Dotternhausen (SW-Germany). It is a lower Jurassic bituminous black shale (lower Toarcian – Lias ε II 1-12), as described by Frimmel et al. (2004) and Röhl et al. (2001).

The selected rock sample had a high TOC-value of 10.76 % and high HI and low OI-values with low $T_{max}$-values (see Table 16). The bulk data is corresponding to results presented by Frimmel et al. (2004), even though the low OI would classify the sample as type-I to type-II kerogen.

***Table 16. Bulk parameter of the used Posidonia shale.***

| Parameter | Posidonia shale |
|---|---|
| **TOC [%]** | 10.67 |
| ***$S_1$ [mg HC/g rock]*** | 4.68 |
| ***$S_2$ [mg HC/g rock]*** | 78.63 |
| ***$T_{max}$ [°C]*** | 428 |
| ***HI [mg HC/g TOC]*** | 730.65 |
| ***OI [mg $CO_2$/g TOC]*** | 10.52 |
| ***extract [mg/g TOC]*** | 108.72 |

## 4.4 Expulsion profile and extract yields

In Figure 36 the expulsion profile of the catagenesis simulation is given. In total, three individual expulsion phases can be distinguished, showing the maxima of extract yields at each temperature and pressure step. The lowest extract yields were reached during the first pyrolysis step at 300°C and low pressure conditions. The second expulsion phase started after a well-established minimum during the second pyrolysis step at 330°C and medium pressure conditions. The minimum in the extract yields after the second maximum was not as pronounced as the first minimum, but still significant. The highest extract yields were reached at the very last expulsion step with the highest temperature (360 °C) and pressure conditions (see Table 17).

***Table 17. Extract yields of the catagenesis experiment.***

| Step | Parameters [Temp.; hyd. & lith. pressure] | Total Extract [mg/g TOC] |
|---|---|---|
| **1st** | 300°C; 200 bar; 600 bar | 88.97 |
| **2nd** | 330°C; 250 bar; 750 bar | 249.32 |
| **3rd** | 360°C; 300 bar; 900 bar | 402.33 |

The extract yields generated and released during the first pyrolysis step are in the same magnitude as the extract yields of the untreated sample. The reason is that at the low temperature of the first pyrolysis step only the in-situ bitumen is mobilised and little or no generation occurs. To the contrary, the high extract yields of the second and the third pyrolysis step were clearly attributed to new generation and expulsion of hydrocarbons.

## 4.5 Compositional changes of *n*-alkanes upon expulsion

In Figure 37.1 the general distribution of short, middle and long chain *n*-alkanes is given of hydrous and anhydrous CSVP, of MSSV and of the catagenesis simulation. Main difference between hydrous and anhydrous CSVP was a significant higher content of middle-chain *n*-alkanes and a much lower amount of *n*-alkanes with long-chain length in case of hydrous CSVP. The amount of short-chain *n*-alkanes was in the same range for both methods. The relative distribution of the *n*-alkanes for MSSV again differed from the values of hydrous and anhydrous CSVP, but was closer to the anhydrous method. Noticeable were higher amounts of short-chain *n*-alkanes and lower contents of middle- and long-chain components. This is due to methodological differences: In case of MSSV, generated products were discharged directly into the GC-system without evaporation losses.

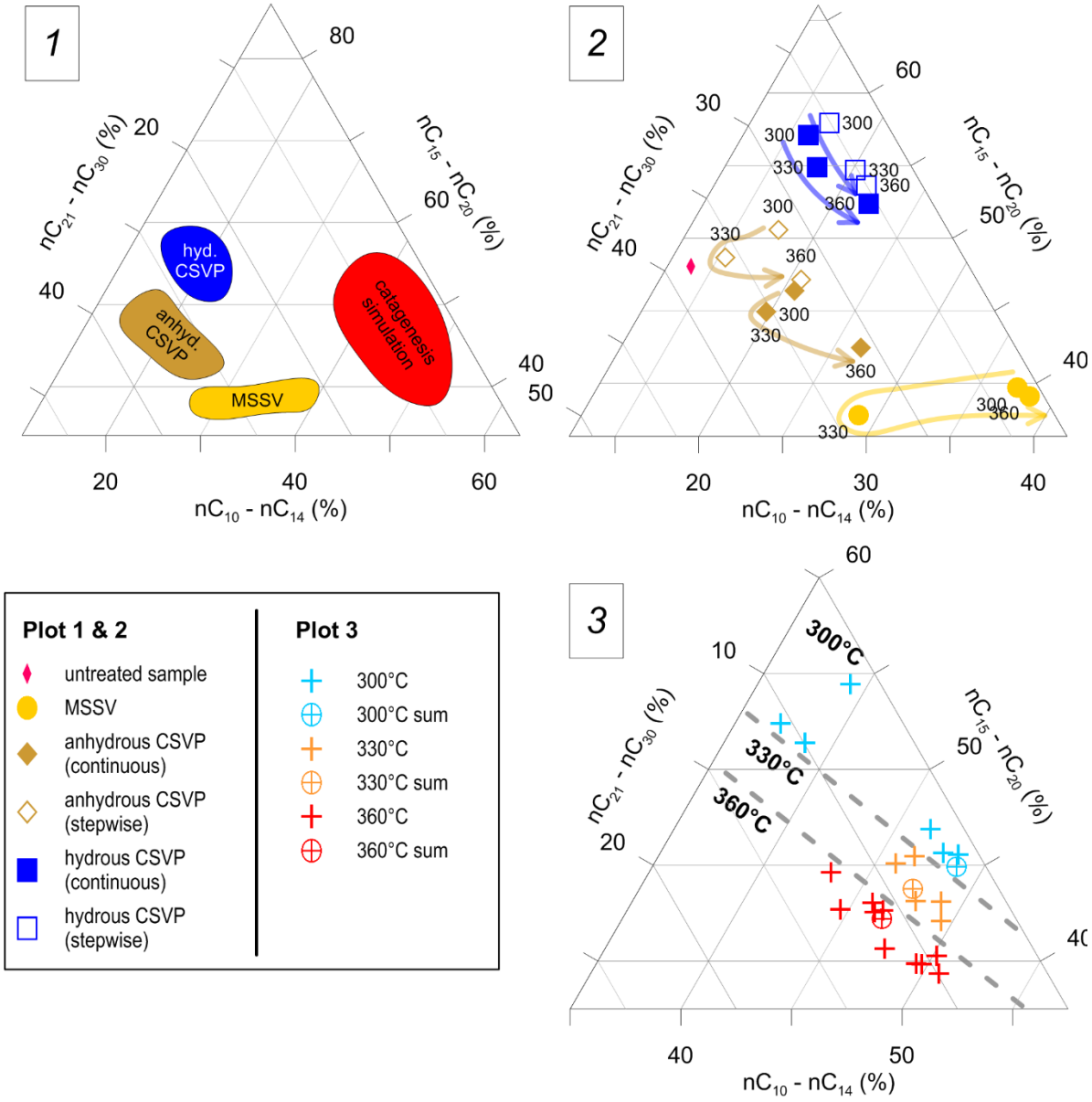


***Figure 37. Distribution of short-, middle- and long-chain n-alkanes of the generated bitumen of CSVP, MSSV and the catagenesis simulation. (1) Overview of the results of the different methodologies; detailed results of the CSVP and MSSV experiments (2) and of the catagenesis simulation (3).***

The differences of the relative amounts of long- and middle-chain *n*-alkanes between the hydrous and anhydrous methodologies in particular, suggest that water plays an important role to support cracking reactions and decomposition processes of the kerogen. Higher yields of bitumen for hydrous pyrolysis in general were observed in various studies (Andresen et al., 1993; Kuangzong et al., 1994; Lewan, 1997; Uguna et al., 2012). Higher yields for $C_{14}$+ components are reported by Behar et al. (2003). The reason therefore is widely seen in supported cracking reactions in case of the hydrous pyrolysis, respectively in condensations reactions in case of anhydrous conditions, leading to the formation of pyrobitumen and char (Behar et al., 2003; Lewan, 1997). Water is supposed to inhibit the aromatization and to prevent cross-linking processes, leading to reduced yields in liquid products in case of anhydrous pyrolysis (Behar et al., 2003; Michels et al., 1995). The origin of the incorporated hydrogen (water or the residual kerogen) could be crucial for the reaction pathway, leading to different hydrogen exchange mechanisms (Michels et al., 1995). This was supported by experiments with isotopic labelled water, which showed large isotopic transfers between water-derived hydrogen and organic hydrogen during maturation and incorporation of hydrogen into the kerogen (Schimmelmann et al., 1999). These effects seemed to affect the relative amounts of short-, middle- and long-chain *n*-alkanes in this study, as well. Propagated cross-linking and condensation reactions in case of anhydrous CSVP reduced the relative amount of *n*-alkanes with short- and middle-chain length and increased the relative amount of long-chain *n*-alkanes. In contrast, cracking reactions, supported by the donation of hydrogen by water, would decrease the relative amount of long-chain *n*-alkanes, as shown by hydrous CSVP.

Remarkable were the differences between the different temperature steps of hydrous and anhydrous CSVP (Figure 37.2). Hydrous CSVP showed a continuous decrease of middle-chain *n*-alkanes to products with shorter chain length with increasing temperature. In contrast, the relative amounts of long-chain *n*-alkanes increased and while the amounts for short-chain *n*-alkanes decreased from 300 °C to 330 °C pyrolysis temperature in case of anhydrous CSVP. However, for the temperature step from 330 °C to 360 °C the trend was similar to the trend of hydrous CSVP (decrease of middle-chain and increase of short-chain *n*-alkanes). The absence of water and its supportive effect to thermal cracking could cause this shift in the relative amounts. At 330 °C, the thermal energy was not sufficient to crack down the hydrocarbons into smaller products without the support of water. Thermally caused condensation and cross-linking processes did not occurr at temperatures around 330 °C (Lewan, 1997). The onset of these processes lowered the relative amount of long- and middle-chain *n*-alkanes in favour of shorter products.

The *n*-Alkane distribution of the catagenesis experiment showed very different behaviour compared to CSVP and MSSV. The differences manifested themselves in much higher relative amounts of *n*-alkanes with short-chain length and significant lower content of long-chain *n*-alkanes (Figure 37.1). The difference was shown more clearly by the behaviour of the composition of short-, middle- and long-chain *n*-alkanes upon increasing maturation and ongoing expulsion (Figure 37.3). Where hydrous CSVP showed a trend towards shorter chain-length with increasing pyrolysis temperature, the catagenesis experiment behaved inverse: The relative amount of short- and middle-chain compounds decreased with ongoing maturation, while the amount of long- chain *n*-alkanes increased. This clearly showed an expulsion effect affecting the distribution of the *n*-alkanes by a preferentially retention of long-chain *n*-alkanes during the expulsion by geochromatographic effects. With increasing simulated subsidence, the increase of the lithostatic pressure with each simulation step lead to the generation of new pathways and enhanced the release of even larger components. The increasing amounts of long-chain *n*-alkanes lead to the decrease of the relative amounts of short and middle-chain *n*-alkanes in the later steps.

Although the relative data indicated an increase of long-chain *n*-alkanes in case of the catagenesis simulation, the absolute data showed that the classical methods (CSVP) produced much higher amounts of long-chain components compared to the expulsion experiment. In Figure 38 the percentage deviations of the yields of *n*-alkanes between the different methodologies are shown. The yields of short-chain *n*-alkanes were much higher for the catagenesis simulation as for CSVP. At the same time, the catagenesis simulation produced significant lower amounts of *n*-alkanes with longer chain-length. In case of hydrous CSVP, the positive deviation focused much more onto the highest temperature stages, but reached from $nC_{15}$ to $nC_{36}$. In contrast, the positive deviation of anhydrous pyrolysis was much broader and already starts at temperatures around 330°C, but includes only a range of *n*-alkanes from $nC_{18}$ to $nC_{36}$. This effect was caused by supported cracking processes due to the presence of water in case of the hydrous CSVP, as already described above. Multi-step and single-step differed mainly in the intensity of the positive deviation, which was much more pronounced for single-step CSVP. In case of the multi-step pyrolysis, generated products of a certain temperature step were removed afterwards and therefore no longer available for further thermal decomposition. This lead to a decrease of the amount of generated *n*-alkanes, as

precursors did not form *n*-alkanes in the following temperature steps.

The shift towards short-chain *n*-alkanes in case of the catagenesis experiment was a result of the impact of expulsion and migration effects. Retaining of components with larger chain-length by geochromatography caused a longer thermal exposure time. Therefore, these components

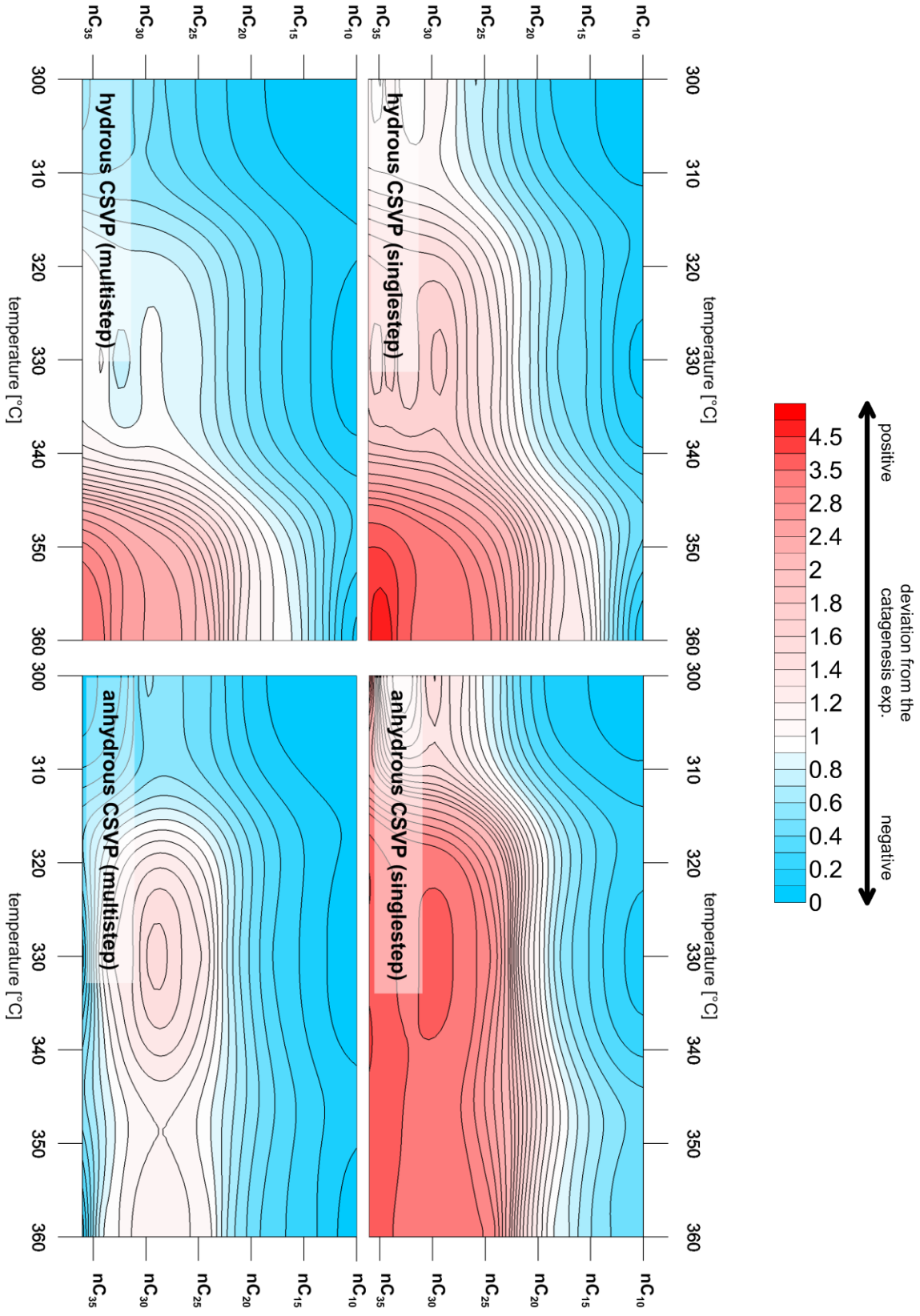


***Figure 38. The percentual deviation of specific n-alkanes of CSVP compared to the catagenesis experiment. Red indicates an higher amount and blue a lower amount compared to the catagenesis experiment. (Gridding callculation parameters: Power: 4; Smoothing: 1; Anisotropy ratio: 3; Anisotropy angle: 0)***

underwent further thermal cracking, leading to a higher content of short- and mid-chain *n*-alkanes.

## 4.6 Influence of generation and expulsion to isoprenoid ratios (pristane/phytane)

The ratio between pristane (Pr) and phytane (Ph) showed to be influenced more by redox conditions of the sedimentation environment as by the maturity of the source-rock (Peters et al., 2005a). Reason is a favoured generation of pristane under oxic conditions, whereby the biological precursor phytol is oxidized by several interim steps to pristane. Conversly, reducing and anoxic conditions caused increased generation of phytane by reduction reactions. However, the Pr/Ph-ratio is also affected by maturation processes, as shown in a variety of studies. Low values for Pr/Ph of immature oils and source-rocks were contrasted by higher values in corresponding samples with higher maturity (Volkman and Maxwell, 1986). Reason therefore could be an increased release of sulphur-bound phytols during early maturation (De Graaf et al., 1992), or a generally higher abundance of pristane precursors bounded within the kerogen (Koopmans et al., 1999). This assumption was supported by results of generation and expulsion experiments, in which the propagated release of pristane from kerogen was reported (Eseme et al., 2006a). Open and closed pyrolysis experiments showed same generation rates for pristane and phytane, but higher rates of decomposition in case of phytane (Tang and Stauffer, 1995), which would lead to an increasing ratio with ongoing maturation. For higher maturity, the Pr/Ph-ratio shows certain inaccuracies and decreasing values were observed by a variety of studies (Albrecht et al., 1976; Brooks et al., 1969; Radke et al., 1980).

***Table 18. Yields of the total extract, the sum of n-alkanes ($nC_{10}$-$nC_{38}$) and pristane and phytane of CSVP experiments.***

| | Hyd. CSVP (multi-step) | Hyd. CSVP (single-step) |
|---|---|---|
| **Extract [mg/g TOC]** | 555 | 463 |
| ***n*-alkanes [µg/g TOC]** | 28939 | 35742 |
| **Pristane [µg/g TOC]** | 649 | 1269 |
| **Phytane [µg/g TOC]** | 348 | 607 |
| ***n*-alkanes/ extract [%]** | 5.21 | 7.72 |
| **Pr+Ph/ extract [%]** | 0.18 | 0.41 |
| **Pr+Ph/ *n*-alkanes [%]** | 3.44 | 5.25 |

The yields of pristane and phytane of the catagenesis simulation, the multi-step CSVP and the single-step CSVP are shown in Table 19. For the catagenesis simulation and the multi-step CSVP the yields were formed by summation of the yields of the previous pyrolysis steps. This method enables the comparison between the methods with stepwise removal of compounds (expulsion experiment and multi-step CSVP) and single-step CSVP. It has to be considered that it was not possible to use pre-extracted material in case of the catagenesis simulation. Therefore it cannot be excluded that larger amounts of expelled isoprenoids were affiliated with already existing in-situ bitumen, especially at the low temperature step (300 °C), where only low generation rates can be expected. However, it can be assumed that larger amounts of the in-situ isoprenoids underwent thermal cracking processes and did not affected the Pr/Ph-ratio drastically, especially at higher temperatures. Nevertheless, the yields of the untreated sample are given in Table 19, along with the isoprenoid yields subtracted by the initial amount (in brackets).

***Table 19. Yields of pristane and phytane of the catagenesis experiment, single- and multi-step CSVP.***

| | | Pristane [µg/g TOC] | | | Phytane [µg/g TOC] | | |
|---|---|---|---|---|---|---|---|
| | | **Catagenesis exp.[1)]** | **Hyd. CSVP (multi-step)[1)]** | **Hyd. CSVP (single-step)** | **Catagenesis exp.[1)]** | **Hyd. CSVP (multi-step)[1)]** | **Hyd. CSVP (single-step)** |
| | **Untreated sample** | 536.2 [2)] | | | 209.1 [2)] | | |
| **Py. temp. [°C]** | **300** | 275.6 (0) [3)] | 28.1 | 74.0 | 162.5 (0) [3)] | 18.0 | 31.2 |
| | **330** | 657.1 (120.9) [3)] | 292.9 | 428.6 | 346.1 (136.9) [3)] | 96.3 | 163.5 |
| | **360** | 1004.7 (468.5) [3)] | 648.9 | 1268.8 | 540.1 (331.0) [3)] | 348.0 | 607.5 |

*[1)] Displayed values included the sum of previous pyrolysis steps to obtain comparable data between the catagenesis experiment, the multi-step CSVP and the single-step variant.*

*[2)] Due to the use of not-extracted material in case of the catagenesis experiment, the isoprenoid-yields of the untreated sample are given.*

*[3)] Values are subtracted by the initial value of the untreated sample. These values are for guidance only, as certain amounts of the initial in-situ isoprenoids will undergo decomposition by cracking and rearrangement reactions.*

In comparison with single-step CSVP, the multi-step variant reached much higher yields for pristane and phytane in all temperature steps. There seemed to be a stronger degradation of isoprenoids in case of multi-step CSVP. At first glance, this is in contrast to observations concerning the yields of total extracts and *n*-alkanes, which are described in detail in chapter 3. The multi-step CSVP reached higher yields of total extract, but produced lower amounts of *n*-alkanes (Table 18), which is explained by an undifferentiated removal of precursors of *n*-alkanes in former pyrolysis steps in case of the multi-step CSVP. Therefore, they are not available for thermal decomposition in the next pyrolysis step, which will result in decreasing yields of *n*-alkanes. However, the ratio of pristane and phytane to *n*-alkanes showed that this effect is not affecting the yields of the isoprenoids. The ratio is smaller in case of the multi-step CSVP, which indicated that a higher rate of thermal decomposition of isoprenoids took place as in the multi-step variant. The reason therefore could be that demethylation processes of the isoprenoids took place at lower energy levels than thermal cracking processes of other components. Therefore, it is quite possible that demethylation processes were amplified by the longer gross pyrolysis time in case of the multi-step CSVP. Each pyrolysis step took 72 h, which means that after termination of the 360 °C-step, the sample was exposed for 432 h in total to different pyrolysis temperatures (starting with 210 °C). If demethylation processes already begin at lower temperatures (e.g. 300 °C), then this could explain higher amounts of total extract, but lower yields of *n*-alkanes and even lower yields of isoprenoids. Additionally the value of the Pr/Ph-ratio at 330 °C was very high in case of multi-step CSVP (Table 20), showing that phytane underwent enhanced degradation. This supports the observation of increased decomposition of isoprenoids, as for phytane higher rates of degradation are already reported (Tang and Stauffer, 1995).

***Table 20. Pr/Ph-ratio of the catagenesis experiement and multi-step (both cumulative) and single-step CSVP.***

| | Pr/Ph | | |
|---|---|---|---|
| **Temp. [°C]** | **Catagen. exp.** | **Hyd. CSVP (multi-step)** | **Hyd. CSVP (single-step)** |
| **300** | 1.70 | 1.56 | 2.37 |
| **330** | 1.90 | 3.04 | 2.62 |
| **360** | 1.86 | 1.86 | 2.09 |

A completely different picture emerged in the case of the catagenesis experiment. Here, the total amounts of the isoprenoids were in between of the multi-step and the single-step CSVP. Considering the existing in-situ isoprenoids, the obtained amounts were below the values reached by multi-step CSVP. However, as mentioned earlier, it can be assumed that a large amount of the i*n*-situ isoprenoids underwent very early demethylation processes and therefore they should not be fully subtracted. In case of the catagenesis simulation, it seems that the isoprenoids were decomposed in a higher grade than in the single-step CSVP, but not as drastically as in the multi-step CSVP. It was not possible to determine a preferred degradation of phytane, as observed in the multi-step pyrolysis. The values of the Pr/Ph-ratio showed a relatively uniform trend (Table 20). Higher degradation rates of the isoprenoids could be due to longer dwell times within the source-rock after their release. That the preferred decomposition of phytane was not observed could be due to catalytic processes, involving active clay minerals, leading to an equable decomposition.

In Figure 39 the Pr/Ph-ratio of the catagenesis experiment, the multi-step and the single-step CSVP is given (mid-part) together with the expulsion profile (lower part). In addition, the influence of the individual isoprenoid onto the ratio is displayed (upper part). During the first pyrolysis step at 300 °C, the i*n*-situ bitumen and the already existing isoprenoids will have larger impact onto the displayed ratio. However, the ratio started a little higher than the value of the untreated sample, showing that the ratio of the expulsion experiment was already influenced by newly released isoprenoids and decomposition of the i*n*-situ components. It is interesting that in this first pyrolysis step a decrease of the ratio was noticeable. This trend is mainly generated by the release of larger amounts of phytane during the increasing phase of the expulsion and by a slightly larger decrease of pristane during the decreasing expulsion stage. The ratio of the sum of the expelled isoprenoids (red triangle) showed nearly no change in the Pr/Ph-ratio during this stage, which is an indication that the observed decrease of the ratio was rather due to expulsion effects, than due to cracking and decomposition effects. The single values of the comparative CSVP experiments at 300 °C were increased compared to the results of the Expulsinator experiment, indicating increased release of pristane and/or increased decomposition of phytane. In contrast, the cumulative value of the multi-step CSVP (blue triangle) showed identical values to the catagenesis simulation. This exhibits a decomposition-related difference, rather than displaying higher releasing-rates of pristane.

With increasing pressure and temperature conditions, the Pr/Ph-ratio increased abruptly to values around 2.2. This offset is caused by a drastic increase of the expelled amounts of pristane compared to phytane, which seems to be a response of a tocopherol and/or chromane breakdown, both components present in large quantities within the source-rock. This abrupt increase to the beginning of the second pyrolysis phase represented the

maximum if the Pr/Ph-ratio, as the general trend decreased in the following, which was also not interrupted by the third expulsion phase.

Looking at the impact of each isoprenoid onto the ratio it is obvious that the decreasing trend was mainly caused by a stronger decrease of pristane than by increasing expulsion of phytane. In conclusion, the ratio was mainly affected by the preferred generation of pristane at the beginning of the second expulsion phase and a slowly decreasing pool of pristane afterwards. Preferred degradation of phytane played only a subordinate role. Lower expulsion potential of pristane was also the reason

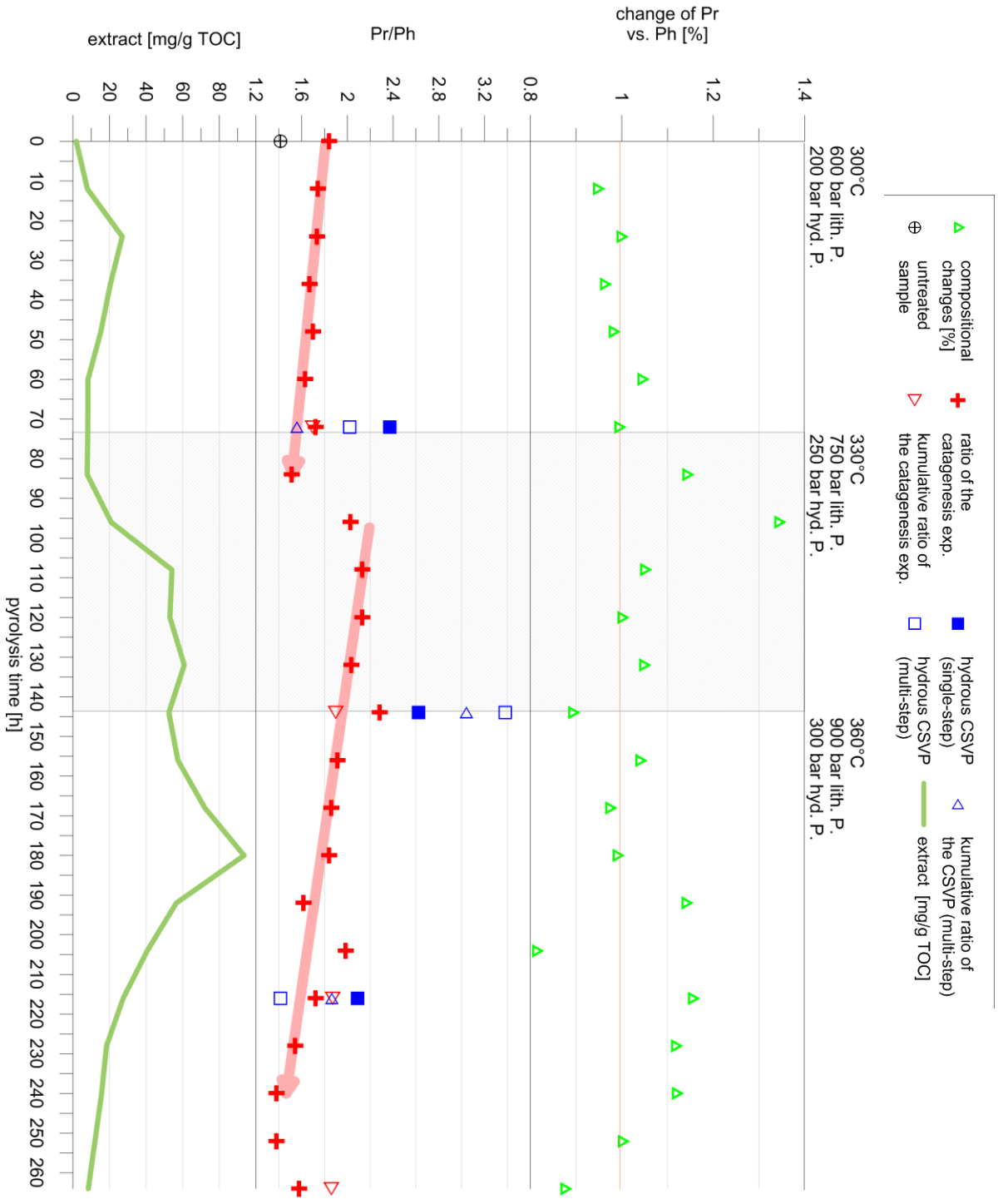


***Figure 39. The expulsion profile (below), the pristane to phytane ratio of the catagenesis experiment together with the corresponding values of hydrous and anhydrous CSVP (middle), and the indication of the causative of the changes of the ratio (above). Values >1 indicate an higher impact of pristane onto changes of the ratio, values <1 an higher impact of phytane.***

for the decreasing trend during the first expulsion step.

The values of the ratio of the CSVP experiments differed extremely at 330 °C compared to the expulsion experiment. Especially the ratio of the multi-step experiment was around 40 to 60 % higher as the values of the catagenesis experiment (single values and cumulative values, see Table 20). The ratio of the single-step CSVP was increased, too, although not as high as the value of the multi-step CSVP. This was due to propagated decomposition of phytane for both methodologies, but especially for the multi-step pyrolysis, as already explained above.

The values of CSVP obtained at 360°C correspond well with the values obtained by the catagenesis experiment. This showed that a general equilibrium is reached at a minimum value around 1.6 to 1.4, which is astonishingly near to the initial value of the untreated sample (1.41). The observed changes of the ratio during the different maturation steps generated by the different methodologies seemed to be generally caused by expulsion effects (catagenesis experiment) or different generation/decomposition rates (CSVP) and overprint the actual signal by varying the amount of pristane (catagenesis experiment) or phytane (CSVP).

In general, first an increase of the Pr/Ph-ratio can be noted for both methodologies, followed by a decrease until the start value is reached again. As already noted above, increasing and decreasing values of this ratio in dependence of the maturity were observed in a variety of studies before (Albrecht et al., 1976; Brooks et al., 1969; Radke et al., 1980). The reason therefore are both fluctuations of the expulsion rate, mainly of pristane, and different decomposition rates of pristane and phytane, mainly as secondary reactions after the release of the isoprenoids. The first effect was shown in the catagenesis experiment, in which secondary reactions played only a minor part. The second effect was observed primarily in the CSVP experiments, where the exposure time to elevated temperatures of both the kerogen and the generated bitumen, is much longer compared to the catagenesis experiment.

## 4.7 Isoprenoid/*n*-alkane ratios as molecular expulsion efficiency proxies

In general, the ratio between isoprenoids and *n*-alkanes decreased with increasing maturity due to increasing *n*-alkane generation by thermal cracking and decreasing isoprenoid yields (Tissot et al., 1971). For the ratio of Pr/*n*-$C_{17}$ and Ph/*n*-$C_{18}$ several studies observed decreasing values with ongoing primary migration. Some of these studies investigated natural systems by sampling a source-rock in different depth and migration distances (Leythaeuser et al., 1984a, 1984b; Leythaeuser and Schaefer, 1984). Others tried to investigate expulsion and migration impact onto the ratio of isoprenoids to *n*-alkanes by laboratory experiments (Lafargue et al., 1990; Mackenzie et al., 1983).

In Figure 40, the Pr/*n*-$C_{17}$-ratio is plotted together with the expulsion profile and the indication of the component with the higher impact onto the change of the ratio. During the first phase of the expulsion experiment, only minor changes could be observed. Again, this was due to in-situ bitumen, which was only little affected by thermal decomposition and new generation. As already described for the Pr/Ph-ratio, an offset was recognizable between the Pr/*n*-$C_{17}$-ratio of the untreated sample and of the expelled extracts. The decrease of the ratio compared to the initial value was explained by a constant rate of demethylation processes, which affected the amount of pristane. Within the first expulsion step, a slight upward trend was recognizable. Since we assumed no significant generation at this low-temperature stage, this effect should not be due to increasing generation of pristane. Rather, this was caused by a minimal retention of pristane by geochromatography, leading to a modest increase of the ratio. Values of the Pr/*n*-$C_{17}$-ratio of the CSVP experiments were consistently lower at 300 °C as the values reached by the expulsion experiment. The values of the multi-step CSVP were even lower as of the single-step variant. In general, the yields of both CSVP variants were low at 300 °C for both, the total extract and *n*-alkanes and isoprenoids. However, for both CSVP variants, a preferred release of *n*-alkanes could be noticed, combined with a higher impact of demethylation reaction, particularly affecting the results of the multi-step CSVP.

With the beginning of the second expulsion step and the onset of the generation phase the value of the ratio dropped abruptly from ~2.25 to ~1.75. The reason therefore was the increasing release of newly generated *n*-$C_{17}$, as shown by the upper diagram in Figure 40. In the following, the ratio continued to decline to values around 1.25 at the end of the 330°C-step. This was caused now by a depletion of the pool of isoprenoids, leading to a decrease of the expelled amounts of pristane. The CSVP experiments reached elevated values compared to the catagenesis simulation (1.75 to 2 vs. 1.25 in case of the expulsion experiment). However, the cumulative calculated value of the expulsion experiment was in the range of the CSVP experiments. This clearly showed that this effect could only be observed with an (semi-) open pyrolysis setup and that closed pyrolysis cannot deliver nature near results in this domain.

The last expulsion step at 360°C started again with generation of *n*-$C_{17}$ and the release of large amounts of *n*-alkanes, leading to a further lowering of the ratio. Subsequent decrease of the ratio was caused by a further depletion of the pool of isoprenoids, until equilibrium was reached at 0.25. This was also mirrored in the values reached by CSVP. The equilibrium between the pristane and *n*-$C_{17}$, which was reached at higher maturity stages, was in dependence of the nature of the source material (Leythaeuser and Schwarzkopf, 1986). Further experiments are necessary to investigate the behaviour of different kerogen types onto the Pr/*n*-$C_{17}$-ratio and their impact onto the equilibrium-value reached at the end of the oil-window.

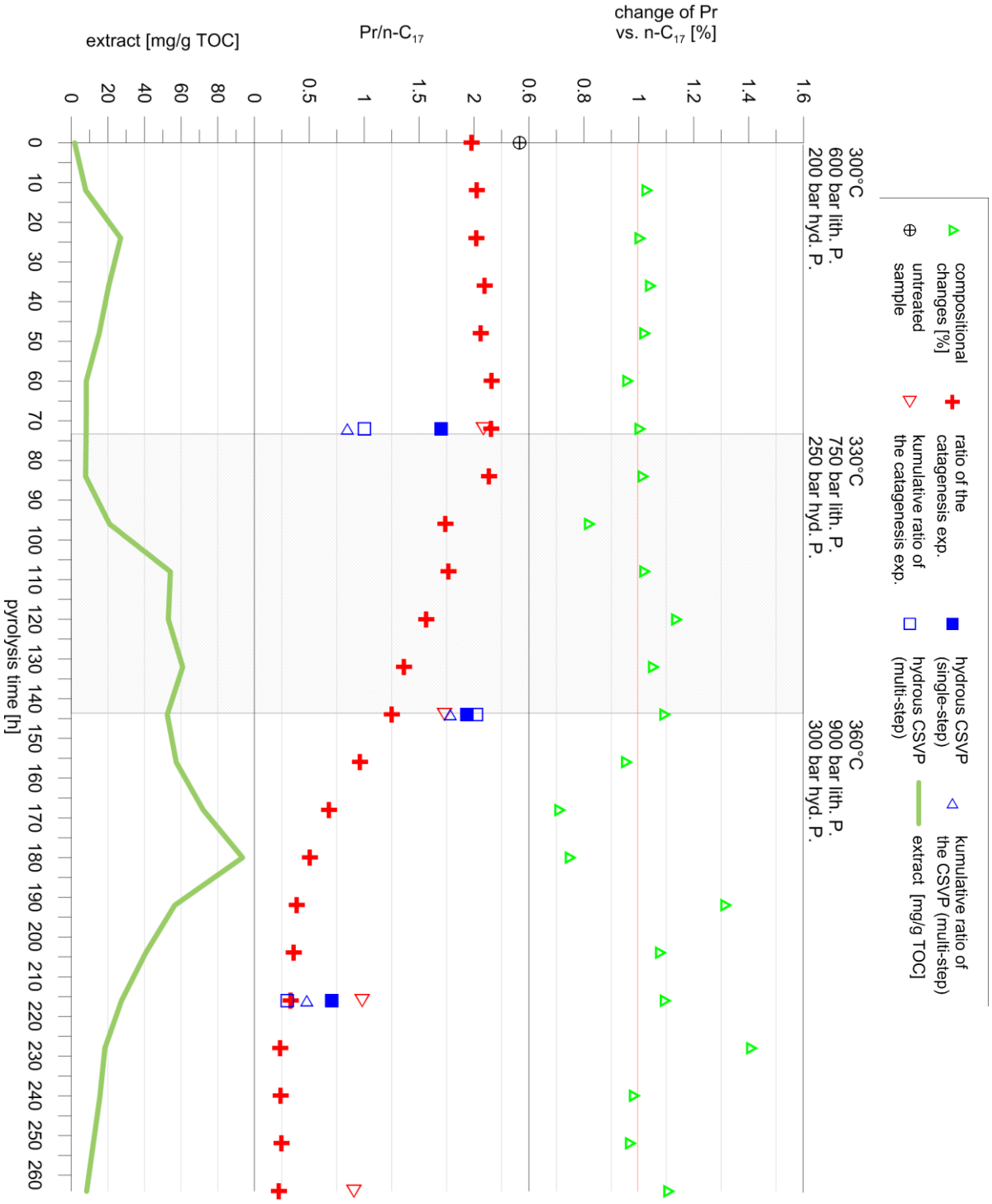


***Figure 40. The expulsion profile (below), the pristane to n-$C_{17}$ ratio of the catagenesis experiment together with the corresponding values of hydrous and anhydrous CSVP (middle), and the indication of the causative of the changes of the ratio (above). Values >1 indicate a higher impact of pristane onto changes of the ratio, values <1 a higher impact of n-$C_{17}$.***

The observed effect of the decrease of the Pr/*n*-$C_{17}$-ratio was mainly associated with decreasing generation rates of pristane during the experiment and not due to geochromatographic retention effects affecting isoprenoids, as stated by several authors (Leythaeuser et al., 1984a, 1984b; Leythaeuser and Schaefer, 1984; Leythaeuser and Schwarzkopf, 1986; Mackenzie et al., 1983). The interpretation of this effect by retention effects affecting isoprenoids is based on a wrong idea of the generation and expulsion/migration process. Source-rocks show increasing values of the Pr/*n*-$C_{17}$-ratio in migration direction towards the reservoir (Leythaeuser et al., 1984b). Here, it is assumed that the bitumen in the middle of the source-rock (or at the point, farthest away of the reservoir rock) is the most unmodified material and that it is more and more affected by expulsion effects towards the boundary to the reservoir (Leythaeuser et al., 1984a, 1984b). However, this is only possible if we have two different processes of generation and migration, separated in time and that the grade of migration is in dependence of the distance to the reservoir rock.

The explanation of said authors would lead to a very low Pr/*n*-$C_{17}$-ratio at the beginning of the expulsion, as here *n*-alkanes would be expelled preferred to isoprenoids. With ongoing migration, the value of the ratio would increase due to time-delayed expulsion of the isoprenoids. This is in opposite to the observations made in this study. Retention effects exist, which affect isoprenoids, but show only a very small impact onto the ratio, as shown by the very first step of the catagenesis experiment. Other studies show a very small effect of preferred retention of pristane (Mackenzie et al., 1983) or no effect at all (Bonilla and Engel, 1986).

In reality, generation and migration are both processes, which cannot be divided and which happen at the same time: New free hydrocarbons are generated, while already generated hydrocarbons migrate through the source-rock simultaneously. Furthermore, migration affects the whole rock body and is not in dependence of the distance to the reservoir rock. With this simultaneous generation and migration model, all of the observed effects are explainable. In Figure 41, a simplified conceptual model is presented to illustrate the processes controlling mostly the Pr/*n*-$C_{17}$-ratio within the source-rock and in the expelled bitumen. Already generated free bitumen is migrating through the source-rock towards the reservoir rock. New free hydrocarbons are generated in the meanwhile, which add to the already migrating hydrocarbons. With ongoing maturation, the pool of isoprenoids decrease and more and more *n*-alkanes are generated, lowering the value of the ratio with increasing maturity. This causes a ratio decrease in the centre of the source-rock (at the point, farthest away of the reservoir rock) and an increase of the ratio towards the source-rock/reservoir rock boundary. Simultaneously, the expelled hydrocarbons will show a ratio decrease with ongoing generation and expulsion.

To estimate the impact of variations of the generation rates of pristane and *n*-$C_{17}$ and of retention effects onto the ratio, a simple numeric model is calculated (Figure 42). For each component C (Pr, *n*-$C_{17}$), the amount is calculated at a migration distance d and expulsion time t (equation 39):

$$C_{(d_i,t_i)} = C_{(d_{i-1},t_{i-1})} * R + C_{(d_i,t_{i-1})} * (R-1) + C_{N\,t_i} \quad (39)$$

$$n\text{-}C_{17\,N\,t_i} = 2.5 * e^{-0.3*Pr_{N\,t_i}} \quad (40)$$

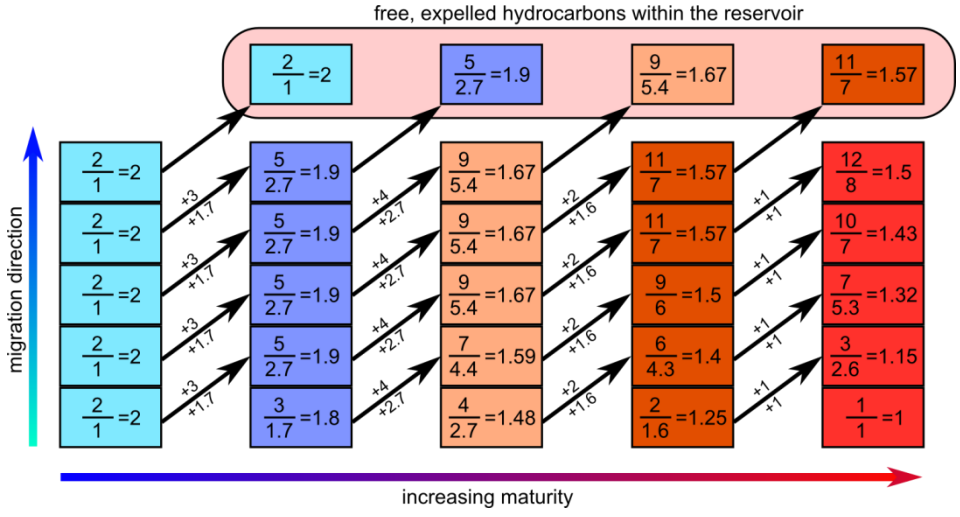


***Figure 41. Conceptual model of the migration of pristane and n-$C_{17}$ through the source-rock (contiguous squares). The denominator is pristane, the counter is n-$C_{17}$ and the result shows the Pr/n-$C_{17}$-ratio. The amount by which the component is increased is indicated by the arrows.***

R is the retention factor (1 is equal to no retention, 0.5 to 50 % retention) resulting in reduced migration speed of pristane. $C_N$ is the amount of new generated components. In case of *n*-$C_{17}$ $C_N$ is calculated with equation 2, assuming an exponential decrease of the generated amount of pristane compared to *n*-$C_{17}$ (also shown in Figure 42). For the numeric model in this study, a generation profile with two generation-maxima is chosen to match the conditions of the presented Expulsinator experiment (see the generation profile in Figure 42). Indeed, there is not a big difference between the results of the calculations for only one or two generation peaks. The calculations for no retention or for 20 % retention well match the presented results of the catagenesis experiment and also to the behaviour of the Pr/*n*-$C_{17}$-ratio in natural samples (Leythaeuser et al., 1984a, 1984b). With increasing retention effectiveness, a

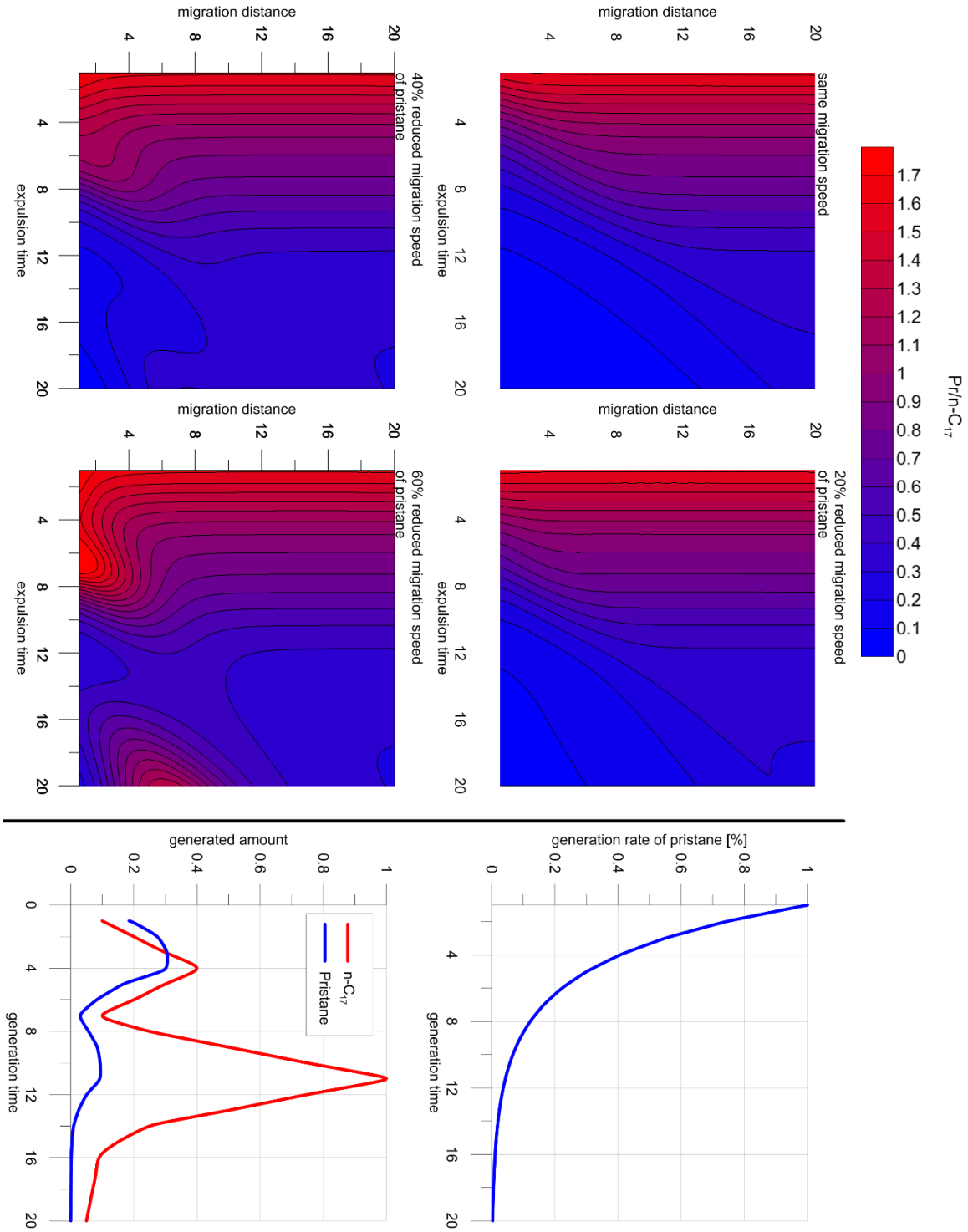


***Figure 42. Calculated evolution of the Pr/n-$C_{17}$ ratio with the assumption of 0 %, 20 %, 40 % and 60 % retention of pristane during migration (contour graphs). In addition, the assumed decrease of the generation of pristane compared to n-$C_{17}$ and the generation profile of pristane and n-$C_{17}$ is given.***

second maximum is generated and increasing ratio values can be observed for small migration distances, standing in actual contrast to all observations, either in laboratory experiments or in nature. This is a strong validation that the decrease of the ratio within the expelled bitumen and the increase of the ratio with increasing migration distance within the source-rock is mainly due to a decrease of the generated amounts of pristane compared to the *n*-alkane amount and not due to retention effects.

However, the Pr/*n*-$C_{17}$-ratio is still a useful expulsion-indicator, as both processes are not divided, but will run simultaneously. In addition, the migration speed will influence the speed of change of the ratio. This effect cannot be investigated with classic pyrolysis methodologies, as the comparison between the catagenesis simulation and the CSVP demonstrates.

## 4.8 Conclusion

The conduction of a catagenesis simulation with intact rock material and pressure regimes prevailing during catagenesis clearly showed a large impact of expulsion effects, like geochromatography and adsorption-absorption processes. The implementation of the experiment as an open hydrous pyrolysis allows the observation of these effects in the experiment course.

Changes of the relative amounts of short-, mid- and long-chain *n*-alkanes to each other showed the impressive impact of geochromatography onto the composition of the expelled petroleum. This study showed retention effects in dependence of the molecular size very clearly, leading to a time delayed expulsion of *n*-alkanes with longer chain-length. Additionally, large differences between classic pyrolysis methodologies and the catagenesis simulation were revealed, manifesting higher amounts of short-chain *n*-alkanes for the catagenesis simulation. This was caused by retention of long-chain *n*-alkanes and the subsequent thermal cracking to shorter components.

In case of the catagenesis simulation, the Pr/Ph-ratio seems to be mainly affected by the preferred release of pristane at the beginning of each generation and the coherently faster decrease of the expelled amount of pristane afterwards. Higher decomposition rates of phytane, as noted by Tang and Stauffer (1995), could not be observed in case of the catagenesis simulation. In contrast, CSVP experiments show higher decomposition rates for phytane compared to pristane. This is caused by higher rates of secondary reactions, showing to have a significant impact onto the decrease of the amounts of phytane. The open setup of the expulsion experiment prevented secondary reactions successfully, lowering the differences between the decomposition of pristane and phytane.

Variations of the ratio of isoprenoids vs. *n*-alkanes, e.g. the Pr/*n*-$C_{17}$-ratio decreased with ongoing maturation and expulsion. This was mainly caused by generation effects, whereby the amounts of expelled isoprenoids decreased in favour to an increasing generation of *n*-alkanes in the course of maturation. Retention effects, causing lower migration speed for pristane, were observed only in a very low range. The impact of this effect was by far not large enough to explain shifts in the Pr/*n*-$C_{17}$-ratio observed in natural systems, as assumed by different studies (Leythaeuser et al., 1984a, 1984b; Leythaeuser and Schaefer, 1984; Leythaeuser and Schwarzkopf, 1986; Mackenzie et al., 1983). The dominance of generation related effects onto the Pr/*n*-$C_{17}$-ratio was proofed by numeric migration models. Results, which were calculated with retention factors of 40 % or 60 %, showed the generation of a second maximum for the Pr/*n*-$C_{17}$-ratio, something not observed in nature or in laboratory experiments.

Both ratios, the Pr/Ph-ratio and especially the Pr/*n*-$C_{17}$-ratio showed a remarkable correlation of decreasing values with ongoing generation and expulsion. This makes the Pr/*n*-$C_{17}$-ratio in particular a suitable expulsion indicator to evaluate the expulsion time and the migration distance of petroleum within an oil system.

# 5 Lab-scaled generation and expulsion simulation of four different kerogen types – maturity assessment and expulsion characteristics.

## 5.1 Abstract

Investigation of expulsion and primary migration usually suffers from inadequate methodologies, failing in the provision of natural conditions prevailing during the genesis of oil and gas. The Expulsinator-device represents a unique methodology to study generation and expulsion of oil and gas under natural pressure conditions and a nature-like constellation of source-rock and reservoir. Eight different source-rocks (two type-I, type-II (-I/II), type-IIS and type-III kerogens each) with different lithologies were used to simulate oil and gas generation and expulsion with increasing subsidence. Therefore a standardised pressure and temperature program was developed, simulating pressure regimes corresponding to 2000 m, 2500 m and 3000 m of depth, thus covering the main oil window. The semi-open setup of the Expulsinator enables the sampling of the generated products during the experiment. By that, it was not only possible to prepare unique generation/expulsion profiles for each source-rock, but also to hinder the formation of condensation products and solid bitumen. These products are common artefacts in case of closed-mode pyrolysis, leading to falsified maturity assessment of the pyrolyzed rock. In particular, the measured $T_{max}$-value is highly affected by solid bitumen formation. The oil and gas generation/expulsion profiles show large differences between the different source-rocks controlled by the nature of the organic matter, but also by lithology influenced factors. Surprisingly, earliest onset of generation is observed for kerogen type-III, followed by sulfur-rich type-IIS, and then type-II kerogen. Common type-I kerogen shows the latest onset of generation. It is assumed that type-III kerogen has an early generation potential, but low expulsion efficiency leads to high condensation and cross-linking rates in most natural systems. In contrast, the Expulsinator-device provides optimal conditions for expulsion, leading to high yields. Pressure resisted lithologies e.g. with high cementation rates, and/or lithologies with low permeability show limited expulsion efficiency. Furthermore, the contribution of inorganic carbon to the overall $CO_2$-yields in case of calcareous source-rocks was observed.

## 5.2 Introduction

Evaluation of hydrocarbon generation and expulsion under natural conditions is aimed by a variety of studies, though they suffer from inadequate methodologies and procedures. In this context, the used methodologies fail to provide adequate pressure regimes concerning the lithostatic (or overburden-) pressure and the hydrostatic (or pore-) pressure. The deconstruction of the kerogen framework and the rock matrix by sample preparation (e.g. grinding, decarbonisation) is problematic as well. Secondary- and condensation reactions, caused by closed mode pyrolysis or methodologies conducted in the absence of water, affect the generated products to a higher grade as in natural systems.

To overcome limitation in simulation of generation and expulsion, a newly designed apparatus, the “Expulsinator”, was developed and built by the Organic Geochemistry Unit at Kiel University in cooperation with ENI S.p.A. With this device, it is possible to perform a semi-open pyrolysis of an intact source-rock (Ø 50 mm) at temperatures of up to 360 °C. The lithostatic- and the hydrostatic pressures are generated independently in magnitudes prevailing during catagenesis. During an experiment, generated and expelled products are released into an artificial reservoir, from where they are flushed out in short intervals. Subsequently, oil and gas are collected separately by an automated sampling system.

In several experiments conducted with Posidonia Shale, the Expulsinator-device has proven to deliver reliable results concerning controlling factors of hydrocarbon generation, expulsion and migration (see chapter 3). Comparison between Expulsinator experiments and classic closed small vessel pyrolysis (CSVP) reveal striking differences concerning product yields and formation of condensates and pyrobitumen. Furthermore, expulsion effects evince high impact onto the composition of hydrocarbons, particularly *n*-alkanes (see chapter 4).

Consequently, the Expulsinator-device has been used for characterization of generation, as well as expulsion and primary migration properties of different kerogen types and source-rock lithologies.

The investigated source-rocks each comprised two type-I, type-II, type-IIS and type-III kerogens. Ductile (e.g. black shale) and brittle lithologies (e.g. lithographic limestone) have been used for the experiments. The source-rocks were of low maturity, with an initial $T_{max}$ between 411 °C and 439 °C.

## 5.3 General experimental conditions

***Expulsinator experiments***

A detailed technical description of the Expulsinator-device is given in chapter 3 and general experimental parameters are described in chapter 3 and chapter 4. Thus, only a brief description of the experimental setup will be given in the following.

To investigate generation and expulsion response of different source-rocks during subsidence, a standardized experimental approach was developed, simulating burial depths of ~2000 m, ~2500 m and ~3000 m. This ensures that the experiment exceeds the oil generation maximum, which is expected to be surpassed in depth of 3 km (Bordenave, 1993; Tissot et al., 1987; Tissot and Welte, 1984). Corresponding pressure regimes comprise overburden pressures of 600 bar, 750 bar and 900 bar and pore pressures of 200 bar, 250 bar and 300 bar. Pyrolysis temperatures are set to 300 °C, 330 °C and 360 °C, respectively.

Each simulation stage was kept constant at least for 72 h or until the expelled hydrocarbon yields reached a significant minimum. This procedure results in different experimental durations, due to the very different generation and expulsion behaviour of the source-rock samples. This makes it necessary to verify the comparability between the expulsion experiments. Therefore, the reached theoretical maturity levels are calculated by the EASY%$R_0$ method (Sweeney and Burnham, 1990). The results show equal maturity levels of the different experiments and confirm the comparability of the experiments (see Figure 43).

During an Expulsinator experiment, generated products are expelled into the artificial reservoir and then flushed out of the Expulsinators high-pressure cell in 20 min intervals with a Volume of 4 ml (144 ml in total after 12 h). The flushed out hydrocarbons are separated into gaseous and liquid products and collected cumulative for time intervals of 12 h. A small amount of a modifier (< 9 ml, *n*-hexane/2-propanol 85:15) was pumped through the artificial reservoir every 5 h for 45 min, to increase the solubility of the expelled petroleum in the water and to prevent precipitation of asphaltenes.

After separation of liquid and gas, the gaseous products are conducted through a gas-washing bottle filled with baryta-water. $CO_2$-content precipitates quantitative as $BaCO_3$ and is determined after that gravimetrically.

Due to an early development stage of the Expulsinator, collecting gas was not possible for the Posidonia Shale experiment and strongly limited for the Foulden Maar experiment. Therefore, no measured data of gaseous products is available for the former mentioned. For the second one only cumulative data can be presented. Data of the Posidonia Shale experiment is already presented in chapter 3 and chapter 4.

***Comparative pyrolysis experiments***

For comparative purposes, closed small vessel pyrolysis (CSVP) are conducted with the different source-rocks. The experimental procedure is widely

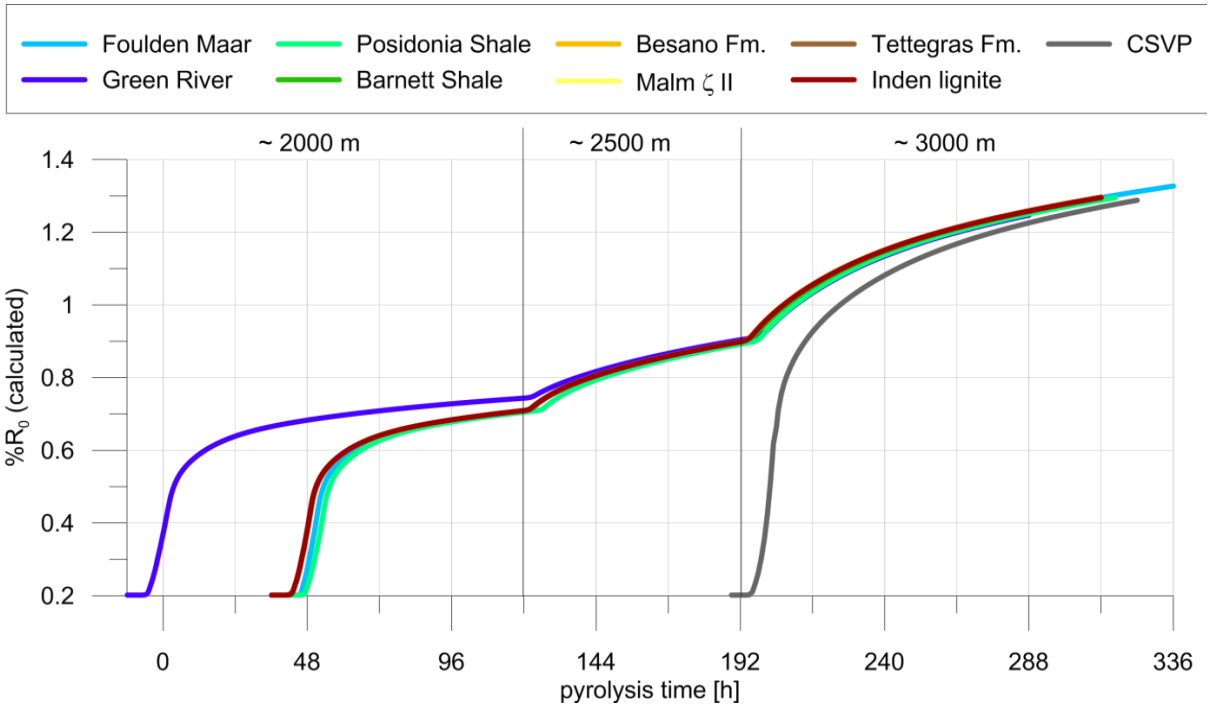


***Figure 43. Reached maturity levels of the experiments, calculated with the EASY%$R_0$ method.***

corresponding to the methodology described in detail in in chapter 3.

Powdered sample (ca. 500 mg) is placed in small stainless steel tubes (30 ml volume) and 20 ml water (HPLC-grade) is added. After that, the tubes are heated up to 360 °C at 25 °C/h. Once the heating-up phase is completed, the temperature is kept constant for 120 h to match maturity levels reached by the Expulsinator experiments (see Figure 43).

With termination of the experiment, the tubes are cooled down passively to ambient temperature, opened and their content filtered to separate the liquid phase from the residual rock. Gaseous products are not collected.

### 5.3.1 Analytical processing

The source-rocks elemental composition (in detail total carbon (TC), total sulphur (S) and total nitrogen (N)) is analysed before and after the Expulsinator experiment by the VARIO EL III elemental analyser. Additionally, source-rock assessment is carried out with a Rock Eval 2 plus analyser.

To prepare the oil-water mixtures of the liquid samples for molecular-geochemical investigation, the samples are treated by liquid-liquid extraction with dichloromethane (DCM). Source-rocks are grinded and ASE-extracted (50 bar, 75 °C; DCM/MeOH (93:7)). In case of CSVP, the extracts from liquid-liquid extraction and from ASE-extraction are merged, concentrated and prepared for further analysis. Subsequently the obtained extracts are separated into an aliphatic, an aromatic and a NSO-fraction by column separation.

GCMS measurements are performed with an Agilent 7820A GC-system, equipped with a HP 5 fused silica capillary column (30 m length, 0.25 mm inner diameter, 0.25 µm film thickness) and coupled to a 5975 MSD Agilent mass-spectrometer. The temperature program begins with 60 °C isothermal for 5 min, then heating to 325 °C at 4 °C/min., which is finally held isothermal for eight minutes.

For gas analysis, a Supel-Q PLOT column is used with a length of 30 m, an inner diameter of 0.53 mm and a film thickness of 1 µm. The temperature program begins at 35 °C and is raised to 250 °C at 16 °C/min. The injection volume of the gaseous sample is 1 ml and injection performed in split-mode (1/20). Helium flow is set to 10 ml/min.

### 5.3.2 Sample description

The artificial maturation and the generation and expulsion behaviour of the different kerogen types are the focus of this study. Thus, it is decided to describe the sample locality and the geological framework for the treated source-rocks superficially. Instead, only brief informations are given of the relevant start conditions of each sample. Bulk data is presented in Table 21 and Rock Eval pyrolysis results are shown in Figure 44 A and B. In general, the source-rocks used are of low maturity, with an initial $T_{max}$ between 411 °C and 439 °C and high generation potential, indicated by high HI-values. All source-rocks, except the kerogen type-III samples, are good to excellent oil sources (Figure 44 C).

***Table 21. Bulk data of the untreated source-rocks.***

| | **Foulden Maar** | **Green River** | **Posidonia Shale** | **Barnett Shale** | **Besano Fm.** | **Malm ζ II** | **Tettegras Fm.** | **Inden lignite** |
|---|---|---|---|---|---|---|---|---|
| ***Kerogen type*** | Type-I | Type-I | Type-I/II | Type-II | Type-IIS | Type-IIS | Type-III | Type-III |
| ***TOC [wt. %]*** | 14.2 | 19.8 | 10.8 | 14.4 | 21.2 | 2.3 | 14.5 | 55.2 |
| ***$TOC_{cf}$ [wt. %]*** | 14.2 | 25.3 | 13.4 | 14.4 | 32.9 | 4.1 | NA | 55.2 |
| ***TN [wt. %]*** | 0.4 | 1.3 | 0.3 | 0.7 | 0.8 | 0.0 | NA | 0.6 |
| ***TS [wt. %]*** | 1.8 | 1.2 | 4.7 | 2.0 | 4.0 | 0.4 | NA | 0.3 |
| ***TIC [wt. %]*** | 0.0 | 2.6 | 2.3 | 0.0 | 4.3 | 5.3 | NA | 0.0 |
| | | | | | | | | |
| ***$S_1$ [mg HC/g rock]*** | 6.2 | 8.0 | 4.7 | 2.3 | 4.9 | 0.3 | 0.3 | 3.8 |
| ***$S_2$ [mg HC/g rock]*** | 85.2 | 156.4 | 78.6 | 102.5 | 111.1 | 13.8 | 27.8 | 35.9 |
| ***$S_3$ [mg $CO_2$/g rock]*** | 7.2 | 1.6 | 1.1 | 1.4 | 1.3 | 0.7 | NA | 58.3 |
| ***$T_{max}$ [°C]*** | 422 | 439 | 428 | 419 | 419 | 411 | 419 | 407 |
| | | | | | | | | |
| ***HI [mg HC/g TOC]*** | 598 | 791 | 731 | 711 | 524 | 610 | 192 | 65 |
| ***OI [mg $CO_2$/g TOC]*** | 50 | 8 | 11 | 10 | 6 | 30 | NA | 106 |

***Foulden Maar (kerogen type-I)***

This source-rock is formed by a freshwater diatomite deposit, accumulated in a small maar lake under anoxic conditions and is located in the south of New Zealand near Dunedin. The early Miocene deposits undergo no diagenetic overprint. Therefore, the sample material represents a very special and unusual source-rock species with limitations in comparability to the other samples. A detailed geological description of the Foulden Maar is given by Lindqvist and Lee (2009).

The bulk data of the used sample material shows high TOC-content of 14.2 % accompanying by a relative high $S_2$-value of 85 mg HC/g rock. Unusual for a kerogen type-I is the high oxygen content represented by the $S_3$-value (7 mg/g TOC). The resulting HI- and OI-values would classify Foulden Maar as kerogen type-II. The missing influence of diagenetic consolidation results in the excellent preservation of oxygen-bearing functional groups, shifting the sample towards HI- and OI-values typical for a type-II kerogen.

***Green River (kerogen type-I)***

As one of the world's largest oil-shale deposits, the Green River Fm. was part of several studies and provides a high grade of comparability to other methodologies. Deposition of this lacustrine lamosite occurs during early through middle Eocene time within an extensive lake system in Colorado, Wyoming and Utha. A general description is given by Dyni (2006) and Killops and Killops (2009). Precipitation of authigenic carbonate and silica minerals leads to a high grade of cementation (Milton, 1977). The sample used in this study is characterized by a high content of TOC (19.8 %) and a high HI- and a low OI-value, corresponding to kerogen type-I. What is striking is the high $T_{max}$ of the Green River, which is also reported in other studies (Lewan and Roy, 2011; Lewan and Ruble, 2002).

***Posidonia Shale (kerogen type-I/II)***

The sample of the Posidonia Shale is originated from the HOLCIM quarry near Dotternhausen (SW-Germany). It is a lower Jurassic bituminous black shale (lower Toarcian – Lias ε II 1-12), as described by Frimmel et al. (2004) Röhl et al. (2001). Posidonia Shale is classified as kerogen type-II (Frimmel et al., 2004). The measured HI- and OI-values of this particular sample allow the assessment to a hybrid-kerogen type-I/II with increased lacustrine influence. The TOC-value of the processed sample is 10.8 %. Noteworthy is its high sulphur content, which is mainly pyrite- and elemental sulphur and only to a smaller scale organic sulphur.

***Mississippian Barnett Shale (kerogen type-II)***

The samples of the Paleozoic (late Mississippian) Barnett Shale are provided by Eni S.p.A. and originate from the Fort Worth Basin in Texas. The sample location is in the south of the basin structure (San Saba), where the lowest maturity levels ($R_0$ < 0.58 %) are reported for this oil shale (Pollastro et al., 2007; Romero-Sarmiento et al., 2014). The sample material is a siliceous mudstone with a corresponding hardness. It has a high TOC content (14.4 %) and remarkable high HI- and low OI-values for a kerogen type-II sample.

***Malm ζ II (kerogen type-IIS)***

The kerogen type-IIS is represented inter alia by the lithographic limestone of the Solnhofen area, Franconian Alb in SW-Germany. The Jurassic age bituminous marls of the Malm ζ II are well laminated and consist of fine-grained carbonate layers, alternating with dark brown, organic rich clay layers (Schwark et al., 1998). Due to the deposition in an iron-limited environment under highly reducing conditions, the organic matter of the Malm limestone contains larger amounts of organic sulphur (Damsté et al., 1990; Schwark et al., 1998).

With 2.3 %, the present sample bears the lowest TOC-values of the treated source-rocks, though the HI-value of 610 mg HC/g TOC represents the high generation potential of this source-rock.

***Besano Fm. (kerogen type-IIS)***

The Besano Fm. (or Grenzbitumenzone) is a sequence of interlayered dolomites, dolomitic marls and black shales in the San Giorgio-Besano region (Bernasconi and Riva, 1993). This middle Triassic deposits were accumulated under anoxic conditions in a basin limited by lagoons, reef-complexes and carbonate platforms. The dolomite content originates from early diagenetic dolomitization. Low availability of reactive iron and early diagenetic reactions with $H_2S$ and elemental sulfur caused an increase of the organically bound sulfur, wherefore the Besano Fm. has to be classified as type-IIS kerogen. The used source-rock sample is provided by Eni S.p.A and is a dolomitic black shale with a very high TOC content of 21.2 %.

***Tettegras Fm. (kerogen type-III)***

The Lower Carboniferous Tettegras Fm. consists of liptinite-rich coals with a high liquid hydrocarbon potential (Van Koeverden et al., 2010). It is located on the Finnmark Platform in the southern Norwegian Barents Sea and was provided to Eni S.p.A by the Norwegian Petroleum Directorate.

This source-rock was available only in very small amounts. To obtain sufficient amounts of generated bitumen and gas with the Expulsinator experiment, it

was necessary to use the entire sample material. Therefore, only limited data (TOC, $S_1$, $S_2$ and $T_{max}$) of the untreated sample is available and no CSVP experiments could be performed. The used Tettegras Fm. sample has a relative low TOC-content for a coal of 14.5 %. However, the HI-value of 192 mg HC/g TOC is high for a coal sample and indicates an elevated generation potential for liquid hydrocarbons.

***Inden Member (kerogen type-III)***

The Inden Member lignite of latest Miocene age is originated from the Lower Rhine Basin (Aachen-Cologne Lignite Mining district), where terrestrial OM accumulated in an paralic environment (Naeth et al., 2004). The high TOC of 55.2 % is contrasted by the typical low HI-value of 65 mg HC/g TOC. This indicates a low generation potential of liquid hydrocarbons of this sample.

## 5.4 Source-rock and maturity assessment

Source-rock classification and potential estimation of both the untreated and the pyrolyzed sample (Expulsinator experiment and CSVP) is done by Rock Eval pyrolysis and TOC determination. In a pseudo Van Krevelen diagram, the untreated

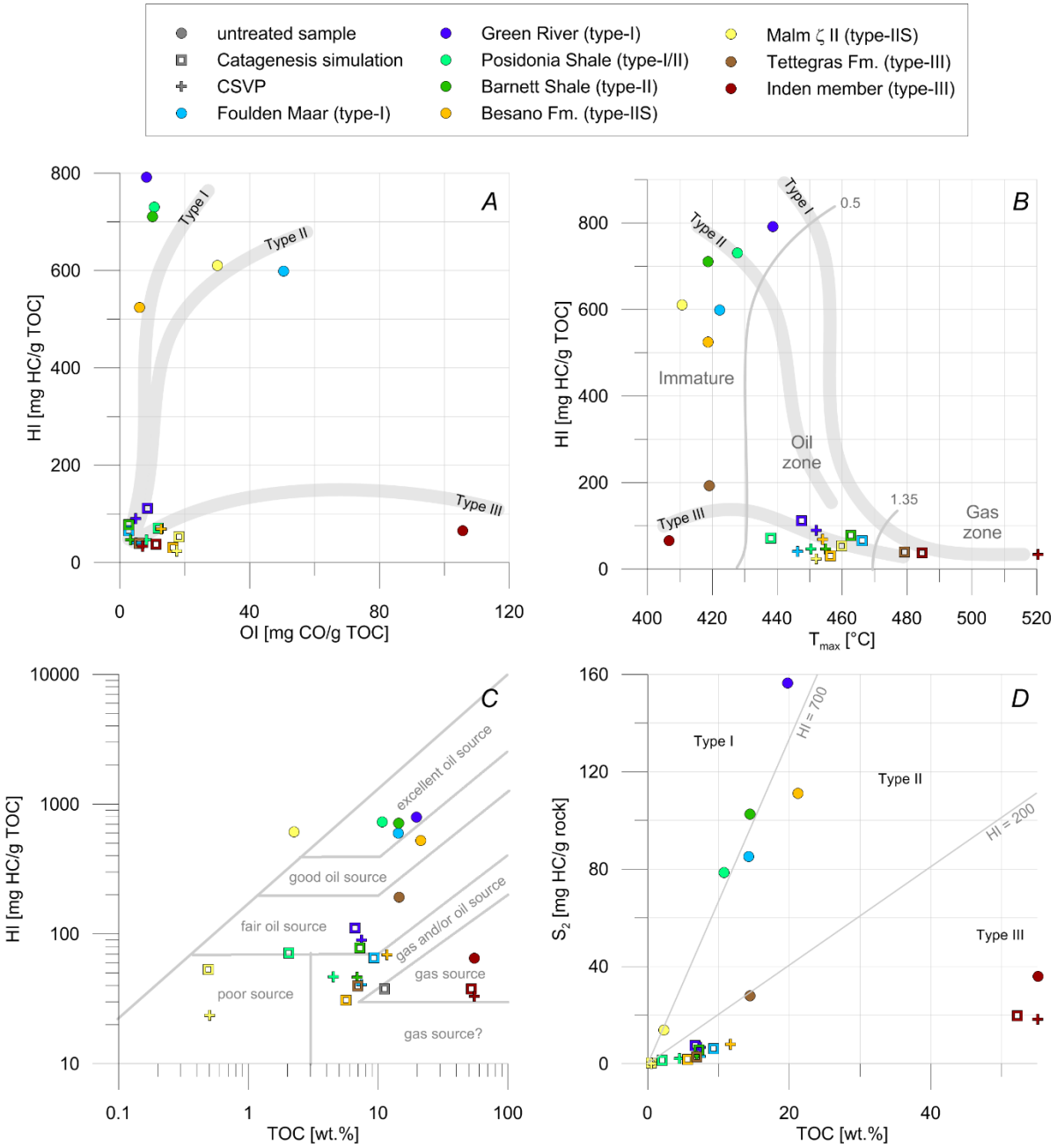


***Figure 44. Rock Eval pyrolysis results (A and B) and HI and $S_2$ vs. TOC (C and D) of the untreated samples, the Expulsinator experiments and the comparative CSVP experiments. For Tettegras Fm., no CSVP experiment was performed, due to a lack of sample material.***

samples differ from the expected results in some cases (Figure 44 A). This is noticeable for Barnett Shale and in a smaller scale for Besano Fm., where the results indicate a kerogen type-I instead of type-II. Though high HI-values accompanied with low OI-values are not unusual and are reported for other kerogen type-II source-rocks as well (e.g. Johannes et al., 2006; Lewan et al., 2006; Rimmer et al., 1993). These results show that a clear separation between kerogen type-I and type-II is not possible by plotting HI vs. OI, as low OI-values are very common even in clearly determined type-II kerogens. Foulden Maar, a kerogen type-I, is plotting as kerogen type-II, caused by a very high OI-value. As afore-noted, oxygen-bearing functional groups are preserved very well in this source-rock, due to missing diagenetic influence. However, there are also relative high OI-values reported for kerogen type-I (e.g. Lewan and Roy, 2011). This leads to the conclusion that HI vs. OI diagrams often deliver a wrong classification of OM, especially concerning type-I and type-II source-rocks. The pyrolyzed samples plot as expected, representing a high maturity stage with low HI- and OI-values.

A much better kerogen classification of the untreated samples is given by the HI-value vs. $T_{max}$ diagram (Figure 44 B). Only Foulden Maar shows a divergent result and plots as kerogen type-II, due to low $T_{max}$- and HI-values caused by extreme immaturity and absence of consolidation. In general the pyrolyzed samples show values corresponding to the end of the oil window (kerogen type-I and type-II/IIS) and beyond (kerogen type-III).

CSVP experiments of kerogen type-I and type-II show values close to each other in a small $T_{max}$-area between 446 °C (Foulden Maar) and 455 °C (Barnett Shale), along with low residual HI-values of 90 mg HC/g TOC in maximum (Green River). In contrast, Expulsinator experiments show different values for kerogen type-I and I/II (with the exception of Foulden Maar) in comparison to kerogen type-II and type-IIS, which is mainly controlled by $T_{max}$-values. Green River (type-I) and Posidonia Shale (type-I/II) are reaching much lower $T_{max}$-values compared to the corresponding CSVP-experiments. Compared to this, $T_{max}$ of kerogen type-II and type-IIS Expulsinator experiments are reaching higher $T_{max}$-values as CSVP experiments, corresponding more to the expected values for this OM type. The different response of the $T_{max}$-values of kerogen type-I and I/II on one hand and kerogen type-II and IIS on the other, could be caused by secondary cross-linking and condensation reactions, leading to the formation of solid bitumen (pyrobitumen) in case of the CSVP experiments. This insoluble solid bitumens form at high thermal maturity levels (Sassen, 1988) and have a graphitic-like structure (Bordenave, 1993). Due to their genesis caused by thermal alteration (Kelemen et al., 2008), they have higher thermal resistance (Huc et al., 2000). As previously mentioned in chapter 3, kerogen Type-I/II (Posidonia Shale) produce higher amounts of pyrobitumen in CSVP experiments as in Expulsion experiments, resulting in higher $T_{max}$-values for the CSVP experiments. The reason is seen in propagated secondary reactions due to the closed setup of CSVP and the thereby increased exposure time of generated bitumen to elevated temperatures.

It can be expected that CSVP-experiments generate higher amounts of pyrobitumen for kerogen type-II and IIS, too. Thus, it is assumed that the $T_{max}$-values of CSVP-experiments represent the thermal resistance of the generated pyrobitumen, rather than of the residual kerogen. In contrast, the Expulsinator experiments do not suffer from propagated pyrobitumen formation due to the open setup of this method. Therefore, it is assumed that the measured $T_{max}$-values correspond to the residual kerogen, as it is not masked by pyrobitumen. Foulden Maar again shows deviancy concerning the $T_{max}$-value and responses like a kerogen type-II. This indicates a higher degree of cross-linking and aromatization reactions for this source-rock.

There is low data density for kerogen type-III, which has to be improved in future work. However, even with the missing CSVP experiment of Tettegras Fm., it is noticeable that the Expulsion experiments are reaching substantive lower $T_{max}$-values (479 °C to 485 °C) as the CSVP experiment of the Inden Member (520 °C). Here too, the formation of pyrobitumen in case of the CSVP experiment is assumed to cause divergence between both methodologies. The high degree of polymerization and cross-linking for kerogen type-III cause the formation of solid bitumen with a very high thermal resistance. Thus, $T_{max}$-values of 520 °C and even higher are not uncommon in nature for terrestrial OM (Bordenave, 1993). The Expulsinator experiment shows a very high expulsion rate for both the Tettegras Fm. and the Inden Member (see Figure 45), preventing further formation of thermally degraded solid bitumen by removal of the products.

The decrease of the source-rock quality (Figure 44 C) after pyrolysis is within the expected range, reflecting a dramatic decrease of the oil generation potential. These results are in line with the reached maturity levels corresponding to the end of the oil window. Only the lignite sample shows almost no change in the source quality, reflecting the mainly gas prone character of this source-rock. The logarithmic scale of Figure 44 C makes it difficult to evaluate the drastic pyrolysis impact onto the oil formation potential of the source-rocks. This is shown by the TOC- and $S_2$-values (Figure 44 D), presenting strong conversion of the OM by pyrolysis. Again, the only exception is the lignite. Weight loss, in the course of hydrocarbon formation in combination with

very low inorganic mineral content, cause a consistent TOC-value and only a moderate decreasing $S_2$-value.

## 5.5 Expulsion profiles and product yields

The revolutionary design of the Expulsinator allows the sampling of the generated products (liquids and gases) within a given time interval in the course of the experiment. Due to this unique feature, every experiment generates a combined generation/expulsion profile of the source-rock for liquid and gaseous hydrocarbons and $CO_2$. In Figure 45, the profiles of eight source-rocks of different kerogen type and lithology are plotted. For Foulden Maar (Figure 45 A) and Posidonia Shale (Figure 45 C), no data of gaseous products are plotted, which has to be attributed to technical shortcomings of the Expulsinator at a very early development stage of the apparatus.

Each profile is divided into the three generation and expulsion stages, simulating depth of 2000 m, 2500 m and 3000 m. Due to technical limitations, it is not possible to produce a pre-extracted, intact rock plug. Thus, it has to be considered that the very first simulation stage shows larger influence by in-situ bitumen, affecting mainly the liquid yields. Gaseous products could be affected as well, but to a minor degree due to low oil-to-gas cracking rates at low temperature conditions (Lewan et al., 2008). However, the solvent extract yields of the untreated sample (Figure 45 and Table 22) have to be considered, to estimate the effective proportion of in-situ bitumen to generated bitumen.

### 5.5.1 Generation/expulsion of liquid products

***Type-I and –I/II kerogen***

The generation/expulsion profile of Foulden Maar represents a very unusual kerogen type-I, with an extreme early onset of generation. The first experiment stage is dominated almost completely by newly generated bitumen, contrasting the results of the Green River and Posidonia Shale experiment. The latter show no new generation, but an exclusive expulsion of in-situ bitumen. The large content of in-situ bitumen in case of Green River and the low-pressure-caused modest expulsion rate give rise to extend the first experiment stage by 48 h. The contrary pattern between Foulden Maar on the one hand and Green River and Posidonia Shale on the other is reflected in the subsequent expulsion stages as well. Already after 24 h, the Foulden Maar experiment is reaching the extract yield maximum at 2500 m depth, while Green River expel the highest bitumen quantity after 48 h and Posidonia shale after

***Table 22. Extract yield of the untreated sample and cumulative extract yields of the first expulsion stage at 300 °C.***

| Sample | Extract yield [mg/g TOC] | Extract $yield_{sum\ 300°C}$ [mg/g TOC] |
|---|---|---|
| **Foulden Maar** | 35.92 | 272.82 |
| **Green River** | 121.96 | 118.18 |
| **Posidonia Shale** | 108.72 | 88.97 |
| **Barnett Shale** | 65.59 | 53.48 |
| **Besano Fm.** | 104.97 | 167.23 |
| **Malm ζ II** | 137.96 | 169.46 |
| **Tettegras Fm.** | 16.87 | 106.69 |
| **Inden lignite** | 3.97 | 84.86 |

60 h. In 3000 m simulated depth, the expulsion maximum of Foulden Maar is reached after 24 h that of Green River and Posidonia Shale after 48 h. Foulden Maar shows only a slow decrease of bitumen expulsion at 3000 m depth. Therefore, this stage had to be extended by 48 h.

In general, Foulden Maar starts with the highest generation/expulsion peak and yields decreasing quantities with ongoing subsidence. This generation/expulsion characteristic contrasts the results obtained from Green River and Posidonia Shale experiments. Both show very late onset of generation and the total generation/expulsion maximum is reached within the last experiment stage at deepest simulated subsidence. However, Green River and Posidonia Shale profiles are in line with data sets presented in literature (e.g. Lewan and Ruble, 2002; Pepper and Corvi, 1995b; Ruble et al., 2001; Tissot et al., 1987), attesting type-I kerogen a late onset of hydrocarbon generation. The timing differences become explainable, taking into account that Foulden Maar lacks diagenetic reworking of the OM, which ensures a good conservation status for thermally weak components, e.g. oxygen baring components. Early conversation of this matter reduce the amount available for further thermal decomposition in subsequent expulsion stages, leading to the resulting Foulden Maar profile.

In addition to the discussed timing differences, the experiments mid-stage shows considerable differences in the course of the expulsion: Foulden Maar generates only a single maximum, while Green River and Posidonia Shale produce an additional minor maximum prior to the main one. For the latter, this could be caused by two different generation processes, involving components with different thermal resistance. Furthermore, secondary cracking processes of restrained products and subsequent expulsion could contribute to the main expulsion maximum. Removal of labile components and

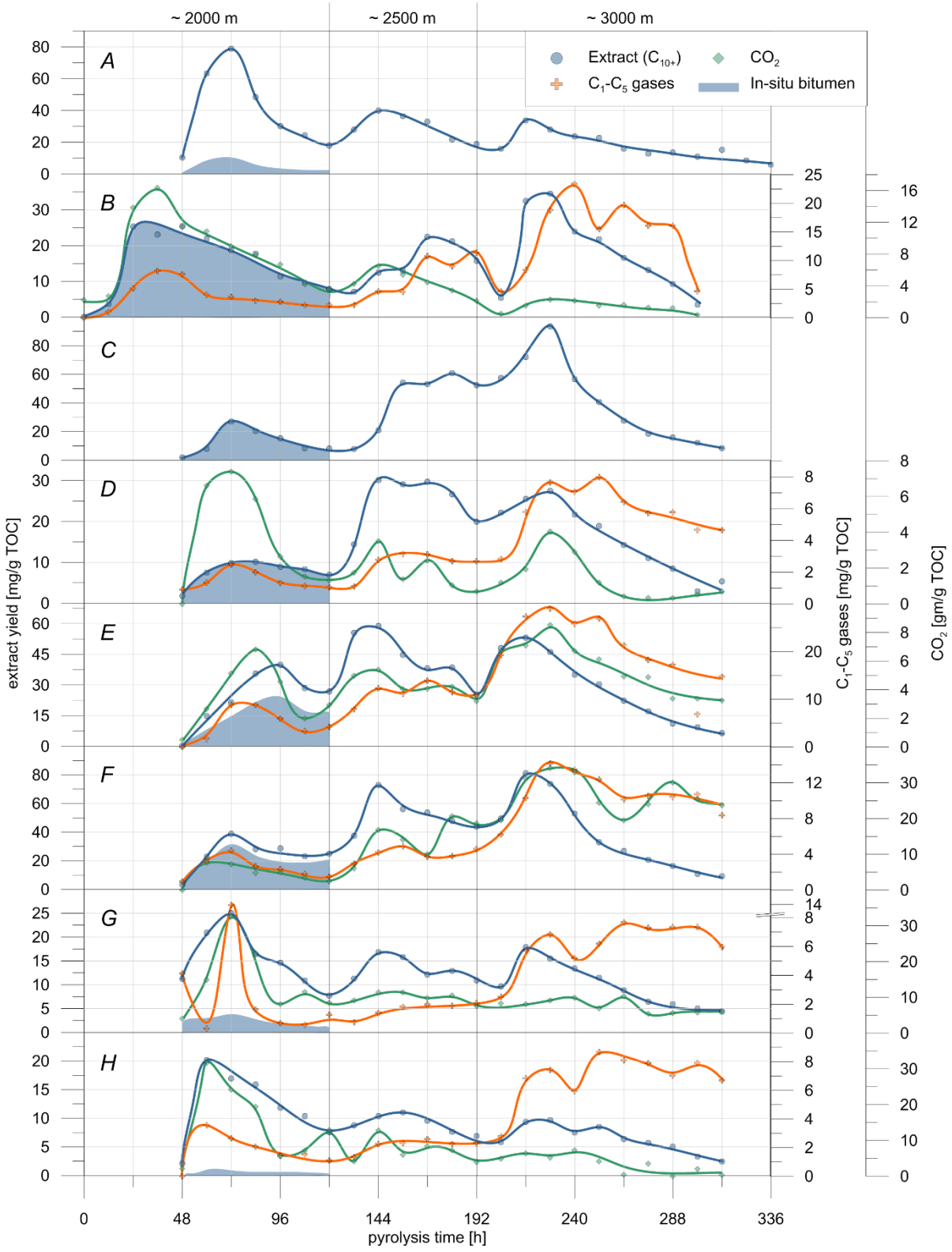


***Figure 45. Expulsion profiles of the Expulsinator experiments: A: Foulden Maar, B: Green River Fm., C: Posidonia Shale, D: Barnett Shale, E: Besano Fm., F: Malm ζ II, G: Tettegras Fm., H: Inden Member. For Foulden Maar and Posidonia Shale experiments, no detailed gas yields are available due to technical limitations at an early Expulsinator development stage. In-situ bitumen quantity distributions are calculated on a percentage basis. For Green River Fm., Posidonia Shale and Barnett Shale, the in-situ bitumen is assumed to be 100 % of the cumulative first stage extract yields (compare Table 22).***

condensation of the OM by diagenetic overprint could model the expulsion curve of the Foulden Maar sample, exposing a similar pattern.

Differences concerning expulsion rates and timing between Green River and Posidonia Shale are apparent for the total experiment duration. Especially

the last stage decreasing-rate of product expulsion cannot be associated to different generation rates of both source-rocks alone, as generation is terminated to this point. Rather, this effect is attributed to the different source-rock litho-types, affecting the expulsion rate of generated hydrocarbons. High grade of cementation in case of Green River (Milton, 1977) causes a more sturdy response onto overburden pressure, reducing expulsion acceleration by squeezing. The consequence is a more constant expulsion rate and a less steep decrease of the expulsion. The elongated expulsion time of the Green River in-situ bitumen supports this assumption. Contrariwise, missing cementation of Posidonia Shale and its ductile response onto overburden pressure reduce the expulsion rate and cause the observed, steep decreasing rate. Further evidence of lithology-influenced expulsion rate could be the slow quantity decrease of expelled products to the mid-stage end of the Posidonia shale experiment, though this could also be related to the mix of type-I and type-II kerogen in this case.

***Type-II and -IIS kerogen***

The Barnett Shale experiment is the only one in the series of Expulsinator experiments performed with a clear type-II kerogen, without pronounced lacustrine influence (Posidonia Shale) or increased sulphur content (Besano Fm. and Malm ζ II). Barnett shale shows no significant generation at the very first experiment stage, which is comparable to the type-I and –I/II samples (Green River and Posidonia Shale). However, in the following stage the Barnett Shale characteristic shows contrasting behaviour by reaching the maximum expulsion of the entire experiment already after 24 h. In this mid stage, the expulsion pattern of Barnett Shale shows again a second expulsion maximum, but now in reverse order: the first one is the major maximum, followed by the minor second one. In the last experiment stage, the Barnett Shale shows a noticeable slower increase of expelled cracking products as kerogen type-I and I/II samples. The stage maximum is reached after 36 h, similar to Green River and Posidonia Shale, but the expulsion/generation rate is lower as in the second stage maximum. The steepness of the subsequent liquid yield decrease, marked by the end of generation, is clearly less pronounced in case of the Barnett Shale sample and steeper for Green River and Posidonia Shale. This could be caused by silification of the Barnett Shale sample, which leads to formation of fractures and migration avenues on the one hand, and reduced expulsion capability by reduced permeability. In fact, the Barnett Shale shows much less response onto lithostatic pressure increase as Green River, suggesting that formation of fracture-caused migration avenues will be less pronounced for the first-mentioned. In general, the generation/expulsion characteristics mirrors generation kinetics of type-II kerogen: a significantly earlier onset of generation compared to kerogen type-I and a relatively constant generation rate with increasing subsidence (Lewan and Ruble, 2002; Pepper and Corvi, 1995b; Tissot et al., 1987).

Type-IIS Kerogen is represented by Besano Fm. and Malm ζ II. For both source-rocks, very early low temperature generation is observable, though Besano Fm. shows a delayed release compared to Malm ζ II. High extract yields at low temperatures mirror the specific generation characteristic of a type-IIS Kerogen. Here, weak C-S bonds and sulfur radicals cause a very early generation and release of hydrocarbons (Lewan, 1998; Lewan et al., 2006; Tissot et al., 1987; Tomić et al., 1995). This characteristic is consistent for the experiments mid-stages and the last stages as well. Maximum expulsion for the mid-stage is reached after 24 h, producing a much more distinct peak as the Barnett Shale experiment and a minor second expulsion peak is noticeable only for Besano Fm. The last experiment stage again shows a distinct generation/expulsion peak for both source-rocks, with a slightly later onset of expulsion for Malm ζ II. The expulsion maximum is reached after 24 h for both experiments, exceeding the mid-stage maximum in case of Malm ζ II and falling below in case of Besano Fm. Different organic source material involved in different generation paths, but also the different lithology could cause the described differences. Malm ζ II has, in opposite to Besano Fm., a very resistant lithology concerning overburden pressure, as no noticeable compaction has been observed in the curse of simulated subsidence. This could reduce the expulsion supporting influence of overburden pressure, similar to the Barnett Shale experiment. In this scenario, products generated within the mid-stage would be partly restrained within the pore space and expelled time-delayed in the last experiment stage, supported by higher lithostatic pressures and newly generated hydrocarbons. However, it is important to note that this has no direct influence onto the peak expulsion timing: The main factor is a more resistible and better-connected pore system in case of Malm ζ II. Peak expulsion will be reached after saturation of the pore space with generated liquids and gas. With ongoing generation and subsequent volume loss by removed OM, the pore space of the Besano Fm. sample is supposed to be stronger influenced by lithostatic pressure and will therefore support further expulsion of generated products. However, the delayed expulsion of the Besano Fm. during the first experiment stage at low-pressure conditions implies low permeability. Thus expulsion after generation termination is more constant due to better response to overburden pressure, but compared to the Barnett Shale only slightly increased due to low permeability.

In case of Malm ζ II, a much sturdier pore system is assumed, which will not collapse even at high lithostatic pressure conditions. As a result, the peak expulsion occurs without time delay after pore space saturation (also supported by the good connected pore system), but the expulsion rate afterwards will be reduced, accompanied with the accumulation of retained bitumen within the pore space. The delayed expulsion of the Besano Fm. during the first experiment stage is not in opposite to this assumption. Low lithostatic pressure conditions in combination with low generation rates lead to a reduction of the expulsion efficiency for this source-rock with low permeability.

***Type-III kerogen***

Both type-III kerogen show a remarkable early release of hydrocarbons already during the first low-temperature stage of the experiments. In the following, the expulsion maxima decrease with every subsequent experiment stage (Inden lignite) or stays constant (Tettegras Fm.), respectively, but is still accompanied by high expulsion rates. However, high expulsion rates are in contrast to the expectation of type-III kerogen as a "bad expeller". The ability of coals to generate liquid hydrocarbons, and not only gas and condensates, has been a matter of controversial debate in a number of studies. Recent investigations tend to attribute generation potential to coals and coaly sediments (e.g. Van Koeverden et al., 2010; Wilkins and George, 2002). In this context, the Expulsinator experiments performed with Tettegras Fm. and Inden Member lignite, support the hypothesis that most type-III kerogens are able to generate substantial amounts of liquid hydrocarbons. The limiting factor for a coal to become oil prone or not is therefore seen in the ability to expel the generated hydrocarbons (Durand and Paratte, 1983; Fleet and Scott, 1994; Wilkins and George, 2002).

Various factors are considered influential for expulsion of hydrocarbons from terrestrial strata. Already the heterogeneity of maceral composition, the variability in microstructure and changes in maceral hydrogen content could influence primary migration (Wilkins and George, 2002 and studies cited therein). Another important point is coal porosity, which is mostly seen as a dynamic structure, changing with ongoing generation and re-distributing the free volume continuously (Wilkins and George, 2002). Molecular sieve-like structures of coal and the resulting extremely narrow connections between pores could act as limiting factor for liquid hydrocarbon expulsion (Radke et al., 1980), but would allow release of gaseous products (Pepper, 1991). A negative impact of hydrocarbon generation onto the micropore system is seen by Bojesen-Koefoed et al. (1996) and Katz et al. (1991), reducing the ability to retain hydrocarbons. However, removal of moderately large molecules ($C_{15}$-$C_{35}$) by common solvent extraction (Wilkins and George, 2002) and even asphaltenes (Groenzin and Mullins, 2000) contradict the model of a migration-restricting pore system, though solvent swelling of the kerogen qualifies this interpretation. Additionally, Larsen et al. (1995) presented indications that pores within coals are isolated and not connected, even though most data are interpreted in favor of interconnected pore systems (e.g. Okolo et al., 2015; Radovic et al., 1997; Walker and Mahajan, 1993). Diffusion through a kerogen network plays an important role for expulsion and the fractionation of the expelled products (Sandvik et al., 1992; Thomas and Clouse, 1990c) and will impact the ability of a coal to expel the generated hydrocarbons as well. However, Sandvik et al. (1992) reported absorption levels of hydrocarbons in coals to be lower than in dispersed kerogens, which conversely lowers the diffusivity of coals. Indirect indication of ensued diffusion is reported by Littke et al. (1989), observing enrichment of aromatics compared to *n*-alkanes in the margin of a coal to an overlying sandstone. However, the authors indicate that only a minor percentage of the generated products were released from the coals.

The observations and theories above suggest that the pore system of a kerogen type-III is of certain importance for the question, if terrestrial strata serve as source for liquid hydrocarbons. It is assumed that bitumen after its generation accumulates within the easily accessible pore space. Findings of exsudatinite within primary pores of coals support this assumption, as it is seen as relic of oil/expelled bitumen (Littke et al., 1989; Teichmüller, 1982). This accumulation process could be supported by diffusion through the kerogen network. Once the generated hydrocarbons will have accumulated within the pore space of the kerogen type-III, further migration seems to be limited either by bottlenecked pore throats (Radke et al., 1980; Wilkins and George, 2002) and/or isolated dead end pores (Larsen et al., 1995). Further limiting factors are adsorption on pore surfaces (Sandvik et al., 1992; Van Koeverden et al., 2010; Wilkins and George, 2002) and limited diffusion levels of kerogen type-III (Sandvik et al., 1992). In accordance with Fleet and Scott (1994) and Wilkins and George (2002), it is assumed that this limitations may be overcome in case of thin coal seams and high amount of clastic insertions, as well as high hydrogen content of the coals. Further, it is assumed that cracks and fractures caused by tectonic stress may increase the expulsion rate dramatically. The cause is increased diffusion initiated by pressure gradients towards the fractures (Hanebeck, 1993; Thomas and Clouse, 1990c).

The observed expulsion behavior of the Tettegras Fm. and the Inden Member lignite are in line with the expulsion model described above. For the Expulsinator experiments, only thin rock disks are used (Tettegras Fm.: 12 mm; Inden Member: 9 mm),

interbedded in a porous artificial reservoir. Additionally the high lithostatic pressures applied (up to 900 bar), combined with the volume loss during simulated catagenesis, will have generated micro- and macro fractures. Therefore, ideal conditions have been provided to reach high expulsion rates. The condensation reactions in case of the CSVP experiment of the Inden Member lignite, reflected in increased $T_{max}$-values and reduced extract yields, better fit to a coal with low expulsion efficiency.

The relatively early onset of generation within the different phases of the Expulsion experiments are not in opposition to oil formation maturity levels reported for coals. Evidence of oil generation has been found for vitrinite reflectivities in the range of 0.43 to 1.18 % $R_0$ (Wilkins and George, 2002), demonstrating that liquid hydrocarbon formation already occurs at lower maturity levels. This is supported by observations of (Behar et al., 1997a), reporting very early generation of liquid products in thermal maturation experiments of type-III kerogen. Additionally, a good example of hydrocarbon generation at low-temperature conditions is given by Teerman and Hwang, (1991).

### 5.5.2 Generation/expulsion of gaseous products

***Type-I and –I/II Kerogen***

Due to reasons already mentioned, gas expulsion profiles of type-I kerogen are only given for the Green River sample. A noticeable amount of $C_1$-$C_5$ components is already released at the beginning of the first expulsion stage at 2000 m. It is assumed that this hump is rather due to decomposition of labile components of in-situ bitumen, than to new generation by thermal cracking of kerogen. With increasing subsidence, the $C_1$-$C_5$ yield rises to its maximum, reached in 3000 m simulated depth. The hydrocarbon gas peak shows a noticeable delay to the bitumen expulsion, clearly indicating gas formation, which ensued bitumen generation. However, the bimodal shape of the last stage expulsion curve is striking for the Green River sample. This suggests that gas generation is mainly controlled by two different processes, gas formation by kerogen decomposition and oil-to-gas cracking, as described by different authors (e.g. Horsfield et al., 1992; Lewan et al., 2008; Pepper and Dodd, 1995). Oil-to-gas cracking requires high pyrolysis temperature and elevated pyrolysis duration (Lewan et al., 2008), suggesting that the second gas expulsion maximum is mainly influenced by oil-to-gas cracking processes.

The largest quantity of $CO_2$ is already expelled in the first low-pressure/low-temperature stage, corresponding to the decomposition of weak oxygen-bearing components of the kerogen and in-situ bitumen. Further $CO_2$-expulsion is recognizable in both the mid-stage and the last stage, but with distinct decreasing quantities. This is in opposition to the assumption that $CO_2$ release only occurs at the beginning of the oil formation (Tissot and Welte, 1984). In contrast to the release of $C_1$-$C_5$ gases, the $CO_2$ expulsion is coupled to a certain degree to the course of liquid expulsion in all three stages. This indicates that at least for the last two stages processes linked to bitumen generation are responsible for the $CO_2$ release. Lewan (1997) sees interactions between bitumen/kerogen dissolved water and carbonyl groups causal for continuing $CO_2$ generation, even at higher maturity stages. Thereby he is drawing on theories suggested by Petit (1991) and Song et al. (1994), concerning weathering of coals and coal liquefaction by water treatment at 350 °C. However, reactions of water molecules with oxygen bearing aldehydes, esters or ketones would cause formation of $CO_2$, explaining the $CO_2$ generation at higher temperature stages and the pairing to liquid expulsion. It has to be mentioned that the pairing of the $CO_2$- and the liquid expulsion curve of the mid-stage is limited to the first liquid expulsion maximum, indicating that no further oxygen bearing components are available at the second liquid expulsion maximum.

***Type-II and -IIS kerogen***

$C_1$-$C_5$ gas generation and expulsion of Barnett Shale, Besano Fm. and Malm ζ II show a relatively similar pattern, regardless of sulphur content or lithology. However, in some parts differences are noticeable: All three source-rocks show similar gas expulsion characteristics in the first expulsion stage. In all three cases, the maximum expulsion is reached after 24 h. This is remarkable for Besano Fm., as here the $C_1$-$C_5$ peak expulsion precedes the maximum yield of liquid hydrocarbons (at 48 h). As already described above, a low permeability and only small overburden pressure influence during the first stage is seen as reason for low liquid expulsion from the Besano sample. However, gas expulsion seems not to be restricted and the permeability is sufficient to provide early gas release, suggesting that the limiting factors only affect components with larger molecular size. The mid-stage is identical for Barnett Shale and Malm ζ II, showing a smooth expulsion curve. In contrast, the $C_1$-$C_5$ gas expulsion of Besano Fm. forms two distinct maxima in the mid-stage. Oil-to-gas cracking is unlikely at this stage, as this process needs higher temperatures (Lewan et al., 2008). Onset of higher pressure conditions, together with generation/expulsion caused volume loss will lead to pore space collapse in case of the weaker lithology of Besano Fm., causing a higher expulsion rate for both liquid and gaseous products. Quite contrary to this gas could be restrained, dissolved in unexpelled bitumen, in case of Barnett Shale and Malm ζ II. For the last stage, an identical patter is

recognisable for Barnett Shale and Besano Fm., showing hydrocarbon gas expulsion with two consecutive maxima. Malm ζ II shows a strongly flattened course of $C_1$-$C_5$ expulsion. The first maximum after 36 h is followed by a long, decreasing flank, which reveals only a very small, not well-established, minor second expulsion maximum. Again, the resistance of the pore system, which is particularly pronounced in case of Malm ζ II, and the resulting retention of hydrocarbons (e.g. gas dissolved in bitumen), is seen as reason for the shape of the expulsion curve of the Malm sample. However, two differentiated expulsion maxima for $C_1$-$C_5$ gases are noticeable again, clearly for Barnett Shale and Besano Fm., not so much for Malm ζ II. As already descripted for the Green River experiment, both maxima are caused by different processes: Kerogen-to-gas cracking (first maximum) and oil-to-gas cracking (second maximum). At experiment termination, all three source-rocks unanimously show high gas formation potential. To evaluate the total gas formation potential, further long-duration experiments have to be conducted in future studies.

$CO_2$ production and expulsion differs strongly between the three experiments. While the first stage shows a similar pattern of $CO_2$ release for type-II and type-IIS kerogen, this fact changes with the second phase. For Barnett Shale, the total $CO_2$ expulsion maximum is reached within the first stage of the Expulsinator experiment. In contrast, Besano Fm. and Malm ζ II release increasing quantities of $CO_2$ in every following experiment stage, reaching the total maximum in the last stage of the experiment. Both samples, the Besano Fm. and Malm ζ II, contain large quantities of inorganic carbon, suggesting decomposition reactions of carbonate and dolomite as source of the increasing $CO_2$ yields. Indeed, both samples show decreasing values of inorganic carbon after the treatment with the Expulsinator (Table 23) In particular, Malm ζ II shows a remarkable loss of inorganic carbon, mirrored in a very high $CO_2$ yield. It is striking that the decomposed inorganic carbon would form much larger quantities of $CO_2$ as obtained by the experiments, suggesting that larger TIC-quantities are removed being dissolved within the water phase. Inorganic sources are reported as origin of $CO_2$ by different authors (e.g. Coudrain-Ribstein et al., 1998; Franks and Forester, 1984; Wycherley et al., 1999). Especially Coudrain-Ribstein et al. (1998) shows correlation between the partial pressure of $CO_2$ and increasing temperature and pressure, suggesting a mainly chemical equilibration controlled process between carbonate minerals and associated water. However, the data presented in this study suggests that there has to be more influencing factors onto $CO_2$ release by carbonate decomposition than temperature and pressure. The Expulsinator is operating in a semi-open modus, releasing the expelled products in short time intervals

***Table 23. Loss of inorganic carbon ($TIC_{loss}$), $CO_2$ potential, possibly formed by $TIC_{loss}$ ($CO_{2\ TIC}$) and total $CO_2$ amount ($CO_{2\ total}$), obtained by the experiments.***

| Sample | Besano Fm. | Malm ζ II |
|---|---|---|
| **$TIC_{loss}$ [mg/g TOC]** | 55.25 | 363.14 |
| **$CO_{2\ TIC}$ [mg/g TOC]** | 202.60 | 1331.52 |
| **$CO_{2\ total}$ [mg/g TOC]** | 105.76 | 382.61 |

of only 20 minutes. The release of $CO_2$ would lead to a chemical imbalance in favour of carbonate minerals, causing further decomposition to $CO_2$. Sustained release of $CO_2$ can be observed for Malm ζ II, but not so much for Besano Fm. A similar pattern of $CO_2$ release is observed by Cai et al. (2001) for the Tarim Basin (China), reporting increasing amounts of $CO_2$ till 5100 depth, followed by decreasing quantities. Oxidation of organic matter, as suggested by Cai et al. (2001), can be excluded in case of Expulsinator experiments. However, significant differences in the mineralogy of both source-rocks, incipient with the different carbonate facies (Besano Fm.: dolomite, Malm ζ II: calcite), could be an explanation for the observed differences. Further investigation (e.g. isotope measurements) is necessary to assess the impact of carbonate decomposition onto the $CO_2$ yields.

### *Type-III kerogen*

$C_1$-$C_5$ gas evolution of both type-III kerogens follows known pattern, as they show an expulsion peak during the first experiment stage, associated to in-situ bitumen and labile kerogen components, followed by increasing gas generation/expulsion in the mid-stage and the last stage. During the first stage, the $C_1$-$C_5$ yield of Tettegras Fm. shows unexpected values after 12 h (almost zero) and after 24 h (~14 mg/g TOC). A malfunction of the Expulsinator, affecting the gas collection, cannot be excluded, but is unlikely, as $CO_2$ shows a very smooth and plausible expulsion curve. Of course, there are additional sources of error, such as leaky gas collection vials. However, retention of gas within the kerogen type-III pore network could be an explanation, taking into account that Tettegras Fm. shows higher resistance to overburden pressure as the Inden lignite. The latter shows high compaction rates already within the first stage of the experiment, causing squeezing effects, which lead to immediate release of liquids and gas. The expulsion behaviour of both source-rocks is in line with this assumption, as within the first stage liquid and gas expulsion of Inden lignite takes place much earlier compared to Tettegras Fm. The mid-stage of both type-III kerogens differs from type-I and -II $C_1$-$C_5$ expulsion in this stage. While type-I and –II kerogen produces a distinct maximum of hydrocarbon gas expulsion,

this maximum is missing in case of type-III kerogen. In fact, type-III kerogen shows only very low $C_1$-$C_5$ gas generation and expulsion in the mid-stage. This is contrasted by the liquid yields, which show a clear generation and a distinct expulsion maximum. The mid-stage pyrolysis temperature seems to be insufficient to generate larger quantities of hydrocarbon gases by thermal kerogen decomposition. This change with the last experiment stage, where high temperature conditions support kerogen-to-gas cracking, leading to a distinct first expulsion maximum of $C_1$-$C_5$ gases. The second gas expulsion phase, which is also observed for the other kerogen types, is also developed in the kerogen type-III experiments. It is striking that this second expulsion phase is much more pronounced than for the other kerogen types, concerning the height and width of the peak. Behar et al. (1995) noted that oil-to-gas cracking of unexpelled hydrocarbons is of large importance for gas formation in case of kerogen type-III, due to the good retention properties of this highly porous kerogen type. As explained for the liquid expulsion profile, we have a very good expulsion rate of oil for a kerogen type-III. Even so, this second gas expulsion phase is a strong evidence for the retention of larger amounts of generated bitumen within the kerogen pore system and subsequent thermal decomposition to gas. However, as described above, unusual high expulsion efficiency is reached by the type-III kerogens, causing high liquid hydrocarbon yields and low $C_1$-$C_5$ gas quantities, due to reduced amounts of source material for oil-to-gas cracking.

$CO_2$ expulsion corresponds very good to the expectations of Tissot and Welte (1984), producing very high yields in the first expulsion stage, followed by much lower generation/expulsion quantities. The high oxygen content of kerogen type-III leads to this large difference between the first stage and the following experiment stages. Nevertheless, comparing the yields reached during the mid-stage and the last stage of kerogen type-III with the quantities released by the other kerogen types shows no large differences. The association to the liquid expulsion seems to exist as well. This suggests that here the same processes takes place, as described for the other kerogen types and interactions between water and carbonyl groups lead to a continued $CO_2$ release.

## 5.6 Expulsion efficiency

The efficiency of expulsion is assessed by determination of the amount of unexpelled solvent extractable bitumen within the pyrolyzed rock sample and comparison with the total extract. In Figure 46, the values are given for the eight source-rocks pyrolyzed with the Expulsinator-device. The effectiveness of expulsion is striking (only ~5 % unexpelled bitumen in maximum) and shows clearly that the setup of the Expulsinator (e.g. sample assembly, arrangement of the artificial reservoirs and pressure regimes) ensures ideal expulsion conditions.

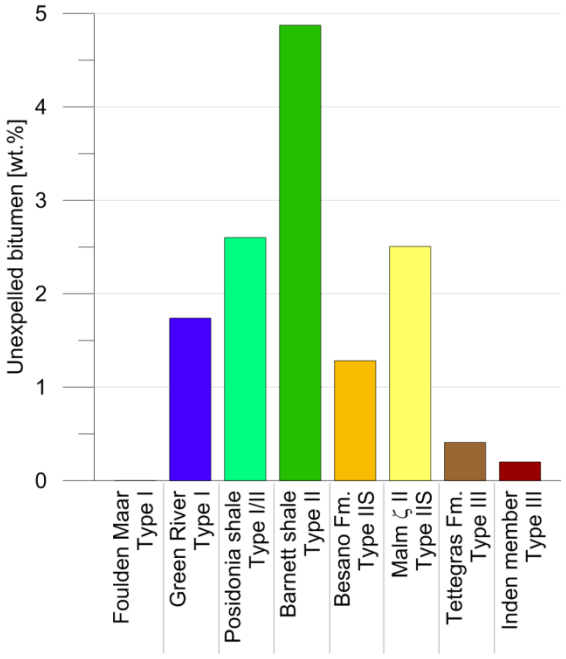


***Figure 46. Part of the unexpelled bitumen in the total extract, determined by solvent extraction of the pyrolyzed rock sample.***

Samples with high compactibility, like Foulden Maar or the type-III kerogens, show low amounts of unexpelled bitumen, though this could also be due to accumulation of solid bitumen, especially in case of the latter. A connection between expulsion efficiency and compaction rate is recognizable for the other samples as well: The high stability of the silicified mudstone of Barnett Shale, in combination with low permeability values, lead to the highest amounts of unexpelled bitumen. The expulsion rate of Malm ζ II, also a sturdy sample, and Posidonia Shale, a more ductile sample, is a little bit higher compared to Barnett Shale, retaining ~2.5 % unexpelled bitumen. Interaction of low permeability, but higher impact by squeezing in case of Posidonia Shale and higher permeability and a better-networked pore system in case of Malm ζ II, is supposed to cause this result. The high expulsion rate of Green River and Besano Fm. (around 1.5 %) could be caused by higher fracturing rates, induced by overburden pressure, leading to migration avenues.

The determined amounts of unexpelled bitumen fit very well to the described expulsion profiles, mirror the influence of lithology and overburden pressure onto the expulsion efficiency.

## 5.7 Conclusion

Expulsion experiments, conducted with eight different source-rocks, reveals striking differences to classic closed pyrolysis and astonishing results, concerning expulsion characteristics and influence of overburden pressure.

Early removal of generated products has great impact onto the maturity assessment, in particular influencing the $T_{max}$ value in dependence of the kerogen type. Formation of solid bitumen in case of missing removal (as shown by CSVP), increase the measured $T_{max}$-value for type-I and -I/II kerogen, but results in lower values for type-II and -IIS kerogen. For type-III kerogen, solid bitumen increased the measured $T_{max}$-value drastically. In contrast, the source-rock quality decreases for both the Expulsinator experiment and for CSVP in a similar range, proving the effective maturation process by the Expulsinator-device.

The common kerogen types -I or -I/II, represented in this study by Green River and Posidonia Shale, show a very late onset of peak generation and release of liquid pyrolysis products. To be exact, kerogen type-I has the latest onset of all kerogen types used. Type-II kerogen shows highest expulsion yields in the experiment mid-stage, though type-IIS owns a high potential for early generation at low temperature conditions and presents a general shift to earlier generation and release of liquid products compared to type-II. The general generation timing is in line with data presented by Lewan and Ruble (2002), Pepper and Corvi (1995b) and Tissot et al. (1987), for example. In contrast, unexpected early release of liquid products is observed for both type-III kerogens. This suggests a high potential for early generation by a type-III kerogen, as also described by (Behar et al., 1997a). In nature, effective expulsion from this kerogen type is hindered by the kerogen porosity and the ability to retain large quantities of generated hydrocarbons within this pore space. As also shown by the small amounts of unexpelled hydrocarbons, the Expulsinator generates an optimum for yielding expulsion: A source-rock with low lateral expansion, surrounded by the reservoir – conditions which are also seen as cause of expulsion from kerogen type-III in natural systems (Fleet and Scott, 1994; Wilkins and George, 2002).

Foulden Maar has to be considered separately, as a missing diagenetic overprint leads to a very different generation/expulsion profile compared to the other type-I and –I/II kerogen. High amounts of thermally labile components show a very early generation at low temperatures and decreasing yields with ongoing simulated subsidence.

The semi-open experimental setup of the Expulsinator enables the observation of timing controlled effects onto generation and expulsion, like the bimodal expulsion curves observed for most source-rock samples during the experiment mid-stage. This suggests two different generation processes and/or secondary cracking processes of restrained products and subsequent expulsion.

Moreover, liquid product expulsion is influenced by the litho-type of the source-rock and its resistance towards overburden pressure. Litho-types, showing a very high grade of overburden pressure resistance, like Barnett Shale (in combination with low permeability) or Malm ζ II, show lower expulsion efficiency. Moderate pressure resistance (Green River and Bessano Fm.) accelerate expulsion at elevated pressures, which is contradicted by lower permeability. A further controlling factor is the low general permeability, which could lead to low expulsion rates in case of Posidonia Shale and Barnett Shale.

Hydrocarbon gas release shows an early expulsion maximum within the first experiment stage for all experiments. This is clearly associated to decomposition of in-situ bitumen, rather than to new generation. In the following stages, $C_1$-$C_5$ gas expulsion is delayed to the expulsion of liquid products. In the last stage, the generation/expulsion curve shows two distinct maxima of gas release in all experiments, but with different shaping, suggesting two different processes: The primary release from kerogen decomposition (first maximum) and oil-to-gas cracking (second maximum). Again, lithology differences are accused to cause shaping differences of the bimodal gas expulsion within the last stage, as larger pore-resistance (no pore collapse), as in case of Malm ζ II, could flatten the expulsion curve.

$CO_2$ expulsion is not limited to the first experiment stage only, but occurs in all stages of the experiments. However, the linkage between liquid product expulsion and $CO_2$ release is striking, supporting suggestions of Lewan (1997) that carbonyl group-water interactions cause a continuing $CO_2$ generation. Not quite clarified is the input of inorganic carbon to the released $CO_2$ quantities in case of Besano Fm. (dolomite) and Malm ζ II (calcite). It is unquestionable that in both cases inorganic carbon contributes to the $CO_2$ content. However, quantities, timing and shape of the expulsion curve differ greatly between both samples, so that a different thermic response of dolomite and calcite can be assumed.

# 6 Summary

Expulsinator experiments are characterized by very high expulsion efficiency, expressed by very low amounts of unexpelled bitumen (< 5 %). Low residue potential of the treated samples testifies the high generation rates produced by the Expulsinator-device.

Results of comparative pyrolysis methodologies differ dramatically from the results delivered by the Expulsinator. The latter exceeded the extract yields of hydrous pyrolysis by 16 % at least and the amount of obtained *n*-alkanes is larger for the Expulsinator experiments, too. The reason is seen in both the closed CSVP pyrolysis versus the open setup of the Expulsinator and in the different pyrolysis duration of these methods. Exhaustive consumption of free hydrogen due to fast generation rates leads to cross-linking reactions in case of CSVP (especially at high temperatures, e.g. 360 °C and 375 °C). This, and the decomposition of already generated hydrocarbons in secondary cracking processes, support the formation of double carbon bonds or cyclization (Lewan, 1997), increasing the amount of solid bitumen products. In contrast, the long-term generation in case of Expulsinator experiments and the consequent removal of generated products, let to a balance between free hydrogen supply and demand by hydrocarbon cracking processes. Higher rates of pyrobitumen formation in closed anhydrous pyrolysis compared to hydrous experiments demonstrate the importance of water as hydrogen donor. However, for Expulsinator experiments with elevated lithostatic pressures, it is questionable whether and to what extent water enters the source-rock to contribute free hydrogen. Alternative hydrogen sources could be mineral transformation (smectite to illite) as described by Colten-Bradley (1987) or secession form kerogen or bitumen aromatization (Weres et al., 1988).

Maturity assessment is highly impacted by pyrobitumen formation as well. $T_{max}$-values of kerogen type-I source-rocks, treated by CSVP, show increased values compared to residues from corresponding Expulsinator experiments. In contrast, source-rocks of type-II kerogen behave reversed, reaching higher $T_{max}$-values after Expulsinator experiments. This suggests that $T_{max}$-values, produced by the residual kerogen, is masked by larger amounts of pyrobitumen in case of the CSVP experiments. Residual type-I kerogen produces lower $T_{max}$-values and residual type-II kerogen higher $T_{max}$-values as pyrobitumen. Type-III kerogen shows a drastic increase of the $T_{max}$-value by pyrobitumen formation.

Removal of generated products suppressed interactions between bitumen, kerogen, pyrobitumen and pyrite in case of Expulsinator experiments. In contrast, CSVP residues show elevated nitrogen content due to incorporation of nitrogen into aromatic pyrobitumen substructures. Lowering of pyrite transformation temperature by pyrobitumen caused a depletion of sulfur and increased the hydrogen shortage by forming $H_2S$. Further, oxygen compounds were re-incorporation into kerogen after the termination of the experiment in case of CSVP, but were removed in the Expulsinator experiment.

Geochromatographic effects, as shown by Expulsinator experiments with Posidonia Shale, strongly affect the composition of expelled products. Greater retention of larger molecules compared to their smaller equivalents leads to time delayed expulsion of *n*-alkanes with longer chain-length. As a side effect, Expulsinator experiments released higher amounts of short-chain *n*-alkanes as comparative CSVP experiments, caused by retention of long-chain *n*-alkanes and the subsequent thermal cracking to shorter components.

The generation and expulsion behaviour of the isoprenoids pristane and phytane were investigated by Expulsinator experiments. Pristane was released preferably compared to phytane, causing a faster quantity decrease of pristane after peak expulsion. Higher decomposition rates of phytane, as noted by Tang and Stauffer (1995), were observed for CSVP (closed setup), but not in case of Expulsinator experiments (open setup). This suggests that mainly secondary reactions affect phytane decomposition.

The ratio of isoprenoids vs. *n*-alkanes, e.g. the Pr/*n*-$C_{17}$-ratio, is mainly controlled by the different generation rates of the *n*-alkane and isoprenoid. Increasing generation of the *n*-alkane and reduced production of pristane causes decreasing values for this ratio with ongoing maturation. In contradiction to various studies (Leythaeuser et al., 1984a, 1984b; e.g. Leythaeuser and Schaefer, 1984; Leythaeuser and Schwarzkopf, 1986; Mackenzie et al., 1983), preferred retention of pristane was found to play only a minor part. Due to the good correlation of Pr/Ph- and the Pr/*n*-$C_{17}$-ratio changes with the generation and expulsion progress, both ratios are considered as indicator for expulsion timing.

The Expulsinator-device delivered reliable generation/expulsion profiles for characterisation of type-I, type-II and type-III kerogens. Onset of generation and expulsion was observed in the following order:

(early) type-III > type-IIS > type-II > type-I (late)

Unexpected early generation and release of hydrocarbons in case of type-III kerogen was attributed to generally high potential for early generation (as also described by Behar et al., (1997a)), combined with excellent conditions for expulsion (thin source-rock, surrounding reservoir, high lithostatic pressures), provided by the Expulsinator. In natural systems, worse conditions for expulsion seems to be more common generally speaking, causing the retention of the generated products within the kerogen pore system. For almost all investigated source-rocks, two deviated generation/expulsion maxima were observed within the 2000 m stage of the Expulsion experiments, suggesting two different generation and/or secondary cracking processes of restrained products and subsequent expulsion.

Expulsion efficiency is highly affected by the source-rock lithology. A reduced expulsion efficiency was observed for very sturdy litho-types or source-rocks with low permeability. In contrast, lithologies with moderate pressure resistance are prone to propagated fracturing, supporting the formation of migration avenues.

In general, the expulsion of gaseous hydrocarbons is time delayed to the liquid product release. The only exception is the very first expulsion stage at 2000 m simulated depth. Here, $C_1$-$C_5$ gas expulsion is clearly associated to decomposition of in-situ bitumen. As to be expected, the main gas generation and expulsion is observed within the last experiment stage (3000 m). Herein, two distinct $C_1$-$C_5$ gas expulsion maxima are recognizable; the first one is attributed to kerogen decomposition, the second one to oil-to-gas cracking. Absent squeezing effects, due to high pore-resistance, affect the shape of the expulsion curve by decreasing the expulsion rate of the hydrocarbon gases.

$CO_2$ expulsion is observed for the entire experiment, even at elevated maturity. This could be caused by interactions between carbonyl groups and water, producing larger amounts of $CO_2$ during the maturation. In case of dolomitic and calcitic litho-types, the inorganic carbon contributes to $CO_2$ on a larger scale, especially at higher pyrolysis temperatures. However, dolomitic and calcitic source-rocks differ in quantity, shape and timing of $CO_2$ generation/expulsion, suggesting different thermic response of both minerals.

# 7 Appendix

The appendix compiles data produced in the scope of this PhD thesis. As the large amount of data is not presentable in printed form, this data is summarized as excel-files and png-files.

The amount of the acquired data exceeds the frame of a single PhD-thesis. Therefore, the appendix includes data, which is not discussed in previous chapters of this thesis. A detailed analysis and interpretation of these data will be part of following publications.

The electronical appendix can be downloaded with the following link:

http://zaphod.gpi.uni-kiel.de/~mst/Appendix_Martin-Stockhausen/

The appendix comprises data sets, associated to the chapters of the thesis:

1. Chapter 3 (Chapter_3.xlsx):
   a. bulk data (extract yields, elementary data, Rock Eval, OM-conversion calculations)
   b. *n*-alkane distribution
   c. BETX-data, derived from MSSV-pyrolysis
2. Chapter 4 (Chapter_4.xlsx):
   a. bulk data (extract yields, elementary data, Rock Eval, OM-conversion calculations)
   b. distribution of aliphatic compounds
   c. calculated data of the Pr/*n*-$C_{17}$ migration model
3. Chapter 5 (Chapter_5.xlsx):
   a. bulk data (extract yields, elementary data, Rock Eval, OM-conversion calculations)
   b. Gas yields ($C_1$-$C_5$ and $CO_2$)

Further, general data sets are included, comprising EASY%$R_O$ calculations (EasyRo_calculation.xlsx) and the pressure, temperature and compression data of each discussed experiment (Experiment-raw-data.xlsx).

Undiscussed data are given as a data file (data_undiscussed.xlsx) and as high-resolution png-files, including bulk data and molecular data of aliphatic and aromatic fractions (raw data, quantifications, bio-/geomarker ratios and migration related ratios of aromatic compounds).

# References


Albrecht, P., Vandenbroucke, M., Mandengué, M., 1976. Geochemical studies on the organic matter from the Douala Basin (Cameroon)—I. Evolution of the extractable organic matter and the formation of petroleum. Geochimica et Cosmochimica Acta 40, 791–799. doi:10.1016/0016-7037(76)90031-4

Alexander, R., Strachan, M.G., Kagi, R.I., Van Bronswijk, W., 1986. Heating rate effects on aromatic maturity indicators. Organic Geochemistry 10, 997–1003. doi:10.1016/S0146-6380(86)80038-9

Allan, J., Larter, S.R., 1983. Aromatic structure in coal maceral extracts and kerogens. Advances in Organic Geochemistry 1981 534–545.

Altaner, S.P., Ylagan, R.F., 1997. Comparison of structural models of mixed-layer illite/smectite and reaction mechanisms of smectite illitization. Clay Clay Min. 45, 517–533. doi:10.1346/CCMN.1997.0450404

Andresen, B., Barth, T., Irwin, H., 1993. Yields and carbon isotopic composition of pyrolysis products from artificial maturation processes. Chemical Geology 106, 103 – 119.

Arneth, J.-D., Matzigkeit, U., 1986. Variations in the carbon isotope composition and production yield of various pyrolysis products under open and closed system conditions. Organic Geochemistry 10, 1067 – 1071.

Artok, L., Schobert, H.H., Nomura, M., Erbatur, O., Kidena, K., 1998. Effects of Water and Molecular Hydrogen on Heat Treatment of Turkish Low-Rank Coalsâ. Energy & Fuels 12, 1200–1211.

Barker, C., 1980. Primary Migration: The Importance of Water-Mineral-Organic Matter Interactions in the Source Rock 29, 19–31.

Behar, F., Kressmann, S., Rudkiewicz, J.L., Vandenbroucke, M., 1992. Experimental simulation in a confined system and kinetic modelling of kerogen and oil cracking. Organic Geochemistry 19, 173–189. doi:10.1016/0146-6380(92)90035-V

Behar, F., Lewan, M.D., Lorant, F., Vandenbroucke, M., 2003. Comparison of artificial maturation of lignite in hydrous and nonhydrous conditions. Organic Geochemistry 34, 575 – 600.

Behar, F., Pelet, R., 1985. Pyrolysis-gas chromatography applied to organic geochemistry: Structural similarities between kerogens and asphaltenes from related rock extracts and oils. Journal of Analytical and Applied Pyrolysis 8, 173–187. doi:10.1016/0165-2370(85)80024-3

Behar, F., Tang, Y., Liu, J., 1997a. Comparison of rate constants for some molecular tracers generated during artificial maturation of kerogens: influence of kerogen type. Organic Geochemistry 26, 281–287. doi:10.1016/S0146-6380(97)00003-X

Behar, F., Ungerer, P., Kressmann, S., Rudkiewicz, J.L., 1991. Thermal Evolution of Crude Oils in Sedimentary Basins: Experimental Simulation in a Confined System and Kinetic Modeling. Oil & Gas Science and Technology 46, 151–181. doi:10.2516/ogst:1991007

Behar, F., Vandenbroucke, M., 1987. Chemical modelling of kerogens. Organic Geochemistry 11, 15 – 24.

Behar, F., Vandenbroucke, M., Tang, Y., Marquis, F., Espitalie, J., 1997b. Thermal cracking of kerogen in open and closed systems: determination of kinetic parameters and stoichiometric coefficients for oil and gas generation. Organic Geochemistry 26, 321–339. doi:10.1016/S0146-6380(97)00014-4

Behar, F., Vandenbroucke, M., Teermann, S.C., Hatcher, P.G., Leblond, C., Lerat, O., 1995. Experimental simulation of gas generation from coals and a marine kerogen. Chemical Geology 126, 247–260. doi:10.1016/0009-2541(95)00121-2

Berg, R.R., Gangi, A.F., 1999. Primary Migration by Oil-Generation Microfracturing in Low-Permeability Source Rocks: Application to the Austin Chalk, Texas. AAPG Bulletin 83, 727–756.

Bernasconi, S., Riva, A., 1993. Organic Geochemistry and Depositional Environment of a Hydrocarbon Source Rock: The Middle Triassic Grenzbitumenzone Formation, Southern Alps, Italy/Switzerland, in: Spencer, D.A.M. (Ed.), Generation, Accumulation and Production of Europe's Hydrocarbons III, Special Publication of the European Association of Petroleum Geoscientists. Springer Berlin Heidelberg, pp. 179–190.

Bishop, A.., Love, G.., McAulay, A.., Snape, C.., Farrimond, P., 1998. Release of kerogen-bound hopanoids by hydropyrolysis. Organic Geochemistry 29, 989–1001. doi:10.1016/S0146-6380(98)00140-5

Bjorøy, M., Solli, H., Hall, K., Leplat, P., 1986. Analysis of source rocks, reservoir rocks and cap rocks by combined thermal extraction and pyrolysis—gas chromatography, in: Thomas, B.M. (Ed.), Petroleum Geochemistry in Exploration of the Norwegian Shelf. Springer Netherlands, pp. 327–337.

Blanc, P., Connan, J., 1992. Generation and expulsion of hydrocarbons from a Paris Basin Toarcian source rock: an experimental study by confined-system pyrolysis. Energy & Fuels 6, 666–677.

Blanksby, S.J., Ellison, G.B., 2003. Bond Dissociation Energies of Organic Molecules. Acc. Chem. Res. 36, 255–263. doi:10.1021/ar020230d

Bojesen-Koefoed, J.A., Christiansen, F.G., Petersen, H.I., Piasecki, S., Stemmerik, L., Nytoft, H.P., 1996. Resinite-Rich Coals of Northeast Greenland - a Hitherto Unrecognized, Highly Oil-Prone Jurassic Source Rock. Bulletin of Canadian Petroleum Geology 44, 458–473.

Boles, J., Franks, S., 1979. Clay Diagenesis in Wilcox Sandstones of Southwest Texas - Implications. Journal of Sedimentary Petrology 49, 55–70.

Bolton, C., Riemer, C., Snape, C.E., Derbushire, F.J., Terrer, M.T., 1988. Effect of low temperature catalytic hydrogenation on pyrolysis and hydropyrolysis of a bituminous coal. Fuel 67, 901–905. doi:10.1016/0016-2361(88)90088-9

Bolton, C., Snape, C.E., O'Brien, R.J., Kandiyoti, R., 1987. Influence of carrier gas flow and heating rates in fixed bed hydropyrolysis of coal. Fuel 66, 1413–1417. doi:10.1016/0016-2361(87)90189-X

Bonilla, J.V., Engel, M.H., 1986. Chemical and isotopic redistribution of hydrocarbons during migration: Laboratory simulation experiments. Organic Geochemistry 10, 181–190. doi:10.1016/0146-6380(86)90021-5

Bordenave, M.L., 1993. Applied Petroleum Geochemistry. Editions OPHRYS.

Bordenave, M.L., Combaz, A., Giraud, A., 1970. Influence de l'origine des matières organiques et de leur degré d'évolution sur les produits de pyrolyse du kérogène. Advances in Organic Geochemistry 1966 389–405.

Braun, R.L., Burnham, A.K., 1992. PMOD: a flexible model of oil and gas generation, cracking, and expulsion. Organic Geochemistry 19, 161 – 172.

Brooks, J.D., Gould, K., Smith, J.W., 1969. Isoprenoid Hydrocarbons in Coal and Petroleum. Nature 222, 257–259. doi:10.1038/222257a0

Brother, L., Engel, M.H., Krooss, B.M., 1991. The effects of fluid flow through porous media on the distribution of organic compounds in a synthetic crude oil. Organic Geochemistry 17, 11–24. doi:10.1016/0146-6380(91)90036-J

Burnham, A., Braun, R., 1985. General Kinetic-Model of Oil-Shale Pyrolysis. In Situ 9, 1–23.

Burnham, A.K., 1993. Relationship Between Hydrous and Ordinary Pyrolysis, NATO Advanced Study Institute on Composition Geochemistry. Lawrence Livermore National Laboratory.

Burnham, A.K., 1991. Oil evolution from a self-purging reactor: kinetics and composition at 2.degree.C/min and 2.degree.C/h. Energy Fuels 5, 205–214. doi:10.1021/ef00025a034

Burnham, A.K., Braun, R.L., 1990. Development of a detailed model of petroleum formation, destruction, and expulsion from lacustrine and marine source rocks. Organic Geochemistry 16, 27–39. doi:10.1016/0146-6380(90)90023-S

Burnham, A.K., Braun, R.L., Gregg, H.R., Samoun, A.M., 1987. Comparison of methods for measuring kerogen pyrolysis rates and fitting kinetic parameters. Energy & Fuels 1, 452–458.

Burnham, A.K., Braun, R.L., Samoun, A.M., 1988. Further comparison of methods for measuring kerogen pyrolysis rates and fitting kinetic parameters. Organic Geochemistry 13, 839–845. doi:10.1016/0146-6380(88)90236-7

Burnham, A.K., Singleton, M.F., 1983. High-Pressure Pyrolysis of Green River Oil Shale, in: Geochemistry and Chemistry of Oil Shales, ACS Symposium Series. AMERICAN CHEMICAL SOCIETY, pp. 335–351.

Cai, C., Hu, W., Worden, R.H., 2001. Thermochemical sulphate reduction in Cambro–Ordovician carbonates in Central Tarim. Marine and Petroleum Geology 18, 729–741. doi:10.1016/S0264-8172(01)00028-9

Campbell, J.H., Koskinas, G.H., Stout, N.D., 1978. Kinetics of oil generation from Colorado oil shale. Fuel 57, 372–376. doi:10.1016/0016-2361(78)90176-X

Carter, S.D., Citiroglu, M., Gallacher, J., Snape, C.E., Mitchell, S., Lafferty, C.J., 1994. Secondary coking and cracking of shale oil vapours from pyrolysis or hydropyrolysis of a Kentucky Cleveland oil shale in a two-stage reactor. Fuel 73, 1455–1458. doi:10.1016/0016-2361(94)90062-0

Cassani, F., Gallango, O., Talukdar, S., Vallejos, C., Ehrmann, U., 1988. Methylphenanthrene maturity index of marine source rock extracts and crude oils from the Maracaibo Basin. Organic Geochemistry 13, 73–80. doi:10.1016/0146-6380(88)90027-7

Chen, H., Li, B., Zhang, B., 2000. Decomposition of pyrite and the interaction of pyrite with coal organic matrix in pyrolysis and hydropyrolysis. Fuel 79, 1627–1631. doi:10.1016/S0016-2361(00)00015-6

Claypool, G.E., Reed, P.R., 1976. Thermal-Analysis Technique for Source-Rock Evaluation: Quantitative Estimate of Organic Richness and Effects of Lithologic Variation: GEOLOGIC NOTES. AAPG Bulletin 60, 608–612.

Clegg, H., Horsfield, B., Wilkes, H., Sinninghe Damsté, J., Koopmans, M.P., 1998. Effect of artificial maturation on carbazole distributions, as revealed by the hydrous pyrolysis of an organic-sulphur-rich source rock (Ghareb Formation, Jordan). Organic Geochemistry 29, 1953–1960. doi:10.1016/S0146-6380(98)00172-7

Colten-Bradley, V.A., 1987. Role of Pressure in Smectite Dehydration-Effects on Geopressure and Smectite-to-Illite Transformation. AAPG Bulletin 71, 1414–1427.

Cooles, G.P., Mackenzie, A.S., Quigley, T.M., 1986. Calculation of petroleum masses generated and expelled from source rocks. Organic Geochemistry 10, 235–245. doi:10.1016/0146-6380(86)90026-4

Coudrain-Ribstein, A., Gouze, P., de Marsily, G., 1998. Temperature-carbon dioxide partial pressure trends in confined aquifers. Chemical Geology 145, 73–89. doi:10.1016/S0009-2541(97)00161-7

Curry, D.J., 2003. New insights on the Green River petroleum system in the Uinta basin from hydrous pyrolysis experiments: Discussion. AAPG Bulletin 87, 1531–1534.

Curtis, C.D., 1983. Geochemistry of Porosity Enhancement and Reduction in Clastic Sediments. Geological Society, London, Special Publications 12, 113–125. doi:10.1144/GSL.SP.1983.012.01.12

Damsté, J.S.S., Kohnen, M.E.L., de Leeuw, J.W., 1990. Thiophenic biomarkers for palaeoenvironmental assessment and molecular stratigraphy. Nature 345, 609–611. doi:10.1038/345609a0

De Graaf, W., Damsté, J.S.S., de Leeuw, J.W., 1992. Laboratory simulation of natural sulphurization: I. Formation of monomeric and oligomeric isoprenoid polysulphides by low-temperature reactions of inorganic polysulphides with phytol and phytadienes. Geochimica et Cosmochimica Acta 56, 4321–4328. doi:10.1016/0016-7037(92)90275-N

Delvaux, D., Martin, H., Leplat, P., Paulet, J., 1990. Geochemical characterization of sedimentary organic matter by means of pyrolysis kinetic parameters. Organic Geochemistry 16, 175–187. doi:10.1016/0146-6380(90)90038-2

Dickey, P.A., 1975. Possible Primary Migration of Oil from Source Rock in Oil Phase: GEOLOGIC NOTES. AAPG Bulletin 59, 337–345.

Dieckmann, V., 2005. Modelling petroleum formation from heterogeneous source rocks: the influence of frequency factors on activation energy distribution and geological prediction. Marine and Petroleum Geology 22, 375–390. doi:10.1016/j.marpetgeo.2004.11.002

Dieckmann, V., Caccialanza, P.G., Galimberti, R., 2002. Evaluating the timing of oil expulsion: about the inverse behaviour of light hydrocarbons and oil asphaltene kinetics. Organic Geochemistry 33, 1501–1513.

Dieckmann, V., Horsfield, B., Schenk, H.J., 2000. Heating rate dependency of petroleum-forming reactions: implications for compositional kinetic predictions. Organic Geochemistry 31, 1333 – 1348.

Durand, B., 1988. Understanding of HC migration in sedimentary basins (present state of knowledge). Organic Geochemistry 13, 445–459. doi:10.1016/0146-6380(88)90066-6

Durand, B., Paratte, M., 1983. Oil Potential of Coals: A Geochemical Approach. Geological Society, London, Special Publications 12, 255–265. doi:10.1144/GSL.SP.1983.012.01.26

Dyni, J.R., 2006. Geology and resources of some world oil-shale deposits (USGS Numbered Series No. 2005-5294), Scientific Investigations Report. U.S. Geological Survey.

Economou, I.G., Heidman, J.L., Tsonopoulos, C., Wilson, G.M., 1997. Mutual solubilities of hydrocarbons and water: III. 1-hexene; 1-octene; C10-C12 hydrocarbons. AIChE Journal 43, 535–546. doi:10.1002/aic.690430226

Eglinton, T.I., 1987. Generation of Water-Soluble Organic Acids from Kerogen During Hydrous Pyrolysis: Implications for Porosity Development. Mineralogical Magazine 51, 495–503. doi:10.1180/minmag.1987.051.362.04

Eltantawy, I.M., Arnold, P.W., 1972. Adsorption of *n*-Alkanes by Wyoming Montmorillonite. Nature 237, 123–125. doi:10.1038/10.1038/physci237123a0

England, W.A., Mann, A.L., Mann, D.M., 1991. Migration from Source to Trap: Chapter 3: PETROLEUM GENERATION AND MIGRATION 37, 23–46.

Ertas, D., Kelemen, S.R., Halsey, T.C., ExxonMobil Research and Engineering Company, 2006. Petroleum Expulsion Part 1. Theory of Kerogen Swelling in Multicomponent Solvents. Energy & Fuels 20, 295–300.

Eseme, E., 2006. Oil shales: Compaction, Petroleum Generation and Expulsion.

Eseme, E., Krooss, B.M., Littke, R., 2012. Evolution of petrophysical properties of oil shales during high-temperature compaction tests: Implications for petroleum expulsion. Marine and Petroleum Geology 31, 110–124. doi:10.1016/j.marpetgeo.2011.11.005

Eseme, E., Littke, R., Krooss, B.M., 2006a. Factors controlling the thermo-mechanical deformation of oil shales: Implications for compaction of mudstones and exploitation. Marine and Petroleum Geology 23, 715–734. doi:10.1016/j.marpetgeo.2006.02.007

Eseme, E., Littke, R., Krooss, B.M., Schwarzbauer, J., 2007. Experimental investigation of the compositional variation of petroleum during primary migration. Organic Geochemistry 38, 1373–1397. doi:10.1016/j.orggeochem.2007.03.003

Eseme, E., Littke, R., Krooss, B.M., Schwarzbauer, J., 2006b. Experimental investigation of the compositional variation of acyclic paraffins during expulsion from source rocks. Journal of Geochemical Exploration 89, 100–103. doi:10.1016/j.gexplo.2005.11.037

Espitalie, J., Deroo, G., Marquis, F., 1986. La pyrolyse Rock-Eval et ses applications. Troisième partie. Oil & Gas Science and Technology 41, 73–89. doi:10.2516/ogst:1986003

Espitalie, J., Deroo, G., Marquis, F., 1985a. La pyrolyse Rock-Eval et ses applications. Première partie. Oil & Gas Science and Technology 40, 563–579. doi:10.2516/ogst:1985035

Espitalie, J., Deroo, G., Marquis, F., 1985b. La pyrolyse Rock-Eval et ses applications. Deuxième partie. Oil & Gas Science and Technology 40, 755–784. doi:10.2516/ogst:1985045

Espitalié, J., Laporte, J.L., Madec, M., Marquis, F., Leplat, P., Paulet, J., Boutefeu, A., 1977. Méthode rapide de caractérisation des roches mètres, de leur potentiel pétrolier et de leur degré d'évolution. Oil & Gas Science and Technology 32, 23–42. doi:10.2516/ogst:1977002

Espitalie, J., Madec, M., Tissot, B., 1980. Role of Mineral Matrix in Kerogen Pyrolysis: Influence on Petroleum Generation and Migration. AAPG Bulletin 64, 59–66.

Espitalié, J., Senga Makadi, K., Trichet, J., 1984. Role of the mineral matrix during kerogen pyrolysis. Organic Geochemistry 6, 365–382. doi:10.1016/0146-6380(84)90059-7

Farrimond, P., Taylor, A., TelnÆs, N., 1998. Biomarker maturity parameters: the role of generation and thermal degradation. Organic Geochemistry 29, 1181–1197. doi:10.1016/S0146-6380(98)00079-5

Fernandez, F., Quigley, R.M., 1985. Hydraulic conductivity of natural clays permeated with simple liquid hydrocarbons. Canadian Geotechnical Journal 22, 205–214. doi:10.1139/t85-028

Fleet, A.J., Scott, A.C., 1994. Coal and coal-bearing strata as oil-prone source rocks: an overview. Geological Society, London, Special Publications 77, 1–8. doi:10.1144/GSL.SP.1994.077.01.01

Franks, S.G., Forester, R.W., 1984. Relationships Among Carbon Dioxide, Pore-Fluid Chemistry, and Secondary Porosity, Texas Gulf Coast: ABSTRACT. AAPG Bulletin 68, 478–478.

Freed, R.L., Peacor, D.R., 1989. Geopressured Shale and Sealing Effect of Smectite to Illite Transition. AAPG Bulletin 73, 1223–1232.

Frimmel, A., Oschmann, W., Schwark, L., 2004. Chemostratigraphy of the Posidonia Black Shale, SW Germany: I. Influence of sea-level variation on organic facies evolution. Chemical Geology 206, 199–230. doi:10.1016/j.chemgeo.2003.12.007

Geng, A., Zhou, Y., Fu, J., Sheng, G., Zhang, Q., 1998. The generation and expulsion of gases in Ya131 gas field, South China Sea: implication of laboratory pyrolysis results. Journal of Asian Earth Sciences 16, 429–436. doi:10.1016/S0743-9547(98)00017-8

Giraud, A., 1970. Application of Pyrolysis and Gas Chromatography to Geochemical Characterization of Kerogen in Sedimentary Rock. AAPG Bulletin 54, 439–455.

Gransch, J.A., Eisma, E., 1970. Characterization of the insoluble organic matter of sediments by pyrolysis. Advances in Organic Geochemistry 1966 407–426.

Green, T.K., Kovac, J., Larsen, J.W., 1984. A rapid and convenient method for measuring the swelling of coals by solvents. Fuel 63, 935–938. doi:10.1016/0016-2361(84)90313-2

Groenzin, H., Mullins, O.C., 2000. Molecular Size and Structure of Asphaltenes from Various Sources. Energy Fuels 14, 677–684. doi:10.1021/ef990225z

Guthrie, J.M., Houseknecht, D.W., Johns, W.D., 1986. Relationships Among Vitrinite Reflectance, Illite Crystallinity, and Organic Geochemistry in Carboniferous Strata, Ouachita Mountains, Oklahoma and Arkansas. AAPG Bulletin 70, 26–33.

Hanebeck, D., 1993. Experimentelle Simulation und Untersuchung der Genese und Expulsion von Erdölen aus Muttergesteinen. Forschungszentrum Jülich.

Heidman, J.L., Tsonopoulos, C., Brady, C.J., Wilson, G.M., 1985. High-temperature mutual solubilities of hydrocarbons and water. Part II: Ethylbenzene, ethylcyclohexane, and *n*-octane. AIChE Journal 31, 376–384. doi:10.1002/aic.690310304

Helgeson, H.C., Knox, A.M., Owens, C.E., Shock, E.L., 1993. Petroleum, oil field waters, and authigenic mineral assemblages Are they in metastable equilibrium in hydrocarbon reservoirs. Geochimica et Cosmochimica Acta 57, 3295–3339. doi:10.1016/0016-7037(93)90541-4

Hill, R.J., Tang, Y., Kaplan, I.R., Jenden, P.D., 1996. The Influence of Pressure on the Thermal Cracking of Oil. Energy Fuels 10, 873–882. doi:10.1021/ef9501408

Hoering, T.C., 1984. Thermal reactions of kerogen with added water, heavy water and pure organic substances. Organic Geochemistry 5, 267–278. doi:10.1016/0146-6380(84)90014-7

Hoffmann, C.F., Mackenzie, A.S., Lewis, C.A., Maxwell, J.R., Oudin, J.L., Durand, B., Vandenbroucke, M., 1984. A biological marker study of coals, shales and oils from the Mahakam Delta, Kalimantan, Indonesia. Chemical Geology 42, 1–23. doi:10.1016/0009-2541(84)90002-0

Horsfield, B., 1990. Evaluating kerogen type according to source quality, compositional heterogeneity and thermal lability. Review of Palaeobotany and Palynology 65, 357 – 365.

Horsfield, B., Disko, U., Leistner, F., 1989. The micro-scale simulation of maturation: outline of a new technique and its potential applications. Geologische Rundschau 78, 361–373. doi:10.1007/BF01988370

Horsfield, B., Schenk, H.J., Mills, N., Welte, D.H., 1992. An investigation of the i*n*-reservoir conversion of oil to gas: compositional and kinetic findings from closed-system programmed-temperature pyrolysis. Organic Geochemistry 19, 191–204. doi:10.1016/0146-6380(92)90036-W

Horsfield, B., Welte, D.H., Baker, D.R., 1996. Petroleum and Basin Evolution: Insights from Petroleum Geochemistry, Geology and Basin Modeling. Springer-Verlag.

Hower, J., Eslinger, E., Hower, M., Perry, E., 1976. Mechanism of Burial Metamorphism of Argillaceous Sediment .1. Mineralogical and Chemical Evidence. Geol. Soc. Am. Bull. 87, 725–737. doi:10.1130/0016-7606(1976)87<725:MOBMOA>2.0.CO;2

Huang, W.-L., 1996. Experimental study of vitrinite maturation: effects of temperature, time, pressure, water, and hydrogen index. Organic Geochemistry 24, 233 – 241.

Huc, A.Y., Nederlof, P., Debarre, R., Carpentier, B., Boussafir, M., Laggoun-Défarge, F., Lenail-Chouteau, A., Bordas-Le Floch, N., 2000. Pyrobitumen occurrence and formation in a Cambro–Ordovician sandstone reservoir, Fahud Salt Basin, North Oman. Chemical Geology 168, 99–112. doi:10.1016/S0009-2541(00)00190-X

Huizinga, B.J., Aizenshtat, Z.A., Peters, K.E., 1988. Programmed pyrolysis-gas chromatography of artificially matured Green River kerogen. Energy Fuels 2, 74–81. doi:10.1021/ef00007a011

Hunt, J.M., 1996. Petroleum Geochemistry and Geology. Freeman.

Jackśon, K.J., Burnham, A.K., Braun, R.L., Knauss, K.G., 1995. Temperature and pressure dependence of *n*-hexadecane cracking. Organic Geochemistry 23, 941–953. doi:10.1016/0146-6380(95)00068-2

Jin, Y., Xiao, Y., Tang, Y., Tian, H., Liu, J., 2009. Influence of water on yields and isotopic fractionations of gas hydrocarbons generated from oil cracking. Geochemical Journal 43, 247–255.

Johannes, I., Kruusement, K., Palu, V., Veski, R., Bojesen-Koefoed, J.A., 2006. Evaluation of oil potential of estonian shales and biomass samples using Rock-eval analyzer. Oil Shale 23, 110–118.

Katz, B.J., Kelley, P.A., Royle, R.A., Jorjorian, T., 1991. Hydrocarbon products of coals as revealed by pyrolysis-gas chromatography. Organic Geochemistry 17, 711–722. doi:10.1016/0146-6380(91)90015-C

Kelemen, S.R., Walters, C.C., Ertas, D., Freund, H., 2006. Petroleum Expulsion Part 3. A Model of Chemically Driven Fractionation during Expulsion of Petroleum from Kerogen. Energy & Fuels 20, 309–319.

Kelemen, S.R., Walters, C.C., Kwiatek, P.J., Afeworki, M., Sansone, M., Freund, H., Pottorf, R.J., Machel, H.G., Zhang, T., Ellis, G.S., Tang, Y., Peters, K.E., 2008. Distinguishing solid bitumens formed by thermochemical sulfate reduction and thermal chemical alteration. Organic Geochemistry 39, 1137–1143. doi:10.1016/j.orggeochem.2008.04.007

Kelemen, S.R., Walters, C.C., Kwiatek, P.J., Freund, H., Afeworki, M., Sansone, M., Lamberti, W.A., Pottorf, R.J., Machel, H.G., Peters, K.E., Bolin, T., 2010. Characterization of solid bitumens originating from thermal chemical alteration and thermochemical sulfate reduction. Geochimica et Cosmochimica Acta 74, 5305–5332. doi:10.1016/j.gca.2010.06.013

Killops, S.D., Killops, V.J., 2009. An Introduction to Organic Geochemistry. John Wiley & Sons.

Koopmans, M.., Carson, F.., Sinninghe Damsté, J.., Lewan, M.., 1998. Biomarker generation from Type II-S kerogens in claystone and limestone during hydrous and anhydrous pyrolysis. Organic Geochemistry 29, 1395–1402. doi:10.1016/S0146-6380(98)00187-9

Koopmans, M.P., Rijpstra, W.I.C., Klapwijk, M.M., de Leeuw, J.W., Lewan, M.D., Sinninghe Damsté, J.S., 1999. A thermal and chemical degradation approach to decipher pristane and phytane precursors in sedimentary organic matter. Organic Geochemistry 30, 1089–1104. doi:10.1016/S0146-6380(99)00088-1

Krooß, B., 1985. Experimentelle Untersuchung der Diffusion niedrigmolekularer Kohlenwasserstoffe in wassergesättigten Sedimentgesteinen.

Krooss, B.M., Brothers, L., Engel, M.H., 1991. Geochromatography in petroleum migration: a review. Geological Society, London, Special Publications 59, 149–163. doi:10.1144/GSL.SP.1991.059.01.11

Kuangzong, Q., Qiushui, Y., Shaohui, G., Qinghua, L., Wei, S., 1994. Chemical structure and hydrocarbon formation of the Huanxian brown coal, China. Organic Geochemistry 21, 333 – 341. doi:10.1016/0146-6380(94)90195-3

Lafargue, E., Espitalie, J., Jacobsen, T., Eggen, S., 1990. Experimental simulation of hydrocarbon expulsion. Advances in Organic Geochemistry 1989; Org. Geochem. Vol. 16, Nos 1-3, 121–131.

Lafargue, W., Espitalie, J., Broks, T.M., Nyland, B., 1994. Experimental simulation of primary migration. Organic Geochemistry 22, 575–586. doi:10.1016/0146-6380(94)90126-0

Larsen, J.W., 1999. A physical-organic chemist looks at hydrous pyrolysis. Abstr. Pap. Am. Chem. Soc. 217, U820–U821.

Larsen, J.W., Hall, P., Wernett, P.C., 1995. Pore Structure of the Argonne Premium Coals. Energy Fuels 9, 324–330. doi:10.1021/ef00050a018

Larter, S., Bowler, B., Clarke, E., Wilson, C., Moffatt, B., Bennett, B., Yardley, G., Carruthers, D., 2000. An experimental investigation of geochromatography during secondary migration of petroleum performed under subsurface conditions with a real rock. Geochemical Transactions 1, 54. doi:10.1186/1467-4866-1-54

Larter, S., Mills, N., 1991. Phase-controlled molecular fractionations in migrating petroleum charges. Geological Society, London, Special Publications 59, 137–147. doi:10.1144/GSL.SP.1991.059.01.10

Larter, S.R., Bowler, B.F.J., Li, M., Chen, M., Brincat, D., Bennett, B., Noke, K., Donohoe, P., Simmons, D., Kohnen, M., Allan, J., Telnaes, N., Horstad, I., 1996. Molecular indicators of secondary oil migration distances. , Published online: 17 October 1996; | doi:10.1038/383593a0 383, 593–597. doi:10.1038/383593a0

Larter, S.R., Horsfield, B., Douglas, A.G., 1977. PYROLYSIS AS A POSSIBLE MEANS OF DETERMINING THE PETROLEUM GENERATING POTENTIAL OF SEDIMENTARY ORGANIC MATTER, in: Jones, C.E.R. (Ed.), Analytical Pyrolysis. Elsevier, pp. 189–202.

Leplat, P., 1967. Application of Pyrolysis-Gas Chromatography to the Study of the Non-Volatile Petroleum Fractions. Journal of Chromatographic Science 5, 128–135. doi:10.1093/chromsci/5.3.128

Lewan, M.D., 1998. Sulphur-radical control on petroleum formation rates. Nature 391, 164–166. doi:10.1038/34391

Lewan, M.D., 1997. Experiments on the role of water in petroleum formation. Geochimica et Cosmochimica Acta 61, 3691 – 3723.

Lewan, M.D., 1983. Effects of thermal maturation on stable organic carbon isotopes as determined by hydrous pyrolysis of Woodford Shale. Geochimica et Cosmochimica Acta 47, 1471 – 1479.

Lewan, M.D., Kotarba, M.J., Curtis, J.B., Więcław, D., Kosakowski, P., 2006. Oil-generation kinetics for organic facies with Type-II and -IIS kerogen in the Menilite Shales of the Polish Carpathians. Geochimica et Cosmochimica Acta 70, 3351–3368. doi:10.1016/j.gca.2006.04.024

Lewan, M.D., Kotarba, M.J., Więcław, D., Piestrzyński, A., 2008. Evaluating transition-metal catalysis in gas generation from the Permian Kupferschiefer by hydrous pyrolysis. Geochimica et Cosmochimica Acta 72, 4069–4093. doi:10.1016/j.gca.2008.06.003

Lewan, M.D., Roy, S., 2011. Role of water in hydrocarbon generation from Type-I kerogen in Mahogany oil shale of the Green River Formation. Organic Geochemistry 42, 31 – 41.

Lewan, M.D., Ruble, T.E., 2002. Comparison of petroleum generation kinetics by isothermal hydrous and nonisothermal open-system pyrolysis. Organic Geochemistry 33, 1457–1475.

Lewan, M.D., Winters, J.C., Mcdonald, J.H., 1979. Generation of Oil-Like Pyrolyzates from Organic-Rich Shales. Science 203, 897–899. doi:10.1126/science.203.4383.897

Leythaeuser, D., Borromeo, O., Mosca, F., di Primio, R., Radke, M., Schaefer, R.G., 1995. Pressure solution in carbonate source rocks and its control on petroleum generation and migration. Marine and Petroleum Geology 12, 717–733. doi:10.1016/0264-8172(95)93597-W

Leythaeuser, D., Littke, R., Radke, M., Schaefer, R.G., 1988a. Geochemical effects of petroleum migration and expulsion from Toarcian source rocks in the Hils syncline area, NW-Germany. Organic Geochemistry 13, 489 – 502.

Leythaeuser, D., Mackenzie, A., Schaefer, R.G., Bjoroy, M., 1984a. A Novel Approach for Recognition and Quantification of Hydrocarbon Migration Effects in Shale-Sandstone Sequences. AAPG Bulletin 68, 196–219.

Leythaeuser, D., Radke, M., Schaefer, R.G., 1984b. Efficiency of petroleum expulsion from shale source rocks. Nature Vol. 311, 745–748.

Leythaeuser, D., Schaefer, R.G., 1984. Effects of hydrocarbon expulsion from shale source rocks of high maturity in upper carboniferous strata of the Ruhr area, Federal Republic of Germany. Organic Geochemistry 6, 671–681. doi:10.1016/0146-6380(84)90088-3

Leythaeuser, D., Schaefer, R.G., Radke, M., 1988b. Geochemical effects of primary migration of petroleum in Kimmeridge source rocks from Brae field area, North Sea. I: Gross composition of C15+-soluble organic matter and molecular composition of C15+-saturated hydrocarbons. Geochimica et Cosmochimica Acta 52, 701 – 713.

Leythaeuser, D., Schwarzkopf, T., 1986. The pristane/*n*-heptadecane ratio as an indicator for recognition of hydrocarbon migration effects. Organic Geochemistry 10, 191–197. doi:10.1016/0146-6380(86)90022-7

Liao, Y., Geng, A., 2009. Stable carbon isotopic fractionation of individual *n*-alkanes accompanying primary migration: Evidence from hydrocarbon generation-expulsion simulations of selected terrestrial source rocks. Applied Geochemistry 24, 2123 – 2132.

Liao, Y., Geng, A., Xiong, Y., Liu, D., Lu, J., Liu, J., Zhang, H., Geng, X., 2004. The influence of hydrocarbon expulsion on carbon isotopic compositions of individual *n*-alkanes in pyrolysates of selected terrestrial kerogens. Organic Geochemistry 35, 1479–1488. doi:10.1016/j.orggeochem.2004.06.011

Li, M., Yao, H., Stasiuk, L.D., Fowler, M.G., Larter, S.R., 1997. Effect of maturity and petroleum expulsion on pyrrolic nitrogen compound yields and distributions in Duvernay Formation petroleum source rocks in central Alberta, Canada. Organic Geochemistry 26, 731–744. doi:10.1016/S0146-6380(97)00053-3

Lindqvist, J.K., Lee, D.E., 2009. High-frequency paleoclimate signals from Foulden Maar, Waipiata Volcanic Field, southern New Zealand: An Early Miocene varved lacustrine diatomite deposit. Sedimentary Geology, Limnogeology: Ancient and modern tales of an evolving Earth 222, 98–110. doi:10.1016/j.sedgeo.2009.07.009

Littke, D.R., Horsfield, D.B., Leythaeuser, P.D.D., 1989. Hydrocarbon distribution in coals and in dispersed organic matter of different maceral compositions and maturities. Geol Rundsch 78, 391–410. doi:10.1007/BF01988372

Littke, R., Baker, D.., Leythaeuser, D., 1988. Microscopic and sedimentologic evidence for the generation and migration of hydrocarbons in Toarcian source rocks of different maturities. Organic Geochemistry 13, 549–559. doi:10.1016/0146-6380(88)90075-7

Love, G.D., Snape, C.E., Carr, A.D., Houghton, R.C., 1995. Release of covalently-bound alkane biomarkers in high yields from kerogen via catalytic hydropyrolysis. Organic Geochemistry 23, 981–986. doi:10.1016/0146-6380(95)00075-5

Mackenzie, A.., Hoffmann, C.., Maxwell, J.., 1981. Molecular parameters of maturation in the Toarcian shales, Paris Basin, France—III. Changes in aromatic steroid hydrocarbons. Geochimica et Cosmochimica Acta 45, 1345–1355. doi:10.1016/0016-7037(81)90227-1

Mackenzie, A.S., 1984. Applications of biological markers in petroleum geochemistry, in: Brooks, J. (Ed.), Advances in Petroleum Geochemistry: 1. Academic Press Inc, pp. 115–206.

Mackenzie, A.S., Leythaeuser, D., Schaefer, R.G., Bjorøy, M., 1983. Expulsion of petroleum hydrocarbons from shale source rocks. Nature 301, 506–509. doi:10.1038/301506a0

Mackenzie, A.S., Quigley, T.M., 1988. Principles of Geochemical Prospect Appraisal. AAPG Bulletin 72, 399–415.

Mandl, G., Harkness, R.M., 1987. Hydrocarbon migration by hydraulic fracturing. Geological Society, London, Special Publications 29, 39–53. doi:10.1144/GSL.SP.1987.029.01.04

Mann, U., Hantschel, T., Schaefer, R.G., Krooss, B.M., Leythaeuser, D., Littke, R., Sachsenhofer, R.F., 1996. Petroleum migration: Mechanisms, pathways, efficiencies and numerical simulations, in: Horsfield, B., Welte, D.H., Baker, D.R. (Eds.), Petroleum and Basin Evolution: Insights from Petroleum Geochemistry, Geology and Basin Modeling. Springer-Verlag, pp. 403–520.

Maters, W.L., Meent, D.V.D., Schuyl, P.J.W., De Leeuw, J.W., Schenck, P.A., Meuzelaar, H.L.C., 1977. CURIE-POINT PYROLYSIS IN ORGANIC GEOCHEMISTRY, in: Jones, C.E.R. (Ed.), Analytical Pyrolysis. Elsevier, pp. 203–216.

Michels, R., Landis, P., Philp, R.P., Torkelson, B.E., 1995. Influence of Pressure and the Presence of Water on the Evolution of the Residual Kerogen during Confined, Hydrous, and (High-Pressure) Hydrous Pyrolysis of Woodford Shale. Energy & Fuels 9, 204–215.

Miles, J.A., 1994. Illustrated Glossary of Petroleum Geochemistry. Oxford University Press, USA.

Milton, C., 1977. Mineralogy of the Green River Formation [Wyoming, Colorado and Utah]. The Mineralogical Record 368–379.

Moldowan, J.M., Lee, C.Y., Watt, D.S., Jeganathan, A., Slougui, N.-E., Gallegos, E.J., 1991. Analysis and occurrence of C26-steranes in petroleum and source rocks. Geochimica et Cosmochimica Acta 55, 1065–1081. doi:10.1016/0016-7037(91)90164-Z

Monthioux, M., Landais, P., Monin, J.-C., 1985. Comparison between natural and artificial maturation series of humic coals from the Mahakam delta, Indonesia. Organic Geochemistry 8, 275 – 292.

Naeth, J., Asmus, S.C., Littke, R., 2004. Petrographic and geophysical assessment of coal quality as related to briquetting: the Miocene lignite of the Lower Rhine Basin, Germany. International Journal of Coal Geology 60, 17–41. doi:10.1016/j.coal.2004.04.002

Okolo, G.N., Everson, R.C., Neomagus, H.W.J.P., Roberts, M.J., Sakurovs, R., 2015. Comparing the porosity and surface areas of coal as measured by gas adsorption, mercury intrusion and SAXS techniques. Fuel 141, 293–304. doi:10.1016/j.fuel.2014.10.046

Ozkaya, I., 1988. A simple analysis of primary oil migration through oil-propagated fractures. Marine and Petroleum Geology 5, 170–174. doi:10.1016/0264-8172(88)90021-9

Pan, C., Geng, A., Zhong, N., Liu, J., 2010. Kerogen pyrolysis in the presence and absence of water and minerals: Steranes and triterpenoids. Fuel 89, 336–345. doi:10.1016/j.fuel.2009.06.032

Pepper, A.S., 1991. Estimating the petroleum expulsion behaviour of source rocks: a novel quantitative approach. Geological Society, London, Special Publications 59, 9–31. doi:10.1144/GSL.SP.1991.059.01.02

Pepper, A.S., Corvi, P.J., 1995a. Simple kinetic models of petroleum formation. Part III: Modelling an open system. Marine and Petroleum Geology 12, 417 – 452.

Pepper, A.S., Corvi, P.J., 1995b. Simple kinetic models of petroleum formation. Part I: oil and gas generation from kerogen. Marine and Petroleum Geology 12, 291 – 319.

Pepper, A.S., Dodd, T.A., 1995. Simple kinetic models of petroleum formation. Part II: oil-gas cracking. Marine and Petroleum Geology 12, 321 – 340.

Peters, K.E., Moldowan, J.M., Sundararaman, P., 1990. Effects of hydrous pyrolysis on biomarker thermal maturity parameters: Monterey Phosphatic and Siliceous members. Organic Geochemistry 15, 249–265. doi:10.1016/0146-6380(90)90003-I

Peters, K.E., Walters, C.C.C., Moldowan, J.J.M., 2005a. The Biomarker Guide: II. Biomarkers And Isotopes In Petroleum Systems And Earth History. Cambridge University Press.

Peters, K.E., Walters, C.C.C., Moldowan, J.J.M., 2005b. The Biomarker Guide: I. Biomakers And Isotopes In The Environment And Human History. Cambridge University Press.

Petit, J.C., 1991. A comprehensive study of the water vapour/coal system: application to the role of water in the weathering of coal. Fuel 70, 1053–1058. doi:10.1016/0016-2361(91)90259-D

Pollastro, R.M., Jarvie, D.M., Hill, R.J., Adams, C.W., 2007. Geologic framework of the Mississippian Barnett Shale, Barnett-Paleozoic total petroleum system, Bend arch–Fort Worth Basin, Texas. AAPG Bulletin 91, 405–436. doi:10.1306/10300606008

Price, P.L., O'Sullivan, T., Alexander, R., 1987. The Nature and Occurrence of Oil in Seram, Indonesia 141–173.

Putschew, A., Schaeffer-Reiss, C., Schaeffer, P., Koopmans, M.P., Leeuw, J.W. de, Lewan, M.D., Damsté, J.S.S., Maxwell, J.R., 1998. Release of sulfur- and oxygen-bound components from a sulfur-rich kerogen during simulated maturation by hydrous pyrolysis. Organic Geochemistry 29, 1875 – 1890.

Quigley, T.M., Mackenzie, A.S., 1988. The temperatures of oil and gas formation in the sub-surface. , Published online: 09 June 1988; | doi:10.1038/333549a0 333, 549–552. doi:10.1038/333549a0

Radke, M., Schaefer, R.G., Leythaeuser, D., Teichmüller, M., 1980. Composition of soluble organic matter in coals: relation to rank and liptinite fluorescence. Geochimica et Cosmochimica Acta 44, 1787–1800. doi:10.1016/0016-7037(80)90228-8

Radke, M., Welte, D.H., 1983. The methylphenanthrene index (MPI). A maturity parameter based on aromatic hydrocarbons, in: Bjorøy, M., Albrecht, C., Cornford, C. (Eds.), Advances in Organic Geochemistry, 1981. Wiley, pp. 504–512.

Radke, M., Welte, D.H., Willsch, H., 1982. Geochemical study on a well in the Western Canada Basin: relation of the aromatic distribution pattern to maturity of organic matter. Geochimica et Cosmochimica Acta 46, 1–10. doi:10.1016/0016-7037(82)90285-X

Radovic, L.R., Menon, V.C., Leon, C.A.L.Y., Kyotani, T., Danner, R.P., Anderson, S., Hatcher, P.G., 1997. On the porous structure of coals: Evidence for an interconnected but constricted micropore system and implications for coalbed methane recovery. Adsorption 3, 221–232. doi:10.1007/BF01650133

Reynolds, J.G., Burnham, A.K., Mitchell, T.O., 1995. Kinetic analysis of California petroleum source rocks by programmed temperature micropyrolysis. Organic Geochemistry 23, 109–120. doi:10.1016/0146-6380(94)00121-G

Riegraf, W., 1985. Mikrofauna, Biostratigraphie und Fazies im Unteren Toarcium Südwestdeutschlands und Vergleiche mit benachbarten Gebieten. Tübinger Mikropaläontologische Mitteilungen 3, 1–232.

Rimmer, S.M., Cantrell, D.J., Gooding, P.J., 1993. Rock-eval pyrolysis and vitrinite reflectance trends in the Cleveland Shale Member of the Ohio Shale, eastern Kentucky. Organic Geochemistry 20, 735–745. doi:10.1016/0146-6380(93)90058-J

Ritter, U., 2003. Solubility of petroleum compounds in kerogen: implications for petroleum expulsion. Organic Geochemistry 34, 319–326.

Ritter, U., Myhr, M.B., Vinge, T., Aareskjold, K., 1995. Experimental heating and kinetic models of source rocks: comparison of different methods. Organic Geochemistry 23, 1 – 9.

Roberts, M.J., Snape, C.E., Mitchell, S.C., 1995. Hydropyrolysis: Fundamentals, Two-Stage Processing and PDU Operation, in: Snape, C. (Ed.), Composition, Geochemistry and Conversion of Oil Shales, NATO ASI Series. Springer Netherlands, pp. 277–293.

Robinson, N., Eglinton, G., Lafferty, C.J., Snape, C.E., 1991. Comparison of alkanes released from a bituminous coal via hydropyrolysis and low temperature hydrogenation. Fuel 70, 249–253. doi:10.1016/0016-2361(91)90160-C

Röhl, H.-J., Schmid-Röhl, A., Oschmann, W., Frimmel, A., Schwark, L., 2001. The Posidonia Shale (Lower Toarcian) of SW-Germany: an oxygen-depleted ecosystem controlled by sea level and palaeoclimate. Palaeogeography, Palaeoclimatology, Palaeoecology 165, 27–52. doi:10.1016/S0031-0182(00)00152-8

Romero-Sarmiento, M.-F., Rouzaud, J.-N., Bernard, S., Deldicque, D., Thomas, M., Littke, R., 2014. Evolution of Barnett Shale organic carbon structure and nanostructure with increasing maturation. Organic Geochemistry 71, 7–16. doi:10.1016/j.orggeochem.2014.03.008

Rouchet, J. du, 1981. Stress Fields, A Key to Oil Migration. AAPG Bulletin 65, 74–85.

Ruble, T.E., Lewan, M. ?d, Philp, R. ?p, 2001. New insights on the Green River petroleum system in the Uinta basin from hydrous pyrolysis experiments. AAPG Bulletin 85, 1333–1371.

Rullkötter, J., Aizenshtat, Z., Spiro, B., 1984. Biological markers in bitumens and pyrolyzates of Upper Cretaceous bituminous chalks from the Ghareb Formation (Israel). Geochimica et Cosmochimica Acta 48, 151–157. doi:10.1016/0016-7037(84)90357-0

Rullkötter, J., Leythaeuser, D., Horsfield, B., Littke, R., Mann, U., Müller, P.., Radke, M., Schaefer, R.., Schenk, H.-J., Schwochau, K., Witte, E.., Welte, D.., 1988. Organic matter maturation under the influence of a deep intrusive heat source: A natural experiment for quantitation of hydrocarbon generation and expulsion from a petroleum source rock (Toarcian shale, northern Germany). Organic Geochemistry 13, 847–856. doi:10.1016/0146-6380(88)90237-9

Rullkötter, J., Spiro, B., Nissenbaum, A., 1985. Biological marker characteristics of oils and asphalts from carbonate source rocks in a rapidly subsiding graben, Dead Sea, Israel. Geochimica et Cosmochimica Acta 49, 1357–1370. doi:10.1016/0016-7037(85)90286-8

Russell, C.A., Snape, C.E., Meredith, W., Love, G.D., Clarke, E., Moffatt, B., 2004. The potential of bound biomarker profiles released via catalytic hydropyrolysis to reconstruct basin charging history for oils. Organic Geochemistry 35, 1441–1459. doi:10.1016/j.orggeochem.2004.07.004

Sahay, B., 1999. Pressure Regimes in Oil and Gas Exploration: Bhagwan Sahay. Allied Publishers.

Sanada, Y., Honda, H., 1966. Swelling Equilibrium of Coal by Pyridine at 25 Degrees C. Fuel 45, 295–&.

Sandvik, E.I., Young, W.A., Curry, D.J., 1992. Expulsion from hydrocarbon sources: the role of organic absorption. Organic Geochemistry 19, 77 – 87.

Sassen, R., 1988. Geochemical and carbon isotopic studies of crude oil destruction, bitumen precipitation, and sulfate reduction in the deep Smackover Formation. Organic Geochemistry 12, 351–361. doi:10.1016/0146-6380(88)90009-5

Schaefer, R.G., Schenk, H.J., Hardelauf, H., Harms, R., 1990. Determination of gross kinetic parameters for petroleum formation from Jurassic source rocks of different maturity levels by means of laboratory experiments. Organic Geochemistry 16, 115–120. doi:10.1016/0146-6380(90)90031-T

Schenk, H.J., Di Primio, R., Horsfield, B., 1997. The conversion of oil into gas in petroleum

reservoirs. Part 1: Comparative kinetic investigation of gas generation from crude oils of lacustrine, marine and fluviodeltaic origin by programmed-temperature closed-system pyrolysis. Organic Geochemistry 26, 467–481. doi:10.1016/S0146-6380(97)00024-7

Schenk, H.J., Horsfield, B., 1998. Using natural maturation series to evaluate the utility of parallel reaction kinetics models: an investigation of Toarcian shales and Carboniferous coals, Germany. Organic Geochemistry 29, 137 – 154.

Schenk, H.J., Horsfield, B., 1993. Kinetics of petroleum generation by programmed-temperature closed-versus open-system pyrolysis. Geochimica et Cosmochimica Acta 57, 623 – 630.

Schimmelmann, A., Boudou, J.-P., Lewan, M.D., Wintsch, R.P., 2001. Experimental controls on D/H and 13C/12C ratios of kerogen, bitumen and oil during hydrous pyrolysis. Organic Geochemistry 32, 1009 – 1018.

Schimmelmann, A., Lewan, M.D., Wintsch, R.P., 1999. D/H isotope ratios of kerogen, bitumen, oil, and water in hydrous pyrolysis of source rocks containing kerogen types I, II, IIS, and III. Geochimica et Cosmochimica Acta 63, 3751 – 3766.

Schoell, M., Teschner, M., Wehner, H., Durand, B., Oudin, J.L., 1983. Maturity related biomarker and stable isotope variations and their application to oil/source rock correlation in the Mahakam Delta, Kalimantan, in: Bjorøy, M., Albrecht, C., Cornford, C. (Eds.), Advances in Organic Geochemistry, 1981. Wiley, pp. 156–163.

Schwark, L., Vliex, M., Schaeffer, P., 1998. Geochemical characterization of Malm Zeta laminated carbonates from the Franconian Alb, SW-Germany (II). Organic Geochemistry 29, 1921–1952. doi:10.1016/S0146-6380(98)00192-2

Seewald, J.S., Benitez-Nelson, B.C., Whelan, J.K., 1998. Laboratory and theoretical constraints on the generation and composition of natural gas. Geochimica et Cosmochimica Acta 62, 1599–1617. doi:10.1016/S0016-7037(98)00000-3

Seifert, W.K., Moldowan, J.M., 1980. The effect of thermal stress on source-rock quality as measured by hopane stereochemistry. Physics and Chemistry of The Earth 12, 229–237. doi:10.1016/0079-1946(79)90107-1

Seifert, W.K., Moldowan, J.M., 1978. Applications of steranes, terpanes and monoaromatics to the maturation, migration and source of crude oils. Geochimica et Cosmochimica Acta 42, 77–95. doi:10.1016/0016-7037(78)90219-3

Smart, G., Clayton, T., 1985. The Progressive Illitization of Interstratified Illite-Smectite from Carboniferous Sediments of Northern England and Its Relationship to Organic Maturity Indicators. Clay Min. 20, 455–466. doi:10.1180/claymin.1985.020.4.02

Snape, C.E., Lafferty, C.J., Stephens, H.P., Dosch, R.G., Klavetter, E., 1991. Effect of catalyst precursors on coal reactivity in catalytic hydropyrolysis. Fuel 70, 393–395. doi:10.1016/0016-2361(91)90128-W

Solli, H., Bjorøy, M., Leplat, P., Hall, K., 1984. Analysis of organic matter in small rock samples using combined thermal extraction and pyrolysis—gas chromatography. Journal of Analytical and Applied Pyrolysis 7, 101–119. doi:10.1016/0165-2370(84)80044-3

Song, C., Saini, A.K., Schobert, H.H., 1994. Effects of Drying and Oxidation of Wyodak Subbituminous Coal on Its Thermal and Catalytic Liquefaction.Spectroscopic Characterization and Products Distribution. Energy Fuels 8, 301–312. doi:10.1021/ef00044a003

Stainforth, J.G., 2009. Practical kinetic modeling of petroleum generation and expulsion. Marine and Petroleum Geology 26, 552 – 572.

Stainforth, J.G., Reinders, J.E.A., 1990. Primary migration of hydrocarbons by diffusion through organic matter networks, and its effect on oil and gas generation. Organic Geochemistry 16, 61–74. doi:10.1016/0146-6380(90)90026-V

Stalker, L., Farrimond, P., Larter, S.R., 1994. Water as an oxygen source for the production of oxygenated compounds (including CO2 precursors) during kerogen maturation. Organic Geochemistry 22, 477–IN4. doi:10.1016/0146-6380(94)90120-1

Stalker, L., Larter, S.R., Farrimond, P., 1998. Biomarker binding into kerogens: evidence from hydrous pyrolysis using heavy water (D2O). Organic Geochemistry 28, 239–253. doi:10.1016/S0146-6380(97)00103-4

Sweeney, J.J., Burnham, A.K., 1990. Evaluation of a Simple Model of Vitrinite Reflectance Based on Chemical Kinetics (1). AAPG Bulletin 74, 1559–1570.

Tang, Y.C., Stauffer, M., 1995. Formation of pristene, pristane and phytane: kinetic study by laboratory pyrolysis of Monterey source rock. Organic Geochemistry 23, 451–460. doi:10.1016/0146-6380(95)00020-F

Tannenbaum, E., Huizinga, B.J., Kaplan, I.R., 1986. Role of Minerals in Thermal Alteration of Organic Matter--II: A Material Balance. AAPG Bulletin 70, 1156–1165.

Teerman, S.C., Hwang, R.J., 1991. Evaluation of the liquid hydrocarbon potential of coal by artificial maturation techniques. Organic Geochemistry 17, 749–764. doi:10.1016/0146-6380(91)90019-G

Teichmüller, M., 1982. Fluoreszenzmikroskopische Änderungen von Liptiniten und Vitriniten mit zunehmendem Inkohlungsgrad und ihre Beziehungen zu Bitumenbildung und Verkokungsverhalten / von Marlies Teichmüller. Geolog. Landesamt Nordrhein-Westfalen, Krefeld.

Terzaghi, K., Peck, R.B., 1967. Soil mechanics in engineering practice. Wiley.

Thomas, M.M., Clouse, J.A., 1990a. Primary migration by diffusion through kerogen: I. Model experiments with organic-coated rocks. Geochimica et Cosmochimica Acta

54, 2775–2779. doi:10.1016/0016-7037(90)90011-9

Thomas, M.M., Clouse, J.A., 1990b. Primary migration by diffusion through kerogen: II. Hydrocarbon diffusivities in kerogen. Geochimica et Cosmochimica Acta 54, 2781–2792. doi:10.1016/0016-7037(90)90012-A

Thomas, M.M., Clouse, J.A., 1990c. Primary migration by diffusion through kerogen: III. Calculation of geologic fluxes. Geochimica et Cosmochimica Acta 54, 2793–2797. doi:10.1016/0016-7037(90)90013-B

Thomas, N.., Windle, A.., 1982. A theory of case II diffusion. Polymer 23, 529–542. doi:10.1016/0032-3861(82)90093-3

Tissot, B., Califet-Debyser, Y., Deroo, G., Oudin, J.L., 1971. Origin and Evolution of Hydrocarbons in Early Toarcian Shales, Paris Basin, France. AAPG Bulletin 55, 2177–2193.

Tissot, B., Deroo, G., Hood, A., 1978. Geochemical study of the Uinta Basin: formation of petroleum from the Green River formation. Geochimica et Cosmochimica Acta 42, 1469–1485. doi:10.1016/0016-7037(78)90018-2

Tissot, B., Espitalié, J., 1975. L'evolution thermique de la matière organique des sédiments : applications d'une simulation mathématique. Potentiel pétrolier des bassins sédimentaires de reconstitution de l'histoire thermique des sédiments. Oil & Gas Science and Technology 30, 743–778. doi:10.2516/ogst:1975026

Tissot, B.P., Pelet, R., Ungerer, P., 1987. Thermal History of Sedimentary Basins, Maturation Indices, and Kinetics of Oil and Gas Generation. AAPG Bulletin 71, 1445–1466.

Tissot, B.P., Welte, D.H., 1984. Petroleum Formation and Occurrence. Springer-Verlag Telos.

Tomić, J., Behar, F., Vandenbroucke, M., Tang, Y., 1995. Artificial maturation of Monterey kerogen (Type II-S) in a closed system and comparison with Type II kerogen: implications on the fate of sulfur. Organic Geochemistry 23, 647–660. doi:10.1016/0146-6380(95)00043-E

Tsonopoulos, C., Wilson, G.M., 1983. High-temperature mutual solubilities of hydrocarbons and water. Part I: Benzene, cyclohexane and *n*-hexane. AIChE Journal 29, 990–999. doi:10.1002/aic.690290618

Uguna, C.N., Carr, A.D., Snape, C.E., Meredith, W., Castro-Díaz, M., 2012. A laboratory pyrolysis study to investigate the effect of water pressure on hydrocarbon generation and maturation of coals in geological basins. Organic Geochemistry 52, 103–113. doi:10.1016/j.orggeochem.2012.09.003

Ungerer, P., 1990. State of the art of research in kinetic modelling of oil formation and expulsion. Organic Geochemistry 16, 1–25. doi:10.1016/0146-6380(90)90022-R

Ungerer, P., Behar, F., Villalba, M., Heum, O.R., Audibert, A., 1988. Kinetic modelling of oil cracking. Organic Geochemistry 13, 857–868. doi:10.1016/0146-6380(88)90238-0

Vandenbroucke, M., Behar, F., Rudkiewicz, J.L., 1999. Kinetic modelling of petroleum formation and cracking: implications from the high pressure/high temperature Elgin Field (UK, North Sea). Organic Geochemistry 30, 1105–1125. doi:10.1016/S0146-6380(99)00089-3

Van Koeverden, J. h., Karlsen, D. a., Schwark, L., Chpitsglouz, A., Backer-Owe, K., 2010. Oil-Prone Lower Carboniferous Coals in the Norwegian Barents Sea: Implications for a Palaeozoic Petroleum System. Journal of Petroleum Geology 33, 155–181. doi:10.1111/j.1747-5457.2010.00471.x

Velde, B., Espitalié, J., 1989. COMPARISON OF KEROGEN MATURATION AND ILLITE/SMECTITE COMPOSITION IN DIAGENESIS. Journal of Petroleum Geology 12, 103–110.

Velde, B., Lanson, B., 1993. Comparison of I/S Transformation and Maturity of Organic-Matter at Elevated-Temperatures. Clay Clay Min. 41, 178–183. doi:10.1346/CCMN.1993.0410206

Volkman, J.K., Maxwell, J.R., 1986. Acyclic isoprenoids as biological markers, in: Biological Markers in the Sedimentary Record. Elsevier, pp. 1–42.

Walker, P.L., Mahajan, O.P., 1993. Pore structure in coals. Energy Fuels 7, 559–560. doi:10.1021/ef00040a017

Waples, D.W., 1980. Time and Temperature in Petroleum Formation: Application of Lopatin's Method to Petroleum Exploration. AAPG Bulletin 64, 916–926.

Wei, Z., Zou, Y.-R., Cai, Y., Wang, L., Luo, X., Peng, P., 2012. Kinetics of oil group-type generation and expulsion: An integrated application to Dongying Depression, Bohai Bay Basin, China. Organic Geochemistry 52, 1–12. doi:10.1016/j.orggeochem.2012.08.006

Welte, D.., Yalçin, M.., 1988. Basin modelling—A new comprehensive method in petroleum geology. Organic Geochemistry 13, 141–151. doi:10.1016/0146-6380(88)90034-4

Weres, O., Newton, A.S., Tsao, L., 1988. Hydrous pyrolysis of alkanes, alkenes, alcohols and ethers. Organic Geochemistry 12, 433–444. doi:10.1016/0146-6380(88)90153-2

Wilkins, R.W.T., George, S.C., 2002. Coal as a source rock for oil: a review. International Journal of Coal Geology, Volume 50 50, 317–361. doi:10.1016/S0166-5162(02)00134-9

Wycherley, H., Fleet, A., Shaw, H., 1999. Some observations on the origins of large volumes of carbon dioxide accumulations in sedimentary basins. Marine and Petroleum Geology 16, 489–494. doi:10.1016/S0264-8172(99)00047-1

Yani, S., Zhang, D., 2010. An experimental study into pyrite transformation during pyrolysis of Australian lignite samples. Fuel 89, 1700–1708. doi:10.1016/j.fuel.2009.07.025

Zumberge, J.E., 1987. Prediction of source rock characteristics based on terpane biomarkers in crude oils: A multivariate statistical approach. Geochimica et

Cosmochimica Acta 51, 1625–1637. doi:10.1016/0016-7037(87)90343-7

# Acknowledgments

Firstly, I would like to thank my advisor Prof. Lorenz Schwark for the support of my Ph.D study and related research. His guidance helped me in all the time of research and writing of this thesis.

Besides my advisor, I would like to thank Dr. Roberto Galimberti and Dr. Rouven Elias from ENI S.p.A. for supporting my research by funding this project and for their insightful comments and encouragement.

My sincere thanks also goes to Prof. Brian Horsfield for reviewing of my thesis and to Prof. Romain Bousquet and PD Dr. Mark Schmidt as members of the board of examiners.

I especially want to thank the student assistances involved in this project, Fanny Aschmann, Viktoria Bass, Theresa Leinkauf, Josh Rochelmeyer, Sabrina Schneider Covachã and Anna Plaß. Without their help the conduction of this project would not have been feasible.

Last but not the least I want to thank the technical stuff, Inge Dold, Petra Fiedler, Eyke Kirchkof and Marieke Sieverding for their help and support.